Oceanic redox conditions across the Cambrian–Ordovician boundary

By

© Alexandre Charest Bisnaire

A thesis submitted to the

School of Graduate Studies

In partial fulfillment of the requirements for the degree of

Masters of Science

Department of Earth Sciences

Memorial University of Newfoundland

May 2018

St. John's, Newfoundland

Abstract

Trace element and isotope geochemistry is used to evaluate paleoenvironments. Uranium and molybdenum geochemistry in particular have been used as reliable paleoredox indicators, leading to valuable developments. Here, these proxies are applied to the transgressive sedimentary succession spanning the Cambrian – Ordovician GSSP boundary section of the Cow Head Group exposed at Green Point, western Newfoundland (Canada).

In Chapter 2, the distal slope environment of deposition is evaluated based on the green to black shales' geochemistry. It underwent significant changes during the transgression occurring around the Cambrian-Ordovician boundary. As the platform became increasingly flooded and more carbonate-dominated, the cratonic siliciclastic supply decreased, lowering the proportion of Al (6.2±1.1 wt% to 5.2±1.0 wt%), Cr (64±12 ppm to 55±10 ppm), Sc (9.1±1.8 ppm to 7.5±1.6 ppm), Th (7.4±1.2 ppm to 5.9±1.4 ppm) and Cs (3.7±1.0 ppm to 2.6±0.8 ppm) and increasing the proportion of Ca (3.8±3.0 wt% to 4.8±2.8 wt%) in the shales. Conditions became more reducing as relative sea level rose, becoming more strongly suboxic, with more frequent anoxic intervals. Due to short-term fluctuations (reflected in the highly variable lithology), this is reflected most accurately by the higher proportion of shales demonstrating significant U and Mo authigenic enrichment above the anomaly level, and their relationship to higher TOC values. Bioproductivity was low throughout the section, based on low P

(494±141 ppm), Ni (32.8±10.5 ppm) and Cu (36.1±16.8 ppm). Bioproductivity variation across the anomaly level could not be ascertained however. The geochemical patterns observed correlate well with the carbonate carbon isotope stratigraphy, clearly defining trends and systems tract.

In Chapter 3, we focus on Mo and U elemental and isotopic geochemistry. We first evaluate the relationship of U/Mo ratio vs U and Mo (both concentrations and EFs) in the Green Point shales and compare the results to several modern and Phanerozoic-aged siliciclastic environments to evaluate repeatability and predictability. Secondly, this method is applied to the Green Point carbonates and modern Bahamas carbonates. In the third part of this chapter, we focus on the δ^{98}Mo ratios from the Green Point carbonates and their reliability as a predictive paleoredox tool. Uranium and Molybdenum were found to have divergent relationships to the U/Mo ratios. In the Green Point shales, the relationship between U/Mo_{auth} vs Mo_{EF} or U_{EF} enrichment factors were found to be reliable redox indicators, particularly U/Mo_{auth} vs Mo_{EF}. When applied to other siliciclastic datasets, plotting U/Mo_{auth} to Mo_{EF} or U_{EF} yielded a different yet consistent pattern relative to the U_{EF} vs Mo_{EF} plot of Algeo and Tribovillard (2009), differentiating oxygen levels, most notably within the suboxic range, and marine basin restriction. Within the carbonates, the main factor controlling the low U concentrations was calcite being the carbonate species present. The decrease across the anomaly is likely due to the TOC decrease; enhanced by low dissolved porewater sulfide levels and the presence of carbonate material. The positive U/Mo vs U trend supports the conclusion that authigenic enrichment was not tot the main control on observed variations. The Mo values were within the range of previously carbonates, indicating pH and carbonate species present may not affect Mo enrichment. The U/Mo vs Mo plot behaved like in the shales, showing potential as a redox indicator. When applied to the Bahamas carbonates, both relationships consistently differentiated low and high pore-water sulfide levels, and shows potential to differentiate paleoenvironments. The Mo isotope ratios were interpreted as being a mixed detrital-authigenic signature, and so are minimum values. The increase across the anomaly level suggests increasingly reducing conditions during the deposition of the Green Point carbonates. This agrees with previous interpretations, indicating δ^{98}Mo ratios are reliable at Green Point.

Acknowledgements

I would first like thank my supervisor Professor Karem Azmy for the chance he gave me to come to Memorial University of Newfoundland, work on a project I found to be very interesting, and the help he afforded me during the editing process. I'd also like to thank Drs. Svend Stouge and Gabriella Bagnoli for the help they gave me, particularly in the field. I would also like to express my sincerest gratitude to Professor Brian Kendall for the help he gave me when I worked in his lab and his very constructive criticism from which I learned much.

I would also like to thank my whole family, particularly my mother, for all the support they've given me since I've started my project. I am grateful for everything they have done to help me.

I would furthermore like to thank Liyan Xing and Joy Hu for their technical assistance when I was working in Professor Kendall's laboratory in Waterloo, Ontario.

Lastly, I also extend my gratitude to PEEP, the Petroleum Exploration Enhancement Program through Professor Azmy, to the NSERC Discovery Grant, through Professor Kendall and to the Carlsberg Foundation, through Professor Stouge, for the financial support which made this project possible.

Table of Contents

List of Tables

List of Figures

List of Appendixes

Co-authorship Statement

The thesis is presented in the format of a manuscript. It consists of 4 separate chapters. Chapter 1 includes a review of the relevant background literature and outlines the main objectives of the study. Chapters 2 and 3 each represent a research paper, including individual introductions, sample localities, analytical methods, results, discussions and conclusion sections. Chapter 5, the last chapter, summarizes the conclusions of this research project.

The mainframe of Chapter 2 and part of Chapter 3 (Molybdenum Isotopic Analysis) were outlined by Profs. Karem Azmy, Brian Kendall and Svend Stouge. The mainframe of the first half of Chapter 3 (U/Mo, Uranium, Molybdenum Covariation) was of my own design. As co-authors, Professors Karem Azmy, Brian Kendall, and Svend Stouge guided my progress during the completion of the project, advised me on my progress and corrected the written manuscript prior to submission. Apart from the sample collection of carbonates and their laboratory analyses (elemental and isotope geochemistry including Mo-isotopes), all aspects of the thesis were my responsibility as the primary author. This includes the literature review, refining the objectives, shale laboratory analyses, data analysis and interpretation and assembling the manuscripts.

Chapter 2, "Trace element variations in the shales across the Cambrian–Ordovician boundary: implications for environmental changes associated with sealevel variations" to be published in "Sedimentology". **Chapter 3**, "Evaluation of uranium and molybdenum enrichments versus U/Mo ratios in shales and carbonates and Mo isotope compositions in carbonates as paleoredox proxies: A case study from the Green Point Cambrian-Ordovician boundary section, Newfoundland" to be published in "Chemical Geology".

Shale samples destined for the interpretation of the Green Point Formation Cambrian-Ordovician section were collected by myself, under the supervision of Dr. Svend Stouge who was collecting samples from the same section, at Green Point, western Newfoundland. Data used for Chapter 3 was also sourced from several published papers to represent both modern and ancient environments.

Chapter 1

Introduction and Overview

Chemostratigraphy has been established as a reliable correlative tool in the study of sedimentary successions, particularly when the biostratigraphic resolution is poor or missing, and thus has significant applications in the evaluation of hydrocarbon plays (Ratcliffe and Wilson, 2014; Ainsaar et al., 2015). Using this tool, isochronous stratigraphic markers, geological boundaries, and geological events/processes are identified by tracking changes in the elemental and isotopic compositions of sedimentary rocks (Saltzman and Thomas, 2012; Ainsaar et al., 2015). Trace element enrichments (or lack thereof) and elemental ratios in shales are known to be reliable proxies for the purpose of identifying variations in paleoredox conditions, source material composition/flux, and bioproductivity (Dill, 1986; Wignall and Myers, 1988; Hatch and Leventhal, 1992; Jones and Manning, 1994; Lécuyer et al., 1998; Schnetger et al., 2000; Piper and Perkins, 2004; Jiang et al., 2006; Lyons and Severmann, 2006; Riquier et al., 2006; Tribovillard et al., 2006; Jiménez-Espejo et al., 2007; Ma et al., 2008; Perkins et al., 2008; Algeo and Tribovillard, 2009; Piper and Calvert, 2009; Poulton et al., 2010; Śliwiński et al., 2010; Zhou et al., 2012; Tripathy et al., 2014; Basu et al., 2014; Gao et al., 2016). Understanding paleoredox conditions has important implications when interpreting ancient marine depositional environments and global ocean oxygen levels in the past oceans and atmosphere (Barling et al., 2001; Siebert et al., 2003; Morford et al., 2009b; Voegelin et al., 2009; Czaja et al., 2012; Lau et al., 2016). Molybdenum and Uranium concentrations and isotopes in particular have been extensively and successfully used as paleoredox indicators in paleoenvironmental reconstructions, particularly in shales but now also in carbonates, due to their sensitivity to changes in water oxygenation, often in combination with total organic content [TOC] (Crusius et al., 1996; Morford and Emerson, 1999; Zheng et al., 2000; 2002a; 2002b; Chaillou et al., 2002; Siebert et al., 2003; Algeo and Maynard, 2004; Tribovillard et al., 2004; McManus et al., 2005; Morford et al., 2005; Tribovillard et al., 2008b; Algeo and Tribovillard, 2009; Morford et al., 2009a; Piper and Calvert, 2009; Poulson Brucker et al., 2009; Voegelin et al., 2009; 2010; Czaja et al., 2012; Scott and Lyons, 2012; Xu et al., 2012; Romaniello et al., 2013; Azmy et al., 2015; Kendall et al., 2015; Wen et al., 2015; Gao et al., 2016; Romaniello et al., 2016). Both trace metals become more authigenically enriched within sediments as pore-water oxygen levels reach anoxic levels and dissolved sulfide increases to reach euxinia (Emerson and Huested, 1991; Jones and Manning, 1994; Crusius and Thomson, 2000; Erickson and Helz, 2000; Adelson et al., 2001; Wignall et al., 2007). Their pattern of enrichment differs in low-O_2 conditions since the intensity of their authigenic enrichment is dependent on different processes and attributes, explained below (Helz et al., 1996; Zheng et al., 2000; 2002a; 2002b; Algeo and Maynard, 2004; Tribovillard et al., 2006; Algeo and Tribovillard., 2009; Zhou et al., 2012).

1.1 Study Area

The succession at Green Point (Fig. 1.1b) spans the Cambrian–Ordovician boundary and was elected as the Global Stratotype Section and Point (GSSP), which defines the lower boundary of the Ordovician system (Cooper et al., 2001a; Fig. 1.1; 1.2). The studied Green Point interval was deposited in a distal slope setting off the Laurentian continental margin (James and Stevens, 1986). Sedimentary rocks from the Green Point locality are typical of mixed siliciclastic-carbonate slope deposits. The interval, part of the Green Point Formation of the Cow Head Group, is composed of deep-water non-carbonaceous to carbonaceous organic-rich green, grey and black shales, siltstones, parted and ribbon limestone as well as breccias and (mega-) conglomerates derived from debris-flows (Fig. 1.2). The sediments were deposited during a period of eustatic sea level fluctuation, which affected ocean circulation (Coniglio, 1986; James and Stevens, 1986; Coniglio and James, 1990; Landing, 2012; Terfelt et al., 2012; Landing, 2013; Terfelt et al., 2014; Azmy et al., 2015). This deep-water environment is characterized by lower bioproductivity, lower organic carbon export fluxes, and lower bottom-water O_2 levels compared with the adjoining continental shelf (Tyson and Pearson, 1991; Landing, 2012, 2013; Azmy et al., 2014). Below the established global Cambrian–Ordovician boundary (Golden Spike) at Green Point, a geochemical anomaly was documented by Azmy et al. (2014; 2015), based on geochemical evidences from the alternating carbonate interbeds in the currently investigated section. The organic-rich black shales of the Green Point Formation is generally considered to be the source rock of the common occurrences of oil seeps seen in the area (Weaver and Macko, 1987). Earlier studies indicated a significant degree of petrographic and geochemical preservation of the carbonates interbedded with the currently investigated shales (Azmy et al., 2014, 2015). This is supported by several lines of evidence, including the insignificant correlations between Mn/Sr ratios vs $\delta^{13}C_{carb}$ or $\delta^{18}O_{carb,}$ TOC values vs $\delta^{13}C_{org}$, $\delta^{15}N_{org}$ and good relationship between Re-Os ages to graptolite stratigraphy (Tripathy et al., 2014; Azmy et al., 2015), which is consistent with the lack of evidence of significant hydrothermal influence, supported by conodont alteration index data T_{max} values of 50-90^{O}C (~1.5; Epstein et al., 1977; Nowlan and Barnes, 1987; Williams et al., 1998) and TOC T_{max} data from Green Point indicating the shallower part of the oil window was reached (Tripathy et al., 2014). Synsedimentary deformation resulting from the slope failures and debris flows did however affect the Green Point section. Later tectonic activity resulted in faulting and overturning beds, causing layer-parallel shortning previously associated with late-diagenetic precipitates and tectonic stylolites (Coniglio, 1986). This did not result in pervasive diagenesis. Furthermore, no evidence of metamorphism was documented. This is to be expected, as metamorphism and deformation within the Humber Zone are known to increase eastward from the western external domain, where the study area is located, to the eastern internal domain (Williams, 1995; Cawood and van Gool, 1998; Waldron et al., 1998).

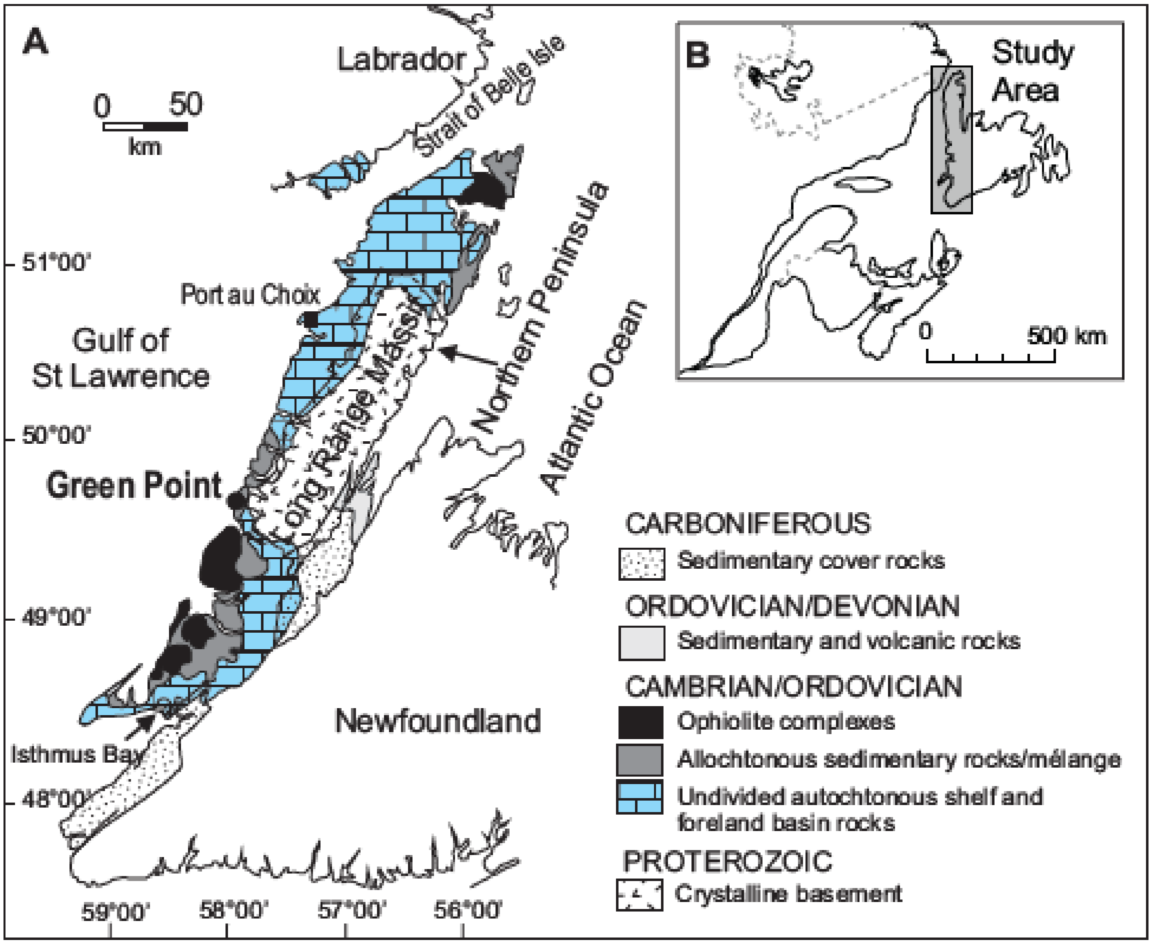

Figure 1.1: A) Geology of western Newfoundland and the location of Green Point. B) Map of eastern Canada, with western Newfoundland marked by the grey box. Modified from Olanipekun et al. (2014).

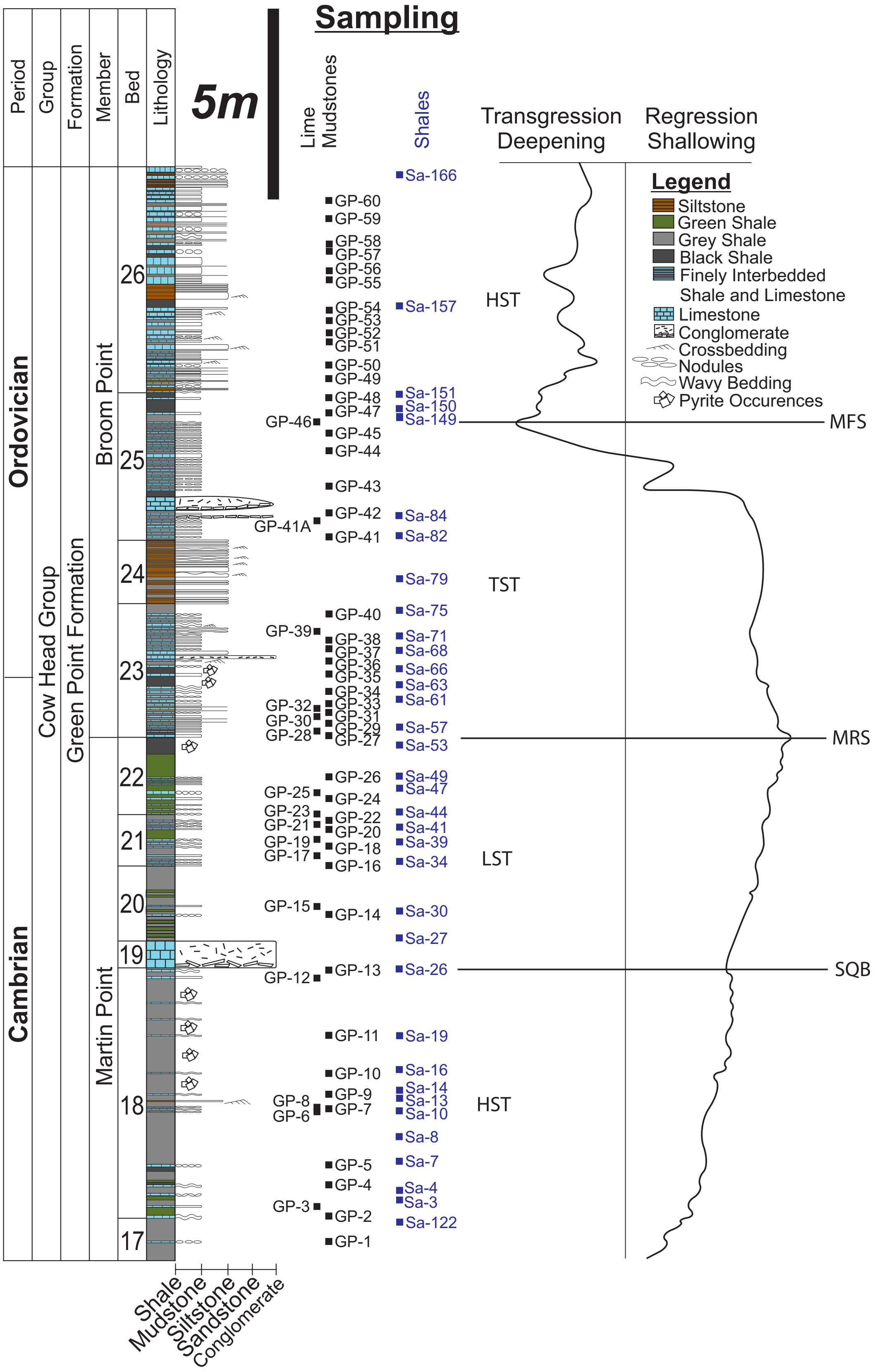
Sampling
Period
Group
Formation
Member
Bed
Lithology
5m
Lime Mudstones
Shales
Transgression Deepening
Regression Shallowing
Legend
Siltstone
Green Shale
Grey Shale
Black Shale
Finely Interbedded Shale and Limestone
Limestone
Conglomerate
Crossbedding
Nodules
Wavy Bedding
Pyrite Occurences
Ordovician
Cambrian
Cow Head Group
Green Point Formation
Broom Point
Martin Point
26
25
24
23
22
21
20
19
18
17
Shale
Mudstone
Siltstone
Sandstone
Conglomerate
GP-60
GP-59
GP-58
GP-57
GP-56
GP-55
GP-54
GP-53
GP-52
GP-51
GP-50
GP-49
GP-48
GP-47
GP-46
GP-45
GP-44
GP-43
GP-42
GP-41A
GP-41
GP-40
GP-39
GP-38
GP-37
GP-36
GP-35
GP-34
GP-33
GP-32
GP-31
GP-30
GP-29
GP-28
GP-27
GP-26
GP-25
GP-24
GP-23
GP-22
GP-21
GP-20
GP-19
GP-18
GP-17
GP-16
GP-15
GP-14
GP-13
GP-12
GP-11
GP-10
GP-9
GP-8
GP-7
GP-6
GP-5
GP-4
GP-3
GP-2
GP-1
Sa-166
Sa-157
Sa-151
Sa-150
Sa-149
Sa-84
Sa-82
Sa-79
Sa-75
Sa-71
Sa-68
Sa-66
Sa-63
Sa-61
Sa-57
Sa-53
Sa-49
Sa-47
Sa-44
Sa-41
Sa-39
Sa-34
Sa-30
Sa-27
Sa-26
Sa-19
Sa-16
Sa-14
Sa-13
Sa-10
Sa-8
Sa-7
Sa-4
Sa-3
Sa-122
HST
TST
LST
HST
MFS
MRS
SQB

Figure 1.2: Detailed stratigraphic column of the investigated Green Point section. Carbonate sampling points shown in black. Shale sampling points shown in blue. Sea level variation curve for the Green Point Formation, Green Point, western Newfoundland, Canada from Azmy et al. (2015). Sea level curve abbreviations are as follows: HST = Highstand Systems Tract, LST = Lowstand Systems Tract, TST = Transgressive Systems Tract, SQB = Sequence Boundary, MRS = Maximum Regressive Surface, MFS = Maximum Flooding Surface.

1.2 Uranium Geochemistry

Within sediments, aqueous authigenic U removal from seawater occurs primarily at the sediment water interface in reducing conditions. Under oxic-suboxic conditions, U is present mainly as unreactive and soluble U(VI) in the form of uranyl carbonates (Langmuir, 1978; Klinkhammer and Palmer, 1991; Calvert and Pedersen, 1993; Algeo and Tribovillard, 2009). These environments typically contain < 5ppm U (Morford et al., 2009b). U becomes reduced to U(IV) at/near the boundary where Fe^{3+} is converted to Fe^{2+} (Cochran et al., 1986; Anderson, 1987; McKee et al., 1987; Barnes and Cochran, 1990; Chaillou et al., 2002; Sani et al., 2004). It forms either highly soluble UO_2^+ or less soluble uranous fluoride complexes that develop within the pore-fluids at the sediment-water interface, either abiotically with $[H_2S]_{aq}$ being the reductant or catalyzed by bacterial enzymes (Barnes and Cochran, 1990; Lovley et al., 1991; Lovley et al., 1993; Zheng et al., 2002a; Hua et al., 2006; Morford et al., 2009a; Brennecka et al., 2011; Romaniello et al., 2013). From these species, authigenic U will be taken up by the reducing sediments as organic-metal ligands in humic acids, uraninite (UO_2), its metastable precursor, U_3O_7 or U_3O_8 (Barnes and Cochran, 1990; Klinkhammer and Palmer, 1991; Zheng et al., 2002a; McManus et al., 2005). In suboxic settings, U may be released from sediments during short-lived oxygenation events (Tribovillard et al., 2006; Algeo and Tribovillard, 2009). In carbonates, uranium can also be readily incorporated within the $CaCO_3$ structures via co-precipitation (Chung and Swart, 1990; Sturchio et al., 1998; Reeder et al., 2000; Kelly et al., 2006). Several factors can affect which U species might be preferentially enriched in the sediments. Controls on abiotic precipitation include the abundance of cations, CO_3^{2-}, the prevalent pH at the time, the primarily precipited carbonate polymorph and whether aqueous species are charged or not (Berner and Kothavala, 2001; Hortia et al., 2002; Lowenstein et al., 2003; Ries et al., 2004; Royer et al., 2004; Ridgwell, 2005; Ries et al., 2010; Chen et al., 2016). Within the environmental pH range (6 to 8), U phases will be more soluble and will tend to form aqueous $UO_2(CO_3)_2^{2-}$ (Krestou and Panias, 2004; Beazly et al., 2011). These can be directly incorporated into aragonite, with no coordination change (Reeder et al,. 2000). Reduced U (IV) will also be substituted preferentially with Ca in calcite relative to U (VI) (Sturchio et al., 1998; Chen et al., 2016). U(VI) will form stable uranyl-tricarbonate-calcium complexes that can substitute for Ca in calcite, adopting the equatorial coordination 4 in the process (Kelly et al., 2003; 2006). In calcite, U(V), via the complex $UO_2(CO_3)_3^{4-}$, can also be incorporated into calcite, with the equatorial coordination number 5 (Reeder et al., 2000; 2001).

1.3 Molybdenum Geochemistry

Molybdenum becomes increasingly authigenically enriched within sediments as bottom-water oxygen levels decrease and dissolved sulfide levels start to increase (Emerson and Huested, 1991; Jones and Manning, 1994; Crusius and Thomson, 2000; Erickson and Helz, 2000; Adelson et al., 2001; Wignall et al., 2007). Within oxidized waters, Mo occurs as soluble and stable MoO_4^{2-}. Authigenic enrichment is limited in the sediments, with Mo_{auth} concentrations normally < 5ppm Mo (Zheng et al., 2000; Morford et al., 2009a). The first mechanism of authigenic Mo enrichment is the formation of Mo bearing Mn-oxides within the Mn-oxidation zone (Lam et al., 2007; Canfield and Thamdrup, 2009; Scott and Lyons, 2012). These Mn-oxides will however undergo reductive dissolution under ferruginous-anoxic conditions, within the Fe-oxide zone, deeper within the sediments. They are only preserved if pore-fluid or water conditions become sulfidic prior to total dissolution (Johnson et al., 1992; Morford and Emerson, 1999; Scott and Lyons, 2012). Under anoxic-sulfidic conditions attained either within the sediment pore-space or water column, molybdate (MoO_4^{2-}) is converted to thiomolybdates ($MoO_xS_{4-x}^{2-}$), a series of particle-reactive ions, when small amounts of dissolved sulfides are present (Helz et al., 1996). Mo scavenging by organic matter and Fe-sulfide phases increases dramatically when $[H_2S_{aq}] \geq 10$ μm, as tetrathiomolybdate formation becomes quantitave under these conditions (Crusius et al., 1996; Helz et al., 1996; Erickson and Helz, 2000; Tribovillard et al., 2004; Vorlicek et al., 2004; Algeo and Lyons, 2006; Helz et al., 2011). Mo concentrations in such sediments can be upwards of 30ppm (Kendall et al., 2011; Scott and Lyons, 2012).

1.4 U/Mo Ratio

U and Mo concentrations and authigenic enrichments have been increasingly applied together to different environments (McManus et al., 2006; Tribovillard et al., 2006; Algeo and Tribovillard, 2009; Tribovillard et al., 2012; Zhou et al., 2012). Comparing patterns of U and Mo enrichment within modern environments can be very informative regarding its redox geochemistry and degree of restriction of its environment of deposition (Algeo and Tribovillard, 2009; Tribovillard et al., 2012). One recent application is the use of the U/Mo ratio (McManus et al., 2006; Zhou et al., 2012; see Chapter 2). Within both modern and ancient environments, it was found to be very sensitive to variations of the bottom-water oxygen content within the suboxic range (McManus et al., 2006; Zhou et al., 2012; see Chapter 2). This reflects U enrichment within the Fe (II) – Fe (III) reducing zone within sediments below suboxic waters, prior to Mo enrichment within the sulfate reducing zone (Helz et al., 1996; Zheng et al., 2000; 2002a; 2002b; Scott and Lyons, 2012). As oxygen levels in the water column become lower and highly suboxic to anoxic conditions are reached, the U/Mo ratio decreases due to the increased Mo uptake relative to U within the sediments as the sulfate reducing zone moves closer to the sediment-water interface (Algeo and Tribovillard, 2009; Canfield and Thamdrup, 2009; Scott and Lyons, 2012).

1.5 Molybdenum Isotope Behavior in Carbonates

The Molybdenum isotope composition of authigenic deposits tends to increase as $[O_2]_{aq}$ decreases and $[H_2S]_{aq}$ increases within the pore fluids and water column. Marine sediment sinks have been identified as being clastic oxic Fe-Mn crusts, suboxic, anoxic, euxinic and carbonate sinks (Barling et al., 2001; Siebert et al., 2003; Arnold et al., 2004; Nägler et al., 2005; Poulson et al., 2006; Siebert et al., 2006; Neubert et al., 2008; Kendall et al., 2009; Poulson Brucker et al., 2009; Voegelin et al., 2009; Scheiderich et al., 2010; Voegelin et al., 2010; Kendall et al., 2011; Nägler et al., 2011; Arnold et al., 2012; Czaja et al., 2012; Zhou et al., 2012; Goto et al., 2014; Romaniello et al., 2016). The isotopic composition of authigenic Mo varies according to its oxidation state and ligand coordination (Anbar, 2004). Several other factors however can affect the final Mo isotopic composition of sediments (Herrmann et al., 2012). Riverine Mo input can vary in magnitude and isotopic composition, even seasonally (Hannah et al., 2007; Archer and Vance, 2008; Dahl et al., 2010; Neubert et al., 2011). This can affect to some degree the local seawater: freshwater mixing ratio and resulting δ^{98}Mo of a local watermass, particularly in limnic and brackish facies (Nägler et al., 2005; Herrmann et al., 2012). The presence of a Mn-particulate shuttle may also affect δ^{98}Mo ratios (Arnold et al., 2004; Herrmann et al., 2012). Reductive dissolution of the sinking particles will release Mo back into the water, eliminating any signature in the sediments, as is the case for the deep Black Sea (Barling et al., 2001; Arnold et al., 2004). If the majority of the particles remain undisolved during descent however and reach the sediments, the resulting δ^{98}Mo composition would be lighter, like in the Cariaco Basin (Arnold et al., 2004; Algeo and Tribovillard, 2009). Global or basinal changes of ocean δ^{98}Mo ratios over time (as little as <100 000y) would also affect sediment isotopic compositions (Arnold et al., 2004; Nägler et al., 2005; Dahl et al., 2010). Greater anoxia would lead to increased Mo drawdown and lower resultant δ^{98}Mo ratios (Dahl et al., 2010; 2011 Herrmann et al., 2012). Application of the δ^{98}Mo paleoredox proxy to carbonates is in its early stages (Voegelin et al., 2009, 2010; Czaja et al., 2012; Romaniello et al., 2016). Mo enrichment in carbonates is controlled by pore-water $[H_2S]_{aq}$ content (Voegelin et al., 2009, Romaniello et al., 2016). Modern skeletal carbonates have lower δ^{98}Mo ratios relative to modern seawater (~2.3‰; Barling et al., 2001; Siebert et al., 2003; Nakagawa et al., 2012; Nägler et al., 2014), suggesting Mo isotope fractionation results in preferential removal of lighter Mo isotopes to carbonate sediments (Voegelin et al., 2009; Romaniello et al., 2016). In non-skeletal primary carbonates such as ooid or carbonate sands, Mo is primarily incorporated during primary precipitation. The resulting Mo concentrations are low (<0.2ppm) and isotopic ratios lighter than in the ocean reservoir. (δ^{98}Mo = 1.09-2.05‰; Voegelin et al., 2009; Romaniello et al., 2013). Concentrations of Mo in such settings remain low, at <0.2ppm, with δ^{98}Mo on average 0.5-1.0‰ lower than the seawater value of 2.3±0.1‰, (Voegelin et al., 2009; Romaniello et al., 2016). Authigenic enrichment starts during very early diagenesis. In conditions with pore-water sulfides levels <20μM H_2S_{aq}, the primary carbonate signatures remain the dominant control. The resulting total Mo concentrations (<0.2ppm) and isotopic ratios (δ^{98}Mo = 1.6‰) are thus very similar (Romaniello et al., 2016). Authigenic enrichment of Mo within the sediments becomes dominant when pore water concentrations of H_2S > 20μM. Above this threshold, Mo uptake by sediments from seawater is quantitative as tetrathiomolybdate, becomes dominant at pore water H_2S_{aq} concentrations of ~23.5μM (Romaniello et al., 2013; 2016). This results in high concentrations of Mo in sediments (1-27ppm). High concentrations of H_2S result from high organic content in these sediments (Romaniello et al., 2016). The resultant $\delta^{98/95}$Mo = 1.6-2.5‰, lower by to 0.7‰ to 0.2 ‰ higher relative to seawater (Romaniello et al., 2016). Hence, the ability of carbonate δ^{98}Mo to record the contemporaneous seawater value may depend on quantitative thiomolybdate formation and scavenging (Romaniello et al., 2016), in a manner analogous to organic-rich, fine-grained siliciclastic sediments (Arnold et al., 2004; Neubert et al., 2008).

1.6 Objectives

There are several objectives in this study. The first is to evaluate the shales from the Green Point locality in Western Newfoundland to reconstruct the paleoenvironment of the Green Point succession in the ocean during the latest Cambrian and the Early Ordovician and subsequent shale diagenesis. To achieve this, several elements of the environment were investigated; interpreted and synthesized. (1) The total organic content and $\delta^{13}C_{org}$ signatures were investigated to evaluate the controls on their variations. (2) The origin of the siliciclastic detrital component and the cause of its flux in magnitude and composition within the shales was investigated, using several elemental and ratio proxies. (3) The prevailing paleoredox conditions within the basin during the Cambrian-Ordovician transition were also defined, using multiple elemental and elemental ratio proxies. (4) The impact of the detrital flux and variations in oxygen levels during deposition on bioproductivity proxies was finally ascertained, using TOC, REE and elemental proxies.

The second objective is to investigate the covariation of U and Mo and the resulting relationship between the U/Mo ratio and both U and Mo. This was first done within the shales at Green Point. This relationship was then evaluated as an indicator of redox conditions and restriction within the depositional environment, verified by comparison to the established paleoredox interpretation of the Green Point shales. This approach is then expanded in scope to include multiple previously investigated sections from different modern and ancient environments, to further evaluate the potential of this relationship as a proxy.

Following the investigation of the shales, the same relationship was evaluated within the lime mudstones in the Green Point carbonates, to study its application as a redox proxy in carbonates. As in the shales, the approach was then applied to modern carbonates from the Bahamas platform and recent carbonates from the Bahamas slope.

Our last objective is to investigate the δ^{98}Mo ratio within the carbonates of the Green Point Formation Cambrian-Ordovician Boundary section to investigate its potential as a redox proxy in slope lime mudstones. This was achieved through comparison with; (1) δ^{98}Mo data from modern carbonates, (2) shale ratios available for the same time period, (3) results from the δ^{238}U data at Green Point and (4) elemental and redox elemental ratio proxies previously evaluated from both the shales and carbonates.

References

Adelson, J.M., Helz, G.R., Miller, C.V., 2001. Reconstructing the rise of recent coastal anoxia; molybdenum in Chesapeake Bay sediments. Geochim. Cosmochim. Acta 65, 237-252.

Ainsaar, L., Truumees, J., Meidla, T., 2015. The Position of the Ordovician-Silurian Boundary in Estonia Tested by High-Resolution δ^{13}C Chemostratigraphic Correlation. Chapter 15. In: Ramkumar, M. Chemostratigraphy: Concepts, Techniques, and Applications. Elsevier Pub. 395-412.

Algeo, T.J., Maynard, J.B., 2004. Trace-element behavior and redox facies in core shales of Upper Pennsylvanian Kansas-type cyclothems. Chem. Geol. 206, 289-318.

Algeo, T.J., Lyons, T.W., 2006. Mo-total organic carbon covariation in modern anoxic marine environments: implication for analysis of paleoredox and –hydrographic conditions. Paleooceanography 21, PA1016 23 pp.

Algeo, T.J., Tribovillard, N., 2009. Environmental analysis of paleoceanographic systems based on molybdenum–uranium covariation. Chem. Geol. 268. 211–225.

Anbar, A.D., 2004. Molybdenum stable isotopes: observations, interpretations and directions. Rev.Mineral. Geochem. 55, 429-454.

Anderson, R.F., 1987. Redox behavior of uranium in an anoxic marine basin. Uranium, 3, 145-164.

Archer, C., Vance, D., 2008. The isotopic signature of the global riverine molybdenum flux and anoxia in the ancient oceans. Nat. Geo. 1, 597-600.

Arnold, G.L., Anbar, A.D., Barling, J., Lyons, T.W., 2004. Molybdenum isotope evidence for widespread anoxia in mid-Proterozoic oceans: Science, 304, 87-90, doi: 10.1126/science.1091785.

Arnold, G.L., Lyons, T.W., Gordon, G.W., Anbar, A.D., 2012. Extreme change in sulfide concentrations in the Black Sea during the Little Ice Age reconstructed using molybdenum isotopes. Geol. 40, 595-598.

Azmy, K., Stouge, S., Brand, U., Bagnoli, G., 2014. High-resolution chemostratigraphy of the Cambrian–Ordovician GSSP in western Newfoundland, Canada: enhanced global correlation tool. Palaeogeogr. Palaeoclim. Palaeoecol. 409. 135-144.

Azmy, K., Kendall, B., Brand, U., Stouge, U., Gordon, G.W., 2015. Redox conditions across the Cambrian-Ordovician Boundary: Elemental and isotopic signatures retained in the GSSP carbonates. Paleogeogr. Paleoclim. Paleoecol. 440. 440-454.

Barling, J., Arnold, G. L. and Anbar, A. D., 2001. Natural mass-dependent variations in the isotopic composition of molybdenum. Earth and Planet. Sci. Lett., 193, 447-457.

Barnes, C.E., Cochran, J.K., 1990. Uranium removal in oceanic sediments and the oceanic U balance. Earth and Planet. Sci. Lett. 97, 94-101.

Basu A., Sanford R. A., Johnson T. M., Lundstron C. C. and Loffler F. E., 2014. Uranium isotopic fractionation factors during U(VI) reduction by bacterial isolates. Geochim. Cosmochim. Acta. 136. 100–113.

Beazly, M.J., Martinez, R.J., Webb, S.M., Sobecky, P.A., Taillefert, M., 2001. The effect of pH and natural microbial phosphatase activity on the speciation of uranium in subsurface soils. Geochim. Cosmochim. Acta. 75 (19), 5648-5663.

Berner, R.A., Kothavala, Z., 2001. GEOCARB III: a revised model of atmospheric CO_2 over Phanerozoic time. Am. J. Sci. 301, 182-204.

Brennecka, G.A., Herrmann, A.D., Algeo, T.J., Anbar, A.D., 2011. Rapid expansion of oceanic anoxia immediately before the end-Permian mass extinction. Proc. Natl. Acad. Sci. USA. Early Edition, 1-4. Doi/10.1073/pnas.1106039108.

Brumsack, H.-J., 2006. The trace trace metal content of recent organic carbon-rich sediments: implications for Cretaceous black shale formation. Paleogeogr. Paleoclim. Paleoecol. 232, 344-361.

Canfield, D.E., Thamdrup, B., 2009. Towards a consistent classification scheme for geochemical environments, or why we wish the term 'suboxic' would go away. Geobiology 7, 385-392.

Cawood, P.A., van Gool, J.A.M., 1998. Geology of the Corner Brook-Glover Island region, Newfoundland: Ottawa, Geological Survey of Canada, Bulletin 427, 96.

Chaillou, G., Anschutz, P., Lavaux, G., Schäfer, J., Blanc, G., 2002. The distribution of Mo, U, and Cd, in relation to major redox redox species in muddy sediments of the Bay of Biscay. Mar. Chem. 80, 41-59.

Chen, X., Romaniello, S.J., Herrmann, A.D., Wasylenki, L.E., Anbar, A.D., 2016. Uranium isotope fractionation during coprecipitation with aragonite and calcite. Geochim. Cosmichim. Acta. 188, 189-207.

Chung, G.S., Swart, P.K., 1990. The concentration of uranium in freshwater vadose and phreatic cements in Holocene ooid cay; a method of identifying ancient water tables. J. Sed. Petrol. 60, 735-746.

Cochran, J.K., Carey, A.E., Sholkovitz, E.R., Suprenant, L.D., 1986. The geochemistry of uranium and thorium in coastal marine sediments and sediment porewaters. Geochim. Cosmochim. Acta. 50, 663-680.

Coniglio, M., 1986. Synsedimentary submarine slope failure and tectonic deformation in deep-water carbonates, Cow Head Group, western Newfoundland. Can. J. Earth Sci. 23, 476-490.

Coniglio, M., James, N.P., 1990. Origin of fine-grained carbonate and siliciclastic sediments in an early Paleozoic slope sequence, Cow Head Group, western Newfoundland. Sedimentology 37. 215-230.

Cooper, R.A., Nowlan, G.S., Williams, S.H., 2001a. Global Stratotype Section and Point for base of the Ordovician System. Episodes 24, 19–28.

Crusius, J., Calvert, S., Pedersen, T., Sage, D., 1996. Rhenium and molybdenum enrichments in sediments as indicators of oxic, suboxic and sulfidic conditions of deposition. Earth. Planet. Sci. Lett. 145, 65-78.

Crusius, J., Thomson, J., 2000. Comparitive behavior of authigenic Re, U and Mo during reoxidation and subsequent long-term burial in marine sediments. Geochim. Cosmochim. Acta. 64, 2233-2242.

Czaja, A.D., Johnson, C.M., Roden, E.E., Beard, B.L., Voegelin, A.R., Nägler, T.F., Beukes, N.J., Wille, M., 2012. Evidence for free oxygen in the Neoarchean ocean based on coupled iron-molybdenu, isotope fractionation. Geochem. Cosmochim. Acta. 86, 118-137.

Dahl, T.W., Hammarlund, E.U., Anbar, A.D., Bond, D.P.G., Gill, B.C., Gordon, G.W., Knoll, A.H., Nielsen, A.T., Schovsbo, N.H., Canfield, D.E., 2010b. Devonian rise in atmospheric oxygen correlated to the radiations of terrestrial plants and large predatory fish. Proc. Natl. Acad. Sci. USA. 107, 17911-17915.

Dahl, T.W., Canfield, D.E., Rosing, M.T., Frei, R.E., Gordon, G.W., Knoll, A.H., Anbar, A.D., 2011. Molybdenum evidence for expansive sulfidic water masses in 750 Ma oceans. Earth. Planet. Sci. Lett. 311, 264-274.

Dill, H., 1986. Metallogenesis of early Paleozoic graptolite shales from the Graefenthal Horst (northern Bavaria-Federal Republic of Germany. Econ. Geol. 81. 889-903.

Emerson, S.R., Huested, S.S., 1991. Ocean anoxia and theconcentrations of molybdenum and vanadium in seawater. Mar. Chem. 34. 177-196.

Epstein, A.G., Epstein, J.B., Harris, L.D. (1977) Conodont Color Alteration – an Index to Organic Metamorphism. U.S. Department of the Interior. Geological Survey Professional Paper 995.

Erickson, B.E., Helz, G.R., 2000. Molybdenum (VI) speciation in sulfidic waters: stability and lability of thiomolybdates. Geochim. Cosmochim. Acta. 64, 1149-1158.

Gao, P., Lia, G., Jia, C., Young, A., Wang, Z., Wang, T., 2016. Redox variations and organic matter accumulation on the Yangtze carbonate platform during late Ediacaran-early Cambrian: Constraints from petrology and geochemistry. Paleogeogr. Paleoclim. Paleoecol. 450. 91-110.

Goto, K.T., Anbar, A.D., Gordon, G.W., Romaniello, S.J., Shimoda, G., Takaya, Y., Tokumaru, A., Nozaki, T., Suzuki, K., Machida, S., Hanyu, T., Usui, A., 2014. Uranium isotope systematics of ferromanganese crusts in the Pacific Ocean: Implications for the marine $^{238}U/^{235}U$ isotope system. Geochim. Cosmochim. Acta. 146, 43-58.

Hannah, J.L., Stein, H.J., Wieser, M.E., de Laeter, J.R., Varner, M.D., 2007. Molybdenum isotope variations in molybdenite: vapor transport and Rayleigh fractionation of Mo. Geology 35, 703-705.

Hatch, J.R., Leventhal, J.S., 1992. Relationship between inferred redox potential of the depositional environment and geochemistry of the Upper Pennsylvanian (Mis- sourian) Stark Shale Member of the Dennis Limestone, Wabaunsee County, Kansas, USA. Chem. Geol. 99. 65–82.

Helz, G.R., Miller, C.V., Charnock, J.M., Mosselmans, J.L.W., Pattrick, R.A.D., Gamer, C.D., Vaughan, D.J., 1996. Mechanisms of molybdenum removal from the sea and its concentration in black shales: EXAFS evidences. Geochim. Cosmochim. Acta. 60, 3631-3642.

Helz, G.R., Bura-Nakić, E., Mikac, N., Ciglenečki, I., 2011. New model for molybdenum behavior in euxinic waters. Chem. Geol. 284, 323-332.

Herrmann, A.D., Kendall, B., Algeo, T.J., Gordon, G.W., Wasylenki, L.E., Anbar, A.D., 2012. Anomalous molybdenum isotope trends in Upper Pensylvanian euxinic facies: Significance for use of δ^{98}Mo as a global marine redox proxy. Chem. Geol. 324-325, 87-98.

Hortia, J., Zimmermann, H., Holland, H.D., 2002. Chemical evolution of seawater during the Phanerozoic: implications from the record of marine evaporates. Geochim. Cosmochim. Acta. 66, 3733-3756.**Hua**, B., Xu, H.F., Terry, J., Deng, B.L., 2006. Kinetics of uranium (VI) reduction by hydrogen sulfide in anoxic aqueous systems: Environ. Sci. Tech. 40, 4666-4671.

James, N. P., Stevens, R. K., 1986. Stratigraphy and Correlation of the Cambrian-Ordovician Cow Head Group, Western Newfoundland. Geological Survey of Canada Bulletin 366.

Jiang, S.-Y., Chen, Y.-Q., Ling, H.-F., Yang, J.-H., Feng, H.-Z., Ni, P., 2006. Trace- and rare-earth element geochemistry and Pb-Pb dating of black shales and intercalated Ni-Mo-PGE-Au sulfide ores in lower Cambrian strata, Yangtze Platform, South China. Miner Deposita, 41. 453-467.

Jiménez-Espejo, F.J., et al., Martínez-Ruiz, F., Finlayson, C., Payton, A., Sakamoto, T., Ortega-Huertes, M., Finlayson, G., Ijima, K., Gallego-Torres, D., Fa, F., 2007. Climate forcing and Neanderthal extinction in Southern Iberia: insights from a multiproxy marine record. Quat. Sci. Rev. doi:10.1016/j.quascirev.2006.12.013

Johnson, K.S., Berelson, W.M., Coale, K.H., Coley, T.L., Elrod, V.A., Fairey, W.R., Iams, H.D., Kilgore, T.E., Nowicki, J.L., 1992. Manganese flux from continental margin sediments in a transect through the oxygen minimum zone. Science. 257, 1242-1245.

Jones, B.J., Manning, A.C., 1994. Comparison of geochemical indices used for the interpretation of palaeoredox conditions in ancient mudstones. Chem. Geol. 111. 111–129.

Kelly, S.D., Newville, M.G., Cheng, L., Kemner, K.M., Sutton, S.R., Fenter, P., Sturchio, N.C., Spotl, C., 2003. Uranyl incorporation into natural calcite. Env. Sci. Tech. 37, 1284-1287.

Kelly, S.D., Rasbury, E.T., Chattopadhyay, S., Kropf, A.J., Kemner, K.M., 2006. Evidence of a stable uranyl site in ancient organic-rich calcite. Env. Sci. Tech. 40, 2262-2268.

Kendall, B., Creaser, R.A., Gordon, G.W., Anbar, A.D., 2009. Re-Os and Mo isotope systematics of black shales from the Middle Proterozoic Velkerri and Wollogorang Formations, McArthur Basin, northern Australia. Geochim. Cosmochim. Acta. 73, 2534-2558.

Kendall, B., Gordon, G.W., Poulton, S.W., Anbar, A.D., 2011. Molybdenum isotope constraints on the extent of late Paleoproterozoic ocean euxinia. Earth. Planet. Sci. Let. 307, 450-460.

Kendall, B., Komiya, T., Lyons, T.W., Bates, S.M., Gordon, G.W., Romaniello, S.J., Jiang, G., Creaser, R.A., Xiao, S., McFadden, K., Sawaki, Y., Tahata, M., Shu, D., Han, J., Li, Y., Chu, X., Anbar, A.D., 2015. Uranium and molybdenum isotope evidence for an episode of widespread ocean oxygenation during the late Ediacaran Period. Geochim. Cosmochim. Acta. 156, 173-193.

Klinkhammer, G.P., Palmer, M.R., 1991. Uranium in the oceans: where it goes and why. Geochim. Cosmochim. Acta. 55, 1799-1806.

Krestou, A., Panias, D., 2004. Uranium (VI) speciation diagrams in the UO22+/CO32-/H2O system at 25OC. Eur. J. Miner. Process. Environ. Prot. 4 (2), 113-129.

Lam, P., Jensen, M.m., Lavik, G., McGinnis, D.F., Muller, B., Schubert, C.J., Amann, R., Thamdrup, B., Kuypers, M.M.M., 2007. Linking crenarchaeal and bacterial nitrification to anammox in the Black Sea. Proc. Nat. Acad. of Sci. USA. 104, 7104-7109.

Landing, E., 2012. Time-specific black mudstones and global hyperwarming on the Cambrian–Ordovician slope and shelf of the Laurentia palaeocontinent. Palaeogeogr. Palaeoclim. Palaeoecol. 367–368. 256–272.

Landing, E., 2013. The Great American Carbonate Bank in northeast Laurentia: its births, deaths, and linkage to continental slope oxygenation (early Cambrian–late Ordovician). In: Derby, J.R., Fritz, R.D., Longacre, S.A., Morgan, W.A., Sternbach, C.A. (Eds.), The Great American Carbonate Bank, Essays in Honor of James Lee Wilson. AAPG Bulletin, Memoir 98. 451–492.

Langmuir, D., 1978. Uranium solution-mineral equilibria at low temperatures with applications to sedimentary ore deposits. Geochim. Cosmochim. Acta 42, 547-569.

Lau, K.V., maher, K., Altiner, D., Kelly, B.M., Kump, L.R., Lehrmann, D.J., Silva-Tamayo, J.C., Weaver, K.L., Yu, M.., Payne, J.L., 2016. Marine anoxia and delayed Earth system recovery after the end-Permian extinction. Proc. Nat. Acad. of Sci. USA. 113 (9), 2360-2365.

Lécuyer, C., Grandjean, P., Barrat, J.-A., Nolvak, J., Emig, C., Paris, F., Robardet, M., 1998. δ^{18}O and REE contents of phosphatic brachiopods: a comparison between modern and lower Paleozoic populations. Geochim. Cosmochim. Acta. 62, 2429-2436.

Lovley, D.R., Phillips, E.J.P., Gorby, Y.A., Landa, E.R., 1991. Microbial reduction of uranium. Nature 350, 413-416.

Lovley, D.R., Roden, E.E., Phillips, E.J.P., Woodward, J.C., 1993. Enzymatic iron and uranium reduction by sulfate-reducing bacteria: Mar. Geol. 113, 41-53.

Lowenstein, T.K., Hardie, L.A., Timofeef, M.N., Demicco, R.V., 2003. Secular variation in seawater chemistry and the origin of calcium chloride basinal brines. Geology. 31, 857-860.

Lyons, T.W., Severmann, S., 2006. A critical look at iron paleoredox proxies: New insights from modern euxinic marine basins. Geochim. Cosmochim. Acta. 70. 5698-5722.

Ma, X.P., Wang, C.Y., Racki, G., Racka, M., 2008. Facies and geochemistry across the Early-Middle Frasnian transition (Late Devonian) on South China carbonate shelf: Comparison with the Polish reference succession. Palaeogeogr. Palaeoclim. Palaeoecol. 269. 130-151.

McKee, B.A., DeMaster, D.J., Nittrouer, C.A., 1987. Uranium geochemistry on the Amazon shelf. Evidence for uranium release from bottom sediments. Geochim. Cosmochim. Acta. 51, 2779-2786.

McManus, J., Berelson, W.M., Klinkhammer, G.P., Hammond, D.E., Holm, C., 2005. Authigenic uranium: relationship to oxygen penetration depth and organic carbon rain. Geochim. Cosmochim. Acta. 69, 95-108.

McManus, J., Berelson, W.B., Severmann, S., Poulson, R.L., Hammond, D.E., Klinkhammer, G.P., Holm, C., 2006. Molybdenum and uranium geochemistry in continental margin sediments: paleoproxy potential. Geochim. Cosmochim. Acta. 70, 4643-4662.

Morford, J.L., Emerson, S., 1999. The geochemistry of redox sensitive trace metals in sediments. Geochim. Cosmochim. Acta. 63, 1735-1750.

Morford, J.L., Emerson, S.R., Breckel, E.J., Kim, S.H., 2005. Diagenesis of oxyanions (V, Y, Re, and Mo) in pore waters and sediments from a continental margin. Geochim. Cosmochim. Acta. 69, 5021-5032.

Morford, J.L., Martin, W.R., Francois, R., Carney, C.M., 2009a. A model for uranium, rhenium, and molybdenum diagenesis in marine sediments based on results from coastal locations. Geochim. Cosmochim. Acta. 73, 2938-2960.

Morford, J.L., Martin, W.R., Carney, C.M., 2009b. Uranium diagenesis in sediments underlying bottom waters with high oxygen content. Geochim. Cosmochim. Acta. 73, 2920-2937.

Nägler, T.F., Siebert, C., Lüschen, H., Böttcher, M.E., 2005. Sedimentary Mo isotope record across the Holocene fresh-brackish water transition of the Black Sea. Chem. Geol. 219, 283-295.

Nägler, T.F., Neubert, N., Böttcher, M.E., Dellwig, O., Schnetger, B., 2011. Molybdenum isotope fractionation in pelagic euxinia: Evidence from the modern Black and Baltic Seas. Chem. Geol. 289, 1-11.

Nägler, T. F., Anbar, A. D., Archer, C., Golderg, T., Gordon, G. W., Greber, N. D., Siebert, C., Sohrin, Y. and Vance, D., 2014. Proposal for an Internatinal Molybdenum Isotope Measurement Standard and Data Representation. Geostand. Geoanal. Res. 38(2), 149-151. doi: 10.1111/j.1751-908X.2013.00275.x.

Nakagawa, Y., Takano, S., Lufti Firdaus, M., Norisuye, K., Hirata, T., Vance, D., Sohrin, Y., 2012. The molybdenum isotopic composition of the modern ocean. Geochem. Journ. 46, 131-141.

Neubert, N., Nägler, T.F., Böttcher, M.E., 2008. Sulfidity controls mylybdenum isotope fractionation into euxinic sediments: Evidence from modern Black Sea. Geology. 36, 775-778.

Neubert, N., Heri, A.R., Voegelin, A.R., Nägler, T.F., Schlunegger, F., Villa, I.M., 2011. The molybdenum isotopic composition in river water: constraints from small catchments. Earth. Planet. Sci. Lett. 304, 180-190.

Nowlan, G.S., Barnes, C.R., 1987. Thermal maturation of Paleozoic strata in Eastern Canada from conodont colour alteration index (CAI) data with implications for burial history, tectonic evolution, hotspot tracts and mineral and hydrocarbon exploration. Geological Survey of Canada Bulletin. 367, 47.

Olanipekun, O.K., Azmy, K., Brand, U. 2014. Dolomites of the Boar Harbour Formation in the Northerm Peninsula, western Newfoundland, Canada: implications for dolomitization history and porosity control. AAPG Bull. 98, 765-

791.

Perkins, R.B., Piper, D.Z., Mason, C.E., 2008. Trace-element budgets in the Ohio/Sunbury shales of Kentucky: Constraints on ocean circulation and primary productivity in the Devonian-Mississippian Appalachian Basin. Palaeogeogr. Palaeoclim. Palaeoecol. 265. 14-29.

Piper, D.Z. & Perkins, R.B., 2004. A modem vs. Permian black shale - the hydrography, primary productivity, and water-column chemistry of deposition. Chem. Geol. 206. 177-197.

Piper, D.Z., Calvert, S.E., 2009. A marine biogeochemical perspective on black shale deposition. Earth-Sci. Rev. 95. 63-96.**Poulson**, R.L., Siebert, C., McManus, J., Berelson, W.M., 2006. Authigenic molybdenum isotope signatures in marine sediments. Geology. 34, 617-620.

Poulson Brucker, R.L., McManus, J., Severmann, S., Berelson, W.M., 2009. Molybdenum behavior during early diagenesis: insights from Mo isotopes. Geochem. Geophys. Geosys. 10 (6). Doi: 10.1029/2008GC002180.

Poulton, S.W., Fralick, P.W., Canfield, D.E., 2010. Spatial variability in oceanic redox structure 1.8 billion years ago. Nat. Geo. 3. 486-490.

Ratcliffe, K., Wilson, A., 2014. Stratigraphy in the Oil Industry. PESA News Resources. Feb/March 2014. 60-63.

Reeder, R.J., Nugent, M., Lamble, G.M., Tait, C.D., Morris, D.E., 2000. Uranyl incorporation into calcite and aragonite; XAFS and luminescence studies. Env. Sci. Tech. 34, 638-644.

Reeder, R.J., Nugent, M., Tait, C.D., Morris, D.E., Heald, S.M., Beck, K.M., Hess, W.P., Lanzirotti, A., 2001. Coprecipitation of uranium(VI) with calcite; XAFS, micro-XAS, and luminescence characterization. Geochim. Cosmochim. Acta. 65, 3491-3503.

Ridgewell, A., 2005. A mid Mesozoic revolution in the regulation of ocean chemistry. Mar. Geol. 217, 339-357.

Ries, J.B., 2004. Effect of ambient Mg/Ca ratio on Mg fractionation in calcareous marine invertebrates: a record of the oceanic MG/Ca ratio over the Phanerozoic. Geology 32, 981-984.

Ries, J.B., 2010. Review: geological and experimental evidence for secular variation in seawater Mg/Ca (calcite-aragonite seas) and its effects on marine biological calcification. Biogeosciences. 7, 2795-2849.

Riquier, L., Tribovillard, N., Averbuch, O., Devleeschouwer, X., Riboulleau, A., 2006. The late Frasnian Kellwasser horizons of the Harz Mountains (Germany): Two oxygen-deficient periods resulting from different mechanisms. Chem. Geol. 233. 137-155.

Romaniello, S.J., Herrmann, A.D., Anbar, A.D., 2013. Uranium concentrations and $^{238}U/^{235}U$ isotope ratios in modern carbonates from the Bahamas: Assessing a novel paleoredox proxy. Chem. Geol. 362, 305-316.

Romaniello, S.J., Herrmann, A.D., Anbar, A.D., 2016. Syndepositional diagenetic control of molybdenum, isotope variations in carbonate sediments from the Bahamas. Chem. Geol. 438, 84-90.

Royer, D.L., Berner, R.A., Montanez, I.P., Beerling, D.J., 2004. CO_2 as primary driver of Phanerozoic climate. GSA Today. 14, 4-10. **Saltzman**, M.R., Thomas, E., 2012. Carbon isotope stratigraphy. In: Gradstein, F.M., Ogg, J.G., Schmitz, M., Ogg, G. (Eds.), The Geologic Time Scale. Elsevier. The Netherlands. 207-232.

Sani, R.K., Peyton, B.M., Amonette, J.E., Geesey, G.G., 2004. Reduction of uranium(VI) under sulfate-reducing conditions in the presence of Fe(III)-(hydr)oxides. Geochim. Cosmochim. Acta. 68, 2639-2649.

Scheiderich, K., Helz, G.R., Walker, R.J., 2010. Century-long record of Mo isotopic composition in sediments of a seasonally anoxic estuary (Chesapeake Bay). Earth. Planet. Sci. Lett. 289, 189-197.

Schnetger, B., Brumsack, H-J., Schale, H., Hinrichs, J., Dittert, L., 2000. Geochemical characteristics of deep-sea sediments from the Arabian Sea: a high-resolution study. Deep-Sea Res. II 47. 2735-2768.

Scott, C., Lyons, T.W., 2012. Contrasting molybdenum cycling and isotopic properties in euxinic versus non-euxinic sediments and sedimentary rocks: Refining the paleoproxies. Chem. Geol. 324-325, 19-27.

Siebert, C., Nagler, T.F., von Blanckenburg, F., and Kramers, J.D., 2003. Molybdenum isotope records as a potential new proxy for paleoceanography: Earth. Planet. Sci. Lett.211, 159–171, doi: 10.1016/ 0012-821X(03)00189-4.

Siebert, C., McManus, J., Bice, A., Poulson, R., Berelson, W.M., 2006. Molybdenum isotope signatures in contental margin marine sediments. Earth. Planet. Sci. Lett. 241, 723-733.

Śliwiński, M.G., Whalen, M.T., Day, J., 2010. Trace element variations in the Middle Frasnian punctata zone (late Devonian) in the western Canada sedimentary Basin–changes in oceanic bioproductivity and paleoredox spurred by a pulse of terrestrial afforestation? Geologica Belgica 4. 459–482.

Sturchio, N.C., Antonio, M.R., Soderholm, L., Sutton, S.R., Brannon, J.C., 1998. Tetravalent Uranium in Calcite. Science 281, 971-973.

Terfelt, F., Bagnoli, G., Stouge, S., 2012. Re-evaluation of the conodont *Iapetognathus* and implications for the base of the Ordovician System GSSP. Lethaia 45. 227–237.

Terfelt, F., Eriksson, M.E., Schmitz, B., 2014. The Cambrian–Ordovician transition in dysoxic facies in Baltica—diverse faunas and carbon isotope anomalies. Paleogeogr. Paleoclim. Paleoecol. 394. 59-73.

Tribovillard, N., Riboulleau, A., Lyons, T., Baudin, F., 2004. Enhanced trapping of molybdenum by sulfurized organic matter of marine orgin as recorded by various Mesozoic formations. Chem. Geol. 213, 385-401.

Tribovillard, N., Algeo, T.J., Lyons, T., Riboulleau, A., 2006. Trace metals as paleoredox and paleoproductivity proxies: an update. Chem. Geol. 232. 12-32.

Tribovillard, N., Lyons, T.W., Riboulleau, A., Bout-Rounazeilles, V., 2008b. A possible capture of molybdenum during early diagenesis of dysoxic sediments. Bulletin de la Société Géologique de France. 179, 3-12.

Tribovillard, N., Algeo, T.J., Baudin, F., Riboulleau, A., 2012. Analysis of marine environmental conditions based on molybdenum-uranium covariation – Applications to Mesozoic paleoceanography. Chem. Geol. 324-325, 46-58.

Tripathy, G.R., Hannah, J.L., Stein, H.J., Yang, G., 2014. Re-Os age and depositional environment for black shales from the Cambrian-Ordovician boundary, Green Point, western Newfoundland. Geochem. Geophys. Geosys. 15 (4). 1021-1037.

Tyson, R. V., Pearson T. H., 1991. Modern and ancient continental shelf anoxia: an overview. In Modern and Ancient Continental Shelf Anoxia. Geololgical Society Special Publications 58. 1–26.

Voegelin, A.R., Nägler, T.F., Samankassou, E., Villa, I.M., 2009. Molybdenum isotopic composition of modern and Carboniferous carbonates. Chem. Geol. 265, 488-498.

Voegelin, A.R., Nägler, T.F., Beukes, N.J., Lacassie, J.P., 2010. Molybdenum isotopes in late Archean carbonate rocks: Implications for early Earth oxygenation. Precambrian Research 182, 70-82.

Vorlicek, T.P., Kahn, M.D., Kasuya, Y., Helz, G.R., 2004. Capture of molybdenum in pyrite-forming ligand-induced reduction by polysulfides. Geochim. Cosmochim. Acta. 68, 547-556.

Waldron, J.W., Anderson, S., Cawood, P.A., Goodwin, L.B., Hall, J., Jamieson, R.A., Palmer, S.E., Stockmal, G.S., Williams, P.F., 1998. Evolution of the Appalachian Laurentian margin: Lithoprobe results in western Newfoundland. Can. J. Earth Sci. 35, 1271-1287.

Weaver, F.J., Macko, S. A., 1988. Source rocks of Western Newfoundland. Advances in Organic Geochemistry. Org. Chem. 13. 411-421.

Wen, H., Fan, H., Zhang, Y., Cloquet, C., Carignan, J., 2015. Reconstruction of early Cambrian ocean chemistry from Mo isotopes. Geochim. Cosmochim. Acta. 164, 1-16.

Wignall, P.B., Myers, K.J., 1988. Interpreting the benthic oxygen levels in mudrocks: a new approach. Geology 16. 452–455.

Wignall, P.B., Zonneveld, J.-P., Newton, R.J., Amor, K., Sephton, M.A., Hartley, S., 2007. The end Triassic mass extinction record of Williston Lake, British Columbia. Paleogeogr. Paleoclim. Paleoecol. 253, 385-406.

Williams, H., 1995. Temporal and spatial subdivisions of the rocks of the Canadian Appalachian region, *in* Williams, H., ed., Geology of the Appalachian-Caledonian orogeny in Canada and Greenland: Ottawa, Geological Survey of Canada , Geology of Canada, p. 21-44.

Williams, S.H., Burden, E.T., Mukhopadhyay, P.K., 1998. Thermal maturity and burial history of Paleozoic rocks in western Newfoundland. Can. J. Earth. Sci. 35 (11), 1307-1322.

Xu, L., Lehmann, B., Mao, J., Nägler, T.F., Neubert, N., Böttcher, M.E., Escher, P., 2012. Mo isotope and trace element patterns of Lower Cambrian black shales in South China: Multi-proxy constraints on the paleoenvironment. Chem. Geol. 318-319, 45-59.

Zheng, Y., Anderson, R.F., van Geen, A., Kuwabara, J., 2000. Authigenic molybdenium formation in marine sediments: a link to pore water sulfide in the Santa Barbara Basin. Geochim. Cosmochim. Acta. 64, 4165-4178.

Zheng, Y., Anderson, R.F., van Geen, A., Fleischer, M.Q., 2002a. Preservation of non-lithogenic particulate uranium in marine sediments. Geochim. Cosmochim. Acta. 66, 3085-3092.

Zheng, Y., Anderson, R.F., van Geen, A., Fleischer, M.Q., 2002b. Remobilization of authigenic uranium in marine sediments by bioturbation. Geochim. Cosmochim. Acta. 66, 1759-1772.

Zhou, L., Wignall, P.B., Su, J., Feng, Q., Xie, S., Zhao, L., Huang, J., 2012. U/Mo ratios and $\delta^{95}/^{95}$Mo as local and global redox proxies during mass extinction events. Chem. Geol. 324–325. 99-107.

Chapter 2

Trace element variations in the shales across the Cambrian–Ordovician boundary: implications for environmental changes associated with sealevel variations

To be published in "Sedimentology"

Alexandre Charest Bisnaire [a*], Karem Azmy [a], Brian Kendall [b], Svend Stouge [c]

[a] Department of Earth Sciences, Memorial University of Newfoundland, St. John's, NL A1B3X5, Canada
[b] Department of Earth and Environmental Sciences, University of Waterloo, Waterloo, ON N2L3G1, Canada
[c] Natural History Museum of Denmark, Geological Museum, Earth and Planetary Systems Science Section, University of Copenhagen, Øster Voldgade 5, DK-1350 Copenhagen K, Denmark

Abstract

Trace element geochemistry and organic carbon data can be used together to accurately track changes in depositional environments over time. In the current study, this approach is used on the Upper Cambrian – Lower Ordovician sedimentary rocks of the Cow Head Group exposed at Green Point, western Newfoundland (Canada) (Fig. 1.1). The investigated interval is part of the Green Point Formation and covers the significant regressive - transgressive event spanning the international Cambrian–Ordovician boundary. The geochemical patterns observed were found to correlate well with the lithology and sequence stratigraphy, clearly defining boundaries between major systems tracts and changes in the

depositional conditions within each systems tract. A prominent geochemical anomaly marks the start of the transgression and reflects a significant change in the depositional conditions of the palaeocontinental slope. As the platform became flooded and carbonate-dominated, the detrital siliciclastic supply from the Laurentian craton to the slope decreased, resulting in lower detrital proxy (Sc, Al, Th, Cr, K/[Fe+Mg]) and higher carbonate proxy (Ca) contents within the shales. The oxygen levels were highest (oxic-slightly suboxic) during the lowstand system tract below the anomaly and the decreased (to strongly suboxic-intermittently anoxic) across the geochemical anomaly as sea level rose, reflected in the greater proportion grey-black shales and samples authigenically enriched in U and Mo. The lower oxygen levels were favorable for the preservation of organic matter. Bioproductivity during this period is thought to have been low, based on P, Ni and Cu signatures.

2.1 Introduction

Trace element enrichments (or lack thereof) and elemental ratios in shales are known to be reliable proxies for the purpose of identifying variations in paleoredox conditions, source material composition/flux, and bioproductivity (Dill, 1986; Wignall and Myers, 1988; Hatch and Leventhal, 1992; Jones and Manning, 1994; Lécuyer et al., 1998; Schnetger et al., 2000; Piper and Perkins, 2004; Jiang et al., 2006; Lyons and Severmann, 2006; Riquier et al., 2006; Tribovillard et al., 2006; Jiménez-Espejo et al., 2007; Ma et al., 2008; Perkins et al., 2008; Algeo and

Tribovillard, 2009; Piper and Calvert, 2009; Poulton et al., 2010; Śliwiński et al., 2010; Zhou et al., 2012; Tripathy et al., 2014; Basu et al., 2014; Gao et al., 2016).

In this study, we apply a wide range of proxies to the sedimentary rocks (shales) from the Green Point locality in Western Newfoundland (Fig. 1.1). The succession at Green Point spans the Cambrian–Ordovician (Cb-O) boundary and was elected as the Global Stratotype Section and Point, abbreviated GSSP, which defines the lower boundary of the Ordovician system (Cooper et al., 2001a; Fig. 1.2). This addresses an important gap in the understanding of the GSSP, namely the depositional environment in the deep waters off of the Laurentian continental shelf during this period and the impact of the global sealevel rise that occurred at the Cb-O transition on deep-water environments.

The studied Green Point interval was deposited in a distal slope setting off the Laurentian continental margin (James and Stevens, 1986). The interval is typical of mixed siliciclastic-carbonate slope deposits, composed of deep-water organic-bearing-to-rich green, grey and black shales, siltstones, parted and ribbon limestone, debris-flow derived breccias and (mega-) conglomerates. It is part of the Green Point Formation of the Cow Head Group. The sediments were deposited during a period of eustatic sea level fluctuation, which affected ocean circulation (James and Stevens, 1986; Landing, 2012; Terfelt et al., 2012; Landing, 2013; Terfelt et al., 2014; Azmy et al., 2015). Below the established global Cambrian–Ordovician boundary (Golden Spike) at Green Point, a geochemical anomaly was documented by Azmy et al. (2014;

2015), based on geochemical evidences from the alternating carbonate interbeds in the section.

The main objectives of the current chapter are to (1) investigate variations in total organic content, $\delta^{13}C_{org}$ and their main controls, (2) investigate variations of the siliciclastic detrital flux to the shales based on elemental and ratio proxies, (3) investigate variations in the paleoredox conditions based on elemental and elemental ratio proxies in shales, (4) investigate bioproductivity along the Laurentian margin and the impact of detrital flux and paleoredox variations on bioproductivity proxies in the ocean during the latest Cambrian and the Early Ordovician, and (5) evaluate how the depositional environment changed in relation to sea-level fluctuations.

2.2 Geological Setting and Stratigraphy

2.2.1 Geological Setting

Western Newfoundland is the north-easternmost extension of the Appalachian foldbelt that extends from Alabama, USA in the south to the west coast of Newfoundland, southeastern Canada (Stevens, 1970; Williams, 1995; Hibbard et al. 2007). It belongs to the tectonostratigraphic Humber Zone of the Appalachian-Caledonian orogen comprising a record of continental platform and margin deposits of Laurentia (Williams, 1975; 1979). The zone consists of crystalline basement of the Greenville province that is unconformably overlain by a succession of rift-related, passive-continental-margin, and foreland-basin units. The zone is divisible into a western external domain and eastern internal domain on the basis of increasing deformation and metamorphism to the east (Williams 1995; Cawood et al. 2001; Waldron et al. 1998).

The allochthon Cow Head Group is well exposed on the western coast of Newfoundland (Fig. 1.1) and is part of the external Humber Zone. It is characterized by tectonically imbricated, west-verging, locally overturned, thrust slice stacks (James and Stevens 1986; Waldron, 1985; Waldron et al., 1988).

The development of the Laurentian plate started by rifting of Rodinia, which resulted in an irregular-shaped continental margin (promontories and reentrants of Thomas, 1977). The rifting period was followed by divergence/drifting forming the opening of the Iapetus Ocean. The rift-related deposits consist of Neoproterozoic to lower Cambrian conglomerate, quartzite arkosic sandstone, siltstone and shale along with a suite of mafic and felsic igneous rocks. The rifting margin transitioned into a passive margin by ca. 550Ma, facing the Iapetus Ocean. The drift-related units are carbonate dominated and range in age from late Early Cambrian to Early Ordovician (Fig. 1.1a; Knight et al. 1995; Cawood et al., 2001; Cooper et al., 2001b). In the late mid Cambrian, the great American carbonate bank was established along the Saint Lawrence promontory (Lavoie et al., 2003; Boyce and Knight, 2005). A sea level rise and subsequent sea level fluctuations were responsible for the establishment of a productive shelf carbonate factory (Cowan and James, 1993). The ramp developed into a platform rimmed by high energy oolitic shoals (Cowan and James, 1993; Lavoie et al., 2003; Boyce and Knight, 2005).

Sedimentation in these environments was controlled by third-order sea level fluctuations, and resulted in deposition of the Port au Port Group (James and Stevens, 1986; James et al., 1989; Cooper et al., 2001b). The carbonate platform persisted into the Late Cambrian (Lavoie et al., 2003). The coeval deep-water slope deposits of the Cow Head Group formed up to the Cambrian–Ordovician boundary and consisted of primarily shale interbedded with parted lime mudstone, ribbon limestone and grainstones. Within this succession, there are also limebreccias and multiple conglomerate beds formed by debris flows. These lithological variations were controlled by sea level fluctuations (James and Stevens, 1986; James et al., 1989). The early Ordovician marks the gradual sea level rise that led to the new flooding of the Laurentian Craton and a large low energy carbonate mud platform - referred to the St. George Group in Western Newfoundland - developed. The associated slope deposits of the Cow Head Group are composed of shale, siltstone, parted and ribbon limestone, interrupted by debris flow-derived breccias and conglomerates (James and Stevens, 1986; James et al., 1989; Cooper et al., 2001b; Knight et al., 2007). These slope failures did result in synsedimentary deformation (Coniglio, 1986). The Laurentian passive margin terminated along with the onset of seafloor subduction and the landward migration of a peripheral bulge (Jacobi, 1981) and caused by tectonic loading of the crust due to the westward transport of the Humber Arm allochthon in the Middle Ordovician (Taconic Orogeny) (Stevens, 1970; Williams and Stevens, 1974; Knight et al., 1991; Cooper et al., 2001b).

The exposed rocks of the former Laurentian margin were deformed during the Taconic Orogeny and again later by the Acadian orogeny (Waldron and Stockmal, 1994). Metamorphism and deformation within the Humber Zone are known to increase eastward. The Green Point locality is at the westernmost edge of the Western External Humber Zone where deformation was at its minimum (Williams, 1995; Cawood and van Gool, 1998; Waldron et al., 1998). The tectonic deformation did result in the studied section being overturned, moderately faulted and undergoing bed-parallel shortening, though the timing of these post-depositional features remains uncertain (Coniglio, 1986; James and Stevens, 1986).

2.2.2 Stratigraphy

2.2.2.1 Green Point Formation

The Green Point Formation comprises the distal fine-grained siliciclastic-carbonate hemipelagite sedimentary rocks of the Cow Head Group allochthonous sequence (Fig. 1.2; James and Stevens, 1986). They are composed primarily of varying proportions of non-calcareous to calcareous hemipelagic lighter green and grey shales and clastic terrigeneous darker green, grey and black shales (Fig. 2.1a). The calcareous component of the shales takes the form of very thin laminations within the laminated shales. Interbedded with the shales are clastic-derived carbonate mustones, siltstones and siliciclastic siltstones previously interpreted to be deposited by turbidity currents (Coniglio and James, 1990). These sediments are interrupted by a few thin lenticular to continuous large coarse-grained conglomerate carbonates, derived from debris flow events and sourced from the Laurentian margin platform and early-lithified upper slope (Fig. 2.1b; James and Stevens, 1986). Visible within the section are isolated very thin beds (<1cm) rich in small cubic pyrite. These and other beds were associated with recent iron oxide staining, which was avoided when sampling.

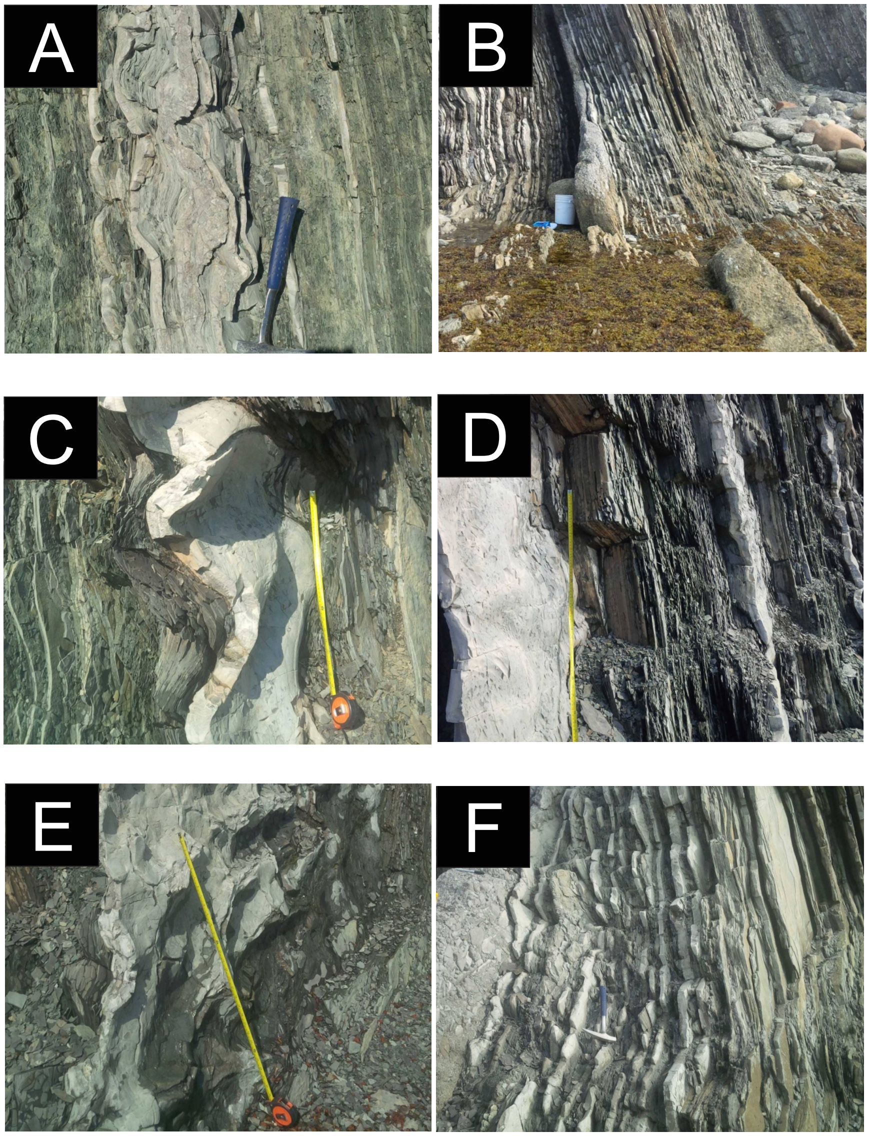

Figure 2.1: Photographs from the Green Point section. (A) Greenish-gray, light-gray and gray shales interbedded with a package of limestone rhythmites demonstrating folding and brecciation resulting from synsedimentary deformation (Bed 21, Martin Point Member). (B) Tectonically-faulted lenticular coarse-grained carbonate conglomerate (Bed 25, Broom Point Member). (C) Wrinkled limestone rhythmite and grey to dark grey shales affected by demonstrating layer-parallel tectonic deformation (Bed 18, Martin Point Member). (D) Finely to coarsely laminated grey shales with interbedded isolated limestone rhythmites (Bed 18, Martin Point Member). (E) Top view of limestone rhythmites demonstrating the tectonic wrinkled fabric (Boundary of beds 17-18; Martin Point Member). (F) Fissile shales closely interbedded with beige siltstones (Right), light grey limestone rhythmites (Center) and overlain by a lenticular carbonate conglomerate (Beds 24-25; Broom Point Member).

At the Green Point locality, the Green Point Formation has been affected by synsedimentary deformation caused by slope failures (Fig. 2.1a; b). The resulting shear zones have been interpreted to occur in the shallow subsurface, below truncation surfaces or in the margins of or slide mass bases (Coniglio, 1986). The succession at Green Point furthermore has been overturned and slightly faulted by latter tectonic activity (James and Stevens, 1986). This caused layer-parallel shortening to occur, forming wrinkled limestone fabrics (Fig. 2.1c). These fabrics have been previously associated with late-diagenetic precipitates, tectonic stylolites and the fault structures (Coniglio, 1986). Visual inspection of the outcrops at Green Point during this study indicate that the observed tectonic and slope failure features did not result in pervasive hydrothermal alteration or metamorphism of the succession within the sediments. Previous geochemical work supports this observation. Recent petrographic, cathodoluminescence and geochemical investigations of the carbonate rhythmites indicate good preservation of primary signatures, noted by the retention of depositional fabrics, micritic grain sizes, dull cathodoluminescense and poor correlation between Mn/Sr ratios and either $\delta^{13}C_{carb}$ or $\delta^{18}O_{carb}$ values (Azmy et al., 2014). The TOC contents of those carbonates were also found to have an insignificant correlation with $\delta^{13}C_{org}$ and $\delta^{15}N_{org}$, thus suggesting good preservation of at least near-primary geochemical signatures (Popp et al., 1997; Faure and Mensing, 2005; Yamaguchi et al., 2010; Azmy et al., 2015). Furthermore, in a separate study on the same section by Tripathy et al. (2014), Re-Os ages of the shales fit very well on the constrained optimization trend of radiometric ages of the Ordovician to Silurian plotted against graptolite stratigraphy (Cooper and Saddler, 2012). This indicates very limited post-depositional alteration and preservation of at least near primary geochemical signatures. Conodont alteration index data (CAI) values are ~1.5, indicating maximum temperatures of 50-90^{O}C (Epstein et al., 1977; Nowlan and Barnes, 1987). This generally agrees with organic matter T_{max} data from Green Point, which falls within the lower part of the oil window (Tripathy et al., 2014).

The Green Point Formation is subdivided into the Martin Point, Broom Point and St. Paul's members (James and Stevens, 1986). The first two members are the focus of this study and are further described below.

2.2.2.1.1 Martin Point Member

The upper Martin Point Member forms the basal section of the currently studied outcrop at Green Point (Fig. 1.2; James and Stevens, 1986). It is dominated by non-carbonaceous to carbonaceous hemipelagites composed of green, grey, dark-grey and black shales. Thin ribbon (<10cm) lime mudstones are intricately interbedded with the shales (Fig. 2.1d). Dark grey and black shales have been interpreted as terrigeneous muddy turbidites derived from gravity flows (Coniglio and James, 1990), which are commonly associated with rhythmites, siltstones and very fine sandstones. Some siltstones may have ferroan dolomite or dolo-siltstones (James and Stevens, 1986). The most common pyrite occurences are located in the top of bed 18. Within the shales and siltstones are 1-20cm thick isolated packages of continuous to nodular ribbon limestones that, at times, were brecciated or folded by syndepositional deformation (Fig. 2.1c; e). A thick conglomerate sequence occurs within the upper part of the sequence (Fig. 1.2). Near the top of the Martin Point Member, a geochemical anomaly was identified in the interbedded carbonate rhythmites based on a $\delta^{13}C_{carb}$ excursion observed, supported by $\delta^{13}C_{org}$, $\delta^{15}N_{org}$, P and REE spikes (Azmy et al., 2014; 2015).

2.2.2.1.2 Broom Point Member

The basal sequence of the Broom Point Member is exposed at Green Point (James and Stevens, 1986). The conformable contact between the Martin Point and Broom Point Members is gradational, located just below the Cambrian-Ordovician boundary level. The Broom Point Member at Green Point is mainly composed of non-carbonaceous to carbonaceous dark grey to black shales that are finely interbedded with much more common continuous to nodular ribbon limestone rhythmites (Fig. 2.1f). Some rhythmites show a crinkled or wavy macrofabric, indicating soft-sediment deformation. In certain intervals, the shales are instead interbedded with rippled to laminar siltstones that are mainly siliciclastic in composition, while a few are composed of carbonate material (ex. Bed 24; Fig. 1.2). The sequence has interbeds of 5cm- to 0.5m-thick conglomerate and a ~2m-thick siltstone unit showing crossbedding occurs near its base (Fig. 2.1b). The first pelagic graptolites within the Cow Head Group appear in Bed 25 (Fig. 1.2; Cooper et al., 2001a). The base of the GSSP for the Ordovician System is located near the base of the Broom Point Member (Fig. 1.2; Cooper et al., 2001a).

2.3 Methodology

2.3.1 Sampling

Shale sampling was conducted at high resolution (down to <10cm intervals between samples) from the upper Martin Point to the lower Broom Point Members of the Green Point Formation at Green Point, focusing on the uppermost Cambrian-Ordovician interval (49^{0} 40’ 51” N; 57^{0} 57’ 36” W, Fig. 1.1b). For shale analyses, ~ 9 g of material was crushed and powdered from each sample using an electric mill with tungsten carbide disks.

2.3.2 Total Organic Carbon and $\delta^{13}C_{org}$

Total Organic Carbon (TOC) and $\delta^{13}C_{org}$ (VPDB) analyses were completed according to the method outlined in Kikumoto et al. (2014). Firstly, 5% HCl was used to determine if the shales were calcareous. Subsequently, 300-500 mg of sample powder was demineralized in 10 mL of 20 volume % HCl for 24 h to eliminate the carbonate content. The sample solutions and acidic residue were then separated in a centrifuge, and the residue was washed by distilled water and ethanol 3 times each. The samples were dried for 3 days at 50-60^{O}C and then stored in plastic tubes. About 2.5mg of each digested sample was weighed and combusted at 1000^{O}C. Measurements were conducted at the isotope labs of the Memorial University of Newfoundland (MUN) using a Delva V Plus isotope ratio mass spectrometer equipped with a conventional elemental analyzer and an interfaced OI Analytical Aurora 1030W TOC analyzer. The reproducibility was better than ±20% for carbon content and ±0.10‰ for $\delta^{13}C_{org}$ (VPDB). Standards used for $\delta^{13}C_{org}$ (VPDB) and TOC calibration were MUN-CO-1 ($\delta^{13}C_{org}$ (VPDB) = -21.02, %C = 11.31), MUN-CO-2 ($\delta^{13}C_{org}$ (VPDB) = -40.11, %C = 11.63) and B2153 ($\delta^{13}C_{org}$ (VPDB) = -26.67, %C = 1.65).

2.3.3 Shale Elemental Compositions

Bulk sample digestions were carried out in a clean room at the Metal Isotope Geochemistry Laboratory, University of Waterloo. Approximately 100-150 mg of shale sample powder was ashed at 550^{O}C for 24 h in a muffle furnace to oxidize organic matter. Following cooling, samples were transferred to 22 mL Savillex Teflon beakers. The samples were digested with multiple combinations of concentrated trace-metal grade acids at 110^{O}C. After each step, the samples were evaporated at 110^{O}C. The first digestion was in 2.5 mL HNO_3 and 0.5 mL HF for 48 hours. The second digestion used 1 mL HNO_3 and 3mL HCl (aqua regia) for 48 hours. A third digestion was conducted using 2 mL HCl for 24 hours. Thereafter, stock solutions containing ~ 5 mL of 6M HCl and 3 drops of 0.5% HF were prepared and stored in 15 mL LDPE vials.

Following dissolution, sample splits were dried, diluted with 2% HNO_3 and analyzed for major, minor, and trace element abundances using a Thermo X-Series 2 quadrupole inductively coupled plasma mass spectrometer (ICP-MS) at the University of Waterloo (cf. Kendall et al., 2010). Instrument accuracy was verified using two shale standards, the United States Geological Survey (USGS) SBC-1 and SGR-1b (Both have a certified deviation value of ≤10%). Instrumental drift during analysis was corrected using internal element standards. The accuracy of reproducibility of elemental concentration data was typically within 5%.

All mean statistical calculations in the current investigation are based on 1▯ values. The *P* values from unpaired two-tailed t-tests were used to determine if there were statistically meaningful differences in the mean values of geochemical proxies above and below the geochemical anomaly. Table 2.1 includes the *P* values derived from comparing data from below and above the geochemical anomaly level.

2.3.4 Equations Used for Interpretation

Throughout this chapter, several geochemical ratios and equations are used. They are listed below.

2.3.4.1 Elemental Ratios

The Y/Ho ratio was used to evaluate the influence of hydrothermal fluids on siliciclastic sediments (Bau, 1996; Bau and Dulski, 1999; Douville et al., 1999).

Mg/Ca and Sr/Ca weight ratios were plotted against one-another to evaluate the composition of the carbonate component within the Green Point shales (Bayon et al., 2007; Picone et al., 2008).

Th/Sc ratios were used as a tool to evaluate sedimentary provenance (McLennan et al., 1993; Zhao and Zheng, 2015).

The K/(Fe+Mg) ratio was used in this study to evaluate the proportion of sediments within shales derived from either detrital terrigenous or volcaniclastic sources (Dean and Arthur, 1998; Werne et al., 2002).

The Cerium anomaly (Ce/Ce^*_{SN}) has previously been used to evaluate redox conditions (Bau and Dulski, 1996; Bolhar et al., 2004; Nozaki, 2001). SN refers to the values used being PAAS-normalized (Bau and Dulski, 1996). It was calculated using two different formulas for this study, using the methods of Bau and Dulski, 1996 (1) and Bolhar et al., 2004 (2), respectively.

$$Ce/Ce^*_{SN} = 2Ce/(La+Pr) \tag{1}$$

$$Ce/Ce^*_{SN} = Ce/(2Pr - Nd) \tag{2}$$

The shale normalized praseodymium anomaly (Pr/Pr^*_{SN}) anomaly was used in concert with the Ce/Ce^*_{SN} (1) to evaluate potential REE anomalies (Bau and Dulski, 1996), using the formula:

$$Pr/Pr^*_{SN} = 2Pr/[Ce+Nd] \tag{3}$$

The Fe_T/Al ratio was used as an indicator of authigenic iron enrichment for the Green Point shales (T refers to total; Lyons et al., 2003; Lyons and Severmann, 2006).

Authigenic U and Th/U were both used to evaluate authigenic uranium enrichment (U – Th/3; Wignall and Myers, 1988; Wignall and Twitchett, 1996), using the formula:

$$\text{Authigenic U} = \text{U} - \text{Th}/3 \tag{4}$$

The U/Mo_{auth} ratio has been used to evaluate the covariation pattern of authigenic U and Mo enrichment within the Gren Point shales (see section 2.3.5 for EF equation; McManus et al., 2006; Zhou et al., 2012), using the formula:

$$U/Mo_{auth} = U\ EF_{PAAS}/Mo\ EF_{PAAS} \tag{5}$$

2.3.4.2 Enrichment Factors

Trace element concentrations (U, Mo, Ni, V, Cr, Cu, P) were converted into enrichment factors to evaluate authigenic tracemetal enrichment. For general analysis, Post-Archean-Australian Shale (PAAS) Al normalized enrichment factors (EF_{PAAS}) were used, based on the formula:

$$EF_{PAAS} = (\text{trace metal/ Al})_{sample} / (\text{trace metal/Al})_{PAAS} \tag{6}$$

(Taylor and McLennan, 1985; Calvert and Pederson, 1993; Tribovillard et al., 2006; Tribovillard et al., 2012). U and Mo concentrations were converted into Average Shale Al-normalized enrichment factors for comparison to previously published results using the formula:

$$EF_{\text{Average Shale}} = (\text{trace metal} / \text{Al})_{\text{sample}} / (\text{trace metal} / \text{Al})_{\text{Average Shale}} \quad (7)$$

(Wedepohl, 1971; 1991; Tripathy et al., 2014). These ratios are used to evaluate authigenic enrichment in the shales. This method eliminates the impact of variable dilution caused by the presence of calcium carbonate muddy laminations and fluxes in organic matter contents within the studied samples (Sageman et al., 2003). The EF values > 1 are generally considered to represent enrichments relative to PAAS and average shale respectively (Wedepohl, 1971; Taylor and McLennan, 1985; Wedepohl, 1991; Calvert and Pederson, 1993; McLennan, 2001; Tribovillard et al., 2006). Table 2.2 summarizes the P values calculated when the data noted to have low U enrichment factors and a high U-Al correlation was compared against the data with high enrichment factors and no U-Al correlation. The division set between these two categories is $EF_{\text{Average Shale}} = 1.25$ (Appendix 2.1; See results and discussion). This separation was done to split samples based on prevailing redox conditions, which as will be discussed later, were found to fluctuate significantly within the same beds.

	Ca	Sr	Al	K	Cr	Sc	Th	Cs	La	Mo	U	V	P	Ni	Cu
	wt%	ppm	wt%	wt%	ppm	ppm	ppm	ppm	ppm	ppm	ppm	ppm	ppm	ppm	ppm
n	34	34	34	34	34	34	34	34	34	34	34	34	34	34	34
Mean	4.2	115	5.8	4.5	60	8.4	6.7	3.2	19.8	2.6	3.1	120	494	32.8	36.1
STDV	2.9	29	1.2	1.2	12	1.9	1.5	1.0	7.2	3.0	2.0	80	141	10.5	16.8
MEDIAN	3.2	115	5.8	4.8	60	8.5	6.9	3.1	19.8	1.4	2.5	88	490	30.2	32.5
MIN	0.7	73	3.2	1.8	33	4.9	3.6	1.2	8.1	0.3	1.0	41	259	17.9	8.5
MAX	13.7	183	7.9	6.8	89	12.3	10.0	5.6	34.8	13.9	9.7	338	896	60.1	105.2
Below Anomaly															
n	19	19	19	19	19	19	19	19	19	19	19	19	19	19	19
Mean	3.8	116	6.2	4.7	64	9.1	7.4	3.7	22.6	2.7	3.2	94	503	33.6	36.3
STDV	3.0	31	1.1	1.2	12	1.8	1.2	1.0	6.4	3.5	1.6	30	116	10.9	12.9
MEDIAN	2.9	114	6.6	4.8	67	9.1	7.4	3.8	23.3	0.8	2.6	86	500	29.6	35.3
MIN	0.7	73	3.3	2.1	34	4.9	4.9	1.2	8.1	0.3	1.4	62	259	18.2	8.5
MAX	13.7	183	7.9	6.8	89	12.3	10.0	5.6	33.2	13.9	6.9	195	732	60.1	56.2
Above Anomaly															
n	15	15	15	15	15	15	15	15	15	15	15	15	15	15	15
Mean	4.8	114	5.2	4.1	55	7.5	5.9	2.6	16.2	2.4	3.1	152	484	31.7	35.9
STDV	2.8	28	1.0	1.3	10	1.6	1.4	0.8	6.7	2.3	2.4	108	171	10.4	21.2
MEDIAN	3.7	117	5.1	4.5	52	7.5	6.1	2.9	13.5	1.5	2.5	110	469	30.7	30.9
MIN	1.0	73	3.2	1.8	33	5.1	3.6	1.2	10.5	0.4	1.0	41	271	17.9	16.2
MAX	11.8	163	7.1	6.3	74	10.9	8.6	3.8	34.8	7.3	9.7	338	896	49.5	105.2
Two-tailed P values	0.3279	0.9159	0.007	0.17	0.0353	0.011	0.898	0.0025	0.0078	0.75	0.90	0.031	0.71	0.62	0.94
Mean Difference	-1.0	-1	1.04	0.60	8.80	1.6	0.09	1.01	6.43	0.34	0.09	-58.67	18.63	1.86	0.43
95% Lower Value	-3.05	-22	0.30	-0.28	0.647	0.393	-1.331	0.38	1.82	-1.77	-1.33	-111.62	-81.78	-5.63	-11.57
95% Upper Value	1.05	19.951	1.78	1.48	16.95	2.807	1.51	1.64	11.04	2.45	1.51	-5.72	119.04	9.35	12.4265

	TOC %	δ^{13}Corg ‰ VPDB	K/(Fe+Mg) Ratio	Th/Sc Ratio	∑REE ppm	Ce/Ce* (1)	Ce/Ce* (2)	Pr/Pr* (3)	V/Cr ratio	Authigenic U (4)	U/Mo_{auth} (5)	Th/U ratio	Fe_T/Al ratio
n	24	24	34	34	34	34	34	34	34	34	34	34	34
Mean	0.97	-29.03	0.72	0.81	106	0.91	0.97	1.02	2.01	0.90	0.74	2.71	0.50
STDV	0.93	0.75	0.28	0.11	36	0.05	0.06	0.03	1.34	1.88	0.56	1.26	0.09
MEDIAN	0.80	-29.04	0.72	0.81	105	0.91	0.96	1.02	1.42	0.43	0.52	2.42	0.49
MIN	0.11	-30.10	0.25	0.63	43	0.81	0.85	0.91	0.90	-0.99	0.15	0.76	0.36
MAX	4.10	-27.52	1.38	1.08	176	1.14	1.19	1.08	5.88	7.27	2.54	5.51	0.77
Below Anomaly													
n	13	13	19	19	19	19	19	19	19	19	19	19	19
Mean	0.95	-28.61	0.75	0.83	118	0.89	0.96	1.02	1.49	0.72	0.88	2.77	0.49
STDV	1.15	0.70	0.29	0.13	33	0.03	0.03	0.02	0.43	1.54	0.67	1.10	0.08
MEDIAN	0.58	-28.79	0.73	0.80	125	0.90	0.96	1.02	1.29	0.14	0.84	2.84	0.47
MIN	0.11	-29.84	0.25	0.63	43	0.81	0.90	0.99	0.90	-0.91	0.16	1.09	0.36
MAX	4.10	-27.52	1.38	1.08	173	0.93	1.01	1.05	2.34	4.41	2.54	4.55	0.66
Above Anomaly													
n	11	11	15	15	15	15	15	15	15	15	15	15	15
Mean	0.98	-29.52	0.68	0.79	90	0.93	0.98	1.01	2.68	1.12	0.57	2.65	0.52
STDV	0.66	0.45	0.28	0.08	35	0.07	0.08	0.04	1.78	2.28	0.30	1.47	0.10
MEDIAN	0.95	-29.71	0.71	0.81	75	0.91	0.97	1.02	2.25	0.54	0.52	2.28	0.51
MIN	0.20	-30.10	0.30	0.68	59	0.86	0.85	0.91	0.90	-0.99	0.15	0.76	0.38
MAX	2.37	-28.82	1.15	0.89	176	1.14	1.19	1.08	5.88	7.27	1.38	5.51	0.77
Two-tailed P values	0.94	0.0012	0.48	0.30	0.020	0.032	0.32	34.83	0.0081	0.55	0.11	0.79	0.34
Mean Difference	-0.03	0.91	0.07	0.04	29	0.04	-0.02	0.01	-1.19	-0.4	0.31	0.12	-0.03
95% Lower Value	-0.84	0.40	-0.13	-0.038	4.95	0.0038	-0.061	-0.011	-2.049	-1.74	-0.07	-0.78	-0.093
95% Upper Value	0.78	0.15	0.27	0.12	52.63	0.076	0.021	0.031	-0.33	0.94	0.69	1.02	0.033

Table 2.1: Mean, standard deviation, median, minimum and maximum values of select elements and ratios in the shales for the whole section, and below/above the geochemical anomaly, as well as two-tailed *P* values, mean differences and 95% confidence intervals using unpaired t-tests for comparing samples below vs above the anomaly. Where necessary, equations' numbers for ratios are included. Sample 166 data is not included here.

	TOC wt%	$\delta^{13}C_{org}$ ‰VPDB	Mo ppm	U ppm	V ppm	V/Cr Ratio	Authigenic U (4)	Th/U Ratio	U/Mo_{auth} (5)	Fe_T/Al Ratio
High EFs, U-Al correlation absent										
n	13	13	19	19	19	19	19	19	19	19
Mean	1.51	-29.5	4.1	4.1	145	2.53	1.90	1.85	0.45	0.49
STDV	0.99	0.4	3.3	2.2	96	1.59	1.98	0.58	0.27	0.09
MEDIAN	1.24	-29.7	3.0	3.2	110	1.92	1.11	1.87	0.41	0.47
MIN	0.45	-30.1	0.6	1.7	43	0.90	0.13	0.76	0.15	0.36
MAX	4.10	-28.8	13.9	9.7	338	5.88	7.27	2.88	1.25	0.66
Low EFs, U-Al correlation present										
n	11	11	15	15	15	15	15	15	15	15
Mean	0.32	-28.5	0.7	2.0	88	1.36	-0.37	3.81	1.12	0.52
STDV	0.28	0.6	0.3	0.6	36	0.40	0.50	1.01	0.61	0.10
MEDIAN	0.20	-28.7	0.6	2.1	86	1.27	-0.54	3.62	0.90	0.50
MIN	0.11	-29.1	0.3	1.0	41	0.90	-0.99	2.35	0.34	0.38
MAX	0.87	-27.5	1.5	2.8	195	2.37	0.52	5.51	2.54	0.77
Two-tailed P values	0.0009	0.0001	0.0004	0.0012	0.036	0.0092	0.0001	0.0001	0.0008	0.36
Mean Difference	1.19	-1.05	3.36	2.1	57.09	1.17	2.27	-1.96	-0.67	-0.03
95% Lower Value	0.55	-1.50	1.63	0.90	3.92	0.31	1.20	-2.52	-1.040	-0.97
95% Upper Value	1.83	-0.60	5.09	3.30	110.26	2.029	3.34	-1.40	-0.30	0.037

Table 2.2: Mean, standard deviation, minimum and maximum values of TOC, $\delta^{13}C_{org}$, and redox indicators including Mo, U, V, V/Cr, Authigenic U, Th/U, U/Mo_{auth} and Fe_T/Al values separated based on U-Al correlation of low U-EF samples, as well as unpaired t-test results for comparing both groups.

2.3.4.3 Uranium Content (%) in Different Phases

To determine the proportions of uranium in different phases, a modified version of the Organo (1997) approach is employed. Uranium is divided in two different categories: detrital and authigenic-biogenic.

2.3.4.3.1 Detrital Phase

The NASC standard (Gromet et al., 1984) was chosen as the basis for the calculation of the detrital phase as the Th/Sc_{NASC} (0.82) is very similar to the average Green Point shales' Th/Sc ratio (0.82) and should be representative of its detrital content.

Scandium is used here to quantify the detrital phase due to its immobile behavior and absence from other sedimentary phases (Chester and Aston, 1976; Brewer et al., 1980; Condie te al., 1995; Nesbitt and Markivics, 1997; Organo, 1997 Zhao and Zheng, 2015). For sample x, the detrital phase content [$(\%ter)_x$] is equal to:

$$(\%ter)_x = (Sc_x \text{ x } 100)/Sc_{NASC} \tag{8}$$

Sc_x = Sc content of Green Point shale sample (x)

Sc_{NASC} = Sc content of the NASC standard, i.e. 15.00 ppm

Next, the expected detrital uranium content [$(U_{ter})_x$] is calculated for each sample (normalized to NASC) using the formula:

$$(U_{ter})_x = [(\%ter)_x \text{ x } U_{NASC}]/100 \tag{9}$$

U_{NASC} = uranium content of the NASC standard, i.e. 2.66 ppm

The percentage of uranium associated with the detrital phase [$(\%U_{ter})_x$] in each sample is found using the formula:

$$(\%U_{ter})_x = [(U_{ter})_x \text{ x } 100]/(U_{tot})_x \tag{10}$$

$(U_{tot})_x$ = total uranium content in Green Point sample (x)

2.3.4.3.2 Authigenic and biogenic phases

As uranium contents within the Green Point carbonates (Azmy et al., 2015) are lower than within the shales, carbonate material within the shales is considered to be a diluting factor with regards to uranium derived from any non-detrital phase. Because of this, the authigenic and biogenic U are grouped together as $(\%U_{bio\text{-}auth})_x$ using the formula:

$$(\%U_{bio\text{-}auth})_x = 100 - (\%U_{ter})_x \tag{11}$$

2.4. Results

2.4.1 Organic Carbon and Organic Carbon Isotopes

The Total Organic Carbon (TOC) content of the studied shales varied from 0.11 to 8.81 wt%, similar to the range documented by earlier studies for carbonates (Azmy et al., 2015) and shales (Weaver and Macko, 1988) deposited at the same time period across western Newfoundland (Table 2.1). However, the range of TOC contents is larger than TOC values reported for black shales of the same section by Tripathy et al. (2014), who analyzed a small number of stratigraphically restricted intervals targeted for Re-Os geochronology. Generally speaking, the lowest TOC contents in the shales are associated with green shales that are most common in beds 20-22 while the highest TOC contents were derived from dark grey or black shales (Fig. 1.2; Fig. 2.2; McLaughlin et al., 2012). The TOC concentrations of the shales average 1.28±0.67 wt%, which is slightly higher than the average reported by Tripathy et al. (2014). Previous evaluation of the interbedded carbonates in the Green Point Formation documented the presence of a geochemical anomaly documenting environmental changes slightly below the biostratigraphic boundary (Golden Spike), based on changes of the $\delta^{13}C_{org}$, $\delta^{15}N$, and $\delta^{238}U$ profiles at this level (Azmy et al., 2014; 2015). Due to its presence, geochemical observations comparing environmental conditions across the Cambrian-Ordovician boundary in this study are made based the same anomaly. Values in this study do not change in any statistically significant manner across the geochemical anomaly level when they are compared solely based on stratigraphic position relative to the anomaly (Table 2.1). However, when comparing values based on their U enrichment factors and U-Al relationship (discussed below), *P* values become statistically significant ($P = 0.01$; Table 2.2). This observation is supported by changes in median values across the geochemical anomaly level, from 0.58 to 0.95wt%. The $\delta^{13}C_{org}$ values of the shales vary between -26.01‰ and -30.10‰, which fall within the range documented for western Newfoundland shales of the same time interval by earlier studies (Weaver and Macko, 1988). Sample 166, located at the top of the section, was found to anomalously have both the highest TOC (8.81 wt%) and $\delta^{13}C_{org}$ (- 26.01‰) values of the whole section, by a noticeable margin (Fig. 2.2). This may indicate potential bituminization of this sample, making it an outlier that may not be representative of environmental conditions within the studied interval (Gao et al., 2016). It is excluded from any further statistical analyses. The $\delta^{13}C_{org}$ values were found to have a moderate inverse correlation to TOC ($R^2 = 0.48$; Fig. 2.3). An overall decrease in $\delta^{13}C_{org}$ values occurs across the geochemical anomaly, from -28.61±0.70‰ to -29.52±0.45‰ (Table 2.1). *P* values are statistically significant whether compared based on the anomaly level (0.0001) or U behavior ($P = 0.0275$; Table 2.2). A similar, though less pronounced, decrease in $\delta^{13}C_{org}$ values was also observed in the concurrent carbonates across the geochemical anomaly (Azmy et al., 2015).

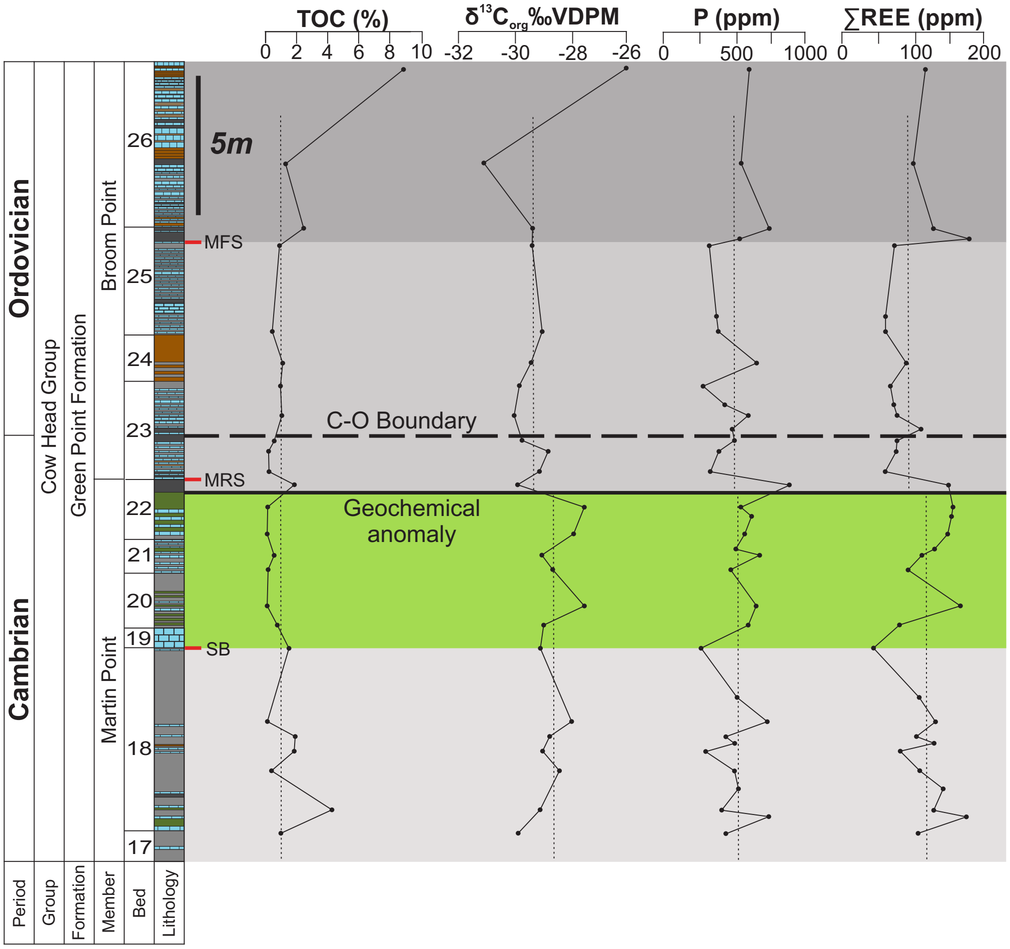

Figure 2.2: TOC (weight %), δ $^{13}C_{org}$ (‰ VDPM), P (ppm) and Σ REE (ppm) profiles across the Cambrian–Ordovician boundary at Green Point (western Newfoundland). The solid black line marks the geochemical anomaly level identified by Azmy et al. (2014; 2015). The horizontal dashed black line marks the current Cambrian-Ordovician boundary (Golden Spike, Cooper et al., 2001a). Vertical dotted black lines represent the mean values below and above the anomaly level (Sample 166 not included). The shading outlines systems tracts: First HST (light grey, beds 17-18), LST (green, beds 19-22), TST (grey, beds 22-25), Second HST (dark grey, beds upper 25-26). SB = Sequence Boundary. MRS = Maximum Regressive Surface. MFS = Maximum Flooding Surface.

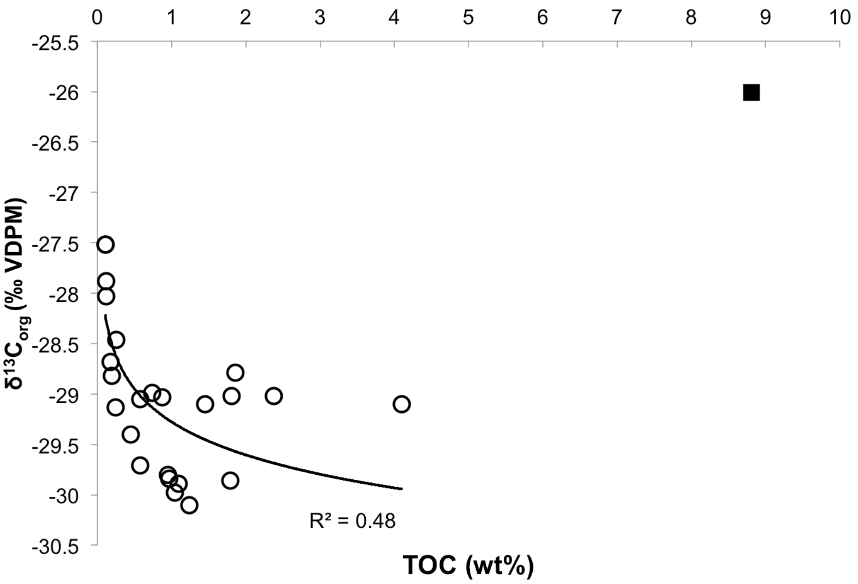

Figure 2.3: Scatter diagram of TOC (wt %) vs $\delta\ ^{13}C_{org}$ (‰ VDPM). Sample Sa-166 is marked by the black square. See text for details.

2.4.2 Carbonate Content Proxies

The elements Ca, Sr and Na were assessed in this study in order to quantify the carbonate material identified within the shales of the Green Point Formation (Chester and Aston, 1976; Nesbitt et al., 1980; Middlebug et al., 1988; Dean and Arthur, 1998; Werne et al., 2002; Babechuk et al., 2014). The Ca content of the shales has a mean of 4.24±2.90wt%, varying widely between 0.68 and 13.66wt% throughout the section (Fig. 2.4). A statistically insignificant increase is observed across the geochemical anomaly level. Sr concentrations have a mean of 116±29ppm and vary from 73 to 183ppm. No statististically significant change is observed across the anomaly. Na concentrations vary between 0.22 and 0.60wt% with a mean of 0.38±0.10wt%. No change is observed across the anomaly level. Ca and Sr have a good correlation ($R^2 = 0.67$) while no noteworthy correlation is observed between Ca and Na ($R^2 = 0.13$; Fig. 2.5).

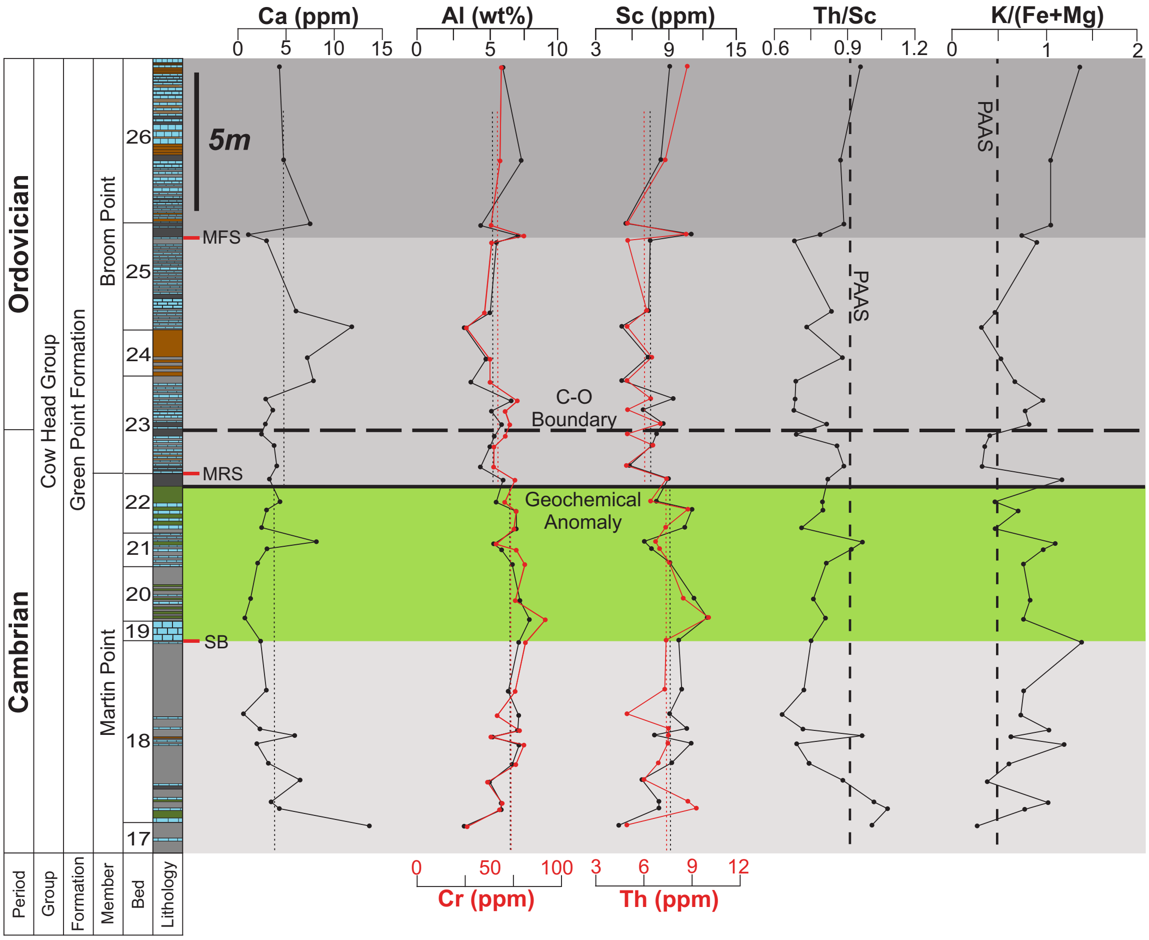

Figure 2.4: Ca (weight %), Al (weight %), Cr (ppm), Sc (ppm), Th (ppm), Th/Sc and K/[Fe+Mg] profiles across the Cambrian–Ordovician boundary at Green Point (western Newfoundland). The solid black line, the horizontal dashed black line, and black dotted lines are defined as in Figure 2.2. Vertical dotted red lines also represent mean values below and above the anomaly level (Sample 166 not included). The vertical dashed black lines represent ratios derived from PAAS.

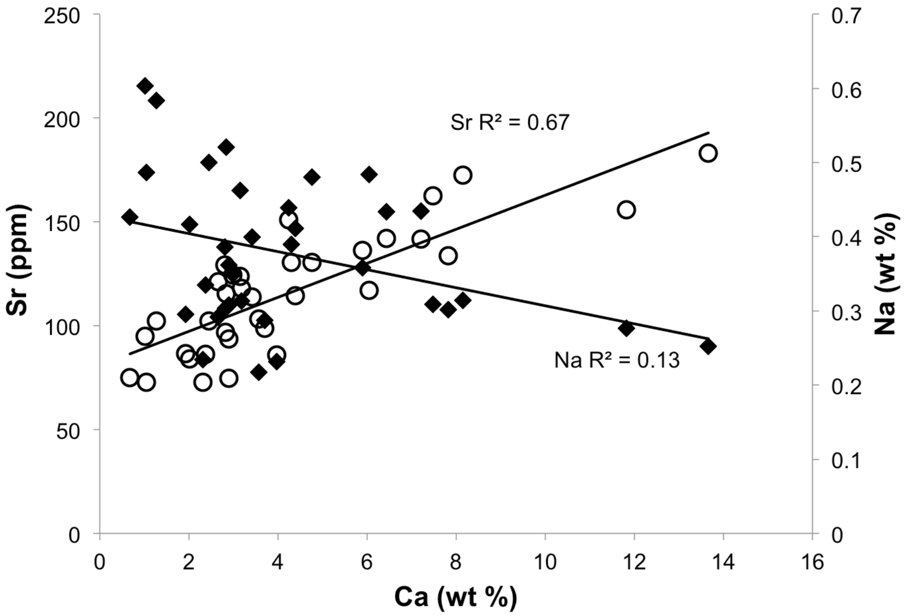

Figure 2.5: Scatter diagram of Ca (wt %) vs Sr (circles) and Na (diamonds; ppm). See text for details.

2.4.3 Siliciclastic Detrital Proxies

Concentrations of several elements; Sc, Al, K, Cr, Th, Cs, and La have been utilized as indicators of siliciclastic input and provenance (e.g., Nesbitt ,1979; Nesbitt et al., 1980; Middleburg et al., 1988; Dean and Arthur, 1998; Schnetger et al., 2000; Jiménez-Espejo et al., 2007; Śliwiński et al., 2010; Zhao and Zheng, 2015). The concentrations of these detrital indicators consistently decrease across the geochemical anomaly (Table 2.1; Fig. 2.4). The observed decrease is statistically significant for all of these elements except K (Table 2.1).

To eliminate the effect of dilution, several elemental ratios are used. The Th/Sc ratio has previously been found to vary depending on provenance (McLennan et al., 1990; McLennan et al., 1993). They vary within the Green Point Shales between 0.63 and 1.08 with a mean of 0.82±0.11, (Table 2.1; Fig. 2.4). No statistically significant variation is observed up-section (Table 2.1; Fig. 2.4).

The K/[Fe+Mg] ratio has been used previously as a proxy for the relative abundance of volcaniclastic and detrital components in hemipelagic sediments. Higher ratios are indicative of a higher siliciclastic detrital input (Dean and Arthur, 1998; Werne et al., 2002). However, it must be used with caution when conditions are euxinic due to the impact of pyrite on sedimentary iron contents (Werne et al., 2002). The mean value of the K/[Fe+Mg] ratio is 0.74±0.27 (Table 2.1). Though its vertical profile indicates variations occur, especially when compared to the systems tracks, these variations are not considered to be statistically significant, as observed for K (Table 2.1; Fig. 2.4).

2.4.4 Rare Earth Elements and Ce/Ce*

The total rare earth element contents (∑REE) vary from 43 to 176 ppm within the studied section (Table 2.1). The shale ∑REE abundances have no correlation with Mo and U abundances (both $R^2 \leq 0.01$). However, the ∑REE abundances have a moderate correlation with the P content in the shales ($R^2 = 0.44$; Fig. 2.6). A comparable correlation ($R^2 = 0.60$) was documented by earlier studies on the alternating carbonates of the same section (Azmy et al., 2014; 2015). The ∑REE abundances in the shales decrease upward across the anomaly level from 118±33 to 90±35 ppm ($P = 0.02$; Table 2.1; Fig. 2.2).

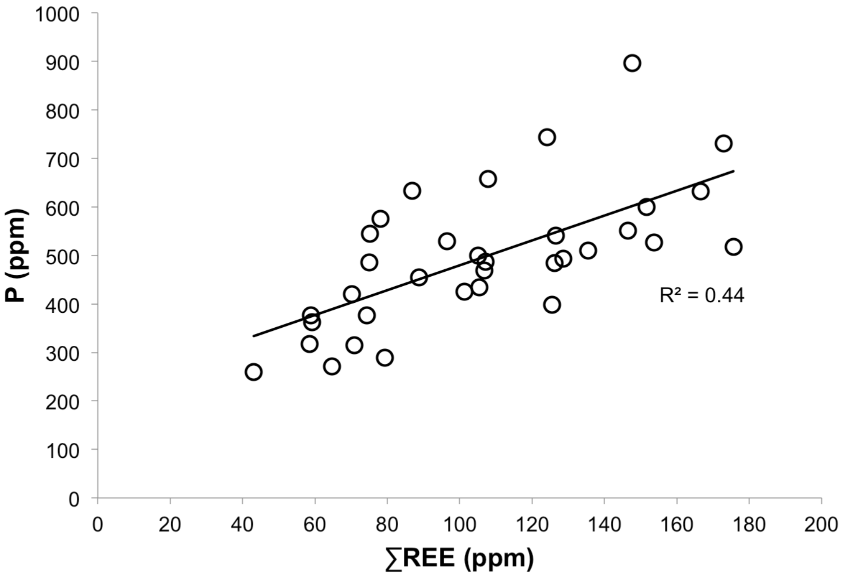

Figure 2.6: Scatter diagram of P (ppm) vs ∑REE (ppm). See text for details.

TThe Y/Ho ratios of the shales throughout the section have a mean value of 29.8±1.3, and do not change across the anomaly level (Appendix 2.1). It varies from 26.6 to 34.1 across the whole section.

The cerium anomaly (Ce/Ce^*_{SN}) was calculated in 2 ways for comparison. Using equation (1), Ce/Ce^*_{SN} ratios in the shales varies from 0.81 to 1.13 across the section, with a mean of 0.91±0.06 (Table 2.1; Bau and Dulski, 1996; Nozaki, 2001), and increases slightly across the anomaly level, from 0.89±0.03 to 0.93±0.07 (P = 0.03; Table 2.1). The Ce/Ce^*_{SN} ratios derived from equation (2) were also used in this study. Its mean value throughout the section is 1.02±0.33 and does not change across the anomaly level. No significant variation across the anomaly was noted when using this equation (P = 0.32; Bolhar et al., 2004).

The Pr/Pr*$_{SN}$ anomaly, see equation (3), was also utilized in order to evaluate potential REE anomalies that have to be taken into account (See discussion; Bau and Dulski, 1996). The Pr/Pr*$_{SN}$ values have a mean of 1.02±0.33 and do not change up-section (Table 2.1).

2.4.5 Redox-Sensitive Trace Elements

Vanadium, uranium and molybdenum concentrations are proxies of redox conditions (e.g., Algeo and Maynard, 2004; Rimmer, 2004; Tribovillard et al., 2006; Śliwiński et al., 2010; Sahoo et al., 2012; Scott and Lyons, 2012; Partin et al., 2013; Gao et al., 2016). The V concentrations increase from 94±30 to 152±108 ppm across the geochemical anomaly (P = 0.0001; Table 2.1; Fig. 2.7). The geochemical anomaly level itself is marked by a positive V spike (Fig. 2.7). The U and Mo concentrations in the shales vary within the whole section from 1.0 to 13.4 ppm and 0.3 to 24.6 ppm respectively (Table 2.1). Not including the outlier Sa-166, U and Mo are moderately correlated (R^2 = 0.56; Fig. 2.8). An abrupt positive spike in their concentrations occurs right at the geochemical anomaly level (Fig. 2.7). The abundances of U and Mo do not however change in any significant way when splitting the dataset stratigraphically based on the anomaly level (Table 2.1; Fig. 2.7). This can be explained by highly variable redox conditions, which is reflected in the variations in shale coloration, the wide range of concentrations and high standard deviations on both sides of the anomaly (Table 2.1; Fig. 1.2). Keeping this in mind, statistically significant results may be derived from comparing samples with respectively low and high enrichment factors and the relationship of U to Al, based on the division set at $EF_{Average\ Shale}$ = 1.25, which is more reflective of the observed lithological variability (Table 2.2; Fig. 2.9; Appendix 2.1). The geochemical change across the anomaly is well represented by the proportions of samples with low and high enrichment. As more samples with high enrichment are present above the anomaly, this indicates an overall increase, reflective of the higher proportion of grey and black shale intervals above the anomaly level (Fig. 1.2; Table 2.2). This approach is supported by the changes in median values below to above the geochemical anomaly level (Table 2.1). Medians for V and Mo increase across it; V from 86 to 110 ppm, Mo from 0.8 to 1.5 ppm. U medians decrease very slightly across the anomaly level (2.6 to 2.5 ppm; Table 2.1). This is however a reflection of decreasing detrital U up section, rather than a lack of change in authigenic enrichments. This is reflected in the consistent median increases observed for the Th/U, authigenic U and U EF_{PAAS} proxies, which are more indicative or redox behavior in this case (see below; Table 2.1).

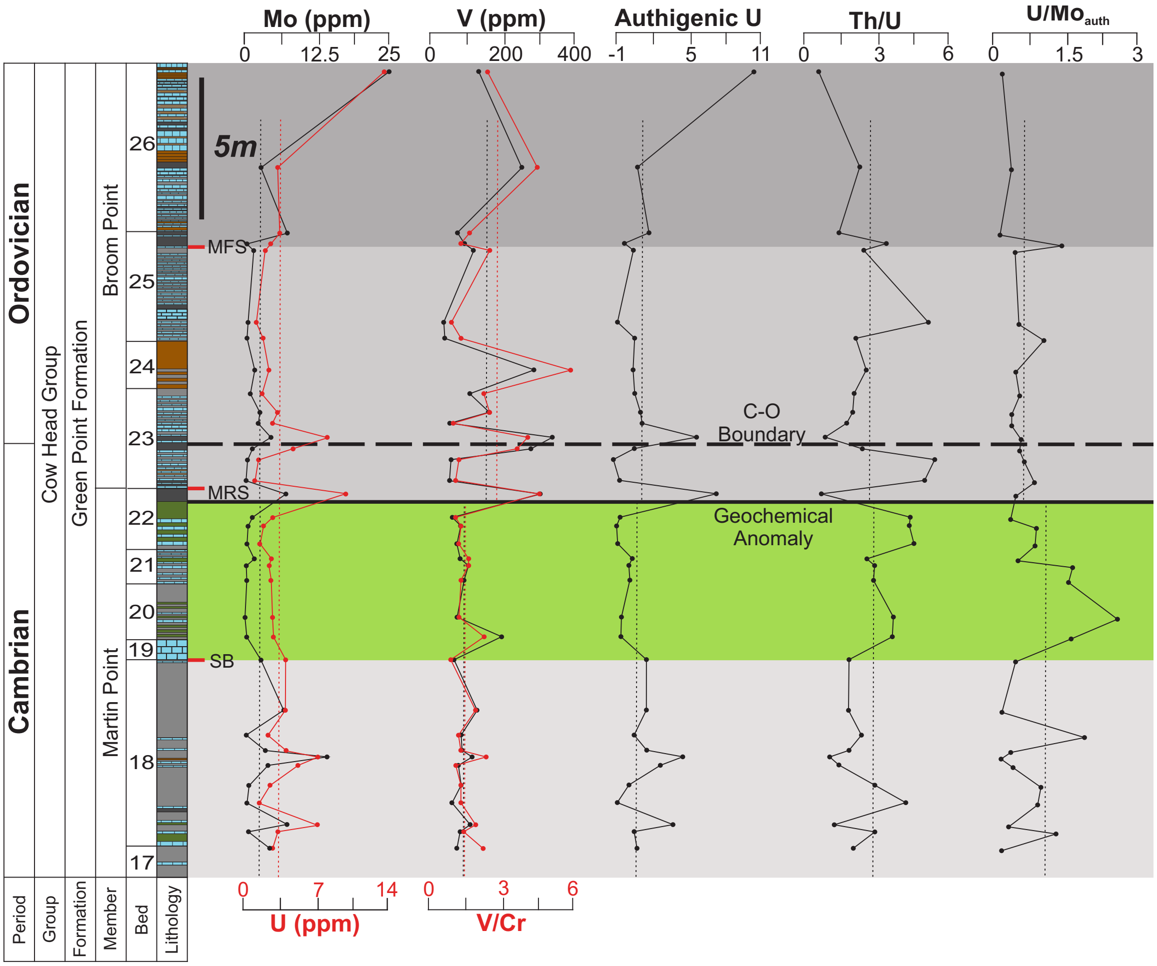

Figure 2.7: Mo (ppm), total U (ppm), V (ppm), V/Cr, authigenic U (ppm), Th/U and U/Mo$_{auth}$ paleoredox profiles across the Cambrian-Ordovician boundary at the GSSP in Green Point (western Newfoundland). The solid black line, the dashed black line, vertical red, and black dotted lines are defined as in Figures 2.2 and 2.4.

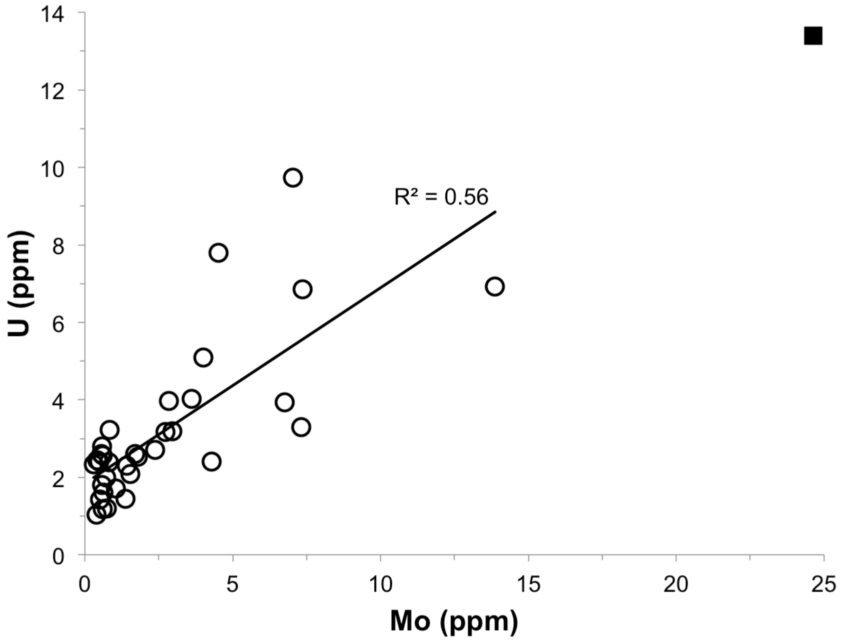

Figure 2.8: Scatter diagram of uranium vs molybdenum concentrations. The outlier Sa-166 is marked by the black square.

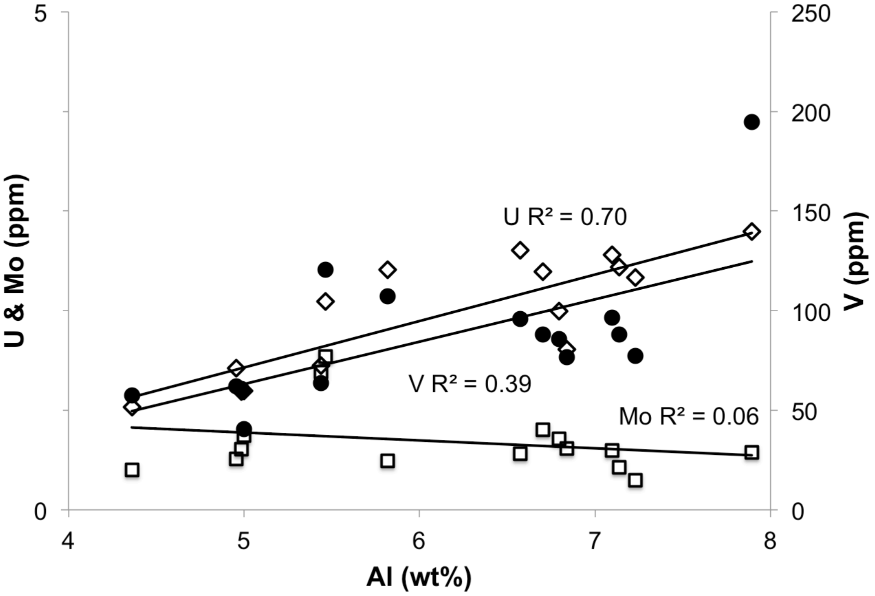

Figure 2.9: Plot of U (diamonds), Mo (squares) and V (circles) vs Al concentrations of the samples that were identified to have low EFs. See Appendix 2.1 for list of samples included and text for details.

2.4.6 Redox-Sensitive Trace-Metal Ratios

Several trace metal ratios have been evaluated as proxies of redox conditions, including V/Cr, V/(V+Ni), authigenic U (Total U – Th/3; Wignall and Myers, 1988), Th/U, U/Mo_{auth} and Fe_T/Al (Wignall and Myers, 1988; Hatch and Leventhal, 1992; Jones and Manning, 1994; Lyons and Severmann, 2006; Algeo and Tribovillard, 2009; Poulton et al., 2010; Zhou et al., 2012). Table 2.1 summarizes the statistics of the most redox-sensitive trace metal ratios for the Green Point shales [V/Cr, authigenic U, U/Mo and Th/U]. The V/Cr ratios range from 0.9 to 5.9 (Table 2.1) and increase upward across the geochemical anomaly level from 1.5±0.4 to 2.7±1.7 (P = 0.008; Table 2.1; Fig. 2.7). The V/(V+Ni) values vary between 0.6 and 0.9 and show insignificant change across the anomaly. The authigenic U values vary between -1.0 and 10.5 and increase considerably across the geochemical anomaly from 0.7±1.6 to 1.1±2.3 (Table 2.1, Fig. 2.7). The Th/U ratio varies between 0.65 and 5.51, and does not change in any statistically significant manner when values below and above the anomaly level are compared. As for U and Mo concentrations, statistically significant results for change across the anomaly cannot be derived by direct comparison but rather by separating samples based on U enrichment factors and comparing proportions of each below and above the anomaly (authigenic U P = 0.0006; Th/U P = 0.0001; Table 2.2). This is supported by median values. The authigenic U median increases across the anomaly level from 0.71 to 1.71. Th/U median decreases across the anomaly level from 2.84 to 2.19 (Table 2.2). The U/Mo_{auth} ratios were calculated as U EF_{PAAS}/Mo EF_{PAAS}. This was done to remove the influence of detrital Mo and U identified within the samples. U/Mo_{auth} ratios vary between 0.12 and 2.03, decreasing across the anomaly from 0.71±0.54 to 0.46±0.26, though not in a significant manner ($P = 0.11$; Table 2.1, Fig. 2.7). The Fe_T/Al ratios (0.50±0.09) are similar to the average ratios for both upper continental crust (UCC; 0.44) and Post-Archean-Australian-Shale (PAAS; 0.50) (Taylor and McLennan, 1985; McLennan, 2001), and range between 0.36 and 0.77. No change in Fe_T/Al ratios occurs across the geochemical anomaly. Comparison of the metal ratios for sample groups defined by low vs high U enrichments, all ratios except V/(V+Ni) and Fe_T/Al exhibit statistically significant differences, clearly indicating 2 populations (Table 2.2).

2.4.7 Bioproductivity-Sensitive Trace Elements

The P, Ni and Cu contents have also been used as indicators of bioproductivity (e.g., Piper and Perkins, 2004; Riquier et al., 2006; Ma et al., 2008; Piper and Calvert, 2009; Śliwiński et al., 2010). Phosphorus concentrations vary throughout the whole section from 259 to 895 ppm and show no change across the anomaly (Table 2.1; Fig. 2.2). Total Ni and Cu contents in the investigated shales are 17.9 to 60.1 ppm and 8.5 to 105.2 ppm, respectively, and do not change in a statistically significant way across the anomaly level (Table 2.1).

2.4.8 Enrichment Factors

The averaged order of EF_{PAAS} magnitudes for the entire section (not including Sa 166) is Mo (3.98) > U (1.49) > V (1.27) > P (1.07) > Cr (0.88) > Ni (0.80) > Cu

(0.70) (Table 2.3). Mean average shale normalized EFs for U and Mo are 1.63 and 3.24, respectively. When comparing values based on the anomaly level, only V EF_{PAAS} demonstrates a significant increase (Fig. 2.10). Uranium samples with low average shale (U $EF_{Average\ Shale} < 1.25$) normalized enrichment factors (n=15) were found to have a very good correlation between U and Al concentrations, supporting low authigenic contents ($R^2 = 0.70$; Table 2.1; 2.4; Fig. 2.9; Appendix 2.2). The dataset was split based on this criteria. A statistically significant difference between the EFs of these samples and the samples with high U enrichment was found for most metals except for P, Cu and Cr. The same statistically significant pattern is present for TOC, trace metals and trace metal ratios (Table 2.2). As low EF values are much more common below the geochemical anomaly, this indicates that though conditions were variable, EFs increased across the geochemical anomaly level (Table 2.4; Fig. 2.10; Appendix 2.1). This is supported by the increase in EF medians across the geochemical anomaly level for Mo, U, V and Ni (Table 2.3).

	Mo	U	V	Ni	Cu	Cr	P	Mo	U
	EF_{PAAS}	EF_{PAAS}	EF_{PAAS}	EF_{PAAS}	EF_{PAAS}	EF_{PAAS}	EF_{PAAS}	$EF_{Average\ Shale}$	$EF_{Average\ Shale}$
n = 35									
Mean	3.98	1.49	1.27	0.80	0.70	0.88	1.07	3.24	1.63
STDV	4.83	0.93	0.87	0.23	0.26	0.07	0.35	3.93	1.01
MEDIAN	2.23	1.26	0.88	0.82	0.68	0.87	0.97	1.81	1.37
MIN	0.34	0.64	0.49	0.48	0.13	0.76	0.44	0.28	0.70
MAX	22.44	4.45	3.66	1.62	1.66	1.04	2.05	18.27	4.86
Below Anomaly, *n = 19*									
Mean	4.11	1.43	0.92	0.77	0.66	0.86	1.01	3.34	1.57
STDV	5.63	0.81	0.28	0.27	0.22	0.06	0.30	4.59	0.89
MEDIAN	1.20	1.12	0.79	0.75	0.67	0.85	0.97	0.98	1.23
MIN	0.34	0.64	0.58	0.48	0.13	0.77	0.44	0.28	0.70
MAX	22.44	3.61	1.48	1.62	1.09	0.97	1.60	18.27	3.95
Above Anomaly, *n = 15*									
Mean	3.83	1.57	1.72	0.85	0.75	0.90	1.14	3.12	1.72
STDV	3.75	1.08	1.14	0.17	0.30	0.08	0.41	3.05	1.18
MEDIAN	2.37	1.33	1.32	0.85	0.74	0.89	0.97	1.93	1.46
MIN	0.71	0.64	0.49	0.52	0.36	0.76	0.69	0.58	0.70
MAX	14.07	4.45	3.66	1.12	1.66	1.04	2.05	11.46	4.86
Two-tailed P values	0.88	0.67	0.0058	0.32	0.32	0.11	0.79	0.87	0.68
Mean Difference	0.28	-0.14	-0.8	-0.08	-0.090	-0.04	-0.13	2.22	-0.15
95% Lower Value	-3.17	-0.80	-1.35	-0.24	-0.27	-0.09	-1.14	-2.59	-0.87
95% Upper Value	3.73	0.52	-0.25	0.08	0.092	0.01	-0.88	3.03	0.57

Table 2.3: Mean, standard deviation, median, minimum and maximum values of the calculated EF_{PAAS} (6) and $EF_{Average\ Shale}$ (7) values of the shales for the whole section, and below/above the geochemical anomaly, as well as two-tailed *P* values, mean differences and 95% confidence intervals using unpaired t-tests for comparing samples below to above the anomaly.

	Mo	U	V	Ni	Cu	Cr	P	Mo	U
	$\mathrm{EF}_{\mathrm{PAAS}}$	$\mathrm{EF}_{\mathrm{PAAS}}$	$\mathrm{EF}_{\mathrm{PAAS}}$	$\mathrm{EF}_{\mathrm{PAAS}}$	$\mathrm{EF}_{\mathrm{PAAS}}$	$\mathrm{EF}_{\mathrm{PAAS}}$	$\mathrm{EF}_{\mathrm{PAAS}}$	$\mathrm{EF}_{\mathrm{Average\ Shale}}$	$\mathrm{EF}_{\mathrm{Average\ Shale}}$
High EFs, no U-Al correlation *n = 19*									
Mean	6.36	2.00	1.61	0.91	0.71	0.88	1.14	5.17	2.19
STDV	5.38	0.97	1.03	0.23	0.18	0.07	0.44	4.38	1.06
	4.11	1.52	1.25	0.85	0.67	0.88	1.10	3.34	1.66
MIN	1.20	1.17	0.58	0.53	0.41	0.79	0.44	0.98	1.28
MAX	22.44	4.45	3.66	1.62	1.09	1.04	2.05	18.27	4.86
Low EFs, U-Al correlation present *n = 16*									
Mean	0.98	0.85	0.84	0.67	0.70	0.87	0.97	0.80	0.93
STDV	0.56	0.17	0.26	0.16	0.35	0.08	0.17	0.46	0.19
MEDIAN	0.78	0.87	0.76	0.61	0.70	0.86	0.91	0.63	0.96
MIN	0.34	0.64	0.49	0.48	0.13	0.76	0.69	0.28	0.70
MAX	2.37	1.12	1.48	0.95	1.66	0.99	1.36	1.93	1.23
Two-tailed P values	0.0005	0.0004	0.0082	0.0017	0.91	0.70	0.17	0.0006	0.0001
Mean Difference	5.38	4.61	0.77	0.24	0.01	0.01	0.17	4.37	1.26
95% Lower Value	2.53	2.22	0.21	0.10	-0.18	-0.042	-0.08	2.05	0.69
95% Upper Value	8.23	7.00	1.33	0.38	0.20	0.062	0.45	6.69	1.83

Table 2.4: Mean, standard deviation, median, minimum and maximum values of the calculated $\mathrm{EF}_{\mathrm{PAAS}}$ (6) and $\mathrm{EF}_{\mathrm{Average\ Shale}}$ (7) values separated based on U-Al correlation of low U-EF samples, as well as unpaired t-test results for comparing samples from both sets.

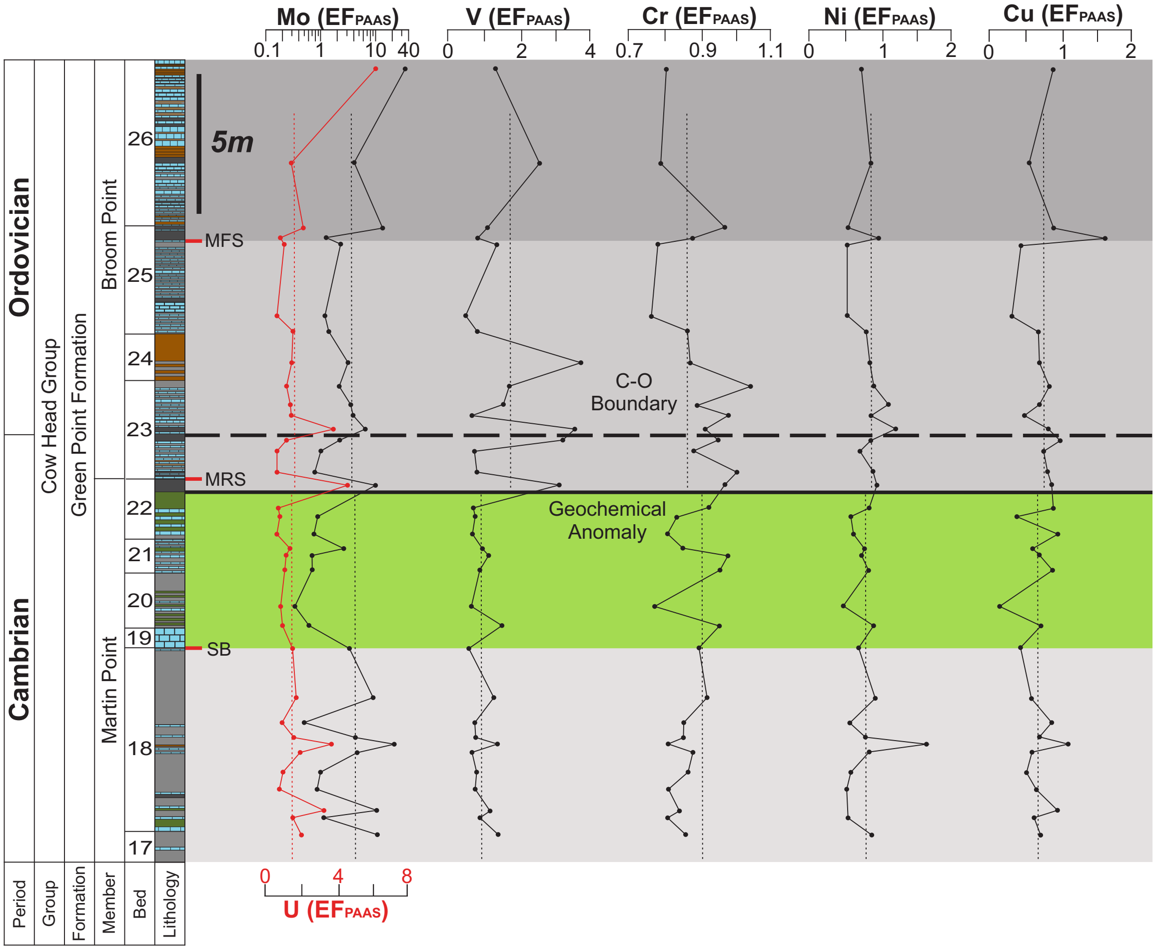

Figure 2.10: Mo EF_{PAAS}, total U EF_{PAAS}, V EF_{PAAS}, Ni EF_{PAAS}, Cu EF_{PAAS}, Cr EF_{PAAS} paleoredox profiles across the Cambrian-Ordovician boundary at the GSSP in Green Point (western Newfoundland). The solid black line, the dashed black line, vertical red, and black dotted lines are defined as in Figures 2.2 and 2.4.

2.4.9 Uranium Content by Phase

Following the method of Organo (1997), the uranium content of the Green Point shales was divided between its calculated detrital and authigenic-biogenic components, presented in Appendix 2.3. The calculated detrital content ($(U_{ter})_x$) of the Green Point shales varies between 0.9 and 2.2 ppm, with a mean of 1.5±0.3. It is closely correlated to detrital proxies other than Sc as well, such as Al ($R^2 = 0.91$) and

Th ($R^2 = 0.67$). $(U_{ter})_x$ was also found to decrease across the anomaly level, from 1.6±0.3 to 1.3±0.3 (Table 2.5). This statistically significant decrease was also observed in detrital proxies (Sc, Th, Al, Cr, Cs; Table 2.1; Fig. 2.4). The calculated percentage of total U (ppm) within the detrital phase ($(\%U_{ter})_x$) varied between 12 and 114%, with a mean of 58.7±28.1 (Table 2.5). There are 3 samples (Sa 44, Sa 61 and Sa 84) that have $(\%U_{ter})_x$ values > 100% and their $(\%U_{bio\text{-}auth})_x$ values are negative. The resulting $(\%U_{bio\text{-}auth})_x$ values vary between -14% and 88% with a mean of 41.3±28.1 (Table 2.5).

	$(\%ter)_x$ (8)	$(U_{ter})_x$ (9)	$(\%U_{ter})_x$ (10)	$(\%U_{bio\text{-}auth})_x$ (11)
n = 35				
Mean	56.00	1.49	58.66	41.34
STDV	12.36	0.33	28.10	28.10
MEDIAN	57.23	1.52	52.20	47.80
MIN	32.79	0.87	12.02	-14.08
MAX	82.28	2.19	114.08	87.98
Below Anomaly, *n = 19*				
Mean	60.50	1.61	60.71	39.29
STDV	12.00	0.32	26.17	26.17
MEDIAN	60.48	1.61	55.79	44.21
MIN	32.79	0.87	20.10	-13.14
MAX	82.28	2.19	113.14	79.90
Above Anomaly, *n = 15*				
Mean	50.66	1.35	56.24	43.76
STDV	10.85	0.29	30.93	30.93
MEDIAN	50.31	1.34	51.67	48.33
MIN	34.30	0.91	12.02	-14.08
MAX	72.46	1.93	114.08	87.98
Two-tailed P values	0.019	0.020	0.51	0.65
Mean Difference	9.84	0.26	4.47	-4.47
95% Lower Value	1.74	-0.04	-9.34	-24.42
95% Upper Value	17.94	0.48	18.28	15.48

Table 2.5: Mean, standard deviation, median, minimum and maximum values of the calculated results, following the method of Organo, 1997, of the shales for the whole section, and below/above the geochemical anomaly. Also present are the two-tailed *P* values, mean differences and 95%

confidence intervals using unpaired t-tests for comparing samples below to above the anomaly. (#) indicates the relevant equation for each ratio used.

2.5 Discussion

2.5.1 Geochemical Preservation of the Green Point Shales

The preservation of the depositional geochemical signatures is a cornerstone of paleoenvironmental studies. Prior petrographic and field examination of the sediments of the Cow Head Group has identified several features that could potentially impact the preservation of primary geochemical signatures in the shales at the Green Point locality (Coniglio, 1986; James and Stevens, 1986; Coniglio and James, 1990). Some of the carbonate muds in certain carbonaceous shales, the "calcilutite-shale facies" of Coniglio and James (1990), have been interpreted to have undergone dissolution of carbonate mud and local precipitation very early during diagenesis (cms to a few meters) within the pore-waters, due to pH changes resulting from anaerobic oxidation of organic matter within these sediments. Apart from undergoing compaction, the detrital siliciclastic component was not affected by this process (Coniglio and James, 1990). The presence of carbonate material, organic matter, the same shale colorations and evidence of some synsedimentary compaction (Fig. 2.1a; d) found in some of the shales this study does indicate that the "calcilutite-shale" facies of Coniglio and James (1990) is likely to be present within the Green Point section. The resulting carbonate dilution effect on the detrital and authigenic components of the Green Point shales is addressed below.

Evidence of later tectonic deformation of the Green Point section was also noted, based on the presence of minor faulting, wrinkled limestones, and associated minor shortening (Fig. c; e). These features have previously been associated with late diagenetic precipitates and tectonic stylolites within the Cow Head Group, which could cause some degree of alteration (Coniglio, 1986; James and Stevens, 1986). The Y/Ho ratio is a good proxy for the degree of preservation of clastic sediments. Values that deviate widely from the average of most clastic and igneous rocks (~28) reflect the influence of hydrothermal fluids (Bau, 1996; Bau and Dulski, 1999; Douville et al., 1999). The Y/Ho ratios of the shales throughout the section has a mean value of 29.8±1.3 (Appendix 2.1), which is very close to the average documented by earlier studies (Bau and Dulski, 1996). Diagenetic alteration of sediments during progressive burial is associated with an increase in temperatures and water/rock interactions with depth. Catagenesis of organic matter occurs above 50^{O}C, resulting in the thermal degradation and release of hydrocarbons, particularly lighter compounds. This causes an overall decrease in TOC content and an increase in its $\delta^{13}C_{org}$ signatures (Popp et al., 1997; Faure and Mensing, 2005). Apart from sample 166, which shows evidence of bituminization (Gao et al., 2016), the $\delta^{13}C_{org}$ values (-29.03±0.75‰; Table 2.1) fall within or close to the expected range of algae or C3 land plants (Meyers, 1994; 1997). This reflects insignificant thermal degradation (Popp et al., 1997; Faure and Mensing, 2005). Based on these observations, the shale geochemistry does appear to have retained primary signatures. These observations are consistent with previous geochemical studies of both the shales and carbonates of the same section, which also indicate little diagenetic change and alteration occured (Azmy et al., 2014; Tripathy et al., 2014; Azmy et al., 2015).

2.5.2 Evaluation of the TOC and $\delta^{13}C_{org}$ signatures

Previous petrographic examination of the shales yielded visible organic matter (Coniglio and James, 1990). In the Green Point Formation, shale $\delta^{13}C_{org}$ varies from -30.10‰ to -26.01‰ (Fig. 2.2). Similar values were observed in the carbonates associated with the shales (Azmy et al., 2015). Due to the restricted biomass on land prior to the Devonian, the $\delta^{13}C_{org}$ values would be mainly indicative of phototrophic and potentially chemotrophic biological activity in the ocean (Gao et al., 2016). The observed values are very close to the range for photoautotrophic carbon fixation based on the Calvin cycle (House et al., 2000; She et al., 2014). Organic matter oxidation leading to chemotrophic pathways on the other hand would be unlikely in slope settings (Azmy et al., 2015; Gao et al., 2016). The shale $\delta^{13}C_{org}$ values in this section gradually increase from beds 17-18 during the first HST to beds 20-22, the LST, reaching their peak. They exhibit a general slight decrease across the geochemical anomaly level ($P = 0.0001$; Table 2.1; Fig. 2.2), and remain consistently lower within the TST and second HST of beds 22-26. This is similar to the $\delta^{13}C_{carb}$ trend of the interbedded carbonates (Azmy et al., 2015).

The final TOC content of sediments has previously been interpreted as a mixed signal, that can reflect both bioproductivity and/or bottom-water oxygenation-mediated preservation (Canfield, 1994; Murphy et al., 2000; Shoepfer et al., 2014). The shale TOC profile of the Green Point shales is moderately inversely correlated to the $\delta^{13}C_{org}$ trend (Table 2.1; Fig. 2.3). TOC decreases in beds 17-18 and stays low within the overlying beds 20 to mid-22 before increasing across the geochemical anomaly rather than decreasing as was observed in the carbonates. This trend is in line with the observed shale coloration within the section. The lowest TOC contents are associated with green shales that are most common in beds 20-22, below the anomaly (Fig. 2.2; McLaughlin et al., 2012). The highest TOC contents were derived from dark grey or black shales (Fig. 2.2; McLaughlin et al., 2012).

The relationship between TOC content and elemental concentrations, elemental ratios, or enrichment factors allow the identification of reliable proxies of the depositional environment and bioproductivity (Hatch and Leventhal, 1992; Dean and Arthur, 1998; Werne et al., 2002; Algeo and Maynard, 2004; Rimmer, 2004; Algeo and Lyons, 2006; Turgeon and Brumsack, 2006; Arnaboli and Meyers, 2007; Piper and Calvert, 2009; Tribovillard et al., 2012; Schoepfer et al., 2014; Azmy et al., 2015; Gao et al., 2016). Upon inspection, the TOC content of the Green Point shales was found to have variable correlations with different proxies both below and above the anomaly. Moderate to very good correlations are observed with the authigenic U ($R^2 = 0.51$), total U ($R^2 = 0.51$) and Mo ($R^2 = 0.78$) concentrations (Fig. 2.11). By contrast, TOC has moderate inverse-correlations with both Th/U ($R^2 = 0.61$) and U/Mo_{auth} ($R^2 = 0.44$). The correlation between TOC content and K/[Fe+Mg] is poor below the geochemical anomaly ($R^2 = 0.26$) and high above it ($R^2 = 0.72$). The P (ppm) and TOC contents have a weak inverse correlation below the anomaly ($R^2 = 0.32$) and a moderate correlation ($R^2 = 0.62$) above it. The ∑REEs show no correlation with TOC content below the anomaly yet have a high correlation above it ($R^2 = 0.71$). There is either a poor or no correlation between TOC content and Ce/Ce*, Fe_T/Al, and Ca, Sr, Ni, Al, K, Sc, Cs, Th and Cr abundance.

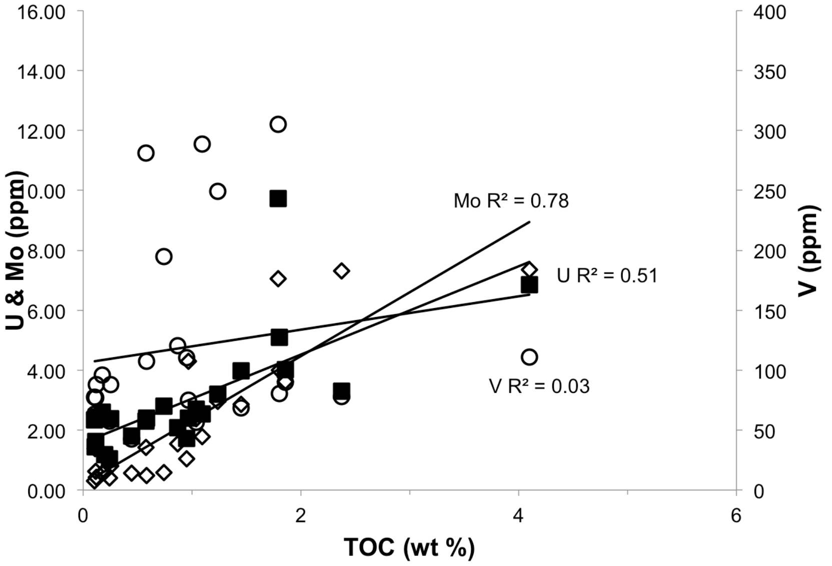

Figure 2.11: Scatter diagram of TOC (wt %) vs. V (ppm; circles), U (ppm; squares) and Mo (ppm; diamonds), showing significant correlations or lack there-of. Sample 166 data is not included. See text for details.

In summary, Mo and U concentrations, enrichment factors, authigenic U, Th/U and U/Mo_{auth} are most closely associated with TOC contents. This indicates that redox conditions, through the preservation of organic matter, is the most influential factor controlling TOC content, and resulting shale coloration (Rimmer et al., 2004; Burdige, 2007; McLaughlin et al., 2012). Redox control of TOC content is associated with low sediment accumulation rates (Canfield, 1994; Schoepfer et al., 2014). The slightly higher TOC correlation with Th/U compared to U is reflective of the Th/U ratio partially correcting for detrital effects (Wignall and Twitchett, 1996; Dean and Arthur, 1998). The lower inverse-correlation between TOC content and U/Mo_{auth} is reflective of U/Mo_{auth}'s sensitivity to variations in oxygen levels associated with suboxic conditions rather than being a good indication of anoxia normally associated with high TOC contents (Algeo and Maynard, 2004; McManus et al., 2006; Zhou et al., 2012). The lack of correlation between V (ppm), V/(V+Ni), V/Cr, Fe_T/Al and Ce/Ce* with TOC indicates these proxies' behaviors' are not closely coupled with TOC, and likely to be less reliable as proxies of redox conditions within the Green Point section.

The correlation of TOC and K/[Fe+Mg] or K was found to increase across the anomaly level. This could be reflective of several processes occurring. It could indicate that TOC concentrations were affected either by changes in the siliciclastic detrital or volcaniclastic flux to the sediments (see below; Dean and Arthur, 1998; Werne et al., 2002). This correlation does not however extend to most other siliciclastic detrital (Al, Cs, Th, Sc and Cr) or carbonate proxies (Ca and Sr). This indicates a direct relationship with either component is unlikely. When considering average TOC (0.97±0.93 wt%) is low compared to Al (5.8±1.2 wt%) or Ca (4.2±2.9 wt%), along with the lack of correlations, any potential organic carbon dilution of the detrital proxies is minimal (Dean and Arthur, 1998; Werne et al., 2002).

The lack of good correlations across the entire section between TOC and bioproductivity proxies such as P, Ni and Cu is further indication that redox conditions and not bioproductivity was the main control on the observed TOC content of the Green Point shales (Murphy et al., 2000; Rimmer et al., 2004). However, the observed and very different correlations below and above the anomaly between TOC and P merits further investigation.

The same importance of good correlations applies when comparing $\delta^{13}C_{org}$ ratios to elemental concentrations, ratios, or enrichment factors (Azmy et al., 2015; Gao et al., 2016). In contrast to TOC, there are no excellent correlations between $\delta^{13}C_{org}$ values and those of any other proxies utilized in the current study. Moderate correlations are observed between $\delta^{13}C_{org}$ and detrital proxies such as K content ($R^2 = 0.51$) and K/[Fe+Mg] ($R^2 = 0.51$) below the geochemical anomaly level. The $\delta^{13}C_{org}$ and ∑REEs values show a moderate correlation below the anomaly level ($R^2 = 0.52$) but none above it. The Th/U proxy has a moderate correlation with the $\delta^{13}C_{org}$ values below the anomaly ($R^2 = 0.49$) and a poor correlation above it ($R^2 = 0.32$). The $\delta^{13}C_{org}$ values have low or no correlation to V/Cr, authigenic U, U/Mo, Ce/Ce*, and Mo, U, V, Cu, Cr, Al, Cs, Th, Sc, Sr, Ca, Ni, and P abundances.

The $\delta^{13}C_{org}$ values exhibit an opposite stratigraphic trend to that of their TOC counterpart, with regards to its correlation to K and K/[Fe+Mg]. No further meaningful correlations are observed with other detrital proxies. This argues against overprint from allochtonous terrigenous sources (Wignall and Twitchett, 1996; Dean and Arthur, 1998; Werne et al., 2002; Śliwiński et al., 2010).

As the $\delta^{13}C_{org}$ composition of the Green Point sediments appears to be derived from photoautotrophic carbon fixation, the two main possible direct controls should be dissolved CO_2 compositions of the water column and the growth rates of the phototrophic organisms, namely phytoplankton, of the depositional environment in question (Popp et al., 1997). It may then be representative of either redox conditions or bioproductivity rates respectively. The moderate inverse correlation observed with TOC and similar, though less clearly defined, relationship with shale coloration would indicate redox variations as the primary control on carbon isotopes. There are however no good consistent correlations with either redox or bioproductivity proxies to either support or refute this. A very similar behavior observed was in the $\delta^{13}C_{carb}$ values of the interbedded carbonate rhythmites (Fig. 2.2; Azmy et al., 2015). This indicates sealevel variations may have affected dissolved CO_2 carbon isotope compositions and/or phototrophic activity, indirectly controlling shale $\delta^{13}C_{org}$ values (Gao et al., 2016).

2.5.3 Green Point Clastic Sediments

Deposition of the Green Point sediments occurred during a period of overall rising sea levels that started during the mid-to-late Cambrian and ended during the Ordovician. This resulted in an overall general transition from a siliciclastic muddy shelf to a carbonate mud-dominated platform (James et al., 1989; Lavoie et al., 2003; Boyce and Knight, 2005; Knight and Boyce, 2009). The sediments being delivered from the shelf to the slope became consequently less siliciclastic-rich and more carbonate-rich (James and Stevens, 1986; James et al., 1989; Cooper et al., 2001b; Knight et al., 2007). This is evident in the Green Point outcrops in Bed 22-23, where there is a change from the shale-dominated Martin Point Member to the interbedded-interlaminated carbonaceous shale and carbonate muds of the Broom Point Member (Fig. 1.2; James and Stevens, 1986).

2.5.3.1 Shale Carbonate Dilution

The potential for carbonate dilution within the shales of the Green Point section needs to be addressed, as visual inspection of hand samples and the application of HCl revealed the presence of carbonate material within several samples, mainly in the form of fine laminations within the laminated shales.

As $CaCO_3$ values were unavailable for this study, here we use Ca as a substitute. First, Ca was plotted against Sr, another mobile element that is enriched in chemical precipitates, and so is also representative of carbonate content (Nesbitt et al., 1980; Fedo et al., 1996; Dean and Arthur, 1998). A good correlation (Fig. 2.5) was found. Ca was also plotted against Na, a mobile element associated with Ca during chemical weathering of magmatic rocks, and no good correlation was found (Fig. 2.5; Nesbitt et al., 1980; Middlebug et al., 1988; Babechuk et al., 2014). This indicates Ca within the Green Point shales was mainly sourced from carbonate material and can be used to evaluate carbonate dilution.

Based on previous petrographic investigations of the interbedded carbonate rhythmites at Green Point and in the shales of the Cow Head Group, its composition is very likely to be calcite (Coniglio and James, 1990; Azmy et al., 2014). The observed calcite could be composed of unaltered clastic carbonate muds, could have undergone dissolution and re-precipitation very early during diagenesis, or a combination of both is present (Coniglio and James, 1990). Owing to the fine grain size and lack of thin sections of the shales at Green Point for this study, the Mg/Ca vs Sr/Ca scatter plot (wt % ratios) is used here to evaluate the origin of the carbonate material (Bayon et al., 2007; Picone et al., 2008). The Green Point data was compared to both the hypothetical end-members of Bayon et al. (2007) and geostandards for several different lithologies derived from Govindaraju (1989) (Fig. 2.12; Appendix 2.1). The Green Point data follows a similar trend to the siliciclastic geostandards (shales, silt, sandstone, most marine sediments), but with lower Sr/Ca ratios (Fig. 2.12). The same observation stands when comparing the Green Point data to the detrital end-member of Bayon et al. (2007). The lower observed Sr/Ca values are closer to the carbonaceous shale, a dolo-limestone and the HMC end-member of Bayon et al. (2007). The carbonate material influencing the siliciclastic variations is thus likely composed of mainly early diagenetic HMC, unlike the interbedded rhythmites. Dilution of the detrital indicators must be evaluated (Dean et al., 1998; Werne et al., 2002).

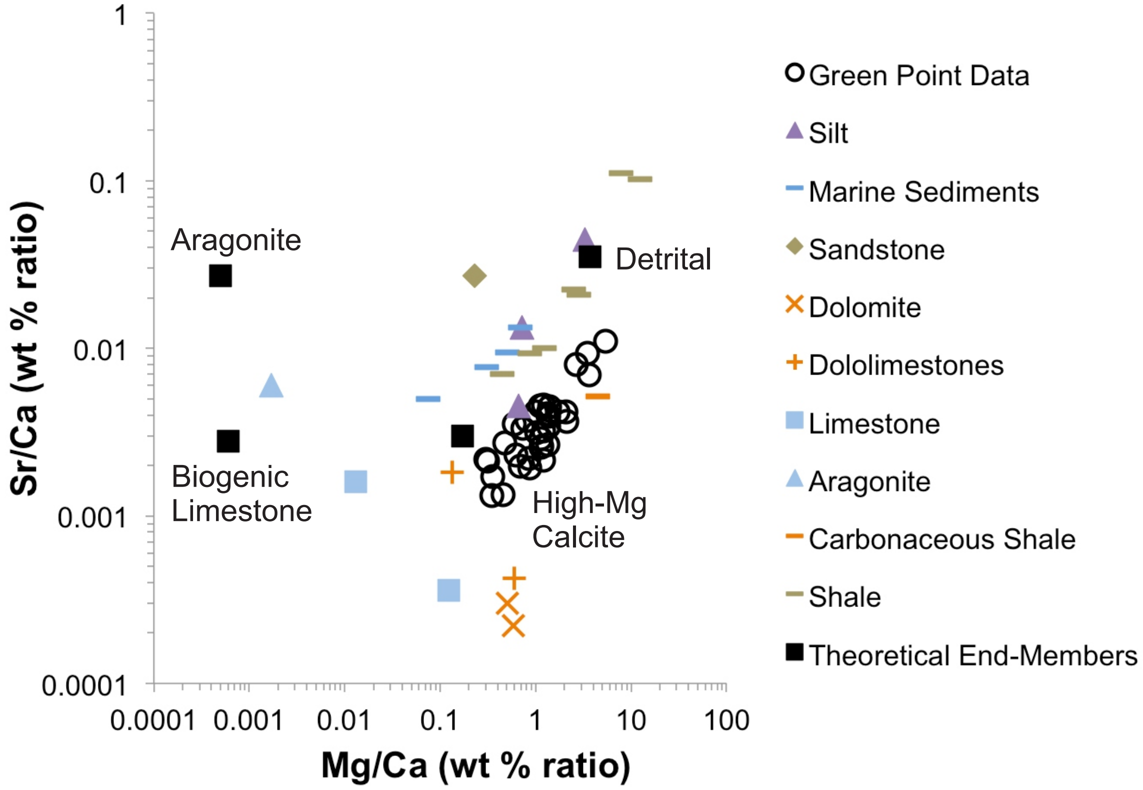

Figure 2.12: Scatter diagram of Mg/Ca (wt % ratio) vs. Sr/Ca (wt % ratio) values from the Green Point shales, lithological data from Govindaraju (1989) and the theoretical end-members of Bayon et al. (2007). See text for details.

Shale elemental detrital indicators were compared to Ca (Fig. 2.13). Variable but consistant negative correlations with Ca are as follows: Cr (R^2 = 0.74), Al (R^2 = 0.74), Sc (R^2 = 0.64), Cs (R^2 = 0.52), K (R^2 = 0.41) and Th (R^2 = 0.33). These consistent negative correlations between Ca and all detrital indicators strongly support carbonate material being the main diluting factor for the detrital fraction (Dean et al., 1998; Werne et al., 2002).

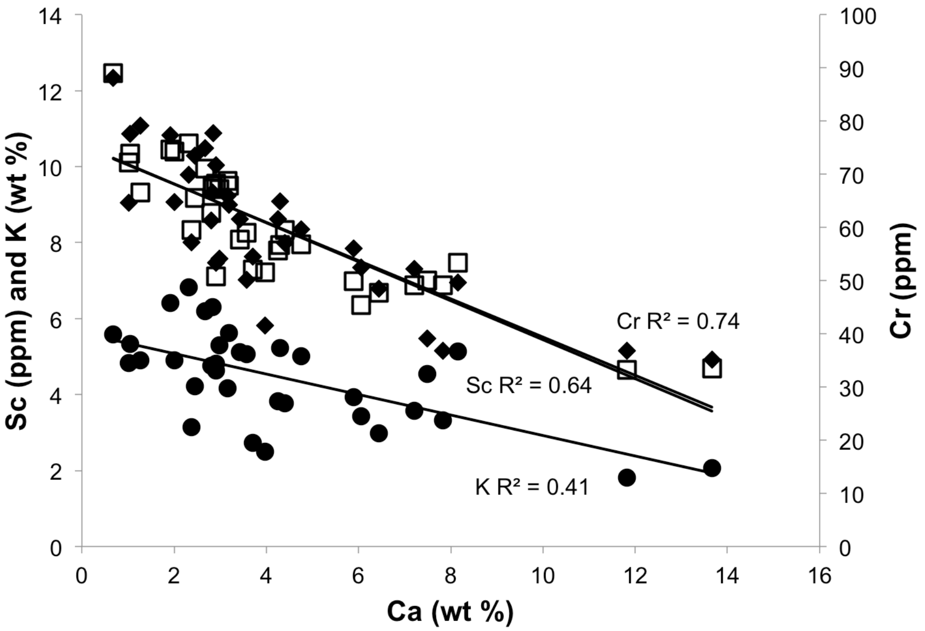

A)

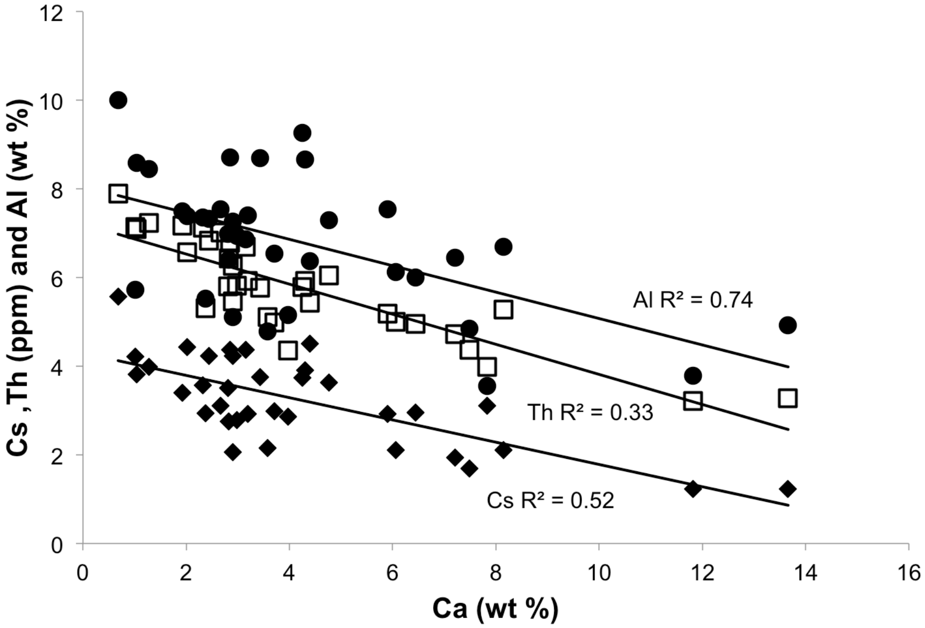

B)

Figure 2.13: Scatter diagram of Ca (wt %) vs detrital proxies. (A) Ca vs Sc (ppm; diamonds), K (wt %; circles) and Cr (ppm; squares) concentrations. (B) Ca vs Cs (ppm; diamonds), Th (ppm; squares) and Al (wt %; circles) values from the Green Point shales. See text for details.

2.5.3.2 Immobile Elements

Several elements that remain immobile during chemical weathering have shone good potential as detrital proxies in shales, as they remain within refractory minerals or are likely to be absorbed by clays and so form part of the detrital input in shales. Their increase indicates stronger weathering and thus higher detrital components (Nesbitt et al., 1980; Middleburg et al., 1988; Condie et al., 1995; Nesbitt and Markovics, 1997; Wei et al., 2003; 2006; Zhao and Zheng, 2014; 2015). Siliciclastic detrital proxies investigated here include Al, K, Cr, Sc, Th and Cs (Nesbitt et al., 1980; Dean and Arthur, 1998; Schnetger et al., 2000; Jiménez-Espejo et al., 2007; Martinez et al., 2007; Śliwiński et al., 2010; Zhao and Zheng, 2015). As scandium is one of the most immobile elements during chemical weathering, strong correlations of other detrital proxies to Sc are a good indicator of immobile behavior (Middleburg et al., 1988; Condie te al., 1995; Nesbitt and Markovics, 1997; Zhao and Zheng, 2015). Correlations to Sc are presented in Figure 2.14. The moderate correlation of K to Sc, the lowest found, indicates some K may have been removed (Nesbitt et al., 1980; Nesbitt and Young, 1989). Good to excellent correlations were found between Sc and Cs, Th, Cr, and Al, indicating they remained dominantly immobile during weathering, and in the case of Cr, unaffected by redox conditions, making them reliable siliciclastic detrital proxies (Fig. 2.14; Nesbitt et al., 1980; Chesworth et al., 1981; Middleburg et al., 1988; Schnetger et al., 2000; Wei et al., 2003; 2006; Śliwiński et al., 2010; Reinhard et al., 2014; Zhao and Zheng, 2014; 2015).

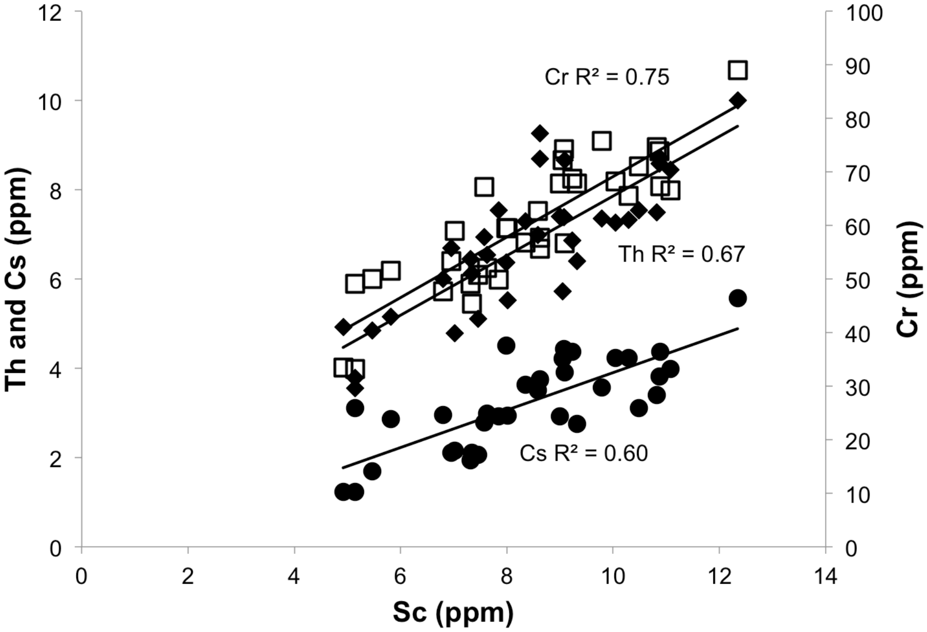

A)

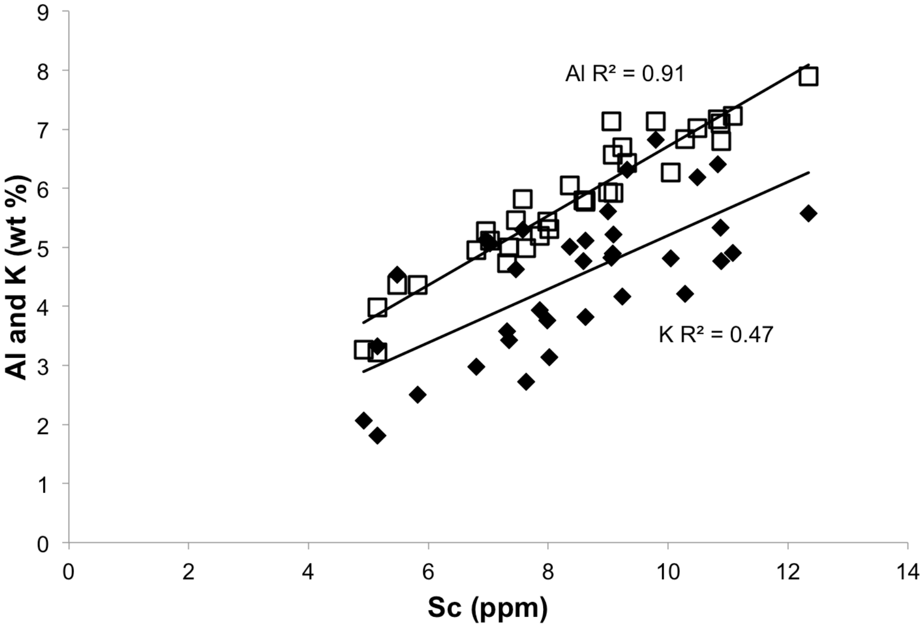

B)

Figure 2.14: Scatter diagram of Sc (ppm) vs other detrital proxies. (A) Sc vs Th (ppm; diamonds), Cs (ppm; circles) and Cr (ppm; squares) concentrations. (B) Ca vs K (wt %; diamonds) and Al (wt %; squares) values from the Green Point shales. See text for details.

2.5.3.3 Siliciclastic Sediment Composition and Provenance

To mitigate the impact of carbonate dilution, elemental ratios are used here to evaluate detrital variations up-section (Werne et al., 2002; Zhao and Zheng, 2015). Th/Sc ratios within the Green Point shales vary between 0.63 and 1.08 (Fig. 2.4). They have a mean of 0.82±0.11, (Table 2.1, similar to PAAS (0.91), UCC (0.79) and NASC (0.82) values in particular (Gromet et al., 1984; Taylor and McLennan, 1986; McLennan et al., 2001). Th/Sc ratios have previously been found to vary greatly, depending on provenance (McLennan et al., 1993). Within the Green Point shales, only minor Th/Sc variations are observed up-section (Table 2.1; Fig. 2.4) indicating little variability in the detrital source potentially occurred (McLennan et al., 1993; Zhao and Zheng, 2015). When compared to modern deep-sea turbidite muds, Th/Sc ratios from the Green Point shales are closest to trailing edge margin basin values (McLennan et al., 1990). This indicates the Green Point siliciclastic sediments were dominantly derived from the Laurentian trailing edge margin, and not the approaching the Taconic island arc. Furthermore, the Th/Sc range for trailing edge margin sediments (McLennan et al., 1990) is quite similar to the observed range of values for the Green Point sediments, implying the variability in the Green Point sediments is a result of variations in the composition of the weathered Laurentian source.

Another good indicator of provenance is the La-Th-Sc system (Bhatia and Crook, 1986; Cullers and Stone, 1991; Cullers, 1994), as LREEs have previously been found to be sensitive indicators of source rock variations, due to immobility during chemical weathering (Nesbitt, 1979; Middleburg et al., 1988). To evaluate LREE immobility in the Green Point section, La was first plotted against Th and Sc. When the whole section was plotted, correlations were very low. When plotted within the La-Th-Sc ternary diagram (Fig. 2.15), nearly all samples plotted within (or very near to) the field of post-Archean shales, which straddles the fields of active-passive margins and continental arcs (Taylor and McLennan, 1985; Bhatia and Crook, 1986; McLennan et al., 1990). They are likely dominantly derived from the Laurentian trailing edge margin (McLennan et al., 1990). There are 4 samples (Sa 26, Sa 27, Sa 71, Sa 84) that did not plot in or near the post-archean shale field, having lower proportions of La relative to Th and Sc. They plotted within the continental arc field (Fig. 2.15). The observed La variability potentially reflects La depletion in those samples or the greater influence of a second minor source with a more La-rich composition that may be more immature.

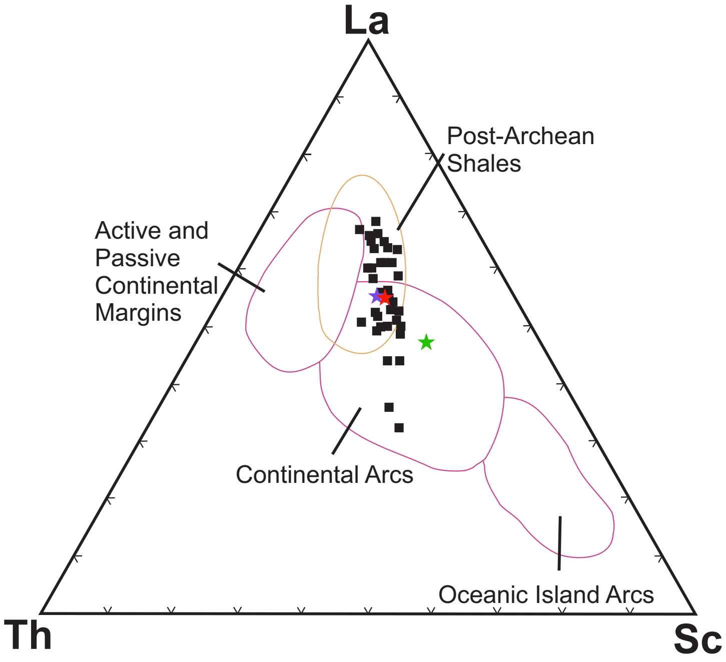

Figure 2.15: Ternary La-Th-Sc system diagram for the Green Point shales. The ocean island arc, continental arc and active-passive continental margin fields are derived from Cullers (1994). The post-Archean shale field is derived from Taylor and McLennan (1985). The stars represent the Japan Arc (green), UCC (red) and PAAS (blue) standard values (Taylor and McLennan, 1985; Togashi et al., 2000; McLennan, 2001). See text for details.

The K/[Fe+Mg] ratio has previously been used as an indicator of clay provenance (Dean and Arthur, 1998; Werne et al., 2002). The K/[Fe+Mg] values (0.74±0.30) of the Green Point section are high (though very variable) relative to PAAS (0.48) and UCC (0.58; Table 2.1; Fig. 2.4; Taylor and McLennan, 1985; McLennan, 2001), indicating a dominantly siliciclastic detrital source for the clays, namely Laurentia, and only a relatively minor input from the likely volcaniclastic ash clay source, the Taconic Arc (Dean and Arthur, 1998; Werne et al., 2002). This agrees with Th/Sc data and the La-Th-Sc ternary plot results. The K/[Fe+Mg] variations also follow the systems tracts based on the carbon isotope stratigraphy (Fig. 1.2;

Azmy et al., 2015) for the section, reflecting variations in sealevel. Overall, the ratios increase during the first HST, decrease during the following LST and TST systems tracks, before increasing slightly again during the final HST. The observed decrease during the LST and TST systems tracks is consistent with the decrease in radiogenic Os fluxes to the basin documented by Tripathy et al. (2014) within the same beds (Fig. 2.4). This suggests either a decrease in material derived from continental weathering or an increase in the input of volcanic ash during this period. However, the associated slight decrease in Th/Sc ratios and elemental detrital proxy concentrations within the same beds (Fig. 2.4) support the former scenario.

2.5.3.4 Sediments Deposited along the Laurentian Slope

As carbonate material within the shales is either clastic in nature or a result of early diagenesis (Coniglio and James, 1990), proportions of Ca and detrital indicators (Sc, Cr, Al, Th, Cs, K) can be used to broadly evaluate the change in the proportions of carbonate and siliciclastic material being deliverered to the slope up-section. The Sc, Th, Al, Cs, K and Cr detrital proxies all consistently decrease upward across the geochemical anomaly level (Fig. 2.4), supported by unpaired t-tests for Sc, Th, Al, Cs and Cr (Table 2.1). This reflects an overall decrease in the fraction of the sediments being derived from weathering of the Laurentian Craton above the anomaly level. Though values are more scattered, resulting in high two-tailed *P* values, the opposite trend is observed for Ca (Table 2.1). This is to be expected as the platform becomes more carbonate dominated, evidenced by the more frequent occurrence of carbonate rhythmites up-section (Fig. 1.2). The variations in detrital proxy concentrations correlate well with the associated relative sea level changes (Fig. 1.2), increasing during the first HST (Beds 17-18), decreasing during the subsequent LST and TST (Beds 20-24), and increasing again during the following HST (Beds 25-26; Figs. 1.2; 2.4). The opposite (though more scattered) trend is observed for Ca. Sealevel variations are interpreted based on the above evidence to be the main control mechanism for the sediments deposited to the slope, most profoundly affecting the magnitude of clastic carbonates' transport to the distal slope.

There does remain some uncertainty in this interpretation as thin sections of the shales and several well-sorted elements (Si, Zr, Ti and Hf) used in detrital sediment investigations are unavailable. This limits our interpretation, notably with regards to sediment sorting and sedimentary recycling (McLennan et al., 1990; Werne et al., 2002; Bouchez et al., 2011; Zhao and Zheng, 2015).

2.5.4 Paleoredox Proxy Variations

2.5.4.1 Elemental Proxies

The redox-sensitive trace metals Mo, U and V are reliable proxies of depositional redox conditions, due to their sensitivity to changes in the oxygen levels of bottom waters and sediment pore fluids (Dill, 1986; Wignall and Myers, 1988; Hatch and Leventhal, 1992; Jones and Manning, 1994; Jiang et al., 2006; Tribovillard et al., 2006; Algeo and Tribovillard, 2009; Scott and Lyons, 2012; Zhou et al., 2012; Partin et al., 2013; Basu et al., 2014; Tripathy et al., 2014). Oxygen levels in the water influence the oxidation state of Mo, U and V, affecting their aqueous solubility and potential for authigenic precipitation (Wignall and Twitchett, 1996; Tribovillard et al., 2006; Arnaboldi and Meyers, 2007; Wignall et al., 2007).

Uranium concentrations within marine sediments are subject to many influences, and so its origin must be evaluated for U to be considered a viable redox proxy. Some U is derived from chemical and physical weathering, having a consistent concentration in purely detrital sediments (2-3ppm; Scott, 1982; Organo, 1997). Uranium is also present within biogenic sediments, namely carbonate and siliceous material. Previous petrographic evaluation of the Green Point sediments did not reveal any siliceous material (Coniglio and James, 1990; Azmy et al., 2014). Uranium concentrations within the Green Point carbonate rhythmites (interbedded with the shales) were found to be low (Azmy et al., 2015) and so carbonate material within the shales is considered a diluting factor (Organo, 1997). Authigenic U is formed within pore-waters or on the seafloor, following sediment deposition. Authigenic U removed from the pore-waters to fine-grained siliciclastic sediments increases with decreasing $[O_2]_{aq}$, thus becoming more efficient from suboxic to anoxic-sulfidic conditions (Cochran, 1992; Morford and Emerson, 1999; Dunk et al., 2002; Algeo and Tribovillard, 2009; Partin et al., 2013; Basu et al., 2014). It is enriched within metalliferous Fe-Mn crusts, mineral phases, organic carbon or organic carbon-coated clays (Kuzendorf et al., 1983; Organo et al., 1997; Cumberland et al., 2016; Bone et al., 2017a). Lastly, it can be derived from hydrothermal activity near mid-ocean ridges, though this last source is not interpreted to be present in the Green Point sediments (Rydell and Bonatti, 1973; Shimmield and Price, 1988). Uranium concentrations within the studied shales are highly variable with a range of 1.04-13.40 ppm (Table 2.1). Calculated PAAS-normalized enrichment factors (U EF_{PAAS} = 0.64 to 4.45; mean U EF_{PAAS} = 1.49±0.93; Table 2.3) indicate that some samples were significantly enriched in U, whereas negligible enrichment and potential depletion is observed in others. To evaluate the proportion of U derived from a detrital source, and resulting depletion or enrichment, the modified method of Organo (1997) was employed. Calculated detrital U ($(U_{ter})_x$; Table 2.5) within the sediments was low relative to purely detrital sediments (Scott, 1982), which is expected within carbonaceous shales. They remained relatively consistent like the detrital proxies (Al, Sc, Th). Its proportion of total U ($(\%U_{ter})_x$) however varies widely (12 to 114%) and was inversely proportional to PAAS-normalized enrichment factors (Fig. 2.16). High $(\%Ut_{er})_x$ values indicate low to no authigenic enrichment. 3 samples (Sa 44, Sa 61 and Sa 84) had values higher than 100%, indicating depletion possibly occurred. Samples that have very low enrichment factors (U $EF_{PAAS} < 1.20$; U $EF_{Average\ Shale} \leq 1.25$; Table 2.4) and high $(\%U_{ter})_x$ values have good correlations between U and Al contents (R^2 = 0.70; Fig. 2.9; Appendix 2.1), supporting a dominant detrital origin for U in these samples, with little or no authigenic contribution normally associated with low O_2 conditions (Table 2.4; Appendix 2.1; Calvert and Pedersen, 1993; Tribovillard et al., 1994; Hild and Brumsack, 1998; Böning et al., 2004; Algeo et al., 2004; Tribovillard et al., 2006). These samples are associated with green shales and low concentrations of organic matter, which if present, would have acted as an adsorption surface for U enrichment within porewaters (Bone et al., 2017a). All 3 samples with indicated U depletion fall within this category. In addition to enhancing authigenic enrichment, organic matter would also have acted as a buffer, which limits changes to porewaters' redox potential due to the oxidizing influence of O_2. The lack of organic matter would increase the potential for U release from the sediments (Bone et al., 2017b). This is further compounded by the presence of early-diagenetic carbonate material within the shales, which would indicate the presence of bicarbonate within the porewaters near the sediment-water interface. This would promote U desorption from these sediments (Alam and Cheng, 2014). The green shale coloration, low organic matter content, low U enrichment factors and some depletion within these samples imply oxic to slightly suboxic conditions during their deposition, or exposure to these same conditions during very early diagenesis (Algeo and Tribovillard, 2009; McLaughlin et al., 2012; Bone et al., 2017b). However, most samples show variable but greater authigenic enrichment in U. The higher U concentrations (4.07±2.22ppm) and enrichment factors (mean EF_{PAAS} = 2.01±0.97; $EF_{Average\ Shale}$ = 2.19±1.06) correlate well with the organic-rich grey and black shales, which are mainly located above the geochemical anomaly level (Fig. 2.7). $(\%U_{ter})_x$ values of these samples are also much lower than within the samples with low EFs (Table 2.5; Appendix 2.3). Black shale samples from Green Point were also analyzed by Tripathy et al., (2014) and were found to have similar enrichment factors ($EF_{Average\ Shale}$ = 2±1) to those of the current study. The presence of black shales associated with elevated U EFs indicates that anoxic conditions were intermittently present within the basin (Algeo and Maynard, 2004; Algeo and Tribovillard, 2009). Though anoxia was reached, no periods of euxinia appear to have occurred within the basin, based on the low Mo concentrations across the whole section (<25ppm; Mean = 3.2±4.7; Scott and Lyons, 2012). This interpretation is supported by a moderate correlation between U and TOC contents ($R^2 = 0.51$; Fig. 2.11), which is typically observed for shales deposited from oxic (low U and TOC contents) to anoxic and non-sulfidic (high U and TOC contents) waters, but not for shales deposited from euxinic waters (more scattered U-TOC covariation) (Algeo and Maynard, 2004; Tribovillard et al., 2006). The observed Cr variations further support this. Authigenic Cr becomes enriched within sediments when sulphidic conditions are prevalent (ex. Cariaco Basin; Reinhard et al., 2014). Within the Green Point section, Cr correlates very well with other detrital proxies such as Sc and has very low enrichment factors (mean EF_{PASS} = 0.88±0.07). This indicates that no significant authigenic Cr enrichment occured, supporting the conclusion that sulfidic conditions were not attained (Reinhard et al., 2014).

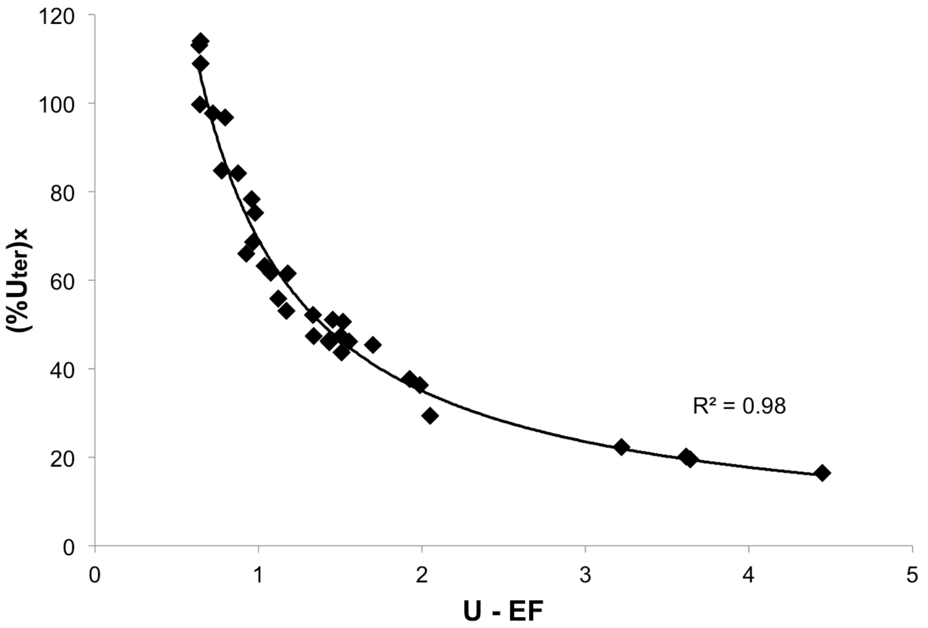

Figure 2.16: Scatter diagram of U-EF (PAAS) vs $(\%U_{ter})_x$ values from the Green Point shales. See text for details.

Molybdenum removal from the water column to sediments increases with decreasing $[O_2]_{aq}$. When bottom water oxygen contents are elevated (oxic to slightly suboxic), resulting in the presence of an oxic zone, strong Mn-oxide zone and no sulfidic zone within the sediment pore-waters, no authigenic enrichment or even Mo depletion is observed (Canfield and Thamdrup, 2009; Scott and Lyons, 2012). Moderate Mo enrichments (<25ppm) are observed in sediments deposited from strongly suboxic bottom waters (smaller oxic and Mn-oxide zones and sulfidic zone present in the sediments), or anoxic/ferruginous bottom waters (where the oxic and Mn-oxide zones are absent in the sediments; Scott and Lyons, 2012). Pronounced Mo enrichment (>25ppm) occurs in sulfidic sediments deposited from euxinic bottom waters (Algeo and Lyons, 2006; Kendall et al., 2010; Scott and Lyons, 2012). A tight correlation between Mo and TOC contents was observed ($R^2 = 0.78$; Fig. 2.11). Molybdenum also has a very similar pattern of enrichment to U, supported by a moderate correlation between the two metals ($R^2 = 0.56$; Figs. 2.7 and 2.8). However, in samples where U EFs are low and U (ppm) is well correlated with Al contents, an insignificant correlation between Mo and either Al or U content is observed, despite the low Mo EFs (Mean: $EF_{PAAS} = 0.98$, $EF_{\text{Average Shale}} = 0.93$; Table 2.4; Fig. 2.9). Some Mo EFs even indicate depletion of Mo relative to PAAS values (Minimum Mo $EF_{PAAS} = 0.34$). This indicates that the detrital component has at most a minor impact on final shale Mo concentrations. This is consistent with the presence of strong oxic and Mn-oxide zones being present in the shallow sediment pore-waters, where either no enrichment or Mo depletion from Mn-nodules occurs (Scott and Lyons, 2012). Thus, the samples with low authigenic Mo, U EFs and non-detrital U components (based on $(\%U_{ter})_x$ values) are consistent with sediments and shales from previously observed oxic to slightly suboxic bottom water conditions (Fig. 2.8; Algeo and Tribovillard, 2009; Tribovillard et al., 2012; Scott and Lyons, 2012). The Mo EF values of the more authigenically enriched samples in this study (Mean: $EF_{PAAS} = 6.36 \pm 5.38$; $EF_{\text{Average Shale}} = 4.06 \pm 3.44$; Table 2.4) are higher than those of the black shale samples (4±3) analyzed by Tripathy et al., (2014). The higher Mo EF and U EF values of the authigenically-enriched samples suggest the sulfate zone within the porewaters was much closer to the water column and resulted in much greater authigenic Mo enrichment. However, Mo concentrations did not exceed 25ppm (Table 2.1). This would indicate the presence of more intensely suboxic to anoxic-ferruginous bottom water conditions being present (Fig. 2.17; Scott and Lyons, 2012). Ocean circulation conditions are interpreted as weakly restricted across the whole section, based on the trend of U EF_{PAAS} and Mo EF_{PAAS} covariation (Fig. 2.17; Algeo and Tribovillard, 2009; Tribovillard et al., 2012).

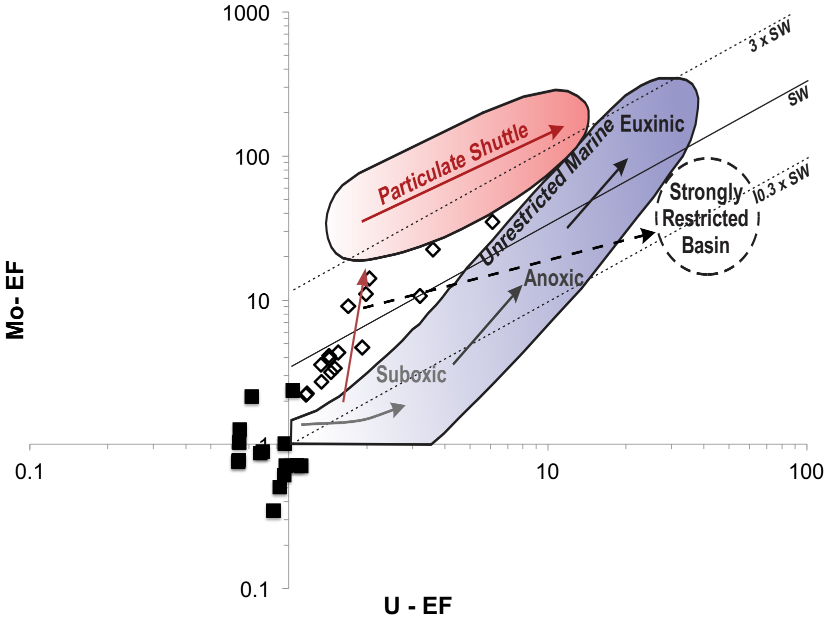

Figure 2.17: General Mo EF vs U EF co-variation for modern marine environments. The blue field represents an open marine unrestricted environment. The red field represents the Fe-Mn particle shuttle field related to weak basin restriction represented by the euxinic Cariaco Basin. The dashed field represents strongly restricted environments, such as the Black Sea. Diagonal lines represent multiples of the Mo:U ratio of modern day seawater, based on an average weight ratio of 3:1 to compare with sediment weight ratios (modified from Algeo and Tribovillard, 2009; Tribovillard et al., 2012). The black square symbols represent samples with both low Mo and U EFs as well as having a good correlation between U and Al (ppm). The unfilled diamonds represent samples with high Mo and U EFs as well as having a low U-Al (ppm) correlation.

Vanadium occurs as a hydrolyzed vanadate species in oxygenated waters (Turner et al., 1981; Sadiq, 1988; Wehrli and Stumm, 1989; Emerson and Huested, 1991). In suboxic to anoxic conditions, it becomes progressively less stable, becoming vanadyl that can be either hydrolyzed or become insoluble $VO(OH)_2$

species (Van der Sloot et al., 1985). In sulfidic conditions, when high dissolved sulfide levels are present, V is reduced to V (III) and precipitated from solution (Wanty and Goldhaber, 1992). The V contents of the shales in the current study increase above the geochemical anomaly (Table 2.1) and the V profile shows a strong positive shift associated with the geochemical anomaly level (Fig. 2.7). The samples with low V enrichments relative to average upper crust correlate well with green shale beds, U (R^2 = 0.55) and have a moderate correlation with Al (R^2 = 0.39 for samples with good U-Al correlations; Fig. 2.9; Appendix 2.1), suggesting a partial detrital V contribution as was noted for U (Lewan and Maynard, 1982). However, the pattern of V enrichment does appear to depart from Mo, U and TOC as evident by the lack of significant correlations (V vs. U: R^2 = 0.29, V vs Mo: R^2 =0.05, V vs TOC: R^2 =0.03; Fig. 2.11). This suggests that TOC was not the main host phase for V and instead a different mechanism was responsible for the high V concentrations observed in the most V-enriched samples (Sa 53; Sa 63; Sa 66; Sa 79; Sa 157). However, no other element appears to behave in the same way as V in these anomalous samples. Neither are there any obvious relationships between the behavior of V and the observed changes in the lithology of the Green Point section. Therefore, V variations must be regarded with caution.

2.5.4.2 Elemental Ratios

The concentration ratios of some elements in shales (e.g., V/Cr, V/[V+Ni], authigenic U, Th/U, U/Mo and Fe_T/Al) are useful paleoredox proxies (Wignall and

Myers, 1988; Hatch and Leventhal, 1992; Jones and Manning, 1994; Wignall and Twitchett, 1996; Webb and Kamber, 2000; Lyons et al., 2003; Lyons and Severmann, 2006; McManus et al., 2006; Algeo and Tribovillard, 2009; Poulton et al., 2010; Śliwiński et al., 2010; Zhou et al., 2012). However, they have to be used with caution, since the redox boundaries developed for several of those ratios (V/Cr, V/[V+Ni] and authigenic U) were derived from studies of shales deposited in shelf conditions (Wignall and Myers, 1988; Hatch and Leventhal, 1992; Jones and Manning, 1994; Wignall and Twitchett, 1996) rather than slope environments. They are also more suitable to differentiate between anoxic/non-sulfidic (ferruginous) and anoxic/sulfidic (euxinic) conditions (Rimmer, 2004; Lyons and Severmann, 2006; Poulton et al., 2010; Śliwiński et al., 2010; Poulton and Canfield, 2011; Zhou et al., 2012; Porter et al., 2014; Azmy et al., 2015) but not for changes between oxic-slightly suboxic and relatively more suboxic/anoxic conditions. Therefore, the stratigraphic trends of their ratios can be used mainly to reflect relative changes of reducing conditions for qualitative evaluation but the exact values cannot be utilized for quantitative assessment of environmental settings.

According to Jones and Manning (1994), V/Cr ratios of <2 indicate oxic conditions, 2 – 4.25 dysoxic conditions, and >4.25 suboxic to anoxic conditions. The V/Cr ratios of the Green Point shales fall in all 3 fields. However, only values above the geochemical anomaly plot in the suboxic to anoxic field, indicating that conditions became relatively more reducing, at least intermittently up section. This agrees closely with the pattern of V enrichment, with a high correlation ($R^2 = 0.91$;

Fig. 2.7) reflecting a minimal influence on the proxy by detrital Cr variations throughout the section.

The V/(V+Ni) ratios of 0.46 to 0.60 have been reported to indicate dysoxic conditions, 0.54 to 0.82 anoxic/non-sulfidic conditions, and >0.84 euxinic conditions (Hatch and Leventhal, 1992; Śliwiński et al., 2010; Porter et al., 2014). The Green Point values plot in the anoxic field across the section as well as in the euxinic field above the geochemical anomaly level, indicating a decrease in water column oxygenation (Table 2.1). Correlation between V/(V+Ni) ratios and V concentrations is lower than for V/Cr ratios versus V concentrations, but still good ($R^2 = 0.63$). The higher than expected V/(V+Ni) values are probably a result of low bioproductivity, which resulted in low Ni enrichment (a bioproductivity proxy; see section 2.5.5). In addition, variations of the profile across the geochemical anomaly are considered statistically insignificant.

The oxidation state of U is influenced by water column and pore-water oxygenation and (potentially microbially mediated) dissolved sulfide content (Anderson et al., 1989; Barnes and Cochran, 1991; Wignall and Twitchett, 1996; Tribovillard et al., 2006; Arnaboldi and Meyers, 2007; Wignall et al., 2007; Rolison et al., 2017). In oxidizing environments, U is present as soluble uranyl carbonate (Wignall and Twitchett, 1996). Its potential for authigenic precipitation and removal to marine shales increases with decreasing pore-water $[O_2]_{aq}$, as U is reduced from U^{+6} to U^{+4} (Wignall and Twitchet, 1996; Partin et al., 2013). Thorium, on the other hand, remains unaffected by changes in redox conditions (Wignall and Twitchet, 1996). According to the work of Wignall and Myers (1988), authigenic U = U – Th/3. Authigenic U ≤1 generally indicates oxygenated environments, whereas authigenic U >1 is an indicator of anoxic conditions. Across the whole section, the authigenic U ratios span the anoxic and oxic fields (1.17±2.47; Table 2.1) and they correlate significantly with U concentrations ($R^2 = 0.94$) and moderately with TOC values ($R^2 = 0.51$). The general increase of authigenic U values above the anomaly level suggest an overall decrease of oxygen levels in the water column (Table 2.2; Fig. 2.7), which is consistent with a general sea level rise (e.g., Azmy et al., 2015). However, some caution has to be taken when interpreting absolute values as some of the lowest values are negative, even if these values are consistent with low U EFs. A Th/U ratio of <2.0 has been known to represent anoxic conditions, whereas Th/U ratios >2.0 may indicate oxic conditions (Wignall and Twitchett, 1996). The Th/U ratio of the Green Point shales decreases above the anomaly level (Table 2.1; Fig. 2.7), thus supporting a decrease in O_2 levels (e.g., Wignall and Twitchett, 1996). These Th/U values are high when compared with those of the interbedded carbonates (Azmy et al., 2015) that all fell within the anoxic field. This difference is due to a higher detrital Th content in the shales.

The U/Mo_{auth} ratios have a generally inverse correlation to increasing basin anoxia, because the Mo burial rate into sediments increases relative to U as conditions become more reducing. High U/Mo_{auth} ratios are associated with oxic to suboxic conditions whereas low ratios indicate anoxic/non-sulfidic to euxinic conditions (McManus et al., 2006; Zhou et al., 2012). The U/Mo_{auth} ratios of the current study are variable and the mean values decrease above the geochemical anomaly level from 0.88±0.67 to 0.55±0.31, suggesting lower O_2 levels (Table 2.2; Fig. 2.7, which is consistent with the sea level rise. The highest U/Mo_{auth} ratios are associated with the samples from green shales that have good U-Al correlations and low TOC contents, primarily within beds 20-22 (Fig. 2.7). These higher values, up to 2.54, should represent slightly suboxic to potentially oxic conditions (Table 2.1). The lower U/Mo_{auth} values above the geochemical anomaly level agree with the change seen in other proxies (Fig. 2.7).

As sedimentary iron becomes authigenically enriched in anoxic conditions, the total iron to aluminum ratio can be another useful redox proxy of anoxia, characterized by $Fe_T/Al > 0.5$ (Lyons et al., 2003; Lyons and Severmann, 2006; Poulton et al., 2010). Though the average Fe_T/Al ratio is 0.50±0.09, several samples have much higher ratios, up to 0.77 (Appendix 2.1). This supports the interpretation of intermittent anoxia being present during the deposition of this section, based on the U and Mo data. Fe_T/Al ratios can also be used in conjunction with Mo concentrations to differentiate between ferruginous and sulfidic conditions. High Fe_T/Al associated with high Mo enrichments indicates sulfidic conditions, but an association with low Mo enrichments suggests ferruginous conditions (Lyons and Severmann, 2006; Kendall et al., 2010; Scott and Lyons, 2012; Sperling et al., 2013). As Mo concentrations at Green Point (<25 ppm) are low when compared to modern euxinic basins (Algeo and Lyons, 2006; Scott and Lyons, 2012), ferruginous conditions likely occurred during the intermittent anoxic intervals. However, a lack of correlation between Fe_T/Al ratios and other redox proxies, including, Mo, U, U/Mo, Th/U and V/Cr was identified. High individual Fe_T/Al were not found to be associated with high occurrences of Mo, U or TOC (Appendix 2.1). Neither was an increase in Fe_T/Al mean values observed at the geochemical anomaly level, as most proxies suggest. This indicates that this proxy must be used with caution here due to its different behavior to other indicators of anoxia.

The stratigraphic trends of the V/Cr, V/(V+Ni) and authigenic U ratios show a general increase across the investigated section based on the change in mean values below and above the geochemical anomaly level (Table 2.1; Fig. 2.7). By contrast, the Th/U and U/Mo ratios decrease instead. This suggests a consistent change towards relatively more reducing conditions, but full bottom water anoxia was likely reached only intermittently (Fig. 2.7; Wignall and Myers, 1988; Hatch and Leventhal, 1992; Jones and Manning, 1994; Wignall and Twitchet, 1996; McManus et al., 2006; Zhou et al., 2012).

2.5.4.3 Ce/Ce* Anomaly

Due to the redox control of cerium in the ocean (i.e., Ce^{3+} is oxidized to Ce^{4+} in oxygenated conditions and is removed from seawater as particulate Ce to Fe-Mn oxides; Sholkovitz et al., 1994), the Ce anomaly (Ce/Ce*) is a reliable proxy for the redox conditions during deposition of marine carbonates (Bau and Dulski, 1996; Nozaki, 2001; Bolhar et al., 2004). However, the same concept was recently applied to clastic sediments such as black shales (Ganai and Rashid, 2015) and found to provide reliable results. The Ce/Ce*$_{SN}$ ratio was calculated using two formulas Ce/Ce*$_{SN}$ (1) = 2Ce/(La + Pr) and Ce/Ce*$_{SN}$ (2) = Ce/(2Pr – Nd) (Bau and Dulski, 1996; Bolhar et al., 2004). The two formulas were evaluated to verify their viabilities, as within the first, used in previous studies of the same section, a majority of the samples demonstrated a positive La anomaly when Ce/Ce*$_{SN}$ (1) was plotted against the Pr/Pr*$_{SN}$ anomaly (3) (Fig. 2.18; Bau and Dulski, 1996). The Ce/Ce* ratios calculated from both equations have a moderate to good correlation ($R^2 = 0.63$), indicating that the Ce/Ce* calculation (1) applied to the Green Point carbonates of this section (Azmy et al., 2014; 2015) may not accurately portray the behavior of Ce. The formula (2) was used.

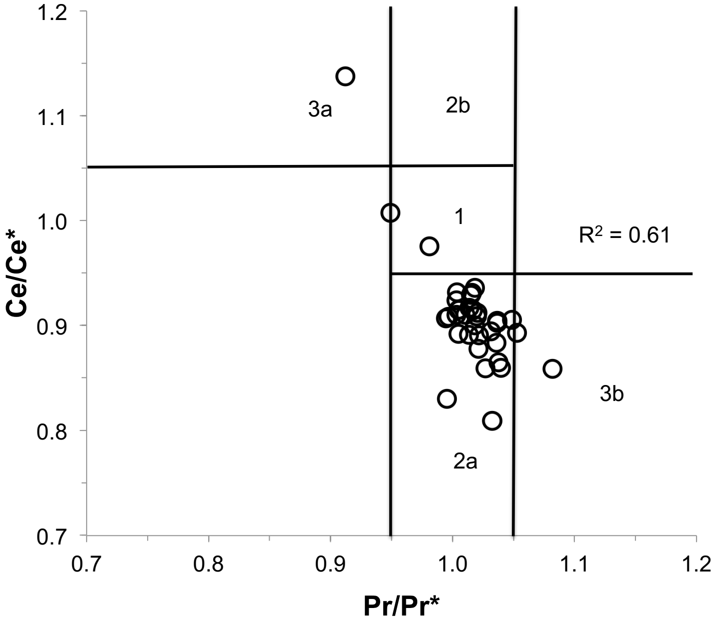

Figure 2.18: Scatter diagram of Ce/Ce* vs Pr/Pr*. 1 = no anomalies, 2a = positive La$_{sn}$ anomaly, no Ce$_{sn}$ anomaly, 2b = negative La$_{sn}$ anomaly, no Ce$_{sn}$ anomaly, 3a = positive Ce$_{sn}$ anomaly. 3b = negative Ce$_{sn}$ anomaly (from Bau and Dulski, 1996).

In terrigeneous sediments, very low Ce/Ce* (2) values (<0.1) are associated with anoxic conditions and higher values (>0.1) with oxic to suboxic conditions (Mir, 2015). Average shale compositions hover around ~1 (Cox et al., 1995; Cullers and Berendsen, 1998). Within the Green Point section, the average Ce/Ce* (2) ratio is 0.97 and shows little variability across the geochemical anomaly level. This suggests oxic to suboxic conditions, (Mir, 2015). This is consistent with geochemical evidence obtained from earlier studies on carbonates of the same section (e.g., Landing et al., 2002; Landing, 2012; 2013; Azmy et al., 2015). The exception is sample 150, which has a ratio of 1.14 and is associated with the top of the maximum flooding surface (MFS; Fig. 1.2; Azmy et al., 2015). The ratios observed do not indicate intermittent anoxia, unlike the other proxies. This could indicate the Ce/Ce^*_{SN} may not record short-term fluctuations in O_2 levels, as the lithological variations and other proxies would indicate occured.

2.5.5 Bioproductivity

Bioproductivity was evaluated using P, Ni, and Cu profiles along with TOC and $\delta^{13}C_{org}$ isotopic signatures (Table 2.1; Fig. 2.2 e.g., Pederson and Calvert, 1990; Canfield, 1994; Lécuyer et al., 1998; Piper and Perkins, 2004; Tyson, 2005; Riquier et al., 2006; Tribovillard et al., 2006; Ma et al., 2008; Perkins et al., 2008; Piper and Calvert, 2009; Śliwiński et al., 2010; Zonneveld et al., 2010; Azmy et al., 2011; Azmy et al., 2015; Schoepfer et al., 2014; Gao et al., 2016). As previously mentioned, evaluation of the $\delta^{13}C_{org}$ values indicates that phototropic activity was the main driver of bioproductivity during the deposition of the Green Point shales (House et al., 2000; She et al., 2014; Gao et al., 2016).

Both Ni and Cu behave as micronutrients in oxic marine environments, being delivered to sediments as organic matter complexes that can be released through organic matter decay (Huerta-Diaz and Morse, 1992; Fernex et al., 1992; Nameroff et al., 2002; 2004; Piper and Perkins, 2004; Algeo and Maynard, 2004; Tribovillard et al., 2006). However, Ni and Cu can also be enriched in Fe-Mn oxyhydroxides during redox cycling (Lewan and Maynard, 1982; Calvert and Pederson, 1993; Piper and Perkins, 2004; Riquier et al., 2006; Tribovillard et al., 2006; Ma et al., 2008; Perkins et al., 2008; Piper and Calvert, 2009). The Ni and Cu concentrations and enrichment factors throughout the studied section are low (Table 2.1; 2.3), indicating no significant enrichment and potential depletion from the sediments. This is consistent with a low organic matter flux to the sediments and low metal scavenging (Tribovillard et al., 2006).

Phosphorus is one of the main bio-limiting nutrients in the natural system (Redfield, 1958; Algeo and Sheckler, 1998). As P is mainly derived from organic sources in marine sediments (Ingall et al., 1993), it has been used as a bioproductivity proxy (Compton et al., 1990; Schenau and De Lange, 2001; Schenau et al., 2005; Brumsack, 2006; Śliwiński et al., 2010; Schoepfer et al., 2014). It must be used with caution however, as burial efficiency and particularly bottom-water oxygenation have a major impact on P retention within marine sediments (Tribovillard et al., 2006). In oxic pore-waters, remineralized P is taken up by organisms via bioaccumulation and adsorption to Fe-oxyhydroxides. It is then retained in the sediments as authigenic precipitates (van Cappellen & Ingall, 1994; Filippelli, 2001; Tribovillard et al., 2006; Díaz et al., 2008; Kraal, 2010; Śliwiński et al., 2010). If pore-water conditions become reducing, P released from sediments to the pore-waters is more likely to diffuse back to the water column (Ingall et al., 2005; Śliwiński et al., 2010). It can however be trapped within apatite phases by sulfide-oxidizing bacteria under reducing conditions, which could limit the P diffusion (Goldhammer et al., 2010). Considering the strong and short-lived oxygenation variations observed in the Green Point shales, based on the observed lithological variations, the main controls of the P signal must be investigated first. The correlation of P (ppm) with TOC contents exhibits a significant change (from R^2 = inverse 0.32 below anomaly to direct 0.62 above it) across the geochemical anomaly level (Fig. 2.2), supported by a similar change in correlations between TOC and P EF_{PAAS} (from R^2 = inverse 0.11 below the anomaly to direct 0.56 above it). This suggests a change in the main mechanism for P enrichment. The low inverse correlations observed below the anomaly level are reflective of more prevalent oxic pore-water conditions, where low preservation of organic carbon (TOC) and enhanced P retention likely occurred (Gächter and Müller, 2003; Ingall et al., 2005; Tyson, 2005). The good correlation between P and TOC contents above the geochemical anomaly reflects relatively higher preservation of phosphorus bearing organic matter in suboxic-anoxic conditions, even though greater diffusion is likely to have occurred (Ingall et al., 2005). There is also the possibility that P trapping by apatite phases occured, which is common in reducing conditions. This is supported by the moderate ∑REE correlation to P content, which commonly occurs as monazite (R^2 = 0.44; Lev et al., 1998; Lev and Filer, 2004; Lev et al., 2008; Goldhammer et al., 2010). Furthermore, ∑REEs have a similar correlation trend (below vs above anomaly level) with TOC as was observed for P (Fig. 2.2). Irrespective of redox influences, the P profile of the Green Point shales exhibits low concentrations (Fig. 2.2) with insignificant change in the mean values above and below the anomaly level. When corrected for carbonate dilution (using PAAS normalized EFs), the mean P EF observed (1.07±0.35) is very close to 1.0, though values vary from 0.44 to 2.05. This would indicate that overall productivity was relatively low and remained consistent (or decreasing slightly in a non-statistically significant way) across the geochemical anomaly level, which agrees with Ni and Cu data. This is consistent with previous studies of pre-Devonian oceans that concluded there was a general lack of terrestrial organic matter input suplementing phototrophic activity (Fig. 2.2; Davies and Gibling, 2010).

2.5.6 Sea level correlation with geochemical signatures

2.5.6.1 Initial Highstand (Beds 17-18)

The initial highstand systems tract covers beds 17 and 18 (Fig. 1.2). This HST tract is marked by positive $\delta^{13}C_{carb}$ and $\delta^{13}C_{org}$ excursions within the interbedded carbonates and shales of this section (Fig. 2.2; Azmy et al., 2014; 2015). This is associated with an increase in the detrital input, reflected by the increase in Al, Sc and Cr contents, K/[Fe+Mg] ratios and decreasing Ca content (Fig. 2.4). Redox conditions appear to have been dominantly suboxic based on the shale coloration, paleoredox indicators and Ce/Ce* of the alternating carbonate interbeds (Azmy et al., 2015). However, rapid fluctuations and high peaks in U, Mo, authigenic U, and TOC contents in the shales indicate intermittent anoxia may have occurred along the open margin, particularly in the base of Bed 18 (Fig. 2.2; 2.7).

2.5.6.2 Lowstand (Beds 19-22)

The lowstand systems tract covers bed 19 to near the top of bed 22 (Fig. 1.2). Its base is the major debris flow deposit that forms bed 19. Beds 20-22 are marked by relatively high $\delta^{13}C_{carb}$ and $\delta^{13}C_{org}$ values in the carbonates and high $\delta^{13}C_{org}$ values in the shales (Fig. 2.2; Azmy et al., 2014; 2015). The water mass during this period of low sea-levels was more oxidizing and had a greater atmospheric influence, which would contribute more $\delta^{13}C$-enriched CO_2. Bottom-water conditions became dominantly oxic-slightly suboxic. This caused greater organic matter degradation (i.e. low TOC values) and relatively high $\delta^{13}C_{org}$ values (Fig. 2.2; Gao et al., 2016). This is consistent with the widespread deposition of green shales during that time interval and the low U, Mo, V, authigenic U, V/Cr ratios as well as high U/Mo_{auth} ratios (Fig. 2.7). Detrital input from Laurentia into the basin during that period made up the majority of the sediments, though its trend indicates it was decreasing nearer to the upcoming transgression, based on Al, Cr, Sc, Th, K/[Fe+Mg] and Ca data (Fig. 2.4).

2.5.6.3 Transgression (Top of Bed 22 to Top of Bed 25)

The base of the transgressive sequence (Fig. 1.2) is marked by the geochemical anomaly documented by Azmy et al. (2014; 2015). It is correlated with a change from green to black shales and a positive spike in multiple proxies including K and K/[Fe+Mg] (detrital), TOC, U, Mo, V, V/Cr, V/(V+Ni), authigenic U (redox), P (bioproductivity), as well as negative spikes in Th/U and $\delta^{13}C_{org}$ values (Figs. 2.12; 2.4; 2.7). This correlates well with the increase in carbonate interbeds, abrupt positive spikes in their $\delta^{13}C_{org}$, $\delta^{15}N_{org}$, P and $\sum$REE profiles, and negative shifts in $\delta^{13}C$ values, Ce/Ce*, and $\delta^{238}U$ values (Azmy et al., 2015; their Fig. 2). This event is proposed to be a slope transgressive-lag deposit sourced from increased erosion along the transgressing margin of Laurentia. The remainder of the transgressive systems tract is marked by much lower $\delta^{13}C_{org}$ signatures. The siliciclastic detrital component of the sediments decreases during the transgression, based on Al, Sc, Th, Cr contents and K/[Fe+Mg] ratios. There is a corresponding increase in carbonate clastic material, based on higher shale Ca content and much more common carbonate rhythmite occurences derived from the platform (Fig. 2.4; James and Stevens, 1986; Azmy et al., 2014). A prevalence of dark grey and black shales and concurrent though very variable increase (Mo, U, V, authigenic U, TOC, V/Cr ratios) and decrease (U/Mo_{auth}) among redox proxies suggests bottom-water redox conditions became relatively more reducing, probably highly suboxic and intermittently anoxic along the margin (Fig. 2.2; 2.7). This decrease in available O_2

near the seafloor and subsequent fluctuations is thought to be the cause of the decrease in radiolarian diversity on the Laurentian slope identified at this time (Cooper et al., 2001b; Lehnert et al., 2005; Terfelt et al., 2012; Pouille et al., 2014; Terfelt et al., 2014).

2.5.6.4 Second Highstand Systems Tract (Top of Bed 25-26)

The the second highstand systems tract (Fig. 1.2) is marked by an increase in detrital proxies (Al, K, Cr, Sc, Th and Th/Sc; Fig. 2.1). Siliciclastic proxies remain high throughtout the second HST, indicating detrital input to the basin rebounded as progradation resumed, even as carbonate rhythmite deposition remained high. Redox proxies (Mo, U, V, V/Cr, authigenic U, Th/U, U/Mo_{auth}) and lithology suggest suboxic and intermittently anoxic conditions remained prevalent within the basin (Fig. 2.7).

2.6 Conclusions

Physical observations, organic carbon and ∑REE data support the preservation of at least near-primary geochemical signatures in the investigated shales from Green Point, with no evidence of significant catagenesis or hydrothermal alteration.

The most influential control of the organic matter content is its potential to be preserved, controlled by the redox conditions on the seafloor and within pore-waters. The $\delta^{13}C_{org}$ values indicate organic carbon is derived from photoautotrophic carbon fixation, and affected by the observed sealevel variations.

As expected, based on the lithology dominated by shales and carbonaceous shales, dilution by carbonate material has a major impact on the geochemical signatures observed, particularly for detrital proxies. Once accounted for however, detrital proxies were found to be a good indicator of clastic input to the basin. The siliciclastic sediments were derived from the Laurentian craton, with little to no input from the approach Taconic Arc. Proportions of detrital proxies (Sc, Th, Al, Cr, Cs, K) and carbonate proxies (Ca) also provided a good indication of relative clastic carbonate and siliciclastic sediment input being delivered concurrently to the slope, especially when evaluated in concert with the lithological variations. A noticeable decrease was observed during the major transition at the Cambrian-Ordovician boundary, which is consistent with the observed shift to the more carbonate-dominated Broom Point Member.

Paleoredox indicators suggest a relative decrease in O_2 levels from the LST systems tract (oxic-slightly suboxic) to the TST systems tract (strongly suboxic and intermittently anoxic) above the anomaly level as sea level rose. The most reliable redox proxies were found to be TOC, Mo, U, authigenic U and U/Mo_{auth}. Caution must be used with absolute authigenic U, due to the negative values observed. Absolute values for several other elemental ratios, such as V/Cr, V/(V+Ni), and Th/U are not reliable for the carbonaceous shales of the Green Point Formation' slope environment. Fe_T/Al and Ce/Ce* should be used with caution as they don't correlate well with other indicators, which is not reflective of the observed lithological variations within the shales.

Evaluation of bioproductivity proxies yielded mixed results. Phototrophic activity within the photic zone was found to be the main driver of bioproductivity within the basin. The overall bioproductivity was found to be low, based on Ni, Cu, P and TOC. Variations within the section could not be ascertained with any certainty however. Preservation potential, the most important factor affecting both TOC and P, was very inconsistent due to the short-term fluctuations in redox conditions within the pore-waters and near the seafloor.

Thus, geochemical changes, when evaluated in concert with lithological changes, track sealevel variations in a predictable manner. The observed variations within the shales could be clearly correlated to the previously interpreted sea-level fluctuations, based on the carbonate isotope stratigraphy of the interbedded carbonates. Clear changes in detrital, redox or bioproductivity proxies mark the transition to different systems tracts and patterns of change within each systems tract.

References

Ainsaar, L., Truumees, J., Meidla, T., 2015. The Position of the Ordovician-Silurian Boundary in Estonia Tested by High-Resolution $\delta^{13}C$ Chemostratigraphic Correlation. Chapter 15. In: Ramkumar, M (Ed.). Chemostratigraphy: Concepts, Techniques, and Applications. Elsevier Pub. 395-412.

Alam, M.S., Cheng, T., 2014. Uranium release from sediments to groundwater: influence of water chemistry and insights into release mechanisms. J. Contam. Hydrol. 164 (0), 72-87.

Algeo, T.J., Scheckler, S.E., 1998. Terrestrial-marine teleconnections in the Devonian: links between the evolution of land plants, weathering processes, and marine anoxic events. Philosophical Transactions of the Roya Society B-Biological Sciences, 353. 113-128

Algeo, T.J., Schwark, L., Hower, J.C., 2004. High-resolution geochemistry and sequence stratigraphy of the Hushpuckney Shale (Swope Formation, eastern Kansas): implications for climate-environmental dynamics of the Late Pennsylvanian Midcontinent Seaway. Chem. Geol. 206. 259-288.

Algeo, T.J., Maynard, J.B., 2004. Trace-element behavior and redox facies in core shales of Upper Pennsylvanian Kansas-type cyclothems. Chem. Geol. 206. 289-318.

Algeo, T.J., Lyons, T.W., 2006. Mo-total organic carbon covariation in modern anoxic marine environments: implications for analysis of paleoredox and paleohydrographic conditions. Paleoceanography 21. 1-23.

Algeo, T.J., Tribovillard, N., 2009. Environmental analysis of paleoceanographic systems based on molybdenum–uranium covariation. Chem. Geol. 268. 211–225.

Anbar, A.D., 2004. Molybdenum stable isotopes: observations, interpretations and directions. Reviews in Mineralogy & Geochemistry 55, 429-454.

Anderson, R.F., Fleisher, M.Q., LeHuray, A.P., 1989. Concentration, oxidation state, and particulate flux of uranium in the Black Sea. Geochim. Cosmochim. Acta. 53, 2215-2224.

Arnaboli, M., Meyers, P.A., 2007. Trace element indicators of increased primary production and decreased water-column ventilation during deposition of latest Pliocene sapropels at five locations across the Mediterranean Sea. Paleogeogr. Paleoclim. Paleoecol. 249. 425-443.

Anderson, R.F., 1987. Redox behavior of uranium in an anoxic marine basin. Uranium, 3, 145-164.

Arnold, G.L., Anbar, A.D., Barling, J., Lyons, T.W., 2004. Molybdenum isotope evidence for widespread anoxia in mod-Proterozoic oceans: Science, 304, 87-90, doi: 10.1126/science.1091785.

Arnold, G.L., Lyons, T.W., Gordon, G.W., Anbar, A.D., 2012. Extreme change in sulfide concentrations in the Black Sea during the Little Ice Age reconstructed using molybdenum isotopes. Geol. 40, 595-598.

Azmy, K., Brand, U., Sylvester, P., Gleeson, S.A., Logan, A. Bitner, M.A., 2011. Biogenic and abiogenic low-Mg calcite (bLMC and aLMC): Evaluation of seawater-REE composition, water masses and carbonate diagenesis. Chem. Geol. 280. 180-190.

Azmy, K., Stouge, S., Brand, U., Bagnoli, G., 2014. High-resolution chemostratigraphy of the Cambrian–Ordovician GSSP in western Newfoundland, Canada: enhanced global correlation tool. Palaeogeogr. Palaeoclim. Palaeoecol. 409. 135-144.

Azmy, K., Kendall, B., Brand, U., Stouge, U., Gordon, G.W., 2015. Redox conditions across the Cambrian-Ordovician Boundary: Elemental and isotopic signatures retained in the GSSP carbonates. Paleogeogr. Paleoclim. Paleoecol. 440. 440-454.

Babechuk, M.G., Widdowson, M., Kamber, B.S., 2014. Quantifying chemical weathering intensity and trace element release from two contrasting basalt profiles, Deccan Traps, India. Chem. Geol. 363, 56-75.

Barnes, C.E., Cochran, J.K., 1991. Geochemistry of uranium in the Black Sea sediments. Deep Sea Res. Part A. Oceanogr. Res. Papers. 38, S1237-S1254.

Basu A., Sanford R. A., Johnson T. M., Lundstron C. C. and Loffler F. E., 2014. Uranium isotopic fractionation factors during U(VI) reduction by bacterial isolates. Geochim. Cosmochim. Acta 136. 100–113.

Bau, M., 1996. Controls on the fractionation of isovalent trace elements in magmatic and aqueous systems: evidence from Y/Ho, Zr/Hf, and lanthanide tetrad effect. Contrib. Mineral. Petrol. 123, 232-333.

Bau, M., and Dulski, P., 1996. Distribution of yttrium and rare-earth elements in the Penge and Kuruman iron-formations, Transvaal Supergroup, South Africa: Precambrian Research 79. 37–55.

Bau, M., Dulski, P., 1999. Comparing yttrium and rare earths in hydrothermal fluids from the Mid-Atlantic Ridge: implications for Y and REE behavior during near-vent mixing and for the Y/Ho ratio of Proterozoic seawater. Chem. Geol. 155. 77–90.

Bayon, G., Pierre, C., Etoubleau, J., Voisset, M., Cauquil, E., Marsset, T., Sultan, N., Le Drezen, E., Fouquet, Y., 2007. Sr/Ca and Mg/Ca ratios in Niger Delta sediments: Implications for authigenic carbonate genesis in cold seep environments. 241 (1-4), 93-109.

Bhatia, M.R., Crook, K.A.W., 1986. Trace element characteristics of graywackes and tectonic setting discrimination of sedimentary basins. Contrib. Mineral. Petrol. 92, 181-193.

Bolhar, R., Kamber, B.S., Moorbath, S., Fedo, C.M., Whitehouse, M.J., 2004. Characterisation of early Archaean chemical sediments by trace element signatures. Earth and Planetary Science Letters 222. 43-60.

Bone, S.E., Dynes, J.J., Cliff, J., Bargar, J.R., 2017A. Uranium (IV) adsorption by natural organic matter in anoxic sediments. PNAS. 114, 711-716.

Bone, S.E., Cahill, M.R., Jones, M.E., Fendorf, S., Davis, J., Williams, K.H., Bargar, J.R., 2017B. Oxidative uranium release from anoxic sediments under diffusion-limited conditions. Environ. Sci. Technol. 51, 11039-11047.

Böning, P., Brumsack, H.-J., Böttcher, M.E., Schnetger, B., Kriete, C., Kallmeyer, J., Borchers, S.L., 2004. Geochemistry of Peruvian near-surface sediments. Geochim. Cosmochim. Acta 68. 4419-4451.

Bouchez, J., Gaillardet, J., France-Lanord, C., Maurice, L., Dutra-Maia, P., 2011. Grain size control of river suspended sediment geochemistry: clues from Amazon River depth profiles. Geochem. Geophys. Geosys. 12 (3), Q03008.

Boyce, W. D., Knight, I., 2005. Cambrian macrofossils from the Phillips Brook and North Brook anticlines, western Newfoundland: Current research: Department of Natural Resources, Geological Survey Report 05-1. 39–62.

Burdige, D.J., 2007. Preservation of Organic Matter in Marine Sediments: controls, Mechanisms, and an Imbalance in Sediment Organic Carbon Budgets? Chem. Rev. 107. 467-485

Calvert, S.E., Pedersen, T.F., 1993. Geochemistry of Recent oxic and anoxic marine sediments: implications for the geological record. Mar. Geol. 113. 67–88.

Canfield, D.E., 1994. Factors influencing organic carbon preservation in marine sediments. Chem. Geol. 114. 315-329.

Canfield, D.E., Thamdrup, B., 2009. Towards a consistent classification scheme for geochemical environments, or why we wish the term 'suboxic' would go away. Geobiology 7, 385-392.

Cawood, P.A., McCausland, P.J.A., Dunning, G.R., 2001. Opening Iapetus: constraints from Laurentian margin in Newfoundland. Geol. Soc. Am. Bull. 113. 443–453.

Chester, R., Aston, S.R., 1976. The geochemistry of deep-sea sediments, in Riley, J.P., Chester, R. (Ed.). Chem. Oceanogr. New York, Academic Press. 6, 281-390.

Chesworth, W., Dejou, J., Larroque, P., 1981. The weathering of basalt and relative mobilities of the major elements at Belbex, France. Geochim. Cosmochim. Acta. 45, 1235-1243.

Cochran, J.K., 1992. The oceanic chemistry of the uranium and thorium series nuclides. In: Ivanoch, M., Harmon, S. (Ed.) Uranium series disequilibrium: applications to earth, marine and environmental sciences,. Oxford-Clarendon Press, 2nd edition, 334-395.

Compton, J.S., Snyder, S.W., Hodell, D.A., 1990. Phosphogenesis and weathering of shelf sediments from the south eastern United States: implications for Miocene $\delta^{13}C$ excursions and global cooling. Geol. 18, 1227-1230.

Condie, K.C., Dengate, J., Cullers, R.L., 1995. Behavior of rare-earth elements in a paleoweathering profile on granodiorite in the Front Range, Colorado, USA. Geochim. Cosmochim. Acta. 59, 279-294.

Coniglio, M., 1986. Synsedimentary submarine slope failure and tectonic deformation in deep-water carbonates, Cow Head Group, western Newfoundland. Can. J. Earth Sci. 23, 476-490.

Coniglio, M., James, N.P., 1990. Origin of fine-grained carbonate and siliciclastic sediments in an early Paleozoic slope sequence, Cow Head Group, western Newfoundland. Sedimentology 37. 215-230.

Cooper, R.A., Nowlan, G.S., Williams, S.H., 2001a. Global Stratotype Section and Point for base of the Ordovician System. Episodes 24, 19–28.

Cooper, M., Weissenberger, J., Knight, I., Hostad, D., Gillespie, D., Williams, H., Burden, E., Porter-Chaudhry, J., Rae, D., Clark, E., 2001b. Basin Evolution in Western Newfoundland: New insights from Hydrocarbon Exploration. AAPG Datapages, Search and Discover Article # 10019.

Cooper, R.A., Sadler, P.M., 2012. The Ordovician period, in "The Geological Time Scale", edited by Gradstein, F. et al., pp. 489-523. Elsevier, Amsterdam.

Cowan, C. A., James, N. P., 1993. The interactions of sea level change, terrigenous-sediment influx, and carbonate productivity as controls on Upper Cambrian grand cycles of western Newfoundland, Canada: Geological Society of America Bulletin 105. 1576-1590.

Cox, R., Low, d.R., Cullers, R.L., 1995. The influence of sediment recycling and basement composition on evolution of mudrock chemistry in the southwestern United States. Geochim. Cosmochim. Acta 59. 2919-2940.

Cullers, R.L., Stone, J., 1991. Chemical and mineralogical comparison of the Pennsylvanian Fountain Formation, Colorado, U.S.A. (an uplifted continental block) to sedimentary rocks from other tectonic environments. Lithos. 27, 115-131.

Cullers, R.L., 1994. The controls on the major and trace element variation of shales, siltstones, and sandstones of Pennsylvanian-Permian age from uplifted continental blocks in Colorado to platform sediment in Kansas, USA. Geochim. Cosmochim. Acta. 58, 4955-4972.

Cullers, R.L., Berendsen, P., 1998. The provenance and chemical variation of sandstones associated with the Mid-continent rift system, USA. Eur. J. Mineral. 10. 987-1002.

Cumberland, S.A., Douglas, G., Grice, K., Moreau, J.W., 2016. Uranium mobility in organic matter-rich sediments: A review of geological and geochemical processes. Earth-Sci. Reviews. 159, 160-185.

Davies, N.S., Gibling, M.R., 2010. Cambrian to Devonian evolution of alluvial systems: the sedimentological impact of the earliest land plants. Earth-Sci. Rev. 98. 171-200.

Dean, W.E., Arthur, M.A., 1998. Geochemical expressions of cyclicity in Cretaceous pelagic limestone sequences: Niobara Formation, Western Interior Seaway, in Stratigraphy in Paleoenvironments of the Cretaceous Western Interior Seaway, USA: Society of Economic Paleontologists and Mineralogists, Concepts in Sedimentology and Paleontology 6. 227-255.

Diaz, J., Ingall, E., Benitez-Nelzon, C., Paterson, D., de Jonge, M.D., McNulty, I., Brandes, J.A., 2008. Marine polyphosphate: a key player in geologic phosphorus sequestration. Science. 320, 652-655.

Dill, H., 1986. Metallogenesis of early Paleozoic graptolite shales from the Graefenthal Horst (northern Bavaria-Federal Republic of Germany. Econ. Geol. 81. 889-903.

Douville, E., Bienvenu, P., Charlou, J.I., Donval, J.P., Fouquet, Y., Appriou, P., Gamo, T., 1999. Yttrium and rare earth elements in fluids from various deep-sea hydrothermal systems. Geochim. Cosmochim. Acta 63. 627-643.

Dunk, R.M., Mills, R.A., Jenkins, W.J., 2002. A reevaluation of the oceanic uranium budget for the Holocene. Chem. Geol. 190. 45-67.

Emerson, S.R., Huested, S.S., 1991. Ocean anoxia and the concentrations of molybdenum and vanadium in seawater. Mar. Chem. 34. 177-196.

Epstein, A.G., Epstein, J.B., Harris, L.D., 1977. Conodont Color Alteration – an Index to Organic Metamorphism. U.S. Department of the Interior. Geological Survey Professional Paper 995.

Faure, G., Mensing, T.M., 2005. Isotopes: Principles and Applications. Third edition. John Willey and Sons, Inc., Hoboken, New Jersey.

Fedo, C.M., Eriksson, K.A., Krogstad, E.J., 1996. Geochemistry of shales from the Archean (~3.0 Ga) Buhwa Greenstone Belt, Zimbabwe: implications for provenance and source-area weathering. Geochim. Cosmochim. Acta 60, 1751-1763.

Fernex, F., Février, G. Benaïm, J., Amoux, A., 1992. Copper, lead and zinc trapping in Mediterranean deep-sea sediments: probable coprecipitation with manganese and iron. Chem. Geol. 98. 293-308.

Filippelli, G.M., 2001. Carbon and phosphorus cycling in anoxic sediments of the Saanich Inlet, British Columbia. Mar. Geol. 174-301-321.

Gächter, R., Müller, B., 2003. Why the phosphorus retention of lakes does not necessarily depend on the oxygen supply to their sediment surface. Limnol. Oceanogr. 48, 929-933.

Ganai, J.A., Rashid, S.A., 2015. Rare earth element geochemistry of the Permo-Carboniferous clastic sedimentary rocks in the Spiti Region, Tethys Himalaya: significance of Eu and Ce anomalies. Chin. J. Geochem. 34. 252-264.

Gao, P., Lia, G., Jia, C., Young, A., Wang, Z., Wang, T., 2016. Redox variations and organic matter accumulation on the Yangtze carbonate platform during late Ediacaran-early Cambrian: Constraints from petrology and geochemistry. Paleogr. Paleoclim. Paleoecol. 450. 91-110.

Goldhammer, T., Brüchert, V., Ferdelman, T.G., Zabel, M., 2010. Microbial sequestration of phosphorus in anoxic upwelling sediments. Nat. Geosci. 3, 557-561.

Govindaraju, K., 1989. Compilation of Working Values and Sample Descriptions for 272 Geostandards. Geostandards Newsletter. 13, special issue, 1-113.

Gromet, L.P., Dymek, R.F., Haskin, L.A., Korotev, R.L., 1984. The "North American shale composite": Its compilation, major and trace element characteristics. Geochim. Cosmochim. Acta. 48, 2469-2482.

Hatch, J.R., Leventhal, J.S., 1992. Relationship between inferred redox potential of the depositional environment and geochemistry of the Upper Pennsylvanian (Mis- sourian) Stark Shale Member of the Dennis Limestone, Wabaunsee County, Kansas, USA. Chem. Geol. 99. 65–82.

Hibbard, J.P., van Staal, C.R., Ranking, D.G., 2007. A comparative analysis of pre-Silurian crustal building blocks of the northern and southern Appalachian orogeny. American Journal of Science 307, 23–45.

Hild, E., Brumsack, H.-J., 1998. Major and minor element geochemistry of lower Aptian sediments from NW German Basin (core Hoheneggelsen KB 40). Cretac. Res. 19. 615-633.

House, C.H., Schopf, J.W., McKeegan, K.D., Coath, C.D., Harrison, T.M., Stetter, K.O., 2000. Carbon isotopic composition of individual Precambrian microfossils. Geology 28. 707–710.

Huerta-Diaz, M.A., J.W., 1992. Pyritisation of trace metals in anoxic marine sediments. Geochim. Cosmochim. Acta 56, 2681-2702.

Ingall, E.D., Bustin, R.M., Van Cappellin, P., 1993. Influence of water column anoxia on the burial and preservation of carbon and phosphorus in marine shales. Geochim. Cosmochim. Ata 57, 303-316.

Ingall, E.D., Kolowith, L., Lyons, T., Hurtgen, M., 2005. Sediment carbon, nitrogen and phosphorus cycling in an anoxic fjord, Effingham Inlet, Btitish Columbia. Am. J. Sci. 305, 240-258.

Jacobi, R.D., 1981. Peripheral bulge – A causal mechanism for the Lower-Middle Ordovician unconformity along the western margin of northern Appalachians. Earth. Plan. Sci. Let. 56, 245-251

James, N. P., Stevens, R. K., 1986. Stratigraphy and Correlation of the Cambrian-Ordovician Cow Head Group, Western Newfoundland. Geological Survey of Canada Bulletin 366.

James, N. P., Stevens, R. K., Barnes, C. R., and Knight, I., 1989. Evolution of a lower Paleozoic continental-margin carbonate platform, northern Canadian Appalachians, in P. D. Crevello, J. L. Wilson, J. F. Sarg, and J. F. Read, eds., Controls on carbonate platform and basin development: SEPM Special Publication 44, 123–146.

Jiang, S.-Y., Chen, Y.-Q., Ling, H.-F., Yang, J.-H., Feng, H.-Z., Ni, P., 2006. Trace- and rare-earth element geochemistry and Pb-Pb dating of black shales and intercalated Ni-Mo-PGE-Au sulfide ores in lower Cambrian strata, Yangtze Platform, South China. Miner Deposita, 41. 453-467.

Jiang, G., Wang, X., Shi, X., Xiao, S., Zhang, S., Dong, J., 2012. The origin of decoupled carbonate and organic carbon isotope signatures in the early Cambrian (ca. 542–520 Ma) Yangtze platform. Earth Planet. Sci. Lett. 317-318, 96–110.

Jiménez-Espejo, F.J., et al., Martínez-Ruiz, F., Finlayson, C., Payton, A., Sakamoto, T., Ortega-Huertes, M., Finlayson, G., Ijima, K., Gallego-Torres, D., Fa, F., 2007. Climate forcing and Neanderthal extinction in Southern Iberia: insights from a multiproxy marine record. Quaternary Science Reviews doi:10.1016/j.quascirev.2006.12.013

Jones, B.J., Manning, A.C., 1994. Comparison of geochemical indices used for the interpretation of palaeoredox conditions in ancient mudstones. Chem. Geol. 111. 111–129.

Kendall, B., Reinhard, C.T., Lyons, T.W., Kaufman, A.J., Poulton, S.W., Anbar, A.D., 2010. Pervasive oxygenation along late Archaean ocean margins. Nature Geoscience 3. 647–652.

Kikumoto, R., Tahata, M., Nishizawa, M., Sawaki, Y., Maruyama, S., Shu, D., Han, J., Komiya, T., Takai, Ken., Ueno, Y., 2014. Nitrogen isotope chemostratigraphy of the

Ediacaran and early Cambrian platform sequence at Three Gorges, South China. Gondwana Res. 25. 1057-1069.

Knight, I., James, N.P., Lane, T.E., 1991. The Ordovician St. George Unconformity, northern Appalcachians: the relationship of plate convergence at the St. Lawrence Promontory to the Sauk/Tippecanoe sequence boundary. GSA Bulletin 103.1200-1225.

Knight, I., Azmy, K., Greene, M., Lavoie, D., 2007. Lithostratigraphic setting of diagenetic, isotopic, and geochemistry studies of Ibexian and Whiterockian carbonates of the St. George and Table Head groups in western Newfoundland. Current Research Newfoundland and Labrador Department of Natural Resources Geological Survey. Report 07-1. 55–84.

Knight, I., Boyce, W. D., 2009. The Reluctant Head Formation, Goose Arm thrust stack, Newfoundland Humber zone: New observations on the stratigraphy, biostratigraphy and implications for the evolution of the Cambrian – Ordovician shelf: Current research: Newfoundland and Labrador Department of Natural Resources, Geological Survey Report 09-1. 183–202.

Kraal, P., 2010. Redox-dependant Phosphorus Burial in Modern and Ancient Marine Sediments. Ph.D. dissertation. Universiteit Utrecht, Netherlands. (176 pp.)

Kuzendorf, H., Plüger, W.L., Friedrich, G.H., 1983. Uranium in pacific deep-sea sediments and manganese nodules. J. Geochem. Exploration. 19, 147-162.

Landing, E., Geyer, G., Bartowski, K.E., 2002. Latest Early Cambrian small shelly fossils, trilobites, and Hatch Hill dysaerobic interval on the east Laurentian continental slope. J. Paleontol. 76. 285-303.

Landing, E., 2012. Time-specific black mudstones and global hyperwarming on the Cambrian–Ordovician slope and shelf of the Laurentia palaeocontinent. Palaeogeogr. Palaeoclimatol. Palaeoecol. 367–368. 256–272.

Landing, E., 2013. The Great American Carbonate Bank in northeast Laurentia: its births, deaths, and linkage to continental slope oxygenation (early Cambrian–late Ordovician). In: Derby, J.R., Fritz, R.D., Longacre, S.A., Morgan, W.A., Sternbach, C.A. (Eds.), The Great American Carbonate Bank, Essays in Honor of James Lee Wilson. AAPG Bulletin, Memoir 98. 451–492.

Lavoie, D., Burden, E., Lebel, D., 2003. Stratigraphic framework for the Cambrian – Ordovician rift and passive- margin successions from southern Quebec to western Newfoundland: Canadian Journal of Earth Science, 40, 177–205; in Tollo, R.P., Bartholomew, M.J., Hibbard, J.P., Karabinos, P.M. (2010) From Rodinia to Pangea: The lithotectonic Record of the Appalachian Region. The Geological Society of America, Memoir 206.

Lécuyer, C., Grandjean, P., Barrat, J.-A., Nolvak, J., Emig, C., Paris, F., Robardet, M., 1998. δ^{18}O and REE contents of phosphatic brachiopods: a comparison between modern and lower Paleozoic populations. Geochim. Cosmochim. Acta 62, 2429-2436.

Lehnert, O., Miller, J.F., Leslie, S.A., Repetski, J.E., Ethington, R.L., 2005. Cambro-Ordovician sea-level fluctuations and sequence boundaries: the missing record and evolution of new taxa. Special Papers in Paleoeontology 74. 117-134.

Lev, S.M., McLennan, S.M., Meyers, W.J., Hanson, G.N., 1998. Apetrographic approach for evaluating trace-element mobility in a black shale. Journal of Sed. Res. 68. 970–980.

Lev, S.M., Filer, J.K., 2004. Assessing the impact of black shaleprocesses on REE and the U–Pb isotope system in the southern Appalachian Basin. Chem. Geol.206. 393–406.

Lev, S.M., Filer, J.K., Tomascak, P., 2008. Orogenesis vs. diagenesis: Can we use organic-rich shales to interpret the tectonic evolution of a depositional basin? Earth Sci. Reviews 86. 1-14.

Lewan, M.D., Maynard, J.B., 1982. Factors controlling enrichment of vanadium and nickel in the bitumen of organic sedimentary rocks. Geoch. Cosmochim. Acta 46. 2547-2560.

Lyons, T.W., Werne, J.P., Hollander, D.J., Murray, R.W., 2003. Contrasting sulfur geochemistry and Fe/Al and Mo/Al ratios across the last oxic-to-anoxic transition in the Cariaco Basin, Venezuela. Chem. Geol. 195. 131-157.

Lyons, T.W., Severmann, S., 2006. A critical look at iron paleoredox proxies: New insights from modern euxinic marine basins. Geochim. Cosmochim. 70. 5698-5722.

Ma, X.P., Wang, C.Y., Racki, G., Racka, M., 2008. Facies and geochemistry across the Early-Middle Frasnian transition (Late Devonian) on South China carbonate shelf: Comparison with the Polish reference succession. Palaeogeogr. Palaeoclim. Palaeoecol. 269. 130-151.

Martinez, N.C., Murray, R.W., Thunnel, R.C., Peterson, L.C., Muller-karger, F., Astor, Y., Varela, R., 2007. Modern climate forcing of terrigenous deposition in the tropics (Cariaco Basin, Venezuela). Earth Planet. Sci. Lett. 264, 438-451.

McLaughlin, P.A., Emsbo, P., Brett, C.E., 2012. Beyond black shales: The sedimentary and stable isotope records of oceanic anoxic events in a dominantly oxic basin (Silurian; Appalachian Basin, USA). Paleogeogr. Paleoclim. Paleoecol. 2012. 153-177.

McLennan, S.M., Taylor, S.R., McCulloch, M.T., Maynard, J.B., 1990. Geochemical and Nd-Sr isotopic composition of deep-sea turbidites: Crustal evolution and plate tectonic associations. Geochim. Cosmochim. Acta. 54, 2015-2050.

McLennan, S.M., Hemming, S., McDaniel, D.K., Hanson, G.N., 1993. Geochemical approaches to sedimentation, provenance, and tectonics. The Geological Society of America, special paper 284.

McLennan, S.M., 2001. Relationships between the trace element composition of sedimentary rocks and upper continental crust. Geochem.Geophys. Geosys. 2. 1021 (2000GC000109).

McManus, J., Berelson, W.M., Severmann, S., Poulson, R.L., Hammond, D.E., Klinkhammer, G.P., Holm, C., 2006. Molybdenum and uranium geochemistry in continental margin sediments: Paleoproxy Potential. Geochim. Cosmochim. Acta 70. 4643-4662.

Meyers, P.A., 1994. Preservation of elemental and isotopic source identification of sedimentary organic matter. Chem. Geol. 144. 289-302.

Meyers, P.A., 1997. Organic geochemical proxies of paleoceanographic, paleolimnologic and paleoclimatic processes. Org. Geochem. 27. 213-250.

Middelburg, J.J., Van der Weijden, C.H., Woitteiz, J.R.W., 1988. Chemical processes affecting the mobility of major, minor and trace elements during weathering of granitic rocks. Chem. Geol. 68, 253-273.

Mir, A.R., 2015. Rare earth element geochemistry of Post- to Neo-Archean shales from Singhbhum mobile belt, Eastern India: implocations for tectonic setting and paleo-oxidation conditions. Chin. J. Geochem. 34(3). 401-409.

Morford, J.L., Emerson, S., 1999. The geochemistry of the redox sensitive trace metals in sediments. Geochim. Cosmochim. Acta 63, 1735-1750.

Murphy, A.E., Sageman, B.B., Hollander, D.J., Lyons, T.W., Brett, C.E., 2000. Black shale deposition in the Devonian Appalachian Basin: siliciclastic starvation, episodic water-column mixing, and efficient recycling of biolimiting nutrients. Paleoceanography 15, 280-291.

Nameroff, T.J., Balistrieri, L.S., Murraym J.W., 2002. Suboxic trace metal geochemistry in the eastern tropical North Pacific. Geochim. Cosmochim. Acta 66. 1139-1158.

Nameroff, T.J., Calvert, S.E., Murray, J.W., 2004. Glacial-interglacial variability in the eastern tropical North-Pacific oxygen minimum zone recorded by redox-sensitive trace metals. Paleooceanogr. 19. PA1010, doi. 1029/2003PA0 00912.

Nesbitt, H.W., 1979. Mobility and fractionation of rare earth elements during weathering of a granodiorite. Nature. 279, 206-210.

Nesbitt, H.W., Young, G.M., 1989. Formation and diagenesis of weathering profiles. J. Geol. 97, 129-147.

Nesbitt, H.W., Markovics, G., 1997. Weathering of granodioritic crust, long-term storage of elements in weathering profiles,, and petrogenesis of siliciclastic sediments. Geochim. Cosmochim. Acta 61, 1653-1670.

Nesbitt, H.W., Markovics, G., Price, R.C., 1980. Chemical processes affecting alkalis and alkaline earths during continental weathering. Geochim. Cosmochim. Acta. 44, 1659-1666.

Nowlan, G.S., Barnes, C.R., 1987. Thermal maturation of Paleozoic strata in Eastern Canada from conodont colour alteration index (CAI) data with implications for burial history, tectonic evolution, hotspot tracks and mineral and hydrocarbon exploration. Bulletin – Geological Survey of Canada, 367, 47.

Nozaki, Y., 2001. Rare earth elements and their isotopes. Encyclopedia of Ocean Sciences, 1st edition, v. 4 (Steele, J.H., Thorpe, S.A., Turekian, K.K., eds) pp. 2354-2366, Academic Press Inc., London.

Organo, C., 1997. Origine et comportement géochimique de l'uranium dans les sediments marins – Utilisation dy rapport ($^{234}U/^{238}U$) en géochimie marine. Doctorat en Sciences. Université de Paris-Sud, U.F.R. Scientifique d'Orsay. Paris, France.

Partin, C.A., Bekker, A., Planavsky, N.J., Scott, C.T., Gill, B.C., Li, C., Podkovyrov, V., Maslov, A., Konhauser, K.O., Lalonde, S.V., Love, G.D., Poulton, S.W., Lyons, T.W., 2013. Large-scale fluctions in Precambrian atmospheric and oceanic oxygen levels from the record of U in shales. Earth and Planetary Science Letters. 369-370. 284-293.

Pederson, S.T., Calvert, S.E., 1990. Anoxia vs. productivity: what controls the formation of organic-rich sediments and sedimentary rocks? AAPG Bull. 74, 454-466.

Perkins, R.B., Piper, D.Z., Mason, C.E., 2008. Trace-element budgets in the Ohio/Sunbury shales of Kentucky: Constraints on ocean circulation and primary productivity in the Devonian-Mississippian Appalachian Basin. Palaeogeogr. Palaeoclim. Palaeoecol. 265. 14-29.

Picone, S., Alvisi, F., Dinelli, E., Morigi, C., Negri, A., Ravaioli, M., Vaccaro, C., 2008. New insights on late Quaternary palaeographic setting in the Northern Adriatic Sea (Italy). J. Quaternary Sci. 23, 489-501.

Piper, D.Z. & Perkins, R.B., 2004. A modem vs. Permian black shale - the hydrography, primary productivity, and water-column chemistry of deposition. Chem. Geol. 206. 177-197.

Piper, D.Z., Calvert, S.E., 2009. A marine biogeochemical perspective on black shale deposition. Earth-Sci. Reviews 95. 63-96.

Popp, B.N., Parekh, P., Tilbrook, B., Bidigare, R.R., Laws, E.A., 1997. Organic carbon $\delta^{13}C$ variations in sedimentary rocks as chemostratigraphic and paleoenvironmental tools. Palaeogeogr. Palaeoclimatol. Palaeoecol. 132. 119–132.

Porter, S.J., Selby, D., Cameron, V., 2014. Characterising the nickel isotopic composition of organic-rich marine sediments. Chem. Geol. 387. 12-21.

Pouille, L., Danelian, T., Maletz, J., 2014. Radiolarian diversity changes during the late Cambrian-early Ordovician transition as recorded in the Cow Head Group of Newfoundland (Canada). Marine Micropaleo. 110. 25-41.

Poulton, S.W., Fralick, P.W., Canfield, D.E., 2010. Spatial variability in oceanic redox structure 1.8 billion years ago. Nat. Geo. 3. 486-490.

Poulton, S.W., Canfield, D.E., 2011. Ferruginous conditions: A dominant feature of the ocean through Earth's history. Elements 7. 107-112.

Redfield, A.C., 1958. The biological control of chemical factors in the environment. Am. Sci. 46 (3), 205-221.

Reinhard, C., Planavsky, N.J., Wang, X., Fischer, W.W., Johnson, T.M., Lyons, T.W., 2014. The isotopic composition of authigenic chromium in anoxic marine sediments: A case study from the Cariaco Basin. Earth. Planet. Sci. Lett. 407, 9-18.

Rimmer, S.M., 2004. Geochemical paleoredox indicators in Devonian-Mississippian black shales, Central Appalachian Basin (USA). Chem. Geol. 206. 373-391.

Rimmer, S.M., Thompson, J.A., Goodnight, S.A., Robl, T.L., 2004. Multiple controls on the preservation of organic matter in Devonian-Mississipian marine black shales: geochemical and petrographic evidence. Paleogr. Paleoclim. Paleoecol. 215. 125-154.

Riquier, L., Tribovillard, N., Averbuch, O., Devleeschouwer, X., Riboulleau, A., 2006. The late Frasnian Kellwasser horizons of the Harz Mountains (Germany): Two oxygen-deficient periods resulting from different mechanisms. Chem. Geol. 233. 137-155.

Rolinson, J.M., Stirling, C.H., Middag, R., Rijkenberg, M.J.A., 2017. Uranium stable isotope fractionation in the Black Sea: Modern calibration of the $^{238}U/^{235}U$ paleo-redox proxy. Geochim. Cosmochim. Acta. 203, 67-88.

Rydell, H.T., Bonatti, E., 1973. Uranium in submarine metalliferous deposits. Geochim. Cosmochim. Acta. 37, 2557-2562.

Sadiq, M., 1988. Thermodynamic solubility relationships of inorganic vanadium in the marine environment. Mar. Chem. 23. 87-96.

Sageman, B.B., Murphy, A.E., Werne, J.P., Ver Straeten, C.A., Hollander, D.J., Lyons, T.W., 2003. A tale of shales: the relative roles of production, decomposition, and dilution in the accumulation of organic-rich strata, Middle–Upper Devonian, Appalachian Basin. Chem. Geol. 195. 229–273.

Sahoo, S.K., Planavsky, N.J., Kendall, B., Wang, X., Shi, X., Scott, C., Anbar, A., Lyons, T.W., Jiang, G., 2012. Ocean oxygenation in the wake of the Marinoan glaciation. Nature 489. 546-549.

Saltzman, M.R., Thomas, E., 2012. Carbon isotope stratigraphy. In: Gradstein, F.M., Ogg, J.G., Schmitz, M., Ogg, G. (Eds.), The Geologic Time Scale. Elsevier. The Netherlands. 207-232.

Schenau, S.J., De Lange, G.J., 2001. Phosphorus regeneration vs. burial in sediments of the Arabian Sea. Mar. Geol. 75, 201-217.

Schenau, S.J., Reichart, G.J., De Lange, G.J., 2005. Phosphorus burial as a function of paleoproductivity and redox conditions in Arabian Sea Sediments. Geochim. Cosmochim. Acta. 69 (4), 919-931.

Schieber, J., Southard, J., Thaisen, K., 2007. Accretion of mudstone beds from migrating floccule ripples. Science 318, 1760-1763.

Schnetger, B., Brumsack, H-J., Schale, H., Hinrichs, J., Dittert, L., 2000. Geochemical characteristics of deep-sea sediments from the Arabian Sea: a high-resolution study. Deep-Sea Res. II 47. 2735-2768.

Schoepfer, S.D., Shen, J., Wei, H., Tyson, R.V., Ingall, E., Algeo, T.J., 2014. Total organic carbon, organic phosphorus, and biogenic barium fluxes as proxies for paleomarine productivity. Earth-Sci. Rev. 149. 08.017.

Scott, M.R., 1982. The chemistry of U and Th series nuclides in rivers. In: Ivanoch, M., Harmon, S. (Ed.) Uranium series disequilibrium: applications to environmental problems,. Oxford-Clarendon Press, 1st edition, 181-201.

Scott, C., Lyons, T.W., 2012. Contrasting molybdenum cycling and isotopic properties in euxinic versus non-euxinic sediments and sedimentary rocks: Refining the paleoproxies. Chem. Geol. 324-325. 19-27.

She, Z.-B., Strother, P., Papineau, D., 2014. Terminal Proterozoic cyanobacterial bloomsand phosphogenesis documented by the Doushantuo granular phosphorites II: microbial diversity and C isotopes. Precambrian Res. 251. 62–79.

Shimmield, G.B., Price, N.B., 1988. The scavenging of U, ^{230Th}, and ^{231}Pa during pulsed hydrothermal activity at 20^{O}S, East Pacific Rise. Geochim. Cosmochim. Acta. 52, 699-677.

Sholkovitz, E.R., Landing, W.M., Lewis, B.L., 1994. Ocean particle chemistry: The fractionation of rare earth elements between suspended particles and seawater. Geochim. Cosmochim. Acta. 58, 1567-1579.

Śliwiński, M.G., Whalen, M.T., Day, J., 2010. Trace element variations in the Middle Frasnian punctata zone (late Devonian) in the western Canada sedimentary Basin–changes in oceanic bioproductivity and paleoredox spurred by a pulse of terrestrial afforestation? Geologica Belgica 4. 459–482.

Sperling, E.A., Halverson, G.P., Knoll, A.H., Macdonald, F.A., Johnston, T., 2013. A basin redox transect at the dawn of animal life. Earth and Planetary Science Letters 371-372. 143-155.

Stevens, R-K. 1970. Cambro-Ordovician flysch sedimentation and tectonics in west Newfoundland and their possible bearing as a proto-Atlantic Ocean. 165-177. *In* Lajoie, J. (ed.). Flysch Sedimentology in North America. G.A.C. Special Paper no 7.

Taylor, S.R., McLennan, S.M., 1985. The continental crust: its composition and evolution. Blackwell, Oxford. 257-277.

Terfelt, F., Bagnoli, G., Stouge, S., 2012. Re-evaluation of the conodont *Iapetognathus* and implications for the base of the Ordovician System GSSP. Lethaia 45. 227–237.

Terfelt, F., Eriksson, M.E., Schmitz, B., 2014. The Cambrian–Ordovician transition in dysoxic facies in Baltica—diverse faunas and carbon isotope anomalies. Paleo. (3) 394. 59-73.

Thomas, W.A., 1977. Evolution of Appalachian-Quachita salient and recesses from reentrants and promontories in the continental margin. American Journal of Science, 277, 1233–1278.

Togashi, S., Okuyama-Kosunose, N., Tanaka, Y., Okai, T., Koma, T., Imai, T., Murata, Y., 2000. Young upper crustal chemical composition of the orogenic Japan Arc. Geochem. Geophys. Geosys. 1, Paper number 2000GC00083.

Tribovillard, N., Algeo, T.J., Lyons, T., Riboulleau, A., 2006. Trace metals as paleoredox and paleoproductivity proxies: an update. Chem. Geol. 232. 12-32.

Tribovillard, N., Algeo, T.J., Baudin, F., Riboulleau, A., 2012. Analysis of marine environmental conditions based on molybdenum-uranium covariation – Applications to Mesozoic paleoceanography. Chem. Geol. 324-235, 46-48.

Tripathy, G.R., Hannah, J.L., Stein, H.J., Yang, G., 2014. Re-Os age and depositional environment for black shales from the Cambrian-Ordovician boundary, Green Point, western Newfoundland. Geochem. Geophys. Geosys. 15 (4). 1021-1037.

Turgeon, S., Brumsack, H-S., 2006. Anoxic vs dysoxic events reflected in sediment geochemistry during the Cenomanian-Turonian Boundary Event (Cretaceous) in the Umbria-Marche Basin of central Italy. Chem. Geol. 234. 321-339.

Turner, D.R., Whitfield, M., Dickson, A.G., 1981. The equilibrium speciation of dissolved components in freshwaterand seawater at 25°C and 1 atm pressure*. Geochem. Cosmochim. 45. 855-881.

Tyson R. V., Pearson T. H., 1991. Modern and ancient continental shelf anoxia: an overview. In Modern and Ancient Continental Shelf Anoxia. Geololgical Society Special Publications 58. 1–26.

Tyson, R.V., 2005. The "productivity versus preservation" controversy; cause, flaws, and resolution. In: Harris, N.B. (Ed.), Deposition of Organic-carbon-rich Sediments: Models, Mechanisms and Consequences. Society for Sedimentary Geology (SEPM-SSG) Special Publication 82. pp. 17-33.

Van der Sloot, H.A., Hoede, D., Wijkstra, J., Duinker, J.C., Nolting, R.F., 1985. Anionic species of V, As, Se, Mo, Sb, Te and W in the Scheldt and Rhine estuaries and the Southern Bight (North Sea). Estuarine Coastal Shelf Sci. 21. 633-651.

van Cappellen, P., Ingall, E.D., 1994. Benthic phosphorus regeneration, net primary production, and ocean anoxia – A model of the coupled marine biogeochemical cycles of carbon and phosphorus: Paleooceanogr. 9. 677-692, doi: 1029/94PA01455.

Waldron, J.W.F., 1985. Structural history of continental margin sediments beneath the Bay of Islands Ophiolite, Newfoundland. Can. Journal of Earth Sci. 22, 1618-1632

Waldron, J.W.F., Turner, D., Stevens, K.M., 1988. Stratal disruption and development of mélange, western Newfoundland: effect of high fluid pressure in an accretionary terrain during ophiolite emplacement. Journ. Struct. Geol. 10, 861-873

Waldron, J.W.F., Stockmal, G.S., 1994. Structural and tectonic evolution of the Humber Zone, western Newfoundland. 2. A regional model for Acadian thrust tectonics. Tectonics 13 #6. 1498-1513.

Waldron, J.W.F., Anderson, S.D., Cawood, P.A., Goodwin, L.B., Hall, J., Jamieson, R.A., Palmer, S.E., Stockmal, G.S., Williams, P.F., 1998. Evolution of the Appalachian Laurentian margin: Lithoprobe results in western Newfoundland. Can. J. Earth Sci. 35, 1271-1287.

Wanty, R.B. and Goldhaber, M.B., 1992. Thermodynamics and kinetics of reactions involving vanadium in naturalsystems: Accumulation of vanadium in sedimentary rocks. Geochim. Cosmochim. Acta. 56. 1471-1483.

Weaver, F.J., Macko, S. A., 1988. Source rocks of Western Newfoundland. Advances in Organic Geochemistry. Org. Chem. 13. 411-421.

Webb, G.E., Kamber, B.S., 2000. Rare earth elements in Holocene reefal microbialites: a new shallow seawater proxy. Geochim. Cosmochim. Acta 64 (9). 1557-1565.

Wedepohl, K.H., 1971. Environmental influences on the chemical composition of shales and clays. In: Ahrens, L.R., Press, F., Runcorn, S.K., Urey, H.C. (Ed.). Physics and Chemistry of the Earth. Pergamon. Oxford. 305-333.

Wedepohl, K.H., 1991. The composition of the upper Earth's crust and the natural cycles of selected metals. In: Merian, E. (Ed.), Metals and their Compounds in the Environment. VCH-Verlagsge-sellschaft, Weinheim. 3-17.

Wehrli, B., Stumm, W., 1989. Vanadyl in natural waters: Adsorption and hydrolysis promote oxygenation. Geochim. Cosmochim. 53. 69-77.

Wei, G.J., Liu, Y., Li, X.H., Shao, L., Liang, X., 2003. Climatic impact on Al, K, Sc and Ti in marine sediments: evidence from ODP Site 1144, South China Sea. Geochem. J. 37, 593-602.

Wei, G.J., Li, X.H., Liu, Y., Shao, L., Liang, X.R., 2006. Geochemical record of chemical weathering and monsoon climate change since the early Miocene in the South China Sea. Paleooceanogr. 21, PA4214.

Werne, J.P., Sageman, B.B., Lyons, T.W., Hollander, D.J., 2002. An integrated assessment of a "type euxinic" deposit: evidence for multiple controls on black shale deposition in the middle Devonian Oatka Creek Formation. Am. J. of Sci. 302. 110-143.

Wignall, P.B., Myers, K.J., 1988. Interpreting the benthic oxygen levels in mudrocks: a new approach. Geology 16. 452–455.

Wignall, P.B., Twitchett, R.J., 1996. Oceanic anoxia and the end Permian mass extinction. Science 272. 1155–1158.

Wignall, P.B., Zonneveld, J.P., Newton, R.J., Amor, K., Sephton, M.A., Hartley, S., 2007. The end-Triassic mass extinction record of Williston Lake, British Columbia. Paleogr. Paleoclim. Paleoecol. 253. 385-406.

Williams, H., 1975. Structural succession, nomenclature and interpretation of transported rocks in western Newfoundland. Can. Journal of Earth Sci. 12, 1874-1894.

Williams, H., 1979. Appalachian Orogen in Canada. Can. Journal of Earth Sci. 16, 792–807.

Williams H. (ed.), 1995. Geology of the Appalachian-Caledonian Orogeny in Canada and Greenland. G.S.C. Geology of Canada 6.

Yamaguchi, K.E., Ogurim, K., Ogawa, N.O., Sakai, S., Hirano, S., Kitazato, H., Ohkouchi, N., 2010. Geochemistry of modern carbonaceous sediments overlain by a water mass showing photic zone anoxia in the saline meromictic Lake Kai-ike, southwest Japan: I. Early diagenesis of organic carbon, nitrogen, and phosphorus. Paleogeogr. Paleoclim. Paleoecol. 294. 72-84.

Zhao, M.-Y., Zheng, Y.-F., 2014. Marine carbonate records of terrigenous input into Paleotethyan seawater: geochemical constraints from Carboniferous limetones. Geochim. Cosmochim. Acta. 141, 508-531.

Zhao, M.-Y., Zheng, Y.-F., 2015. The intensity of chemical weathering: Geochemical constraints from marine detrital sediments of Triassic age in South China. Chem. Geol. 391, 111-122.

Zhou, L., Wignall, P.B., Su, J., Feng, Q., Xie, S., Zhao, L., Huang, J., 2012. U/Mo ratios and $\delta^{98/95}$Mo as local and global redox proxies during mass extinction events. Chem. Geol. 324–325. 99-107.

Zonneveld, K.A.F., Versteegh, G.J.M., Kasten, S., Eglinton, T.I., Emeis, K.C., Huguet, C., Koch, B.P., de Lange, G.J., Midelburg, J.J., Mollenhauer, G., Prahl, F.G., Rethmeyer, J., Wakkeham, S.G., 2010. Selective preservation of organic matter in marine environments; processes and impact on the sedimentary record. Biogeosciences 7. 483-511.

Chapter 3

Evaluation of uranium and molybdenum enrichments versus U/Mo ratios in shales and carbonates and Mo isotope compositions in carbonates as paleoredox proxies: A case study from the Green Point Cambrian-Ordovician boundary section, Newfoundland

To be published in Chemical Geology

Alexandre Charest Bisnaire [a*], Karem Azmy [a], Brian Kendall [b], Svend Stouge [c]

[a] Department of Earth Sciences, Memorial University of Newfoundland, St. John's, NL A1B3X5, Canada
[b] Department of Earth and Environmental Sciences, University of Waterloo, Waterloo, ON N2L3G1, Canada
[c] Geological Museum, University of Copenhagen, Øster Voldgrade 5, DK-1350 Copenhagen K, Denmark

Abstract

Uranium and molybdenum concentrations, enrichments, patterns of covariation, and isotope compositions have been used with increasing frequency as indicators of redox and hydrographic conditions in modern and ancient environments. In the current study, we evaluate the relationship between uranium, molybdenum and the U/Mo ratio in the shales and carbonates of the Cambrian-Ordovician Green Point Formation (Green Point, western Newfoundland) and several other modern and ancient siliciclastic and carbonate environments.

Secondly, we evaluate the δ^{98}Mo isotope ratios of the Green Point carbonates as a paleoredox proxy. U and Mo were found to have different relationships to U/Mo ratios in the shales or carbonates at Green Point. Within the shales, the covariation patterns of authigenic U/Mo (U/$\mathrm{Mo_{auth}}$) ratios with Mo ($\mathrm{Mo_{EF}}$) and to a lesser extent U ($\mathrm{U_{EF}}$) enrichment factors (EF) were found to be a reliable redox indicator. Other datasets representing many environments, when plotting U/$\mathrm{Mo_{auth}}$ to $\mathrm{Mo_{EF}}$ or $\mathrm{U_{EF}}$, yielded different, yet consistent, patterns relative to the $\mathrm{U_{EF}}$ vs $\mathrm{Mo_{EF}}$ covariation plot, differentiating oxygen levels (including within the suboxic range) and the extent of basin restriction from the open ocean. Evaluation of U/Mo ratios, Mo or U in the carbonates yielded different results. The very low U concentrations (mean = 0.93±0.81) are due to the carbonates being composed of calcite. The decrease across the anomaly level is not representative of redox variations. The main control is the low and decreasing organic matter content, within mainly suboxic conditions, which would increase pH and impede U enrichment. This is reflected in the poor positive correlation between U and U/Mo ratios. Mo concentrations (mean = 0.27±0.34) are in the range of modern and ancient carbonates, suggesting the type of carbonate and pH may not have a significant impact on Mo enrichment. The Mo increase across the anomaly, the same observed in the shales, is a good indication that conditions became relatively more reducing, supported by the good inverse correlation between Mo and U/Mo ratios. Within modern carbonates from the Bahamas, U/Mo concentration ratios (U/$\mathrm{Mo_{conc}}$) were found to differentiate sediments with low and high pore-water sulfide levels. The variation in the slope between U/$\mathrm{Mo_{conc}}$ versus

Mo_{ppm} or U_{ppm} in carbonates may also provide an indication of basin restriction. The δ^{98}Mo ratios were found to be a mixed detrital and authigenic signal, and so represent minimum values, instead of the Cambrian-Ordovician seawater. The increase in δ^{98}Mo ratios upsection suggests pore-water conditions became relatively more reducing, consistent with previous interpretations.

3.1 Introduction

Paleoenvironmental reconstructions of ancient environments require the application of multiple proxies, including major, trace and rare earth elements as well as isotopic ratios. Molybdenum and uranium concentrations and isotopes have been extensively and successfully used as paleoredox indicators, particularly in shales but now also in carbonates, due to their sensitivity to changes in water column oxygenation, particularly when in combination with total organic content [TOC] (Dean et al., 1999; Siebert et al., 2003; Algeo and Maynard, 2004; Algeo and Lyons, 2006; McManus et al., 2006; Tribovillard et al., 2006; Algeo and Tribovillard, 2009; Morford et al., 2009a; Voegelin et al., 2009; Czaja et al., 2012; Tribovillard et al., 2012; Scott and Lyons, 2012; Xu et al., 2012; Partin et al., 2013; Romaniello et al., 2013; Azmy et al., 2015; Kendall et al., 2015; Wen et al., 2015; Gao et al., 2016; Romaniello et al., 2016). Both trace metals become more authigenically enriched within sediments as bottom-water oxygen levels reach anoxia and dissolved sulfide increases to reach euxinia (Emerson and Huested, 1991; Jones and Manning, 1994; Crusius and Thomson, 2000; Erickson and Helz, 2000; Adelson et al., 2001; Wignall et al., 2007). Their pattern of enrichment differs in low-O_2 conditions since the intensity of their authigenic enrichment is dependent on different processes and attributes (Helz et al., 1996; Zheng et al., 2000; 2002a; 2002b; Algeo and Maynard, 2004; Tribovillard et al., 2006; Algeo and Tribovillard., 2009; Zhou et al., 2012).

Aqueous authigenic U removal from seawater occurs primarily at or below the sediment-water interface (i.e. within pore-waters) in reducing conditions. Under oxic-suboxic conditions, U is present mainly as unreactive and soluble U(VI) in the form of uranyl carbonate complexes in seawater and additionally as other complexes, $UO_2(OH)^-$ and UO_2^{2+} within groundwaters (Langmuir, 1978; Klinkhammer and Palmer, 1991; Calvert and Pedersen, 1993; Algeo and Tribovillard, 2009; Brennecka et al., 2011; Chen et al., 2016). The fine-grained siliciclastic sediments in these environments typically contain < 5ppm U (Morford et al., 2009a). U(VI) becomes reduced to U(IV) at/near the boundary where Fe^{3+} is reduced to Fe^{2+}, either abiotically with $[H_2S]_{aq}$ being the reductant or catalyzed by bacterial enzymes (Cochran et al., 1986; Anderson, 1987; McKee et al., 1987; Barnes and Cochran, 1990; Lovley et al., 1991; Lovley et al., 1993; Chaillou et al., 2002; Zheng et al., 2002a; 2002b; Sani et al., 2004; Hua et al., 2006; Morford et al., 2009a; 2009b; Brennecka et al., 2011; Romaniello et al., 2013). Authigenic U will form as organic-metal ligands in humic acids, or precipitated as uraninite (UO_2), U_3O_7 or U_3O_8 in anoxic sediments (Barnes and Cochran, 1990; Klinkhammer and Palmer, 1991; Zheng et al., 2002a; McManus et al., 2005; Bone et al., 2017a). Upon short-lived exposure to oxygenated waters, U may be released from sediments. This is mainly dependant on organic matter content (Tribovillard et al., 2006; Algeo and Tribovillard, 2009; Bone et al., 2017b). Uranium can also be included in carbonates. Within the environmental pH range (6 to 8), U phases will be more soluble and will tend to form aqueous $UO_2(CO_3)_2^{2-}$ (Krestou and Panias, 2004; Beazly et al., 2011). Oxidized U (VI) can be incorporated within aragonite without any coordination change, while a coordination change is required within incorporation into calcite (Reeder et al., 2000; Chen et al., 2016). Stable UO_2^{2+} can also substitute for Ca in calcite (Kelly et al., 2003; 2006). Within calcite, reduced U(IV) can substitute for Ca(II) in reducing settings (Sturchio et al., 1998). Furthermore, during diagenesis, U may be released and then reincorporated from ambient pore-water fluids (Land, 1986).

Molybdenum enrichment within sediments is dependant on the environmental chemistry, namely organic matter input and the prevailing metabolic processes occurring, within sediment pore-waters and the overlying water column (Crusius et al., 1996; Canfield and Thamdrup, 2009; Poulson Brucker et al., 2009; Scott and Lyons, 2012). Total Mo becomes increasingly authigenically enriched within sediments as pore-water & water column oxygen levels decrease and dissolved sulfide levels thereafter start to increase (Emerson and Huested, 1991; Jones and Manning, 1994; Crusius and Thomson, 2000; Erickson and Helz, 2000; Adelson et al., 2001; Wignall et al., 2007; Scott and Lyons, 2012). Within the oxic zone, Mo occurs as soluble and stable MoO_4^{2-}. Authigenic enrichment is limited, with Mo_{auth} concentrations normally < 5ppm Mo for fine-grained siliciclastic sediments

(Zheng et al., 2000; Morford et al., 2009a). In sediments deposited from well-oxygenated bottom waters (O_2 >> 10 μM), Mo enrichment occurs as Mo-bearing Mn-oxides within the Mn-oxidation zone. Mo enrichment to a lesser extent also occurs as Mo-bearing Fe-oxides in the Fe-oxide zone (Canfield and Thamdrup, 2009; Scott and Lyons, 2012). After reductive dissolution of these oxides at deeper depths in the sediments, Mo is recycled back into the oceans unless a sulfate-reducing zone is present deeper within the sediments (bottom water O_2 < 10 μM; Scott and Lyons, 2012). If a sulfate-reducing zone is present, Mo released as MoO_4^{2-} from Fe-Mn oxide dissolution will be re-adsorbed permanently as MoS_4^{2-} (Johnson et al., 1992; Morford and Emerson, 1999; Scott and Lyons, 2012). Under anoxic-sulfidic conditions attained either in the sediment pore fluids or water column, molybdate (MoO_4^{2-}) is converted to thiomolybdate ($MoO_xS_{4-x}^{2-}$) and Mo-polysulfides (Dahl et al., 2013). Mo scavenging by organic matter and Fe-sulfide phases increases under these conditions, with concentrations in sediments of >25 Mo ppm for euxinic conditions (Scott and Lyons, 2012).

U and Mo concentrations and authigenic enrichments have been increasingly applied together to help reconstruct the nature of different depositional environments (McManus et al., 2006; Tribovillard et al., 2006; Algeo and Tribovillard, 2009; Tribovillard et al., 2012; Zhou et al., 2012; see Chapter 2). Comparing patterns of U and Mo enrichment in sediments from modern marine environments can be very informative regarding its redox geochemistry and degree of restriction of its environment of deposition (Algeo and Tribovillard, 2009;

Tribovillard et al., 2012). One application is the use of the U/Mo ratio (McManus et al., 2006; Zhou et al., 2012; see Chapter 2). Within both modern and ancient environments, the U/Mo ratio was found to be very sensitive to variations of the bottom-water oxygen content within the suboxic range (McManus et al., 2006; Zhou et al., 2012; see Chapter 2). This reflects U enrichment within the Fe(III) reducing zone within sediments below suboxic waters, prior to Mo enrichment within the sulfate-reducing zone (Helz et al., 1996; Zheng et al., 2000; 2002a; 2002b; Scott and Lyons, 2012). As oxygen levels in the water column become lower and highly suboxic to anoxic conditions are reached, the U/Mo ratio decreases due to the increased Mo uptake relative to U within the sediments as the sulfate-reducing zone moves closer to the sediment-water interface (Algeo and Tribovillard, 2009; Canfield and Thamdrup, 2009; Scott and Lyons et al., 2012).

The Mo isotope composition of sediments tends to increase as $[O_2]_{aq}$ decreases and $[H_2S]_{aq}$ increases within the pore fluids and water column. Marine sinks are categorized as oxic, suboxic, anoxic, and euxinic siliciclastic sediments, as well as carbonate sediments (Barling et al., 2001; Siebert et al., 2003; Poulson et al., 2006; Siebert et al., 2006; Neubert et al., 2008; Tribovillard et a., 2008b; Poulson Brucker et al., 2009; Voegelin et al., 2009; Scheiderich et al., 2010; Nägler et al., 2011; Goto et al., 2014; Romaniello et al., 2016). Application of the δ^{98}Mo paleoredox proxy to carbonates is in its early stages (Voegelin et al., 2009, 2010; Czaja et al., 2012; Romaniello et al., 2016). The Mo enrichment in carbonates may be controlled by pore-water $[H_2S]_{aq}$ content (Romaniello et al., 2016). Modern skeletal carbonates have lower δ^{98}Mo values compared to modern seawater (~2.3‰; Barling et al., 2001; Siebert et al., 2003; Nakagawa et al., 2012; Nägler et al., 2014), suggesting Mo isotope fractionation results in preferential removal of lighter Mo isotopes to carbonate sediments (Voegelin et al., 2009; Romaniello et al., 2016). In non-skeletal carbonates, Mo is primarily incorporated in carbonates during primary precipitation at low pore-water sulfide levels (<20μM H_2S_{aq}), such as in ooid sands (Voegelin et al., 2009; Romaniello et al., 2016). Concentrations of Mo in such settings remain low, at <0.2ppm, with δ^{98}Mo on average 0.5-1.0‰ lower than the global seawater value of 2.3±0.1‰ (Voegelin et al., 2009; Romaniello et al., 2016). Authigenic enrichment of Mo within the sediments during early diagenesis becomes pronounced when pore water H_2S exceeds 20μM. Under these conditions, Mo uptake by sediments from pore waters is quantitative as tetrathiomolybdate becomes dominant at pore water H_2S_{aq} concentrations of ~23.5μM (Romaniello et al., 2016). This results in high concentrations of Mo in sediments (1-27ppm). High concentrations of H_2S result from high organic content in these sediments, which favors high rates of microbial sulfate reduction (Romaniello et al., 2016). The δ^{98}Mo of the sulfidic carbonate sediments is 1.6-2.5‰, ranging from 0.7 lighter to 0.2 ‰ higher than seawater δ^{98}Mo (Romaniello et al., 2016). Hence, the ability of carbonate δ^{98}Mo to record the contemporaneous seawater value may depend on quantitative thiomolybdate formation and scavenging (Romaniello et al., 2016), as is also the case for organic-rich, fine-grained siliciclastic sediments (Arnold et al., 2004; Neubert et al., 2008).

In this study, the objectives are threefold. First, the U/Mo ratios of the shales are compared to U and Mo concentrations and enrichment factors of the Green Point Formation Cambrian-Ordovician boundary section as an indicator of the boundary between suboxic and anoxic conditions in the local depositional environment. This approach is then expanded to include multiple previously investigated sections from different modern and ancient environments.

Secondly, the U and Mo contents of the Green Point carbonates are evaluated. The U-Mo covariation approach is then taken and reapplied to the carbonates of the same section in addition to modern carbonates from the Bahamas platform and slope to evaluate its use as a novel carbonate paleoredox proxy (Romaniello, 2012; Romaniello et al., 2013; 2016).

Our third objective is to evaluate the δ^{98}Mo ratios of the Green Point Formation carbonates as a redox proxy through comparison with previously published δ^{238}U data on the same samples (Azmy et al., 2015), modern and ancient carbonates from other sections (Voegelin et al. 2009; 2010; Romaniello et al., 2016), late Cambrian and early Ordovician shales from other sections (Dahl et al., 2010), and independent constraints on local redox conditions at Green Point based on shale and carbonate geochemistry (this study; Tripathy et al., 2014; Azmy et al., 2015).

3.2 Geological Setting

3.2.1 Green Point Geological History

For a more complete description of the Green Point Formation Cambrian-Ordovician section, please see James et al., 1986; Barnes, 1988; Cooper et al., 2001a; Azmy et al., 2014; 2015 and Chapter 2 of this thesis. Western Newfoundland is the north-easternmost extension of the Appalachian fold-belt and belongs to the tectonostratigraphic Humber Zone of the Appalachian-Caledonian orogen comprising a record of continental platform and margin deposits of Laurentia (Stevens, 1970; Williams, 1975; 1979; 1995; Hibbard et al. 2006; 2007).

The allochthon Cow Head Group is well exposed on the western coast of the Great Northern Peninsula, Newfoundland (Fig. 1.1). It is preserved in tectonically imbricated, west-verging, locally overturned, thrust slice stacks (James and Stevens 1986; Waldron, 1985; Waldron et al., 1988). Deposition of the Cow Head Group occurred on the continental slope of the Laurentian margin along the great American carbonate bank during the early Cambrian to early Ordovician (Fig. 1.1; James and Stevens, 1986; James et al., 1989; Knight et al. 1995; Cawood et al., 2001; Cooper et al., 2001b; Lavoie et al., 2003; Boyce and Knight, 2005; Knight et al., 2008; Lavoie et al., 2012). The associated slope deposits of the Cow Head Group are composed of shale, siltstone, parted and ribbon limestone, interrupted by breccias and conglomerates (James and Stevens, 1986; James et al., 1989; Cooper et al., 2001b; Knight et al., 2007). The Laurentian passive margin was terminated by the onset of seafloor subduction and the landward migration of a peripheral bulge (Jacobi, 1981;

Knight et al., 1991), which was caused by tectonic loading of the crust due to the westward transport of the Humber Arm allochthon in the Middle Ordovician (Taconic Orogeny) (Stevens, 1970; Williams and Stevens, 1974; Knight et al., 1991; Stockmal et al., 1995; 1998; Cooper et al., 2001b).

3.2.2 Green Point Formation Cambrian-Ordovician Section

The Cambrian-Ordovician boundary section studied here is exposed at Green Point, Western Newfoundland. The Green Point Formation comprises the distal fine-grained sedimentary rocks of the Cow Head Group. At Green Point, the formation is composed of slope rhythmites (siliciclastic-carbonate sequence) with a few carbonate debris flows (Fig. 1.2; 2.1b; James and Stevens, 1986; Cooper et al., 2001a; see Chapter 2). The sequence is composed primarily of green, grey and black-coloured shales and carbonaceous shales associated with oxic to slightly suboxic, highly suboxic, and anoxic (probably ferruginous) conditions, respectively. The carbonate content of the shales is early-diagenetic in nature (Coniglio and James, 1990). The shales are interbedded with unaltered primary carbonates (composed of in-situ micrite and detrital carbonate material derived from the slope) and siltstones (Fig. 1.2; James and Stevens, 1986; Coniglio and James, 1990; Azmy et al., 2014; see Chapter 2). The previous evaluation of both the carbonates and shales at Green point indicates that post-depositional diagenesis of the section was minimal (Azmy et al., 2014; 2015; see Chapter 2). At the Green Point locality, the Green Point Formation has been overturned and slightly faulted (James and Stevens, 1986; see Chapter 2), but shows little visual evidence of hydrothermal alteration or metamorphism (Nowlan and Barnes, 1987; Tripathy et al., 2014; see Chapter 2). The Green Point Formation is subdivided into the Martin Point Member, Broom Point Member, studied here, and lastly the St. Paul's Member (James and Stevens, 1986). The upper Martin Point Member, present in outcrop, is dominated by green and grey shales with few occurrences of black shales and few packages of thin lime mudstone rhythmites (Fig. 1.2; 2.1d; see Chapter 2). Near the top of the upper Martin Point Member, a geochemical anomaly was identified in both the carbonates and shales, and is defined by a negative $\delta^{13}C_{carb}$ excursion (Azmy et al., 2014; 2015; see Chapter 2). The lower Broom Point Member is composed of mostly grey and black shales interbedded with abundant limestone rhythmites and siltstones compared with the upper Martin Point Member (Fig. 1.2; see Chapter 2). The Cambrian-Ordovician boundary is located near the base of the Broom Point Member, based on the biostratigraphy (Cooper et al., 2001a).

Redox conditions within the Cambrian-Ordovician boundary section varied widely between potentially oxic-slightly suboxic to anoxic (James and Stevens, 1986; Azmy et al., 2015; see Chapter 2). Oxic to slightly suboxic conditions were previously characterized by very high proportions of green shales (Fig. 1.2), which have elevated Th/U, U/Mo_{auth} and $(\%U_{ter})_x$ values, very low Mo (ppm & EFs), U (ppm & EFs), authigenic U, V (ppm and EFs), V/Cr, and TOC, as well as good correlations between U or V versus Al concentrations (See Chapter 2). More highly suboxic conditions were characterized by the presence of mostly grey shales (Fig. 1.2) paired with lower Th/U and $(\%U_{ter})_x$ values, as well as low U/Mo_{auth}, Mo (ppm and EFs), U (ppm and EFs), authigenic U, V (ppm and EFs), V/Cr and TOC. Anoxic conditions (Fig. 1.2; See Chapter 2) were identified by the presence of mostly black shales, which have low Th/U, $(\%U_{ter})_x$ and U/Mo_{auth} values, and higher Mo (ppm and EFs), U (ppm and EFs), authigenic U, V (ppm and EFs), V/Cr and TOC. Anoxic conditions were interpreted to be ferruginous, and not euxinic, based on Fe/Al ratios and Mo concentrations (see Chapter 2).

3.2.3 Other Datasets

In addition to the data from Green Point, several other published datasets from both modern and ancient environments were used in this study, and are summarized in Tables 3.1 and 3.2 (Berelson et al., 1987; Berelson et al., 1996; Eberli et al., 1997; Henderson, 2002; McManus et al., 2003; Hammond et al., 2004; Berelson et al., 2005; McManus et al., 2006; Poulson et al., 2006; Tribovillard et al., 2008a; Piper and Calvert, 2011; Romaniello, 2012; Tribovillard et al., 2012; Zhou et al., 2012; Romaniello et al., 2013; Romaniello et al., 2015; Calvert et al., 2015; Piper et al., 2016; Romaniello et al., 2016).

Locations	Age	Redox Condition
Central California Margin, b, d, f, j		
Sta. 02	Modern	Suboxic*
Sta. 03	Modern	Oxic*
Sta. 09	Modern	Suboxic*
Southern California, a, b, d, f, i, j, k, l		
Patton Escarpment	Modern	Oxic*
Tanner Basin	Modern	Severely Suboxic*
Catalina Basin	Modern	Severely Suboxic*
Santa Monica Basin	Modern	Anoxic*
San Clemente Basin	Modern	Suboxic-Anoxic*
San Pedro Basin	Modern	Severely Suboxic*
Pacific Mexico Margin, c, j, k		
San Blass	Modern	Anoxic*
Soledad Basin	Modern	Anoxic*
Mazatlan Margin	Modern	Anoxic*
Chile Margin, i, j		
MC22	Modern	Oxic*
MC24	Modern	Suboxic*
MC39	Modern	Suboxic*
MC42	Modern	Suboxic*
Peru Margin, g, i, j		
MC82	Modern	Anoxic-Euxinic*
Orca Basin, m	Modern	Anoxic-Euxinic
Black Sea, n, r		
GC-14	Older Dryas - Modern	Oxic-Limnic to Anoxic-Euxinic
BC-3	Modern	Anoxic-Euxinic
BC-7	Modern	Anoxic-Euxinic
BC-15	Modern	Anoxic-Euxinic
BC-16	Older Dryas - Modern	Oxic-Limnic to Anoxic-Euxinic
GGC79	15kyr - Modern	Oxic-Limnic to Anoxic-Euxinic
Cariaco Basin, r	Modern	Anoxic-Euxinic
South-Central China, p		
Wufeng Fm.	Late Ordovician	Anoxic-Euxinic
Lungmachi Fm.	Early Silurian	Anoxic-Euxinic
Upper Dalong Fm.	Late Permian	Suboxic to Anoxic
Mid. Dalong Fm.	Late Permian	Anoxic
Lower Dalong Fm.	Late Permian	Slightly Anoxic
Argiles de Wilmereux, o	Tithonian	Oxic to Suboxic
La Charce Section, o	Hauterivian	Oxic to Suboxic

Table 3.1: Summary of siliciclastic modern depositional environments or ancient successions and their redox characteristics. Data from a. Berelson et al., 1987; b. Berelson et al., 1996; c. Eberli et al., 1997; d. McManus et al., 1997; e. Henderson, 2002; f. McManus et al., 2003; g. Böning et al., 2004; h. Hammond et al., 2004; i. Berelson et al., 2005; j. McManus et al., 2006; k. Poulson et al., 2006; l. Chan et al., 2008 ; m. Tribovillard et al., 2008a; n. Piper and Calvert, 2011; o. Tribovillard et al., 2012; p. Zhou et al., 2012; q. Calvert et al., 2015; r. Piper, 2016. * indicates redox conditions for specific locations are at least partially inferred based on bottom-water O_2 conditions (Savrda and Bottjer, 1991; Wignall, 1994; Algeo and Tribovillard, 2009).

Locations	Age	Pore-Water Sulfides
Bahamas West Grand Bank, a, b		
Site 1003	~780 ka	High
Site 1004	~780 ka	High
Site 1005	228ka	High
Site 1006	Holocene-Pleistocene (11-783ka)	Intermittently high and low
Site 1008	204-356ka	High
Site 1009	192-336ka	High
Bahamas Platform, b, c, d		
Drill Core 1	Modern	High
Drill Core 2	Modern	Low
Drill Core 3	Modern	High
Drill Core 4	Modern	High

Table 3.2: Summary of carbonate datasets along with pore-water characteristics. High $H_2S_{aq} > 20\ \mu M$. Low $H_2S_{aq} < 20\ \mu M$. Data from a. Eberli et al. 1997; b. Romaniello, 2012; c. Romaniello et al., 2013; d. Romaniello et al., 2016.

3.3 Methodology

3.3.1 Sampling

Samples of both the interbedded shales and carbonates were collected at high resolution (up to <10cm per sample) at Green Point, western Newfoundland (49^{O} 40’ 51” N; 57^{O} 57’ 36” W), encompassing the Cambrian-Ordovician GSSP level within the upper Martin Point and Lower Broom Point Members (Fig. 1.2). Lime mudstone samples were petrographically examined using a polarizing microscope (Azmy et al., 2014). The samples were stained with alizarin Red-S and potassium ferricyanide solutions (Dickson, 1966; Azmy et al., 2015). Cathodoluminescence was conducted at 8 kV and 0.7mA (Azmy et al., 2015).

3.3.2 Powder extraction

In preparation for carbonate microsampling, mirror image slabs of thin sections were polished, washed with deionized water, and dried overnight at 50^{O}C. The finest-grained areas were identified through petrographic examination and were separated from the secondary cements. About ~ 10 mg was extracted from each sample following the method described in Azmy et al. (2015).

For shale analyses, ~ 9 g of material was crushed and powdered from each sample using an electric mill with tungsten carbide disks.

3.3.3 Elemental compositions

For carbonates, the protocol for analysis of the elemental composition of carbonates has been documented and discussed by Azmy et al. (2014; 2015). Results were obtained by digesting ~ 10 mg of powdered sample in 5% (v/v) acetic acid for 70-80 min, followed by analysis using an Elan DRC II inductively coupled plasma mass spectrometer (ICP-MS) at Memorial University of Newfoundland for major, minor, and trace elements (including REEs). Standards used to verify instrument accuracy were the international DLS-88a and CCH-1 standards, along with internal standards. Uncertainties were < 5% for elemental analyses. Results were normalized to 100% carbonate.

Shale elemental compositions were analyzed and discussed in detail in Chapter 2. Approximately 100-150 mg of bulk shale powder was ashed at 550°C and digested in multiple metal-grade acid-combinations of HF, HNO_3 and HCl.

Following dissolution, splits of each sample were analyzed for major, minor, and trace element abundances using a Thermo X-Series 2 quadrupole ICP-MS at the University of Waterloo (cf. Kendall et al., 2010). Instrument accuracy was verified using the USGS SBC-1 and SGR-1b standards (certified deviation: ≤10%). Instrumental drift during analysis was corrected with internal element standards. The accuracy of reproducibility of elemental concentrations was typically within 5%.

3.3.4 Mo isotope analyses

For Mo isotope measurements in the carbonates, ~9 g of each powdered sample was ashed at 750^{O}C to calcinate the carbonate matrix and destroy organics (Romaniello et al., 2013; Azmy et al., 2015). Authigenic Mo was extracted using a 2-step cold leach, first with 1M HCl until no further reaction with the sample was visible, and then with 1M HNO_3, which minimized detrital contamination.

A portion of the sample solution splits from the carbonates was equilibrated with an appropriate amount of Mo double spike (^{97}Mo-^{100}Mo; Dahl et al., 2010; Herrmann et al., 2012; Lu et al., in press). The double spike enables correction for instrumental and column chromatography mass fractionation as well as precise calculation of the Mo concentration in the sample solution. Molybdenum was separated from the sample-spike mixture using a two-step anion and cation exchange chromatography method (Barling et al., 2001; Arnold et al., 2004; Duan et al., 2010). Samples were reacted with a HNO_3-H_2O_2 mixture to destroy residual organic material from the anion and cation resins (Romaniello et al., 2013) and were then taken up in 2% HNO_3 for mass spectrometry. Molybdenum isotope compositions were measured on a Thermo Scientific Neptune multi-collector inductively coupled plasma mass spectrometer (MC-ICP-MS) at Arizona State University using an ESI Apex desolvating nebulizer (Lu et al., in press). Sample Mo isotope compositions were reported relative to NIST SRM 3134 = 0.25 ‰ (Goldberg et al., 2013; Nägler et al., 2014; Kendall et al., 2017):

$$\delta^{98/95}\mathrm{Mo}_{\mathrm{sample}}(‰) = 1000 \times [{}^{98/95}\mathrm{Mo}_{\mathrm{sample}}/{}^{98/95}\mathrm{Mo}_{\mathrm{NIST\ SRM\ 3134}} - 1] + 0.25$$

Samples were run at least in duplicate during different mass spectrometry sessions. Full powder replicates for three carbonate samples (GP 7, GP 40, and GP 48) yielded identical δ^{98}Mo within analytical uncertainties (10‰; Kendall et al., 2017).

3.4. Results

3.4.1 U and Mo Concentrations

The Mo and U concentrations in shales have often successfully been used as proxies of redox conditions (Algeo and Maynard, 2004; Algeo and Lyons, 2006; Tribovillard et al., 2006; Algeo and Maynard, 2008; Algeo and Tribovillard., 2009; Śliwiński et al., 2010; Sahoo et al., 2012; Scott and Lyons, 2012; Partin et al., 2013; Gao et al., 2016). Within the shales at Green Point (Sample 166 not included; see Chapter 2), U concentrations vary from 1.0 to 9.7 ppm (mean = 3.1±2.0 ppm, *n*=34; see Chapter 2). The shale Mo concentrations vary from 0.3 to 13.9 ppm (mean = 2.6±3.0 ppm, *n*=35; Fig. 3.1; Appendix 3.1). The Mo and U concentrations are moderately-correlated ($R^2 = 0.56$; Fig. 2.8) Their behavior across the anomaly level of Azmy et al. (2015) was evaluated in Chapter 2.

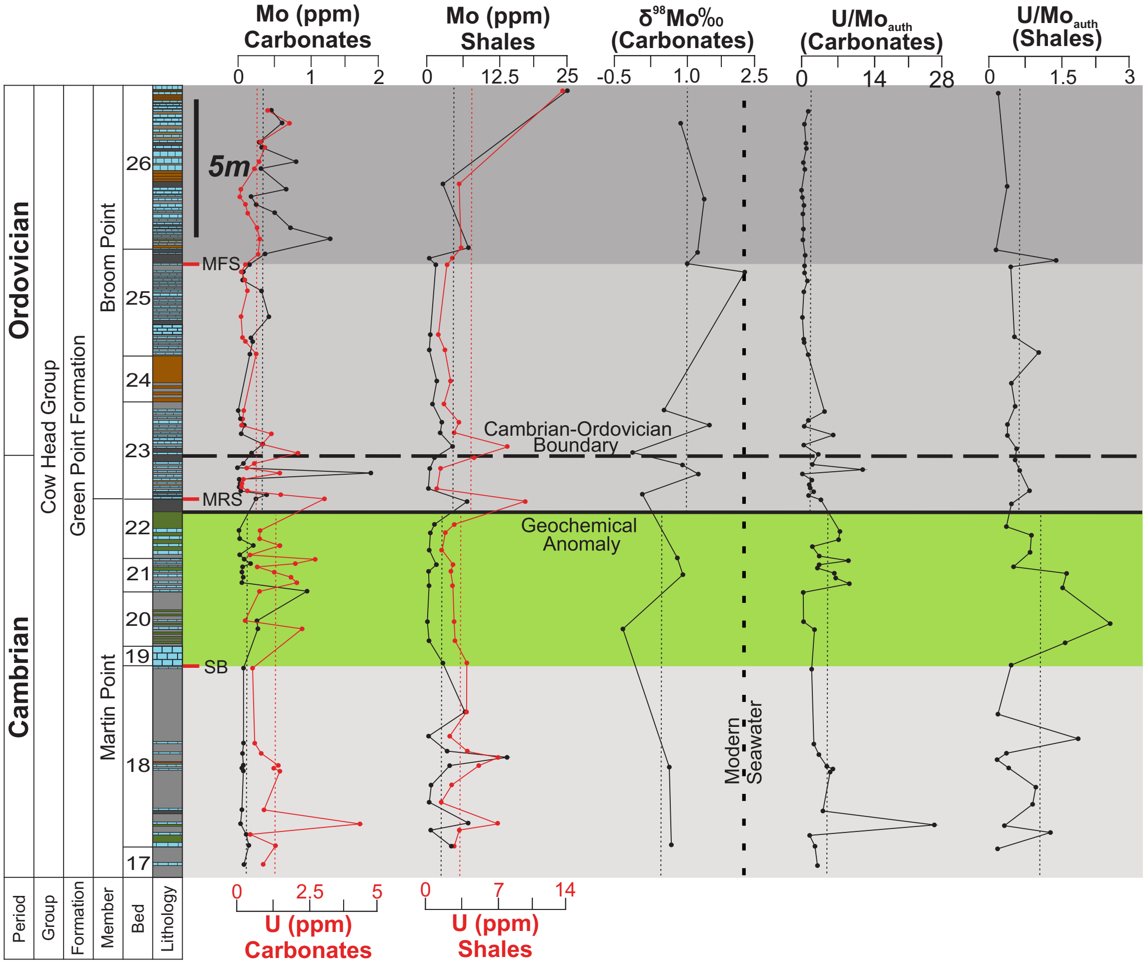

Figure 3.1: Mo (ppm), U (ppm), and U/Mo$_{auth}$ paleoredox profiles for both the shales and carbonates and the δ^{98}Mo for the carbonates across the Cambrian-Ordovician boundary at the GSSP in Green Point (western Newfoundland). The solid black line, the dashed black line, vertical red, and black dotted lines are defined as in Figures 2.2 and 2.4.

Uranium and molybdenum have been investigated as redox proxies in carbonates, often in conjunction with analysis of δ^{98}Mo and δ^{238}U (Voegelin et al., 2009; 2010; Czaja et al., 2012; Romaniello et al., 2013; Azmy et al., 2015; Chen et al., 2016; Gao et al., 2016; Romaniello et al., 2016; Elrick et al., 2017). Carbonate U concentrations within the studied section vary between 0.1 and 4.3 ppm, with a mean of 0.93±0.81 ppm. The U concentrations decrease across the geochemical anomaly level from 1.32±0.89 to 0.67±0.64 ppm, opposite to the trend seen in the shales (Table 3.3; Azmy et al., 2015; see Chapter 2). Molybdenum concentrations in the mudstone rhythmites vary from 0.01 to 1.91 ppm. Unlike U, Mo concentrations increase above the geochemical anomaly level from 0.15±0.19 to 0.35±0.39 ppm. Mo and U concentrations are not well-correlated in the carbonates ($R^2 < 0.01$), which contrasts with the moderate correlation observed for the shales (Fig. 2.8).

	Al ppm	δ^{98}Mo ‰	Mo ppm	U ppm	U/Mo$_{conc}$ Ratio	Mo$_{EF}$ Ratio	U$_{EF}$ Ratio	U/Mo$_{auth}$ Ratio
n	60	16	60	60	60	60	60	60
Mean	1093	0.9	0.27	0.93	9.03	36.75	36.94	2.91
STDV	1552	0.6	0.34	0.81	12.46	65.80	40.89	4.02
MEDIAN	691	0.9	0.15	0.74	4.81	15.48	20.34	1.55
MIN	230	-0.3	0.01	0.10	0.20	0.76	2.47	0.06
MAX	11754	2.3	1.91	4.31	80.49	468.49	216.62	25.96
Below Anomaly								
n	26	5	24	24	24	24	24	24
Mean	1474	0.6	0.15	1.32	15.68	18.39	58.04	5.06
STDV	2322	0.5	0.19	0.89	15.83	24.97	53.90	5.11
MEDIAN	667	0.7	0.09	1.10	10.69	11.24	44.25	3.45
MIN	302	-0.3	0.03	0.29	0.81	1.76	2.47	0.26
MAX	11754	0.9	0.96	4.31	80.49	125.16	216.62	25.96
Above Anomaly								
n	34	11	34	34	34	34	34	34
Mean	817	1.0	0.35	0.67	4.60	48.99	22.87	1.48
STDV	405	0.7	0.39	0.64	6.83	80.64	19.99	2.20
MEDIAN	706	1.0	0.21	0.37	1.83	29.77	14.27	0.59
MIN	230	-0.1	0.01	0.10	0.20	0.76	5.10	0.06
MAX	2010	2.3	1.91	3.00	36.35	468.49	92.21	11.72
Two-tailed P values	0.11	0.29	0.024	0.002	0.0006	0.078	0.0009	0.0006
Mean Difference	657	-0.4	-0.2	0.65	11.08	-30.6	35.17	3.58
95% Lower Value	-154	-1.18	-0.37	0.25	4.98	-64.75	15.08	1.61
95% Upper Value	1468	0.38	-0.027	1.05	17.18	3.55	55.26	5.55

Table 3.3: Mean, standard deviation, minimum and maximum values for Al, δ^{98}Mo, U and Mo concentrations, U/Mo$_{conc}$, Mo$_{EF}$, U$_{EF}$, and U/Mo$_{auth}$ ratios in the carbonates for the whole section as

well as both below and above the geochemical anomaly level, in addition to unpaired t-test results for comparing values from both sets.

3.4.2 Enrichment Factors

For the purpose of evaluating U/Mo ratios on a comparative basis, the concentrations of U and Mo from the shales and carbonates were converted into Al-normalized enrichment factors (EF) relative to Post-Archean-Australian-Shale (PAAS) using the formula $EF = (\text{trace metal} / \text{Al})_{\text{sample}} / (\text{trace metal} / \text{Al})_{\text{PAAS}}$ (6) (Taylor and McLennan, 1985). An EF value > 1 is considered to represent enrichments relative to PAAS (Taylor and McLennan, 1985).

Within the shales, U_{EF} has a mean of 1.49±0.93, and varies between 0.64 and 4.45 across the entire section (*n*=34; Table 2.3). The Mo_{EF} values are comparably higher, with a mean of 3.98±4.83 (*n*=34; Sa 166 not included), and a range of 0.34 to 22.44 (Table 2.3). The Mo_{EF} values strongly correlate with Mo concentrations (R^2 = 0.95; Fig. 3.2a). The enrichment factors (EF) are strongly correlated to concentrations, indicating Al had little impact on enrichment factors (Fig. 3.2a). The Mo_{EF} and U_{EF} are moderately well correlated (R^2 = 0.60; Fig. 3.3).

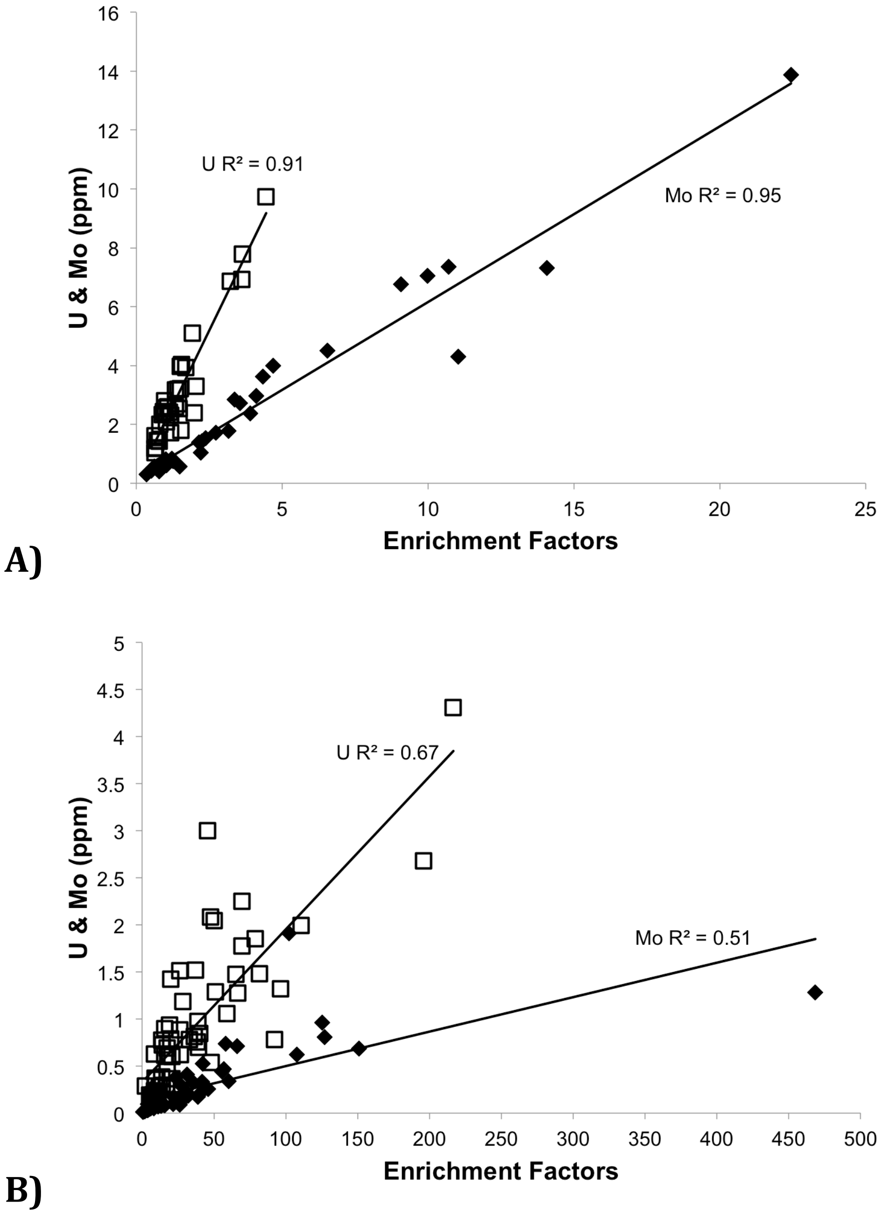

Figure 3.2: (A) Scatter plot of U concentrations vs U_{EF} values (diamonds) and Mo concentrations vs Mo_{EF} values (squares) in the shales. (B) Scatter plot of U concentrations vs U_{EF} values (diamonds) and Mo concentrations vs Mo_{EF} values (squares) in the carbonates.

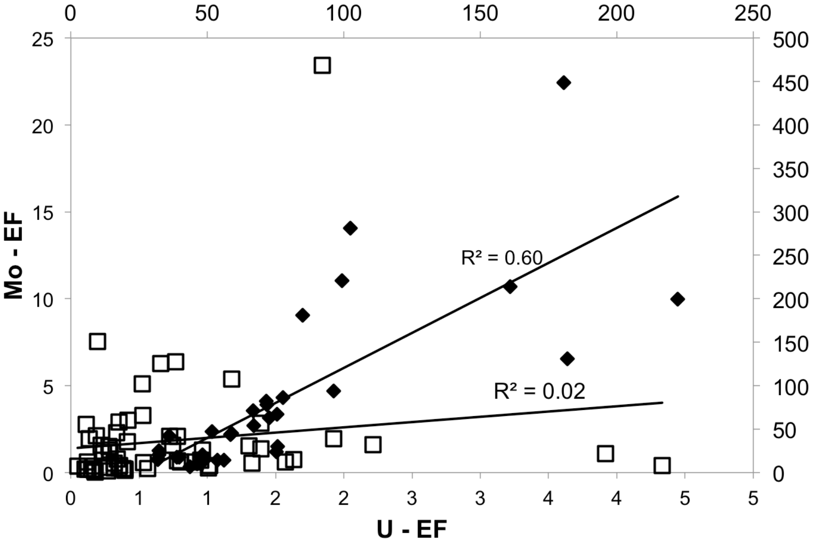

Figure 3.3: Scatter plot of U and Mo PAAS-normalized enrichment factors within the shales (diamonds), on the primary axes (lower and left), and carbonates (squares), on the secondary axes (upper and right).

Within the carbonates, U_{EF} has a mean of 36.94 ± 40.89, and varies between 2.47 and 216.62 (Table 3.3). There is a good correlation between U_{EF} values and U concentrations ($R^2 = 0.67$; Fig. 3.2b). The mean Mo_{EF} is 46.75±65.80, and varies between 0.76 and 468.49. The Mo_{EF} values and Mo concentrations are moderately correlated ($R^2 = 0.51$; Fig. 3.2b). No correlation exists between Mo_{EF} and U_{EF} behavior in the carbonates ($R^2 = 0.02$; Fig. 3.3). Carbonate EF_{PAAS} values are much higher than those found in the shales because of lower detrital Al content in the carbonates.

3.4.3 U/Mo Ratios

The U/Mo ratio was calculated in two different ways. It was first calculated using the formula $U/Mo_{conc} = U_{ppm}/Mo_{ppm}$ (12) (McManus et al., 2006; Zhou et al., 2012). Within the shales, the U/Mo$_{conc}$ varies between 0.45 and 7.88 (mean = 2.31±1.73, *n*=34), and decreases across the anomaly level from 2.85±2.07 to 1.77±0.94. Within the carbonates, the U/Mo$_{conc}$ varies between 0.20 and 80.49, with a mean of 9.03±12.46, and the values decrease across the anomaly level from 15.68±15.83 to 4.60±6.83, indicating that much greater variability between U and Mo contents is present within the carbonates, compared to the shales (Table 3.3).

The U/Mo$_{auth}$ ratio was also calculated using the formula U/Mo$_{auth}$ = U EF$_{PAAS}$/Mo EF$_{PAAS}$ (5) where Al data was available (Appendix 3.1; 3.2; see Chapter 2). This was done to eliminate the potential influence of variable detrital U and Mo contents in the samples. Shale U/Mo$_{auth}$ ratios are on average much lower than those found in carbonates, with a mean of 0.73±0.56, and a range of 0.15 to 2.54 (Appendix 3.1). A decrease in shale U/Mo$_{auth}$ ratios is observed across the geochemical anomaly level from 1.53±1.11 to 0.91±0.51 (see Chapter 2). The carbonate U/Mo$_{auth}$ ratios vary between 0.06 and 25.96 throughout the section (mean = 4.84±6.68, Table 3.3), and decrease across the anomaly level from 5.06±5.11 to 1.48±2.20 (Table 3.3; Appendix 3.2). As seen using the U/Mo$_{conc}$ ratio, the U/Mo$_{auth}$ ratio in the carbonates shows much greater variability than in the shales. To verify that results derived from the U/Mo$_{conc}$ and U/Mo$_{auth}$ equations behaved consistently, they were plotted against one-another. They have an excellent correlation (R^2 = 1.0; Fig. 3.4), indicating that no equation-related deviations occured.

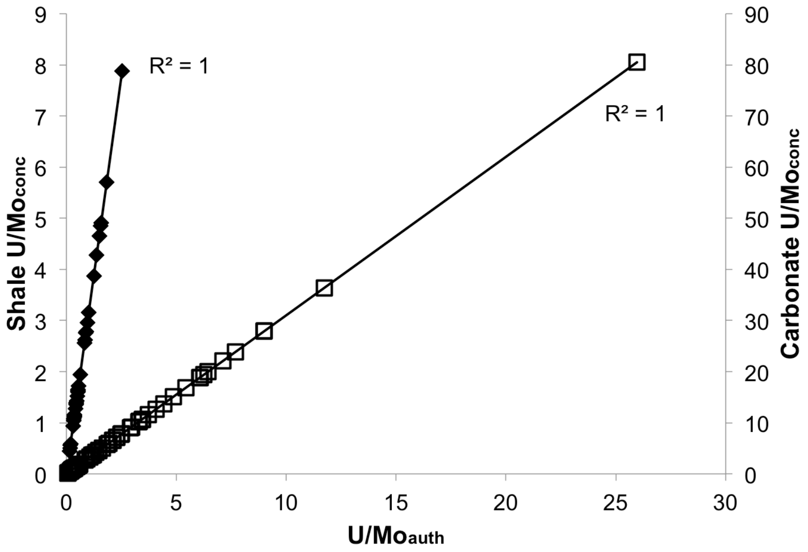

Figure 3.4: Scatter plot of U/Mo$_{auth}$ vs U/Mo$_{conc}$ for both the shales (diamonds) on the primary axis (lower and left) and carbonates (squares) on the secondary axis (lower and right).

U/Mo$_{conc}$ ratios were plotted against U and Mo concentrations within both the shales and carbonates in order to investigate their relationship. For the shales, U/Mo$_{conc}$ shows variable patterns of inverse covariation with U and Mo concentrations (Fig. 3.5). High U/Mo$_{conc}$ ratios are associated with very low U (≤3ppm) and Mo (<1ppm) concentrations (Appendix 3.1; Fig. 3.5a). As U/Mo$_{conc}$ decreases below <2 to near 0, the concentrations of U and Mo increase drastically, to maximum values of 9.74 ppm and 13.9 ppm, respectively (Sa 166 not included). Using a power function, the correlations with U/Mo$_{conc}$ are are poor for U ($R^2 = 0.12$) and good for Mo ($R^2 = 0.77$) (Appendix 3.1; Fig. 3.5). The much higher concentration observed with Mo indicates U/Mo$_{conc}$ is mainly controlled by variations in Mo in the Green Point shales. U/Mo$_{auth}$ ratios were then plotted against U$_{EF}$ and Mo$_{EF}$. In the shales, the observed pattern of enrichment is the same as noted when comparing U and Mo concentrations with the U/Mo$_{conc}$ ratios (Fig. 3.5; 3.6). The U/Mo$_{auth}$ and Mo$_{EF}$ values have an even higher correlation than observed when comparing with Mo concentration data ($R^2 = 0.84$; Fig. 3.6). A slightly higher, but still low correlation is also noted between U/Mo$_{auth}$ and U$_{EF}$ values when compared to the U/Mo$_{auth}$ versus U concentration data ($R^2 = 0.28$; Fig. 3.6).

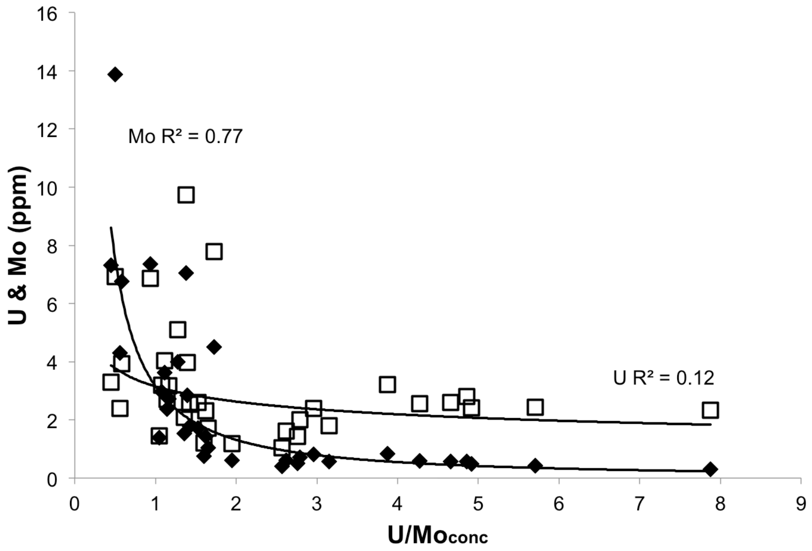

A)

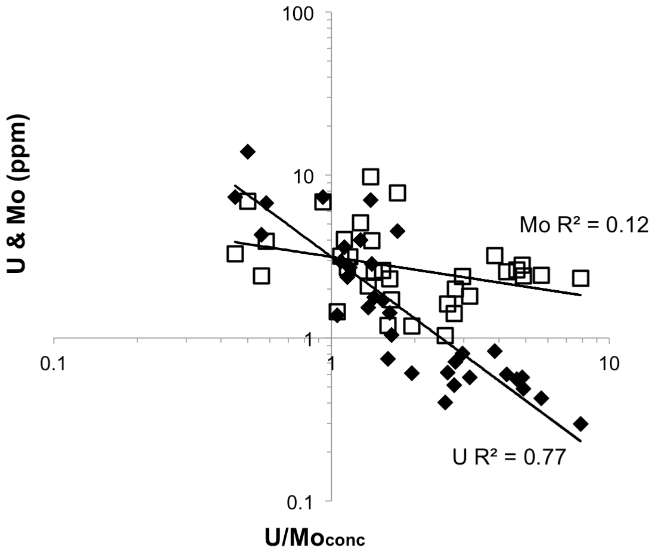

B)

Figure 3.5: (A) Scatter plot of the U/Mo$_{conc}$ ratios plotted against Mo (diamonds) and U (squares) elemental concentrations within the shales. (B) Same plot shown in log form.

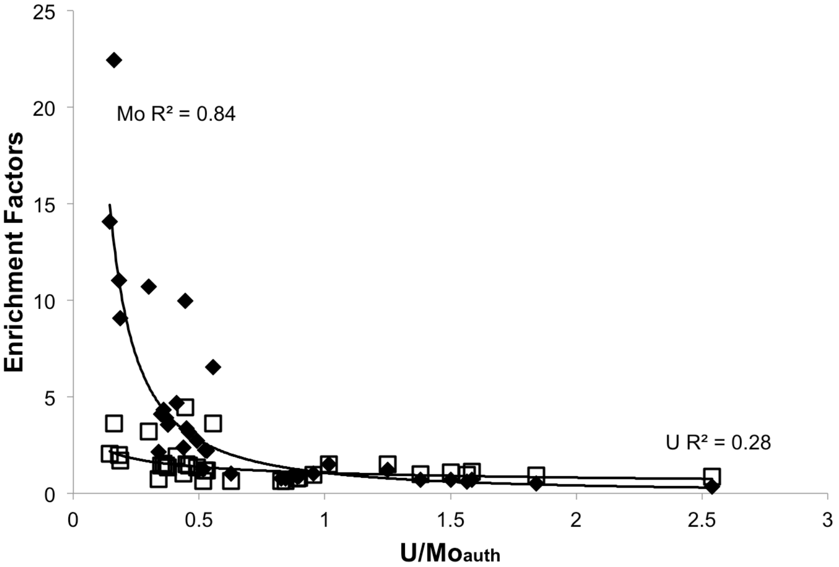

A)

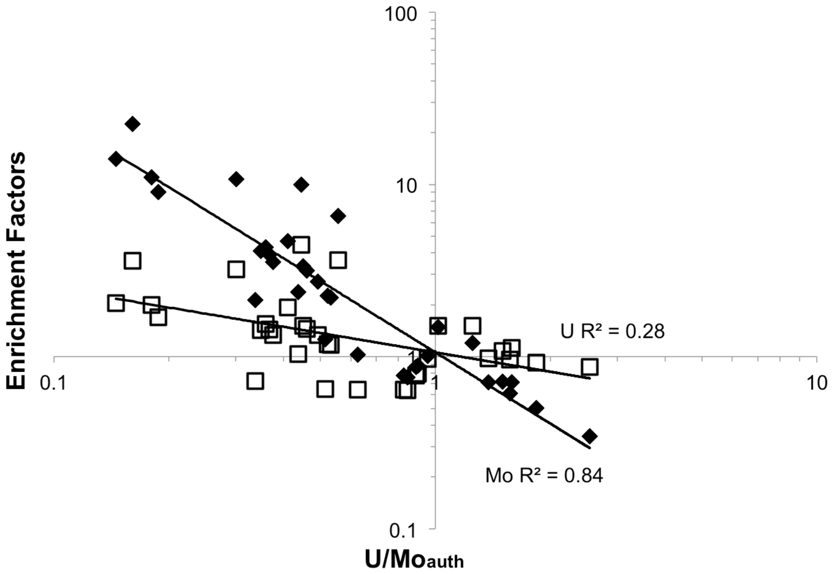

B)

Figure 3.6: (A) Scatter plot of the U/Mo$_{auth}$ ratios plotted against Mo (diamonds) and U (squares) enrichment factors within the shales. (B) Same plot shown in log form.

As was done for the shales, U/Mo$_{conc}$ was plotted against U and Mo concentrations in the carbonates (Fig. 3.7). U/Mo$_{conc}$ and Mo concentrations have a similar, moderate inverse covariation as that observed in the shales ($R^2 = 0.54$; Fig. 3.7). In contrast, U concentrations and U/Mo$_{conc}$ have a moderate positive correlation ($R^2 = 0.31$; Fig. 3.7). As observed in the shales, the carbonate U/Mo$_{auth}$ vs U$_{EF}$ and Mo$_{EF}$ shows the same pattern as seen when comparing U/Mo$_{conc}$ vs U and Mo concentrations. The U/Mo$_{auth}$ and U$_{EF}$ values have a slightly lower correlation than when comparing U/Mo$_{conc}$ and U concentration data ($R^2 = 0.18$; Fig. 3.8). When comparing U/Mo$_{auth}$ to Mo$_{EF}$, the correlation remains moderate though also slightly lower than the correlation between U/Mo$_{conc}$ and Mo concentrations ($R^2 = 0.52$; Fig. 3.8).

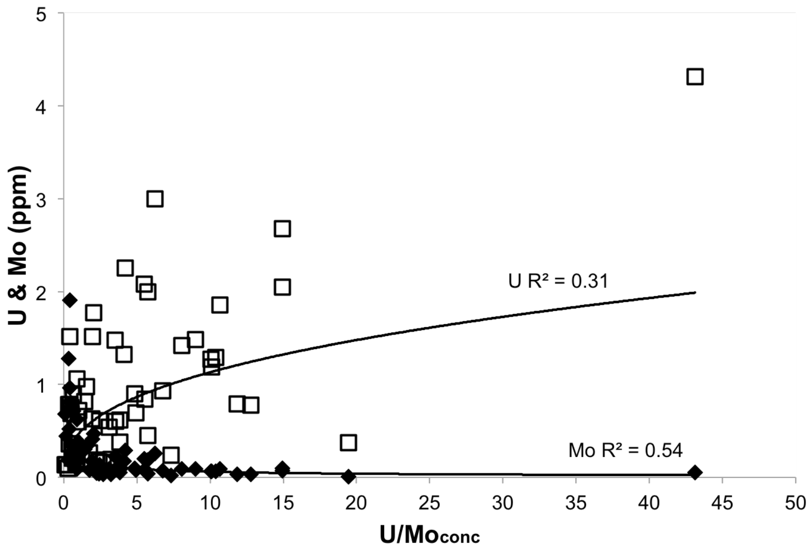

A)

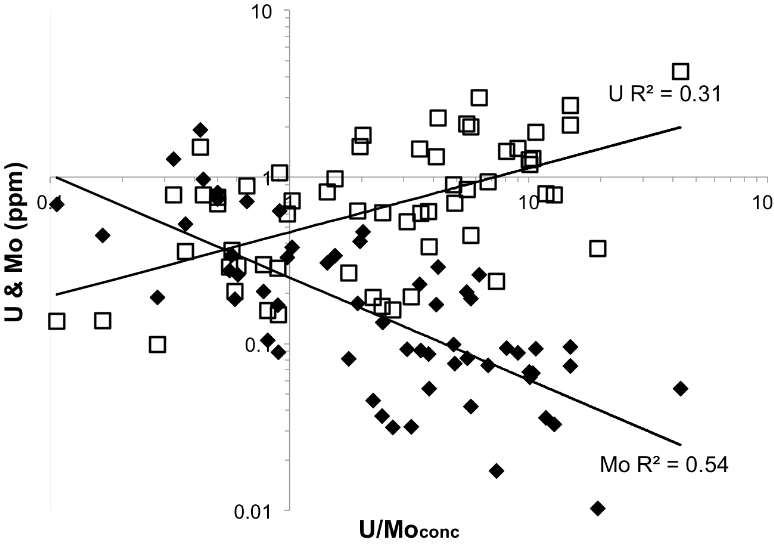

B)

Figure 3.7: (A) Scatter plot of the U/Mo$_{conc}$ ratios plotted against Mo (diamonds) and U (squares) elemental concentrations within the carbonates. (B) Same plot shown in log form.

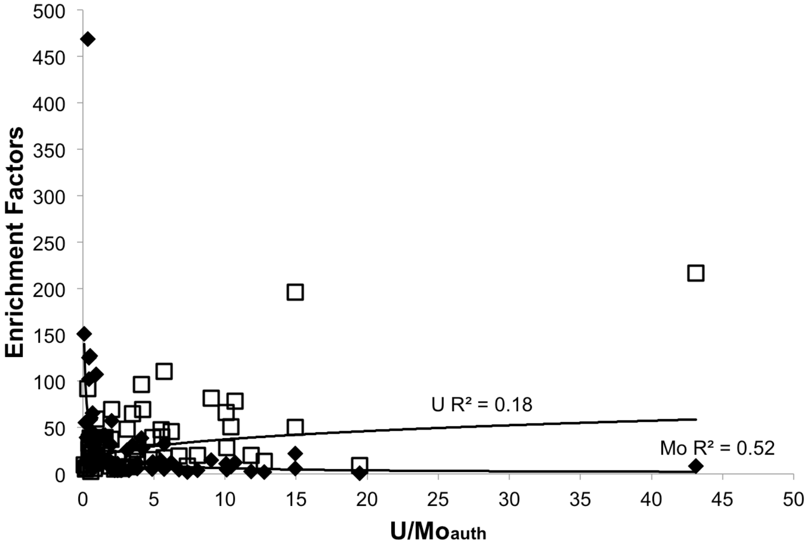

A)

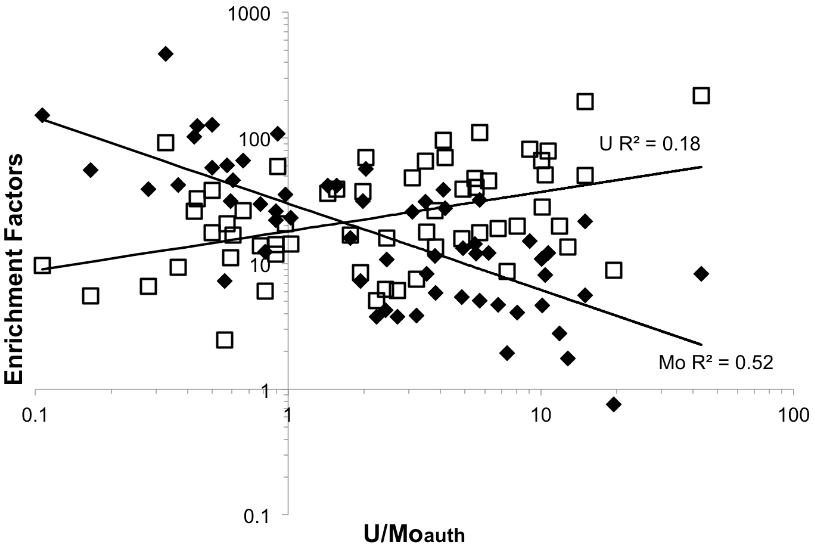

B)

Figure 3.8: (A) Scatter plot of the U/Mo_{auth} ratios plotted against Mo (diamonds) and U (squares) enrichment factors within the carbonates. (B) Same plot shown in log form.

3.4.4 Mo isotopes in the Green Point carbonates

The δ^{98}Mo values from the carbonates at Green Point vary between -0.30 and 2.34 ‰, with a mean of 0.87±0.64 ‰ (Table 3.3; Appendix 3.2). An overall increase in δ^{98}Mo is observed along with a drop in the TOC contents above the geochemical boundary defined by a negative $\delta^{13}C_{carb}$ excursion (Azmy et al., 2014). The δ^{98}Mo values have an insignificant correlation with the $\delta^{13}C_{org}$ values (Azmy et al., 2015). There is no correlation between Mo concentrations and δ^{98}Mo values ($R^2 < 0.1$). Except for one sample (GP46 = 2.34 ‰), the δ^{98}Mo values of the carbonates are lower than modern seawater (~2.3 ‰, Siebert et al., 2003; Nakagawa et al., 2012).

3.5. Discussion

3.5.1 The U/Mo ratio and U, Mo Enrichments in the Shales

3.5.1.1 Mo_{EF} and U_{EF} Covariation at Green Point

Many studies have been conducted on the behavior of Mo and U for various conditions of bottom-water oxygenation (e.g., Algeo et al., 2004; Algeo and Maynard, 2004; McManus et al., 2006; Tribovillard et al., 2006; Algeo and Tribovillard, 2009; Śliwiński et al., 2010; Tribovillard et al., 2012; Zhou et al., 2012; Tripathy et al., 2014; Lu et al., in press). A recent development of this line of research is the covariation diagram of Mo_{EF} and U_{EF} (Algeo and Tribovillard, 2009; Tribovillard et al., 2012). This diagram is a very useful tool when interpreting changes in redox conditions from the suboxic to the euxinic range. It also allows for differentiation between open-marine, partially restricted, and highly restricted environments (Algeo and Tribovillard, 2009; Tribovillard et al., 2012). Based on this diagram, the Green Point shales were deposited from mainly variably suboxic bottom waters, though ranging from oxic to anoxic, on a weakly restricted marine margin with an intermittent particle shuttle operating (Fig. 2.17). Similar interpretations were reached based on other sources of data from the same section (Cooper et al., 2001a; Azmy et al., 2014; Tripathy et al., 2014; Azmy et al., 2015; see Chapter 2). However, the covariation diagram of Mo_{EF} versus U_{EF} in its current form is of limited use when interpreting bottom water O_2 levels for weakly-restricted margins in greater detail within the suboxic range due to the low and variable enrichment factors observed under those conditions (Fig. 2.17). To remedy this, the U/Mo ratio (more sensitive to variations within the suboxic range) was taken and compared to U and Mo variations (McManus et al., 2006; Algeo and Tribovillard, 2009; Zhou et al., 2012; see Chapter 2).

3.5.1.2 Shale U/Mo$_{auth}$ vs. Mo$_{EF}$ and U$_{EF}$ at Green Point

Pore-water oxygen levels during deposition of the Green Point sediments varied widely. The Green Point samples were classified as having been deposited under bottom waters being ranging from oxic to anoxic conditions, though mainly in the suboxic range. The fluctuations observed are due to sealevel variations occurring along the margin during the overall rise in sealevel that occurs at the Cambrian-Ordovician boundary (see Chapter 2).

For the purpose of determining predictable fields based on the redox behavior of the Green Point U and Mo data, as was done for the U-Mo plot by Algeo and Tribovillard (2009), three redox categories were tentatively set, based on the work of Scott and Lyons (2012). Mo$_{EF}$ was chosen as the primary basis for comparison to U/Mo$_{auth}$, as it was previously found to be much more sensitive to redox variations in weakly restricted basins with bottom water oxygenation in the oxic-anoxic range (Algeo and Tribovillard, 2009; Tribovillard et al., 2012). This is supported by Mo having the highest correlation to U/Mo$_{auth}$ in the Green Point shales (Fig. 3.6), indicating it was the main control on U/Mo$_{auth}$ variations.

The first field combines oxic and slightly suboxic conditions. Suboxic conditions were split in two as they encompass a wide redox range approaching both oxic and anoxic values (100 μM > O_2 > 10 μM; Scott and Lyons, 2012). Oxic sediments (O_2 > 100 μM; Collier, 1985) are characterized by low TOC and high oxidant input to the sediments, resulting in the lack of a sulfate zone within the shallow pore-waters and complete dissolution of Mo-bearing Mn-oxides (Bertine and Turekian, 1973; Calvert and Pedersen, 1996). Slightly suboxic conditions would behave in a similar manner. They are considered to have low organic carbon content and bottom water O_2 levels approaching fully oxic conditions. It is likely to have been heavily affected by reductive dissolution of Mo-bearing Mn-oxides and unlikely that a strong-enough sulfidic zone developed (Morford and Emerson, 1999; Scott and Lyons, 2012). Negligeable to low Mo enrichment is retained in the rock record. It was thus grouped with the oxic range into one category. The exact lower dissolved O_2 cutoff is not certain and so the designation O_2 >> 10 μM is appropriate (Scott and Lyons, 2012). Resulting Mo_{auth} enrichments in the oxic-slightly suboxic range are either low or indicate depletion (Mo_{EF} < 2) relative to crustal values (UCC range = 1-2 ppm; Mo EF_{UCC} = 0.67-1.33; Taylor and McLennan, 1985; Algeo and Tribovillard, 2009; Tribovillard et al., 2012). Green Point samples that fall in the oxic to slightly suboxic field are characterized by Mo_{EF} ≤ 1.49 (mean of 0.86±0.30), U/Mo_{auth} > 0.52 (mean of 1.22±0.53), and U_{EF} = ≤ 1.52 (mean of 0.94±0.28; *n*=15; Fig. 3.9; Appendix 3.1). Almost all of these values are from green shale samples with high $(\%U_{ter})_x$ values and low TOC that define the good U/Al correlation and sit at the most oxygenated end of the observed spectrum (see Chapter 2) based on the pattern of enrichment of U_{EF} and Mo_{EF} (Fig. 2.17).

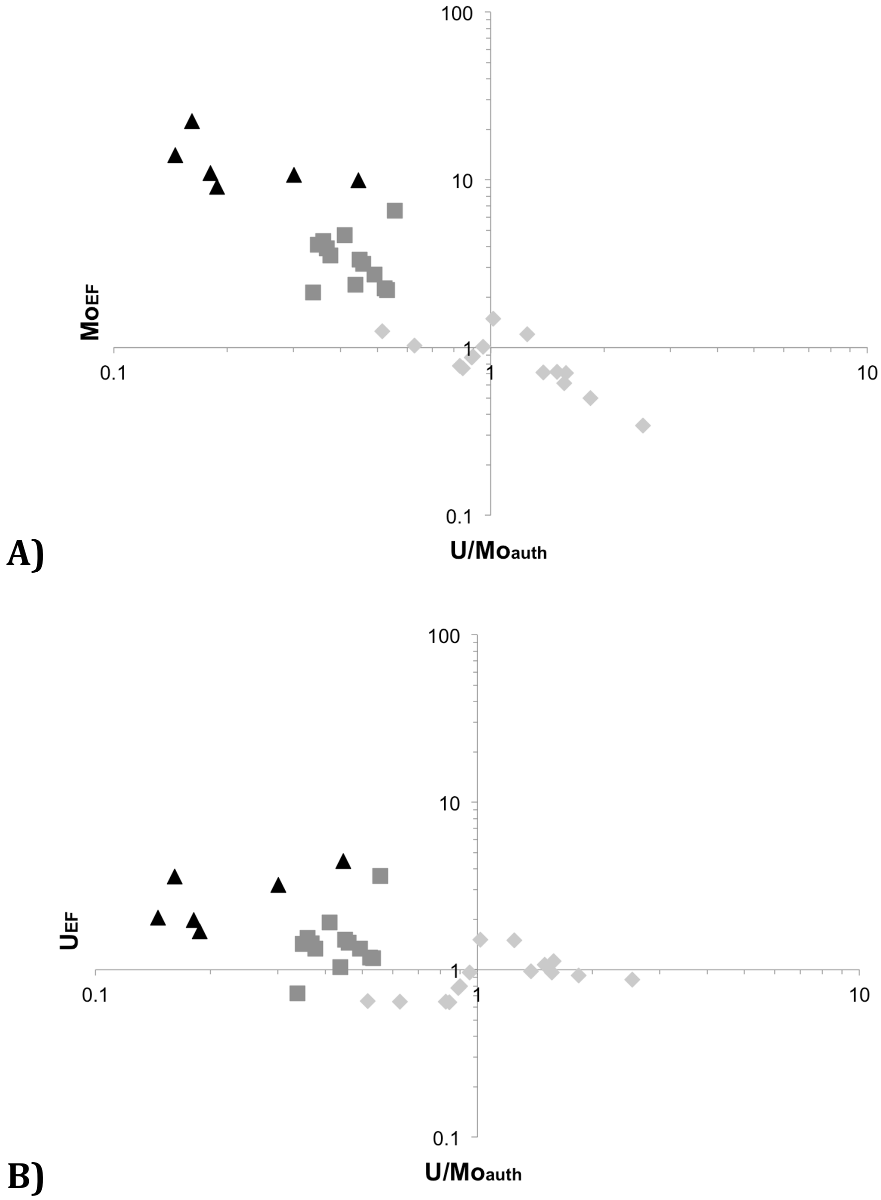

Figure 3.9: (A) U/Mo$_{auth}$ vs Mo$_{EF}$ plot of the Green Point data split based on interpreted redox conditions, including the 3 observed fields: oxic to slightly suboxic (light grey); highly suboxic (dark grey); and anoxic (black). (B) U/Mo$_{auth}$ vs U$_{EF}$ plot of the Green Point data split based on interpreted redox conditions. See Fig. 3.9a for legend.

The highly suboxic range is defined by having a sulfidic zone develop in the pore-waters close enough to the sediment-water interface for significant authigenic Mo to be sequestered to the sediments and retained in the rock record (Reitz et al., 2007). Mo can be retained either in the form of Mo bearing Mn-oxides that were not fully dissolved, or as Mo re-sequestered within the sulfidic zone (Klinkhammer and Bender, 1980; Shaw et al., 1990; Johnson et al., 1992; Calvert and Pederson, 1996; Morford and Emerson, 1999; Reitz et al., 2007). A weak particle shuttle is inferred to operate within this redox range (Tribovillard et al., 2012; see Chapter 2). As the upper O_2 cutoff is not certain, it can be classified as $O_2 > 10$ μM (Scott and Lyons; 2012). Highly suboxic conditions are characterized by $2 < Mo_{EF} < 8$ with a mean of 3.49±1.26 (*n*=13). U/Mo_{auth} ratios are in the range of 0.43 to 0.56 (0.43±0.07), becoming much lower as Mo authigenic enrichment becomes greater relative to U authigenic enrichment (Algeo and Tribovillard, 2009). U_{EF} increases as well (though less than Mo) and varies from 0.72 to 3.64 with a mean of 1.52±0.70 (Fig. 3.9). The samples falling within this range are grey shales with a higher organic carbon content, lower $(\%U_{ter})_x$ values and no U-Al correlation (See Chapter 2). Mo_{EF} and U_{EF} values are similar to previously interpreted suboxic sections deposited in weakly restricted basins (Tribovillard et al., 2012).

Anoxic conditions are characterized by the lack of an oxic and Mn-oxide zone within the sediment pore-waters. A more intense particle shuttle operates can operate under these conditions (Tribovillard et al., 2012). Bottom-water oxygen levels are very low ($O_2 < 10$ μM) but dissolved sulfides are still restricted to the pore-waters (McManus et al., 2006; Scott and Lyons, 2012). The anoxic field in the Green Point section is characterized by $Mo_{EF} > 8$ with a mean of 12.88±4.98. U/Mo_{auth} ratios decrease again, to a range of 0.15-0.56 (mean = 0.424±0.12, *n*=6). U_{EF}

increases as expected to a range of 1.70 – 4.45, with a mean of 2.84±1.09 (Fig. 3.9). These samples are derived from black shale intervals characterized by the highest organic carbon contents and very low $(\%U_{ter})_x$ values with no U-Al correlation (See Chapter 2). The magnitude of Mo and U enrichment is also similar to other sections interpreted as anoxic (Algeo and Tribovillard, 2009; Tribovillard et al., 2012).

U/Mo_{auth} was found to have markedly different inverse correlations with Mo_{EF} ($R^2 = 0.84$) and U_{EF} ($R^2 = 0.28$) (Fig. 3.6). The slope with Mo_{EF} is much steeper and has less variability than observed with U_{EF}, which is at odds with the moderate correlation observed between Mo_{EF} and U_{EF} ($R^2 = 0.60$; Fig. 3.3). This contrast is further highlighted when U_{EF} vs U/Mo_{auth} and Mo_{EF} vs U/Mo_{auth} values from the 3 redox groupings (oxic to slightly suboxic, highly suboxic, and anoxic) were plotted (Fig. 3.9). Although the presence of three populations demonstrating a gradual transition is evident in both plots, Mo_{EF} appears much more sensitive to changes in redox conditions than U_{EF} (Fig. 3.9). This difference is explained by the enrichment mechanisms of U and Mo and how the U/Mo ratio is affected in turn (McManus et al., 2006; Tribovillard et al., 2006; Algeo and Tribovillard, 2009; Tribovillard et al., 2012; Zhou et al., 2012). Authigenic U enrichment begins in the ferruginous zone (Canfield and Thamdrup, 2009) within less reducing conditions than needed for Mo (Zheng et al., 2002a; 2002b; Morford et al., 2009a; 2009b; Scott and Lyons, 2012). The U/Mo ratio sensitively records this phase of authigenic U enrichment (Fig. 3.9; McManus et al., 2006; Algeo and Tribovillard, 2009; Zhou et al., 2012). Substantial authigenic Mo enrichment requires the presence of a shallow sulfidic zone below the sediment-water interface, consistent with high oxidant demand (Helz et al., 1996; Zheng et al., 2000; Algeo and Tribovillard, 2009; Canfield and Thamdrup, 2009; Scott and Lyons, 2012; Romaniello et al., 2013). Mo_{EF} is further characterized by a much higher rate of change as conditions become increasingly reducing. For example, in siliciclastic sediments deposited in open-marine conditions, as bottom-water conditions change from suboxic to euxinic, $Mo_{EF} = \sim 1$ increases to $Mo_{EF} > 100$, compared to a potential change of $U_{EF} = \sim 2$ to $U_{EF} > 30$ (Algeo and Tribovillard, 2009; Tribovillard et al., 2012). The Mo_{EF} versus U/Mo_{auth} relationship thus appears very promising as a highly sensitive redox indicator in the suboxic to anoxic/non-sulfidic range, based on the results from the Green Point Formation (Fig. 3.9a). U_{EF} vs. U/Mo_{auth} also shows some promise but the much lower covariation between U_{EF} and U/Mo_{auth} indicates it is less reliable (Fig. 3.9b).

3.5.1.3 Comparison with other Datasets

As part of this study, the shale co-variation plots (Fig. 2.17; 3.6b) were compared to equivalent plots for various modern and Phanerozoic marine environments ranging in redox conditions from oxic to euxinic (Fig. 3.10). These other datasets are summarized in Table 3.1 (Berelson et al., 1987; Berelson et al., 1996; Eberli et al., 1997; McManus et al., 1997; McManus et al., 2003; Hammond et al. 2004; Berelson et al., 2005; McManus et al., 2006; Poulson et al., 2006; Tribovillard et al., 2008a; Piper and Calvert, 2011; Tribovillard et al., 2012; Zhou et al., 2012; Calvert et al., 2015; Piper, 2016).

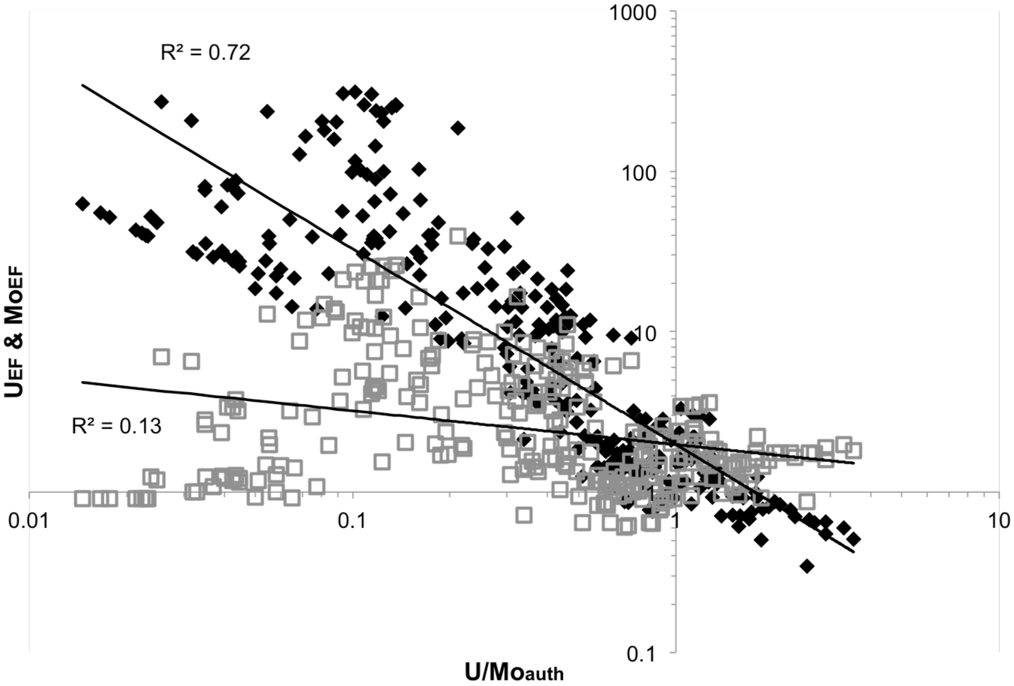

Figure 3.10: U/Mo$_{auth}$ vs Mo$_{EF}$ (diamonds)& U$_{EF}$ (squares) scatter plot in logarithmic format of all samples from all siliciclastic datasets (McManus et al., 2006; Tribovillard et al., 2008a; Piper and Calvert, 2011; Tribovillard et al., 2012; Zhou et al., 2012; Calvert et al., 2015; Piper, 2016). See Table 3.1 for more details.

The other datasets were first plotted on the Mo$_{EF}$ vs U$_{EF}$ diagram of Algeo and Tribovillard (2009) for comparison (Fig. 3.11). Regarding modern datasets (3.11b), the same data used in Algeo and Tribovillard (2009) for open marine environments was available (McManus et al., 2006). However, not all of same data was available (i.e., not listed in Table 3.1) for weakly restricted and highly restricted euxinic basins. Though the same data for the Orca Basin (Tribovillard et al., 2008a) was available, data for the Cariaco Basin came from Calvert et al. (2015). The new Cariaco data from the latter study is characterized by lower U$_{EF}$ values than reported by Algeo and Tribovillard (2009). Data for the highly restricted Black Sea Basin presented here was sourced from Piper and Calvert (2011) and Piper (2016). The Black Sea data covers the flood-transition from a lacustrine oxic-limnic environment to the modern stratified highly restricted basin. It generally follows the trend for strongly restricted basins from Algeo and Tribovillard, 2009. The more recent euxinic data (Units 1 and 2 from cores GC-7607 and GC-14; Piper and Calvert, 2011; and core GCC79; Piper 2016) is however characterized by higher Mo_{EF} values compared to the Black Sea Basin data presented in Algeo and Tribovillard (2009) (Fig. 3.11b).

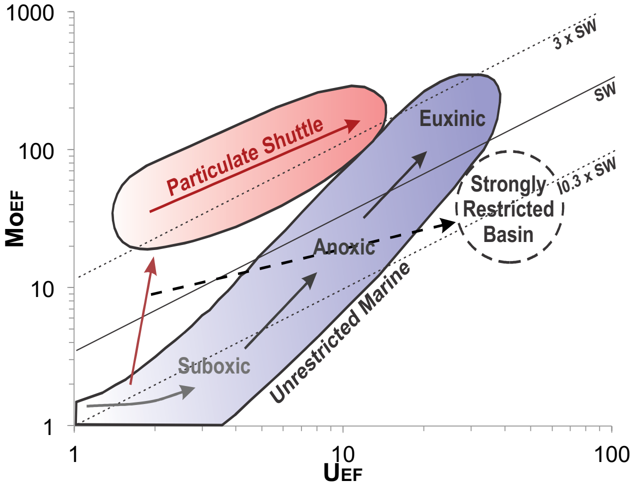

A)

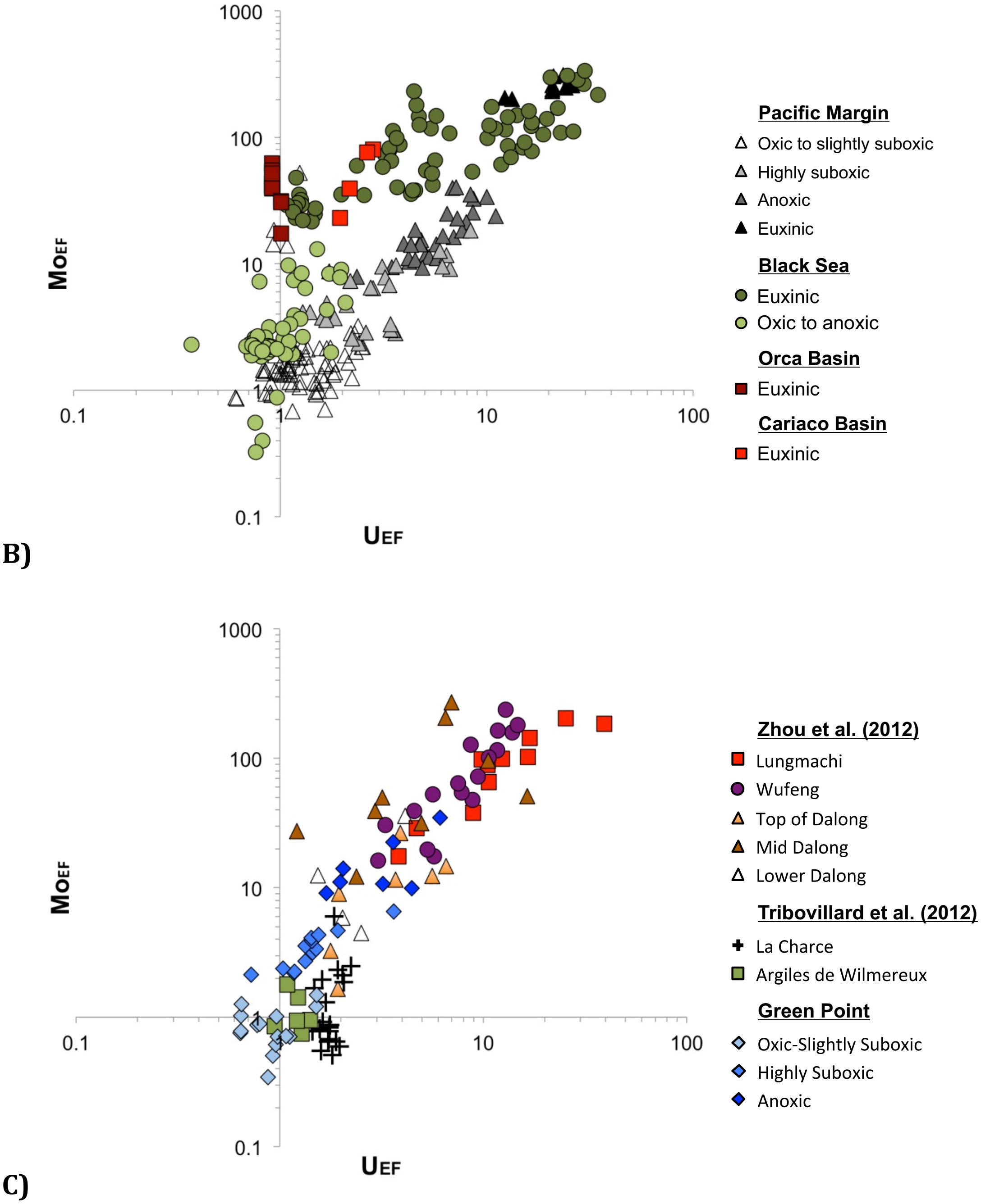

Figure 3.11: (A) General $\mathrm{Mo_{EF}}$ vs $\mathrm{U_{EF}}$ co-variation for marine environments. The blue field represents an open marine unrestricted environment. The red field represents the Fe-Mn particle shuttle field related to weak basin restriction represented by the euxinic Cariaco Basin. The dashed field represents strongly restricted environments, such as the euxinic Black Sea. Diagonal lines represent multiples of the Mo:U ratio of modern day seawater, based on an average weight ratio of 3.1 to compare with sediment weight ratios (modified from Algeo and Tribovillard, 2009; Tribovillard et al., 2012). (B) $\mathrm{Mo_{EF}}$ vs $\mathrm{U_{EF}}$ co-variation diagram of recent-modern siliciclastic data used in this study (McManus et al., 2006; Tribovillard et al., 2008a; Piper and Calvert, 2011;

Calvert et al., 2015; Piper, 2016). For more detail on the different environments, see Table 3.1. (C) Mo_{EF} vs U_{EF} co-variation diagram of Phanerozoic siliciclastic data used in this study (Tribovillard et al., 2012; Zhou et al., 2012; this study).

As expected based on the conclusions derived from the Green Point data, a much better correlation is present between U/Mo_{auth} vs. Mo_{EF} ($R^2 = 0.72$) compared to U/Mo_{auth} vs. U_{EF} ($R^2 = 0.13$) when all the datasets are taken into consideration together (Fig. 3.10). Values for different datasets were also plotted separately, using the U/Mo_{auth} vs Mo_{EF} (Fig. 3.12) and U/Mo_{auth} vs U_{EF} (Fig. 3.13) diagrams. They were then compared to the diagram of Algeo and Tribovillard (2009) (Fig. 3.11).

When analyzing the trends within the U/Mo_{auth} vs Mo_{EF} diagram, data previously interpreted to be oxic to slightly suboxic (Table 3.1; 3.2) plots as expected within the diagram of Algeo and Tribovillard (2009) (Fig. 3.12a), demonstrating depletion to negligeable enrichment. The same data also plots as expected for nearly all sections in the U/Mo_{auth} vs. Mo_{EF} diagram, with relatively high U/Mo_{auth} ratios and low Mo_{EF} values (Fig. 3.12a; 3.12b). An inverse relationship is observed between U/Mo_{auth} and Mo_{EF}. The highly suboxic to euxinic data are characterized by three divergent trends (Fig. 3.12c). Each trend is characterized by different patterns of changes in Mo_{EF} relative to U/Mo_{auth}. The open marine field, based on Pacific margin data, is characterized by higher Mo_{EF} values relative to the observed decrease in U/Mo_{auth} values (Fig. 3.12a; c). The weakly restricted data follows a trend of lower Mo_{EF} increase relative to the decrease in U/Mo_{EF}, though the particle field of Algeo and Tribovillard (2009) is not well defined based on available data (Fig. 3.12c). The trend for highly restricted basins initially follows the same pattern of lower Mo_{EF} relative to U/Mo_{auth} observed in weakly restricted basins. As U/Mo_{auth} approaches 0.05 and Mo_{EF} approaches 10, the patterns diverge. As Mo_{EF} continues to increase, the U/Mo_{EF} change becomes positive and converges with the euxinic range observed for open-marine environments, due to strong U enrichment associated within euxinia. When comparing both diagrams, the U/Mo_{auth} versus Mo_{EF} diagram does a good job of visualizing the same fields present in the diagram from Algeo and Tribovillard (2009).

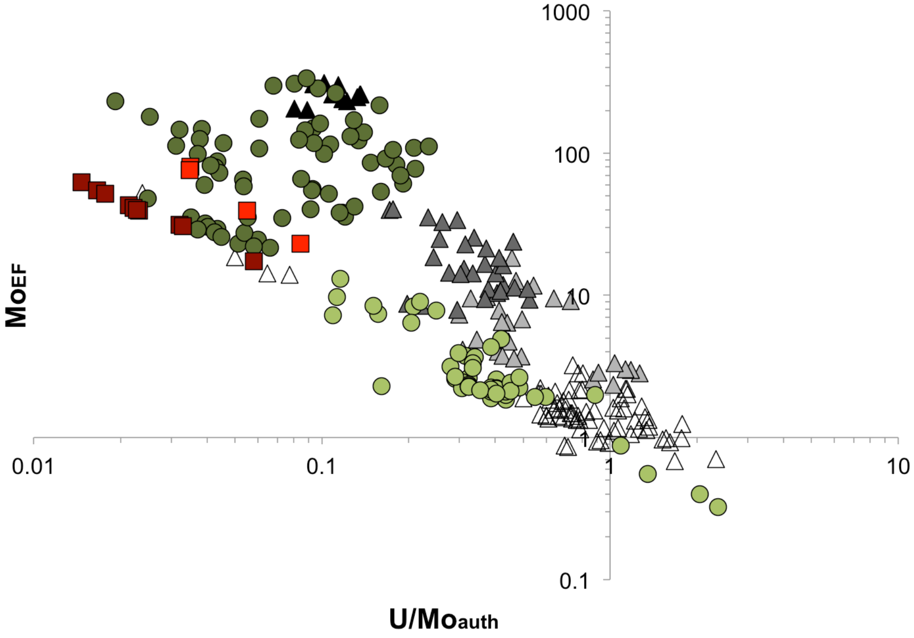

A)

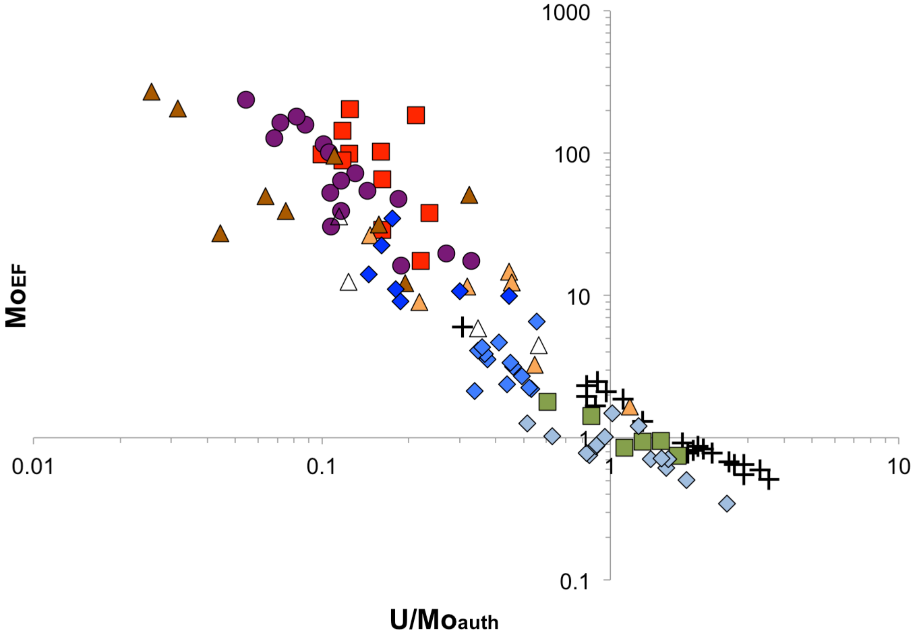

B)

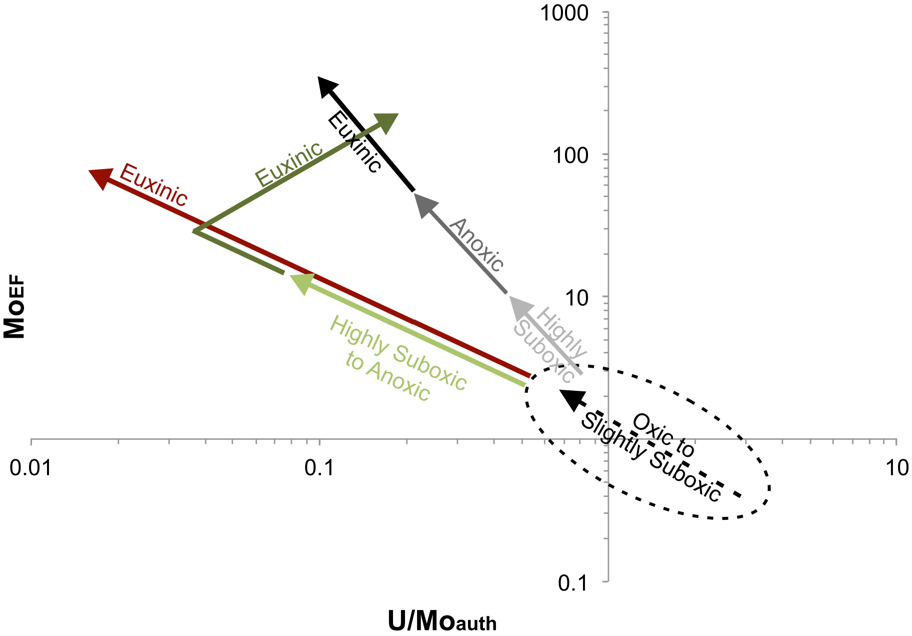

C)

Figure 3.12: (A) U/Mo$_{auth}$ vs Mo$_{EF}$ plot of modern-recent siliciclastic datasets. See Figure 3.11b for legend. (B) U/Mo$_{auth}$ vs Mo$_{EF}$ plot of Phanerozoic siliciclastic datasets. See Figure 3.11c for legend. (C) U/Mo$_{auth}$ vs Mo$_{EF}$ plot of the observed trends. The dashed circle represents the oxic-slightly suboxic field. The dashed line indicates the enrichment trend observed within the oxic-slightly suboxic field. The grey to black lines represent the enrichment trend observed in open-marine environments. The red line indicates the inferred trend observed in weakly restricted basins. The green lines represent the change observed in strongly restricted basins.

When comparing U/Mo_{auth} to U_{EF} using the same datasets, a similar pattern appears to be present in highly suboxic to sulfidic datasets, albeit with lower observed U_{EF} values (Fig. 3.12c; 3.13). However, a consistent positive trend between U/Mo_{auth} and U_{EF} is observed in the oxic-slightly suboxic environments, opposite to the observed trend when Mo_{EF} is compared to U/Mo_{auth} (Fig. 3.12c; 3.13). This observation suggests very little to no Mo enrichment relative to the initial U enrichment retained within the rock record. Within the diagram of Algeo and Tribovillard (2009), this area would be represented by the initial flat section of the open marine field (Fig. 3.11a). It reflects U enrichment within a Fe-reducing zone in the sediment pore-waters or water column and a lack of Mo enrichment normally associated with a sulfidic zone being present (Helz et al., 1996; Zheng et al., 2000; 2002a; 2002b; Scott and Lyons, 2012). As for the U/Mo_{auth} vs Mo_{EF} diagram, three divergent trends of authigenic enrichment patterns are present in the U/Mo_{auth} vs U_{EF} diagram as conditions become more reducing. This shift signals the start of authigenic Mo enrichment associated with the presence of a sulfate-reducing zone (Scott and Lyons, 2012). Within sediments deposited in open-marine conditions, a similar trend is present in both the U/Mo_{auth} vs U_{EF} and U/Mo_{auth} vs Mo_{EF} diagrams, with concurrent U_{EF} and Mo_{EF} increases being observed. The U_{EF} increase is not as significant as the Mo_{EF} increase, resulting in the decreasing U/Mo_{auth} ratios (Fig. 3.12c; 3.13c; McManus et al., 2006; Zhou et al., 2012). The weakly restricted basin trend of Algeo and Tribovillard (2009) is outlined by the Orca Basin and Cariaco Basin data. This trend is characterized by low U_{EF} enrichment (< 5 ; Fig. 3.13) and

U/Mo_{auth} ratios becoming very low (< 0.1) as conditions become euxinic. The evolving water-mass trend of strongly restricted basins, such as the highly restricted Black Sea data, initially follows the same trend present for weakly restricted environments when conditions are highly suboxic-anoxic (Fig. 3.13c). As U/Mo_{auth} approaches 0.05, the highly restricted basin trend diverges as authigenic U enrichment increases to U_{EF} ~ 30 within the evolving water mass (Algeo and Tribovillard, 2009). The U/Mo_{auth} values change accordingly and increase ~ 0.1 (Fig. 3.13c).

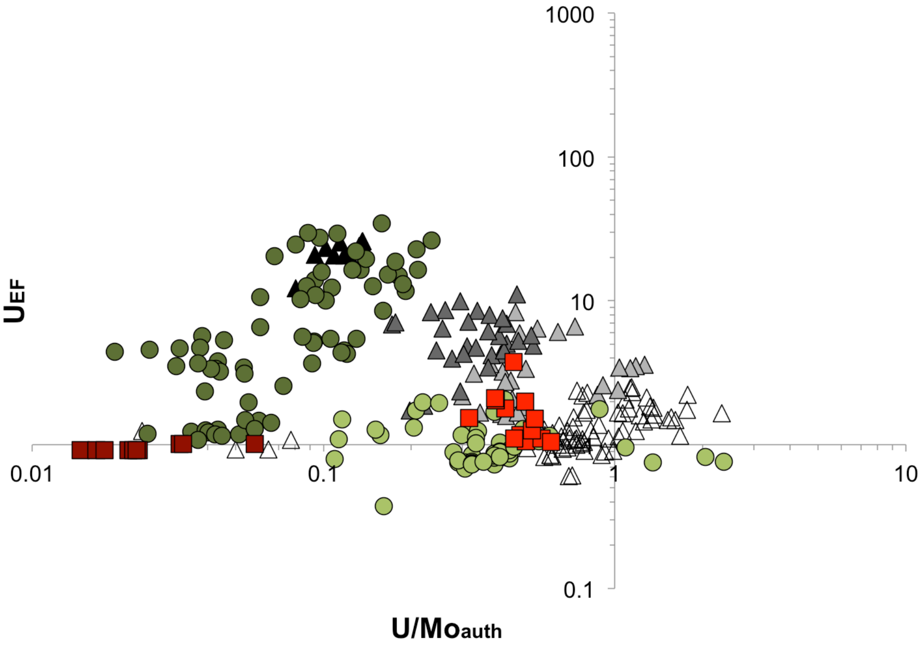

A)

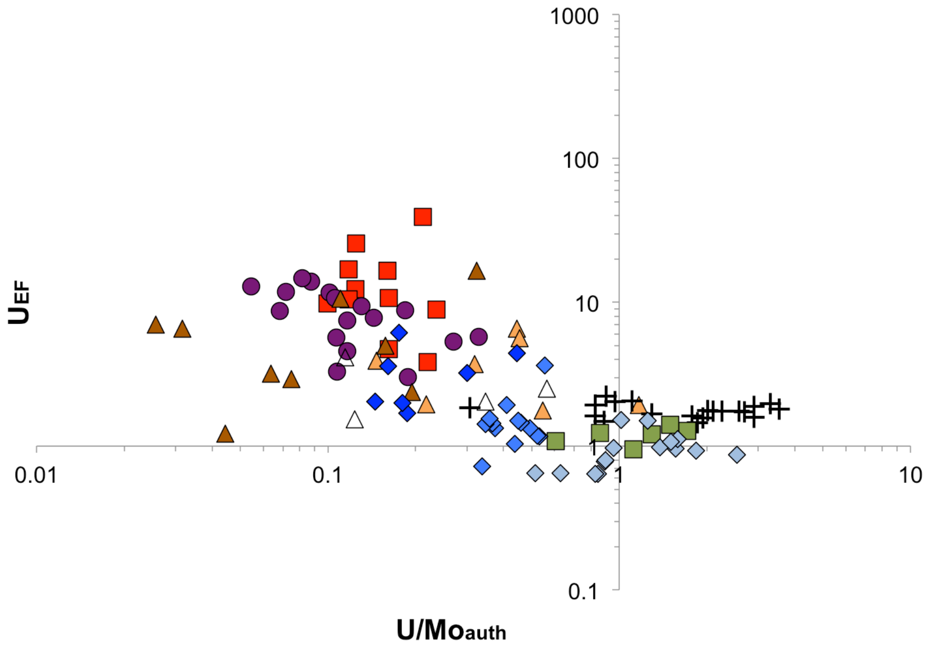

B)

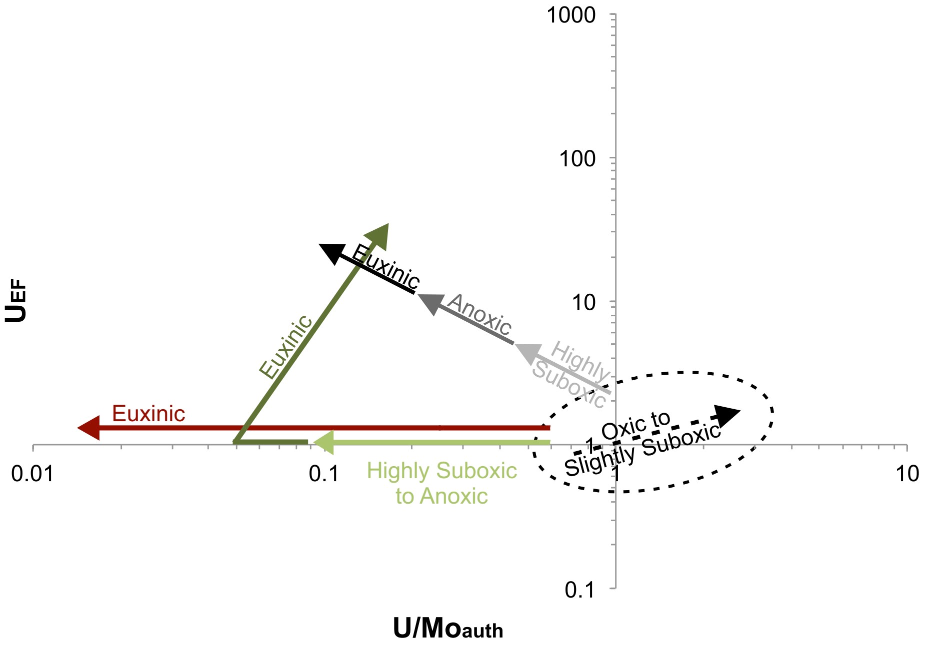

C)

Figure 3.13: (A) U/Mo$_{auth}$ vs U$_{EF}$ plot of modern-recent siliciclastic datasets. See Figure 3.11b for legend. (B) U/Mo$_{auth}$ vs U$_{EF}$ plot of Phanerozoic siliciclastic datasets. See Figure 3.11c for legend. (C) U/Mo$_{auth}$ vs U$_{EF}$ plot of the observed trends. The dashed circle represents the oxic-slightly suboxic field. The dashed line indicates the enrichment trend observed within the oxic-slightly

suboxic field. The grey to black lines represent the enrichment trend observed in open-marine environments. The red line indicates the inferred trend observed in weakly restricted basins. The green lines represent the change observed in strongly restricted basins.

When comparing the Mo_{EF} vs U/Mo_{auth} and U_{EF} vs U/Mo_{auth} diagrams, Mo_{EF} was found to have a much greater control on U/Mo_{auth} variations observed. Regardless, both diagrams were found to consistently track changes observed as conditions change from highly suboxic to euxinic conditions, while differentiating open marine, weakly restricted and highly restricted environments in a similar manner (Fig. 3.12; 3.13). However, within the oxic-slightly suboxic range, very low Mo_{EF} values and opposite patterns of U/Mo_{auth} change are observed as U_{EF} and Mo_{EF} increase. This indicates a sulfidic zone was unlikely to have been present. Using these diagrams in tandem could help evaluate whether a sulfidic oxidation zone developed within sediment pore-waters in suboxic conditions.

3.5.2 Relationship of Uranium and Molybdenum Enrichments with U/Mo Ratios in the Carbonates

3.5.2.1 U and Mo Covariation in the Green Point Carbonates

Uranium concentrations in the Cambrian-Ordovician micritic mudstones (mean = 1.0±0.8 ppm) were found to be lower than in modern marine counterparts, even if little evidence for diagenetic depletion was found (Fig. 3.1; Table 3.3; Azmy et al., 2014; 2015). The lower concentrations are expected, as the Green Point carbonates are composed of low-Mg calcite, rather than aragonite (Romaniello et al., 2013; Azmy et al., 2015; Chen et al., 2016). U concentrations decrease along with

TOC contents across the geochemical anomaly level (Azmy et al., 2015). This observation indicates authigenic U may have formed as organic-metal ligands in humic acids (Barnes and Cochran, 1990; Klinkhammer and Palmer, 1991; Zheng et al., 2002a). The previous interpretation of these low U concentrations as reflecting dominantly suboxic conditions agrees with the geochemical evidence for oxic-slightly suboxic to anoxic-ferruginous conditions during shale deposition. However, the decrease in carbonate U concentrations across the geochemical anomaly is at odds with the shale U data, where the opposite trend occured (Azmy et al., 2015; see Chapter 2).

The Mo contents in the Cambrian-Ordovician micritic calcite lime mudstones (0.01 to 1.91 ppm; mean = 0.27±0.34; Table 3.3) are mainly within the range documented for their modern and ancient non-skeletal carbonate counterparts (e.g. Voegelin et al., 2009; 2010; Czaja et al., 2012; Romaniello et al., 2016). A few high Mo concentrations are associated with high Si contents (Appendix 3.2), which may reflect the influence of siliciclastic inclusions and thus are not included in any further redox analyses. A few other high Mo concentrations are associated with a few beds containing peloidal to algal grainstones, reflected in relatively high P contents (Azmy et al., 2014, Appendix 3.2). Most samples have Mo concentrations comparable to those found in modern aragonitic sediments with low pore-water sulfide levels or Carboniferous calcitic detrital micrites, marine cements and calcified algal mats (Voegelin et al., 2009; Romaniello et al., 2016). This indicates mechanisms for Mo incorporation within the Green Point calcites and previously studied primary carbonates are likely similar, whether Mo is incorporated within calcite or aragonite. As little evidence for diagenesis was observed (Azmy et al., 2014; 2015), it would also suggest porewater sulfide levels were low during the deposition of the Green Point carbonates, supported by low observed TOC contents within most samples. Several other samples have Mo concentrations significantly higher than 0.2 ppm, which indicates intermittently higher pore-water sulfide levels were present, which was also observed in the shales (ex. GP 33: Mo ppm = 1.91; Romaniello, 2012; Romaniello et al., 2016; see Chapter 2). Mo carbonate concentrations also increase across the geochemical anomaly, from 0.15±0.19 to 0.35±0.39 ppm, consistent with the trend observed for the shales, indicating they are likely to be more representative of redox conditions across the section than U (see Chapter 2).

No correlation was found within the carbonates at Green Point between U and Mo enrichments, which differs from their behavior in the shales ($R^2 = 0.02$; Fig. 3.3; see Chapter 2). Their opposite behavior further indicates that different processes were responsible for their final concentrations (Fig. 3.1; Azmy et al., 2015). As previous studies of the Green Point lime mudstone rhythmite petrography and geochemistry indicate, post-authigenic diagenesis was minor. It is unlikely to have been the cause of the observed U and Mo concentrations (Azmy et al., 2014; 2015). The low U concentrations relative to their modern aragonitic counterparts can be explained by abiotic calcite being the dominant carbonate species in the Green Point sediments, which requires a coordination change during U inclusion within calcite, but not in abiotic aragonite (Reeder et al., 2000; Chen et al., 2016). Other additional factors would also discourage U inclusion in calcite. The dominantly suboxic redox setting would only encourage limited substitution of U (IV) for Ca into the calcite structure, particularly when conditions were oxic-slightly suboxic (Sturchio et al., 1998). The low organic matter content of the carbonates would also limit organic matter oxidation, especially under suboxic conditions. The pore-water pH would thus remain higher, and increase the solubility of U (VI) phases, particularly in the presence of bicarbonates and at pH > 5.5 (Langmuir, 1978; Krestou and Panias, 2004; Kelly et al., 2006). The presence of carbonate material would have been effective at keeping U(IV) in solution within suboxic conditions (Sturchio et al., 1998; Luo and Gu, 2008). On the other hand, the magnitude of Mo uptake into the Green Point samples was similar to concentrations observed within both aragonite and calcite samples previousy analyzed (Voegelin et al., 2009; Romaniello et al., 2016). As pore-water conditions in the Green Point samples were the same during both U and Mo enrichment, it is unlikely that pH variations affected Mo inclusion differently in calcite or aragonite structures, as for U (Romaniello et al., 2016). A possible explanation is that the primary Mo species in low-porewater H_2S conditions, MoO_4^{2-}, has similar enrichment mechanisms during inclusion within both aragonite and calcite, unlike U (Reeder et al., 2000; Anbar et al., 2004; Chen et al., 2016; Romaniello et al., 2016). This is supported by U and Mo concentrations observed within different biological and abiological primary carbonates. Romaniello et al. (2013; 2016) evaluated both U and Mo concentrations in corals, mollusks, green algae, red algae and ooids. Mollusk results are not evaluated as U concentrations in mollusks are partially diagenetic, decreasing over time to values below detection levels (Gillikin and Dehairs, 2013). The Mo concentrations of the other carbonates are all similar and consistent (< 0.2 ppm; Romaniello et al., 2016), regardless of whether they are aragonite (corals, green algae, ooid) or calcite (red algae) precipitates. Their U concentrations are not consistent, however. Red algae (calcite) samples have much lower U concentrations then within all coral, ooid and the majority of green algae (aragonite) samples (Romaniello et al., 2013). Regardless, more work would be needed for verification. Most needed would be evaluating how Mo is incorporated within calcite and aragonite crystal structures and sediments, as has been done for U (Reeder et al., 2000; 2001; Chen et al., 2016).

Enrichment factors in the carbonates were found to be much more variable, and in some cases, much higher than for the shales. As Mo and U concentrations are higher in the shales (See Appendix 3.1; 3.2), the higher enrichment factors (mean Mo EF = 36.75±65.80; mean U EF = 36.96±65.80) of the carbonates at Green Point are a result of the low Al contents (mean Al = 1092±1552 ppm; Appendix 3.2; Table 3.3). The lower concentrations of Mo and U in the carbonates relative to the shales are consistent with previous observations, indicating much higher Mo and U concentrations in shales deposited in comparable bottom water redox conditions or porewater sulfide levels (Arnold et al., 2004; McManus et al., 2006; Neubert et al., 2008; Voegelin et al., 2010; Romaniello et al., 2013; 2016). In addition to the difference in the relative authigenic enrichment intensity of U and Mo, other mechanisms affect their final concentrations within the sediments. Generally, much less Mo and U in carbonates are derived from a detrital source relative to shales, based on comparison to the Post-Archean-Australian-Shale or Average Shale compositions (Wedepohl, 1971; Taylor and McLennan, 1985; Wedepohl, 1991; Romaniello et al., 2013; 2016). Carbonate structures also affect the uptake of U within sediments. Uranium fits into the structure of calcite, whereas Mo does not (Sturchio et al., 1998; Kelly et al., 2006; Chen et al., 2016). The presence of bicarbonates or carbonate material also increases the solubility of U, particularly within the environmental pH range (Langmuir et al., 1978; Krestou et al., 2004; Luo and Gu, 2008; Beazly et al., 2011). Small observed U and Mo variations should therefore be interpreted cautiously, as many factors may affect their concentrations during early diagenesis. High Mo_{EF} and U_{EF} values, associated with high U and Mo concentrations, may indicate high pore-water sulfide levels were present during deposition and early diagenesis (Romaniello et al., 2013; 2016). Based on the observed differences between the carbonate and shale enrichment factors, the diagram of Algeo and Tribovillard (2009), calibrated in its current form for shales, would not be suitable for studying the carbonates at Green Point (Fig. 3.3).

The U/Mo ratio has been used successfully when interpreting siliciclastic environments (McManus et al., 2006; Zhou et al., 2012; see Chapter 2). Here we apply it to interpret the redox changes during deposition of the carbonate rhythmites at Green Point for comparison. Whether using U/Mo_{auth} or U/Mo_{conc}, The ratio demonstrates a consistent decrease across the anomaly level of Azmy et al.

(2014), whether using the U/Mo$_{auth}$ (5.06±5.11 to 1.48±2.20) or U/Mo$_{conc}$ (15.68±15.83 to 4.6±6.83) ratios (Fig. 3.1; Table 3.3). The relative change in the carbonate ratios across the geochemical anomaly level is similar to that observed for the shales (see Chapter 2). Exact values however are much more variable (0.06 to 25.96) than within siliciclastic environments and should not be compared directly to those values (McManus et al., 2006; Zhou et al., 2012; see Chapter 2).

3.5.2.2 Carbonate U/Mo$_{auth}$ vs. U$_{EF}$ and Mo$_{EF}$ at Green Point

Following the investigation of the covariation of U/Mo$_{auth}$ versus Mo$_{EF}$ and U$_{EF}$ in the shales, the same analysis was applied to the carbonates for comparison (Fig. 3.8). The U enrichment factors have a very low positive correlation with U/Mo$_{auth}$ ($R^2 = 0.18$; Fig. 3.8). This pattern, opposite to the shales, appears to be a reflection of the lack of correlation between U and Mo in the carbonates, rather than a good reflection of redox variations. The low correlation observed indicates a disconnection between U authigenic enrichment and the U/Mo$_{auth}$ ratio, which is further supported by the higher correlation between U (ppm) and U/Mo$_{conc}$ ($R^2 = 0.43$; Fig. 3.7). This observation adds to the interpretation that other environmental factors besides redox conditions, specifically the effects of pH and U species speciation on U inclusion into the calcite structure, affected U uptake in the carbonates. Thus, the U/Mo$_{auth}$ vs. U$_{EF}$ plot must be used with great caution when applied to carbonates, based on the results from the Green Point succession.

When Mo_{EF} was plotted against U/Mo_{auth} in the carbonates, a moderate inverse correlation is observed, similar to the pattern observed within the shales ($R^2 = 0.52$; Fig. 3.8). This pattern is also present when Mo concentrations are compared to U/Mo_{conc} ($R^2 = 0.54$; Fig. 3.7). The same behavior of authigenic ratios and concentration data suggests that redox-controlled authigenic enrichment played the dominant role in determining the Mo content of the carbonates. As the shales and carbonates were deposited concurrently in the same environment and the same redox regime, the U/Mo_{auth} vs Mo_{EF} plot in the carbonates should reflect the same conditions, specifically oxic-suboxic with intermittent occurrences of anoxia (Azmy et al., 2015). Using the U/Mo_{auth} vs Mo_{EF} and the U/Mo_{conc} vs Mo_{ppm} plots together when evaluating the carbonates does appear to be a reliable tool to evaluate authigenic Mo enrichment in the context of the presence or absence of pore-water dissolved sulfides, and possibly interpret the redox conditions during deposition of the carbonates at Green Point.

3.5.2.3 Comparison with the Bahamas

In order to verify the conclusions based on the Green Point carbonates, the same analysis was applied to carbonates from both a recent slope environment, the western slope of the Great Bahama Bank along the Santaren Channel, and from the modern shallow carbonate platform of the Bahamas Banks (Eberli et al., 1997; Romaniello, 2012; Romaniello et al., 2013; 2016). Several cores were drilled at different locations along the slope (Site 1003; 1004; 1005; 1008; 1009) and near the center of the Santaren Channel off the slope (Site 1006). The carbonate samples are Holocene-Pleistocene in age (Eberli et al., 1997; Romaniello, 2012). Pore-water sulfide is present within the cores, or there is evidence that it was present in the past (only intermittently at Site 1006; Eberli et al., 1997; Romaniello, 2012). The pore water sulfide availability resulted in higher concentrations of redox-sensitive trace metals (Mo, Re, U), which become more enriched up the slope where the sediment organic carbon flux is greater (Eberli et al., 1997; Romaniello, 2012). In addition to the slope data, available data are from 4 shallow cores (0.5 to 4m) that were drilled in various modern shallow marine environments in the southern Exuma Islands area; including tidal flats, a lagoon and a tidal pond (Romaniello, 2012; Romaniello et al., 2013; 2016). High down-core Mo and U concentrations were noted in cores 1, 3 and 4, which correlated with the presence of high pore-water sulfide levels ($[H_2S]_{aq}$ up to >400 μM). No Al data was available from Romaniello (2012). Al data was available from Romaniello et al. (2013) but demonstrated significations variations (118 - 8920 ppm) that would affect EF values. As such, U/Mo_{conc} was calculated and compared directly to Mo and U concentrations in this investigation.

When U/Mo_{conc} was compared to Mo_{ppm}, both the shallow platform and slope carbonates behaved as expected based on the Green Point carbonate and shale data. The slope carbonates demonstrated an excellent inverse correlation, following the trend of changing redox conditions and pore water sulfide concentrations, relative to different locations along the slope ($R^2 = 0.98$; Fig. 3.14a; Romaniello, 2012). The same pattern, related to pore-water sulfide thiomolybdate scavenging, exists in the shallow platform carbonates as well, with again an excellent correlation ($R^2 = 0.99$; Fig. 3.14a; Romaniello, 2013; Romaniello et al., 2016). The difference in the steepness of the inverse slopes also mirrors the trends for partially restricted and open marine environments in the shales, with the latter being steeper (Fig. 3.12; 3.13; 3.14a). This indicates the different slope and platform environments have different patterns of enrichment as conditions become more reducing and sulfidic. The Mo concentrations for the Bahamas slope environment are also much higher than in the Green Point carbonates, apart from Site 1006, the only site characterized by the intermittent presence of pore-water sulfide and most distal to the Greater Bahamas platform (Fig. 3.13c; 3.14a; Romaniello, 2012). These modern observations suggest that the presence of high pore-water sulfide was unlikely, or at most intermittent based on rare higher Mo concentrations (GP-33; Appendix 3.2), during the deposition of the Green Point carbonates, also deposited within a distal slope setting.

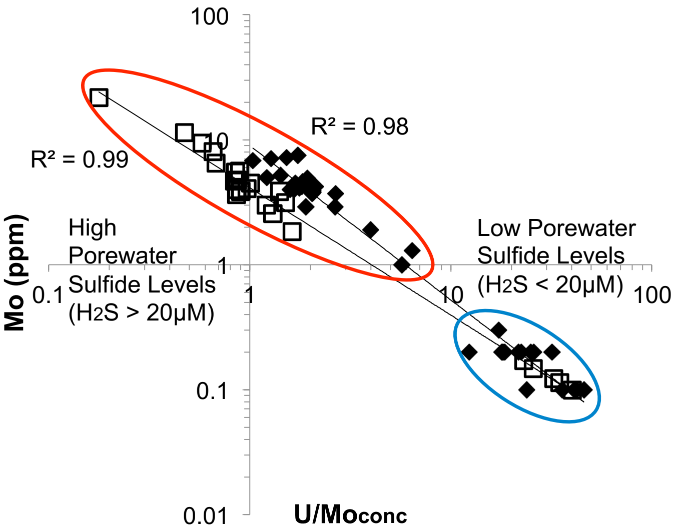

A)

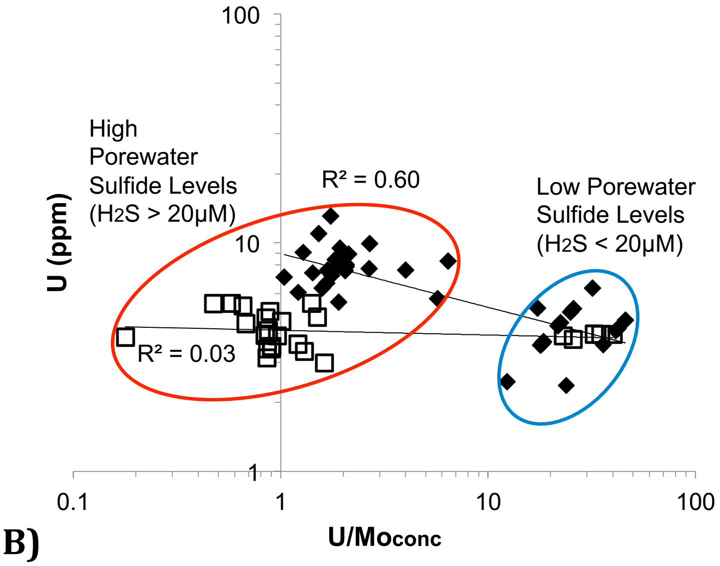

Figure 3.14: (A) U/Mo$_{conc}$ vs Mo$_{ppm}$ scatter logarithmic plots of the slope (diamonds) and platform (squares) Bahamas carbonates. (B) U/Mo$_{conc}$ vs U$_{ppm}$ scatter logarithmic plots of the slope (diamonds) and platform (squares) Bahamas carbonates (Romaniello, 2012; Romaniello et al., 2013; 2016).

When U/Mo$_{conc}$ was compared to U$_{ppm}$, very different results were found for the modern environments compared to the Green Point carbonates. The modern slope carbonates behaved very much like the Green Point shales, demonstrating a moderate-good inverse correlation between U/Mo$_{conc}$ and U$_{ppm}$ ($R^2 = 0.6$; Fig. 3.14b) that reflects U enrichment in response to the pore-water sulfide levels present at different locations (Eberli et al., 1997; Romaniello, 2012). Higher U concentrations and lower U/Mo$_{conc}$ values indicate higher pore-water sulfide levels (i.e., the carbonates sequestered Mo more efficiently than U; Romaniello et al., 2013; 2016). On the other hand, the modern Bahamian platform carbonates demonstrated no noticeable increase in U concentrations, regardless of the change in the U/Mo$_{conc}$ ratio, so no correlation was observed between the two ($R^2 = 0.03$; Fig. 3.14b). In this case, the U/Mo$_{conc}$ ratio alone behaves as expected, becoming lower according to increasing pore-water sulfide levels (Romaniello, 2012; Romaniello et al., 2013; 2016). This relationship is analogous to the trend for partially restricted environments within shales, again indicating that the different environments could have affected the pattern of U and Mo enrichment (Fig. 3.13c; 3.14b). This can potentially be attributed to three factors. One could simply be that the zone of U enrichment was deeper than captured by the shallow Bahamas cores. However, this scenario is not likely considering that substantial Mo enrichment occurred at the same locations (Romaniello, 2012; Romaniello et al., 2013; 2016). The second possibility, based on observations derived from the various shale environments, is that within these clean modern or recent carbonates, the difference in trends observed as pore-water sulfide levels increase is a result of their different environments of deposition. The slope carbonates have high U concentrations when compared to the shallow platform carbonates, which may indicate that available aqueous U was not as abundant within the shallow sediments on the platform (Romaniello, 2012; Romaniello et al., 2013). The last possibility is that U and Mo concentrations in the slope carbonates cores were affected by marine burial diagenesis down-core, which was observed to have resulted in substantial subsurface fluid flow, dissolution (preferentially aragonite) and reprecipitation of solid-phase carbonate species (preferentially low magnesium calcite; Romaniello, 2012). This is unlikely however, as the observed U and Mo concentrations were interpreted to represent authigenic enrichment (Romaniello, 2012). The second possibility, authigenic enrichment representative of environmental conditions, seems most likely though comparison with more data from different modern environments would be needed for verification. The inverse correlation and much higher U concentrations in the Bahamas slope samples, compared to that observed in the Green Point carbonates, also supports the interpretation that persistently high pore-water sulfide levels did not occur during deposition of the Green Point carbonates.

As with the shales, comparing U/Mo_{conc} to U and particularly Mo concentrations shows promise as a valuable tool when applied to carbonates. The application of this concept to more environments would be necessary, as was done by Algeo and Tribovillard (2009), particularly to investigate the potential effect of water-mass restriction during carbonate deposition. This also indicates that a carbonate diagram analogous to the U_{EF} vs Mo_{EF} plot of Algeo and Tribovillard (2009) could potentially work, though it would have to be calibrated based on modern carbonate datasets. This would require Al data from the studied Bahamas carbonates as well as necessary data from other carbonate environments for comparison.

3.5.3 Mo isotopes in the Green Point Carbonates

The $\delta^{98}Mo$ values from the carbonates at Green Point were found to vary widely (-0.30 to 2.34 ‰), with a mean of 0.87±0.64 ‰ (Table 3.3; Appendix 3.2). There is no correlation between Mo concentrations and $\delta^{98}Mo$ values ($R^2 < 0.1$). An overall δ^{98}Mo increase is observed along with a drop in the TOC contents above the geochemical boundary defined by a negative $\delta^{13}C_{carb}$ excursion (Azmy et al., 2014). The δ^{98}Mo values have an insignificant correlation with the $\delta^{13}C_{org}$ values (Azmy et al., 2015). Except for one sample (GP46 = 2.34 ‰), the δ^{98}Mo values of the carbonates are lower than modern seawater (~2.3 ‰, Siebert et al., 2003; Nakagawa et al., 2012). The wide range of δ^{98}Mo values observed within the Green Point samples is similar to previously studied Carboniferous carbonates, including micritic material (Voegelin et al., 2009). Some of these samples (those from Spain) were altered by early diagenetic processes, resulting in light δ^{98}Mo values (Voegelin et al., 2009). Thus, the potential for diagenetic alteration of the primary and authigenic δ^{98}Mo signatures must be assessed. Knowledge of diagenetic controls on the redistribution of Mo in carbonates remains limited. Previous studies have identified authigenic enrichment as a major control on Mo enrichment within carbonates (Voegelin et al., 2009; Romaniello et al., 2016). Mo concentrations have also been found to be unaffected by the progressive marine and burial diagenesis occurring along the western margin of the Grand Bahamas Bank (Romaniello, 2012). A previous petrographic investigation of the studied carbonates indicated insignificant recrystallization of the sampled micritic lime mudstones (Azmy et al., 2014). Poor correlations were also observed between U (ppm) and δ^{238}U against Sr, which becomes depleted with progressive diagenesis (Brand and Veizer, 1980; Veizer, 1983; Azmy et al., 2015). The same poor correlations against Sr were also observed when δ^{98}Mo values ($R^2 = 0.001$) and Mo concentrations ($R^2 = 0.17$) were plotted with Sr contents (Fig. 3.15). This argues against a post-authigenic diagenetic fluid influence on Mo values, suggesting the preservation of at least near-primary and authigenic Mo signatures (Voegelin et al., 2009; 2010; Romaniello, 2012). Though a wide scatter of δ^{98}Mo signatures is observed, the lightest δ^{98}Mo value (-0.3‰) is higher than the range for Fe-Mn oxides (Siebert et al., 2003; Poulson Brucker et al., 2009). There was also no visual or petrographic indication of iron oxide staining previously associated with Mo derived from redissolved Fe-Mn oxide phases (Voegelin et al., 2009). This indicates that, even if present, isotopically light Mo derived from Fe-Mn oxides was unlikely to have been an important source of the Mo permanently sequestered to the Green Point sediments. Most sample δ^{98}Mo ratios are higher, with a very similar mean (δ^{98}Mo = 0.87±0.64 ‰) to a single unaltered Carboniferous micrite sample from China as well as modern aragonites formed from fluids with low pore-water sulfide levels (Voegelin et al., 2009; Romaniello et al., 2016). As the carbonate micritic mudstones at Green Point are allochtonous sediments, they are likely to be at least partially affected by the δ^{98}Mo composition of the calcareous debris making up the micritic material. This is reflected in the wide scatter of δ^{98}Mo values observed (Flügel, 2004; Voegelin et al., 2009). The overall mean of the observed δ^{98}Mo ratios, combined with the Mo (ppm) data interpretation, is likely a good indication that low pore-water sulfide levels were present within the majority of the Green Point interval, and was one of the main influences on the δ^{98}Mo values observed. This is consistent with the interpreted dominantly suboxic redox setting, based on shale data (see Chapter 2).

Therefore, the δ98Mo values of the Green Point carbonates may represent minimum values rather than Cambrian-Ordovician seawater values.

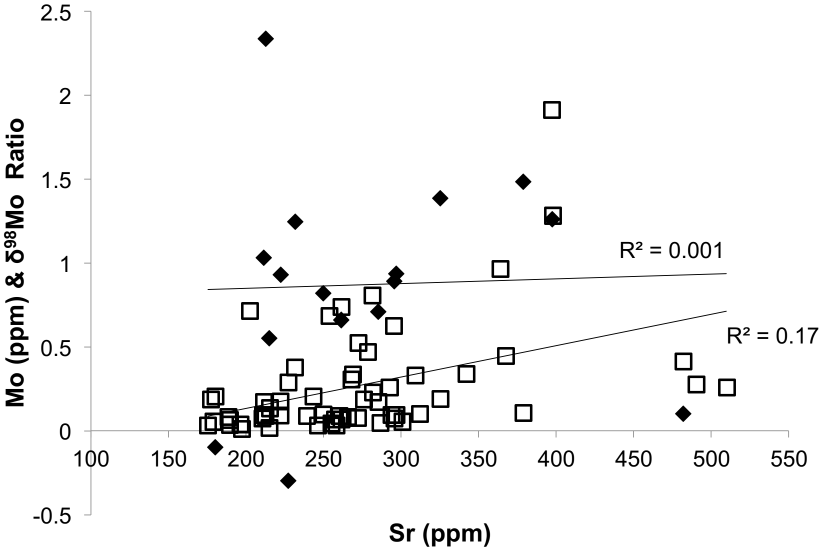

Figure 3.15: Scatter plot of Sr (ppm) vs Mo (ppm) and δ 98Mo ratios.

The base of the negative $\delta^{13}C_{carb}$ and positive $\delta^{15}N_{org}$ excursions on the GSSP C-isotope profile marks a geochemical anomaly level that was caused by a noticeable sealevel rise (Azmy et al., 2014; 2015). The mean δ^{98}Mo values below and above the anomaly are 0.57±0.49 ‰ and 1.01±0.67 ‰, respectively (Table 3.3). The slight increase of the δ^{98}Mo values (Fig. 3.1; Table 3.3) follows the same trend, along with the increase in Mo concentrations. Decreasing oxygen levels during deposition of the Green Point section would reduce the magnitude of Mo isotope fractionation between seawater and sediments. Thus, the increase in the Green Point δ^{98}Mo mean (Fig. 3.1) upsection suggests a change to relatively more reducing pore-water conditions, agreeing with the conclusions based on the shale data (see Chapter 2). It is unlikely that the observed variation is caused by a significant change in the composition of the detrital material being transported to the distal slope. This is based on the petrographic analysis of the sampled material (Azmy et al., 2014) and the lack of evidence within the studied outcrops for variations in the composition of the studied carbonates.

Local and global ocean redox conditions influence the rate of incorporation of Mo into marine sediments and the fractionation of its isotopes between seawater and sediments. The largest extent of Mo isotope fractionation between seawater and sediments (~3‰) is observed during Mo adsorption to Fe-Mn oxides and crusts in well-oxygenated settings, causing the high δ^{98}Mo ratio of modern global seawater. Mass-balance models based on studies of modern sediments and ancient organic-rich shales show that an ancient ocean with a greater global extent of marine anoxia (and especially euxinia) than today will have a global seawater δ^{98}Mo that is lower compared to modern seawater, assuming that the riverine δ^{98}Mo in the past is broadly similar to today (Arnold et al., 2004; Dahl et al., 2010, 2011; Kendall et al., 2011). By comparison, a change from more oxidizing to more reducing conditions at a single locality without a significant change in global ocean redox conditions generally leads to a smaller Mo isotopic offset between seawater and sediments at that locality, and thus higher δ^{98}Mo in the sediments (with the possible exception of a change to weakly euxinic conditions; see Kendall et al., 2017, for a review). Results from the shales indicated that the basin in which the Green Point section was deposited was weakly restricted (see Chapter 2). The δ^{98}Mo values observed are thus likely to be representative of the local marine basin rather than the global ocean signature (see Kendall et al., 2017 for discussion of Mo isotopes as a global ocean redox proxy). The δ^{98}Mo signature of the seawater of the basin during the Cambrian-Ordovician transition may have had generally lower values than in the modern global ocean (~2.3 ‰; only sample GP 46 has a similar value; Fig. 3.2, Table 3.3, Appendix 3.2). This inference may hold even when taking into account a likely Mo isotope fractionation (up to ~1‰) between the carbonate sediments and seawater, based on the lack of evidence for consistently high pore-water sulfide levels during the deposition of the Green Point section (Romaniello et al., 2016; see Chapter 2). This interpretation is consistent with other estimates of Middle Cambrian to Ordovician seawater δ^{98}Mo based on organic-rich mudrocks (Dahl et al., 2010; Zhou et al., 2012; Lu et al., in press).

3.6 Conclusions

The relationships between U and Mo concentrations and enrichment factors versus U/Mo$_{conc}$ or U/Mo$_{auth}$ ratios provide significant clues about the redox changes in a marine sedimentary environment and the degree of basin restriction. Within the shales of the Green Point Formation, the correlations between U/Mo$_{auth}$ ratios and Mo$_{EF}$ or U$_{EF}$ provide a good indicator of changes in redox conditions. The U/Mo$_{auth}$ and Mo$_{EF}$ in particular were found to have significant correlations. When applying this concept to multiple other datasets representing a wide range of redox environments, the plots of U/Mo$_{auth}$ vs Mo$_{EF}$ or U$_{EF}$ demonstrate the same redox and basin restriction patterns relative to the U_{EF} vs Mo_{EF} plot of Algeo and Tribovillard (2009). Most promising, these plots provide a sensitive proxy of variations within the suboxic range, helping to evaluate whether a sulfidic zone developed within the sediment pore-waters.

For the carbonates at Green Point, evaluating U, Mo and U/Mo ratios yielded very different results. The main control on low U concentrations observed is the type of carbonate, namely calcite. The decrease across the anomaly level is likely due to the observed decrease in organic carbon. Combined with the low dissolved pore-water sulfide levels, suboxic conditions and presence of carbonate material, this leads to low authigenic enrichment. By contrast, the Mo concentrations are mainly within the range for modern and ancient carbonates deposited in environments with low pore-water sulfides, whether composed of calcite or aragonite. This may be an indication that, unlike for U, Mo is not affected by the carbonate species or pH during enrichment. More work would be needed for verification. The increase in Mo concentrations and enrichment factors across the anomaly level is marked by several samples indicating high pore-water sulfide levels, which is the same trend observed in the shales. It is therefore likely to be a good redox indicator. U/Mo ratios (EF or ppm) exhibited a decrease across the anomaly level of Azmy et al. (2014), as was observed in the shales. When they were compared to U and Mo (EF or ppm) in the Green Point carbonates, opposite trends were observed. The U/Mo vs U plots exhibited a slight positive correlation. This indicates U is not reflective of authigenic enrichment, and affected by other factors, possibly related to inclusion within the calcite structure. The U/Mo vs Mo plots exhibited a similar behavior to the trend in the shales, with a consistent inverse correlation. They are likely a much better reflection of authigenic enrichment, thus the dominantly suboxic redox conditions. When these two plots were applied to carbonates from the Bahamas, they were found to consistently differentiate between environments with low and high pore-water sulfide levels, respectively, and may prove to be a reliable tool. Although more data is required for verification, variations in the slope of change between U/Mo_{conc} vs Mo_{ppm} and U_{ppm} may provide a proxy for potential restriction within the water column as it does for shales.

The $\delta^{98}Mo$ ratios in the Green Point section are interpreted to represent a mixed detrital and authigenic signal. Post-authigenic diagenesis is however unlikely to have affected the signatures. Therefore, the $\delta^{98}Mo$ values may represent minimum values rather than Cambrian-Ordovician seawater values. The increase observed along with Mo concentrations also suggests increasing pore-water sulfide levels across the geochemical anomaly in the local marine basin. This agrees with the conclusion of earlier studies of biostratigraphy, lithostratigraphy, shale geochemistry, and $\delta^{15}N$ and $\delta^{13}C$ trends of the carbonates at Green Point.

References

Adelson, J.M., Helz, G.R., Miller, C.V., 2001. Reconstructing the rise of recent coastal anoxia; molybdenum in Chesapeake Bay sediments. Geochim. Cosmochim. Acta 65, 237-252.

Algeo, T.J., Maynard, J.B., 2004. Trace-element behavior and redox facies in core shales of Upper Pennsylvanian Kansas-type cyclothems. Chem. Geol. 206, 289-318.

Algeo, T.J., Lyons, T.W., 2006. Mo-total organic carbon covariation in modern anoxic marine environments: implication for analysis of paleoredox and –hydrographic conditions. Paleooceanography 21, PA1016 23 pp.

Algeo, T.J., Tribovillard, N., 2009. Environmental analysis of paleooceanographic systems based on molybdenum-uranium covariation. Chem. Geol. 268, 211-225.

Anbar, A.D., 2004. Molybdenum stable isotopes: observations, interpretations and directions. Reviews in Mineralogy & Geochemistry 55, 429-454.

Anderson, R.F., 1987. Redox behavior of uranium in an anoxic marine basin. Uranium 3, 145-164.

Arnold, G.L., Anbar, A.D., Barling, J., Lyons, T.W., 2004. Molybdenum isotope evidence for widespread anoxia in mid-Proterozoic oceans: Science, 304, 87-90, doi: 10.1126/science.1091785.

Azmy, K., Stouge, S., Brand, U., Bagnoli, G., Ripperdan, R., 2014. High-resolution chemostratigraphy of the Cambrian-Ordovician GSSP: Enhanced global correlation tool. Paleogr. Paleoclim. Paleoecol. 409, 135-144.

Azmy, K., Kendall, B., Brand, U., Stouge, U., Gordon, G.W., 2015. Redox conditions across the Cambrian-Ordovician Boundary: Elemental and isotopic signatures retained in the GSSP carbonates. Paleogeogr. Paleoclim. Paleoecol. 440. 440-454.

Barling, J., Arnold, G. L. and Anbar, A. D., 2001. Natural mass-dependent variations in the isotopic composition of molybdenum. Earth Planet. Sci. Lett., 193, 447-457.

Barnes, C.R., 1988. The proposed Cambrian-Ordovician global boundary stratotype and point (GSSP) in western Newfoundland, Canada. Geological Magazine, 125, 381-414.

Barnes, C.E., Cochran, J.K., 1990. Uranium removal in oceanic sediments and the oceanic U balance. Earth Planet. Sci. Lett. 97, 94-101.

Berelson, W.M., Hammond, D.E., Johnson, K.S., 1987. Benthic fluxes and the cycling of biogenic silica and carbon in two southern California borderland basins. Geochim. Cosmochim. 51, 1345-1363.

Berelson, W.M., McManus, J., Coale, K.H., Johnson, K.S., Kilgore, T., Burdige, D.J., Oilskaln, C., 1996. Biogenic matter diagenesis on the sea floor: a comparison between two continental-margin transects. J. Mar. Res. 54, 731-762.

Berelson, W.M., Prokopenko, M., Sansone, F.J., Graham, A.W., McManus, J., Bernhard, J., 2005. Anaerobic diagenesis of silica and carbon in continental margin sediments: Discrete zones of TCO_2 production. Geochim. Cosmochim. 69, 4611-4629.

Bertine, K., Turekian, K., 1973. Molybdenum in marine deposits. Geochim. Cosmochim. Acta. 37, 1415-1434.

Bone, S.E., Dynes, J.J., Cliff, J., Bargar, J.R., 2017A. Uranium (IV) adsorption by natural organic matter in anoxic sediments. PNAS. 114, 711-716.

Bone, S.E., Cahill, M.R., Jones, M.E., Fendorf, S., Davis, J., Williams, K.H., Bargar, J.R., 2017B. Oxidative uranium release from anoxic sediments under diffusion-limited conditions. Environ. Sci. Technol. 51, 11039-11047.

Böning, P., Brumsack, H.-J., Böttcher, M.E., Schnetger, B., Kriete, C., Kallmeyer, J., Borchers, S.L., 2004. Geochemistry of Peruvian near-surface sediments. Geochim. Cosmochim. Acta. 21, 4429-4451.

Boyce, W. D., Knight, I., 2005. Cambrian macrofossils from the Phillips Brook and North Brook anticlines, western Newfoundland: Current research: Department of Natural Resources, Geological Survey Report 05-1. 39–62.

Brand, U., Veizer, J., 1980. Chemical diagenesis of a multicomponent carbonate system: 1. Trace elements. J. Sediment. Petrol. 50, 1219-1236.

Brennecka, G.A., Wasylenki, L.E., Bargar, J.R., Weyer, S., Anbar, A.D., 2011. Uranium Isotope Fractionation during Adsorpotion to Mn-Oxyhydroxides. Environ. Sci. Technol. 45, 1370-1375.

Brumsack, H.J., Gieskes, J.M., 1983. Interstitial water trace-metal chemistry of laminated sediments from the Gulf of California, Mexico. Mar. Chem. 14, 89-106.

Calvert, S.E., Pedersen, T.F., 1993. Geochemistry of Recent oxic and anoxic marine sediments: implications for the geological record. Mar. Geol. 113. 67–88.

Calvert, S.E., Pederson, T.F., 1996. Sedimentary geochemistry of manganese: implocations for the environment of formation of manganiferous black shales: Econ. Geol. 91, 3-37.

Calvert, S.E., Piper, D.Z., Thunell, R.C., Astor, Y., 2015. Elemental settling and burial fluxes in the Cariaco Basin. Marine Chemistry 177, 607-629.

Canfield, D.E., Thamdrup, B., 2009. Towards a consistent classification scheme for geochemical environments, or why we wish the term 'suboxic' would go away. Geobiology 7, 385-392.

Cawood, P.A., McCausland, P.J.A., Dunning, G.R., 2001. Opening Iapetus: Constraints from the Lautentian margin in Newfoundland. G.S.A. Bul. 113 (4), 443-453.

Chaillou, G., Anschutz, P., Lavaux, G., Schäfer, J., Blanc, G., 2002. The distribution of Mo, U, and Cd, in relation to major redox redox species in muddy sediments of the Bay of Biscay. Mar. Chem. 80, 41-59.

Chan, F., Barth, J.A., Lubchenco, J., Kirincich, A., Weeks, H., Peterson, W.T., Menge, B.A., 2008. Emergence of anoxia in the California Current large marine ecosystem. Sci. 319, 920.

Chen, X., Romaniello, S.J., Herrmann, A.D., Wasylenki, L.E., Anbar, A.D., 2016. Uranium isotope fractionation during coprecipitation with aragonite and calcite. Geochim. Cosmochim. Acta 188, 189-207.

Cochran, J.K., Carey, A.E., Sholkovitz, E.R., Suprenant, L.D., 1986. The geochemistry of uranium and thorium in coastal marine sediments and sediment porewaters. Geochim. Cosmochim. Acta 50, 663-680.

Collier, R.W., 1985. Molybdenum in the Northeast Pacific-Ocean. Limnol. Oceanogr. 30, 1351-1354.

Coniglio, M., James, N.P., 1990. Origin of fine-grained carbonate and siliciclastic sediments in an early Paleozoic slope sequence, Cow Head Group, western Newfoundland. Sedimentology 37. 215-230.

Cooper, R.A., Nowlan, G.S., Williams, S.H., 2001a. Global Stratotype Section and Point for base of the Ordovician System. Episodes 24, 19–28.

Cooper, M., Weissenberger, J., Knight, I., Hostad, D., Gillespie, D., Williams, H., Burden, E., Porter-Chaudhry, J., Rae, D., Clark, E., 2001b. Basin Evolution in Western Newfoundland: New insights from Hydrocarbon Exploration. AAPG Datapages, Search and Discover Article # 10019.

Crusius, J., Calvert, S., Pedersen, T., Sage, D., 1996. Rhenium and molybdenum enrichments in sediments as indicators of oxic, suboxic and sulfidic conditions of deposition. Earth Planet. Sci. Lett. 145, 65-78.

Crusius, J., Thomson, J., 2000. Comparitive behavior of authigenic Re, U and Mo during reoxidation and subsequent long-term burial in marine sediments. Geochim. Cosmochim. Acta 64, 2233-2242.

Czaja, A.D., Johnson, C.M., Roden, E.E., Beard, B.L., Voegelin, A.R., Nägler, T.F., Beukes, N.J., Wille, M., 2012. Evidence for free oxygen in the Neoarchean Ocean based on coupled iron-molybdenu, isotope fractionation. Geochem. Cosmochim. 86, 118-137.

Dahl, T. W., Hammarlund, E. U., Anbar, A. D., Bond, D. P. G., Gill, B. C., Gordon, G. W., Knoll, A. H., Nielsen, A. T., Schovsbo, N. H. and Canfield, D. E., 2010. Devonian rise in atmospheric oxygen correlated to the radiations of terrestrial plants and large predatory fish. *Proceedings of the National Academy of Sciences, 107*(42), 17911-17915. doi: 10.1073/pnas.1011287107/-/DCSupplemental.

Dahl, T.W., Canfield, D.E, Rosing, M.T., Frei, R.E., Gordon, G.W., Knoll, A.H., Anbar, A.D., 2011. Molybdenum evidence for expansive sulfidic water masses in ~750 Ma oceans. Earth Planet. Sci. Lett. 311, 264-274.

Dahl, T.W., Chappaz, A., Fitts, J.P., Lyons, T.W., 2013. Molybdenum reduction in a sulfidic lake: Evidence from X-ray absorption fine-structure spectroscopy and implications for the Mo paleoproxy. Geochim. Cosmochim. Acta 103, 213-231.

Dean, W.E., Piper, D.Z., Peterson, L.C., 1999. Molybdenum accumulation in Cariaco Basin sediment over the last 24 ky: a record of water-column anoxia and climate. Geology 27, 507-510.

Dickson, J.A.D., 1966. Carbonate identification and genesis as revealed by staining. K. Sediment. Petrol. 36, 491-505.

Duan, Y., Anbar, A. D., Arnold, G. L., Lyons, T. W., Gordon, G. W. and Kendall, B., 2010. Molybdenum isotope evidence for mild environmental oxygenation before the Great Oxidation Event. Geoch. Cosmoch. Acta, 74 (23), 6655-6668. doi: 10.1016/j.gca.2010.08.035

Eberli, G.P., Swart, P.K., Malone, M.J. et al., 1997. Proceedings of the ocean drilling program. Initial Reports. V. 166, 5-12.

Elrick, M., Polyak, V., Algeo, T.J., Romaniello, S., Asmerom, Y., Hermann, A.D., Anbar, A.D., Zhao, L., Chen, Z.-Q., 2017. Global-ocean redox variation during the middle-late Permian through Early Triassic based on uranium isotope and Th/U trends of marine carbonates. G.S.A. v. 45, no. 2, p. 163-166.

Emerson, S.R., Huested, S.S., 1991. Ocean anoxia and the concentration of molybdenum and vanadium in seawater. Mar. Chem. 34, 177-196.

Erickson, B.E., Helz, G.R., 2000. Molybdenum (VI) speciation in sulfidic waters: stability and lability of thiomolybdates. Geochim. Cosmochim. Acta 64, 1149-1158.

Flügel, E., 2004. Microfacies of Carbonate Rocks. Analysis, Interpretation and Application. Springer, Berlin Heidelberg New York. 976.

Gao, P., Liu, G., Jia, C., Young, A., Wang, Z., Wang, T., Zhang, P., Wang, D., 2016. Redox variations and organic matter accumulation on the Yangtze carbonate platform during Late Ediacaran-Early Cambrian: Constraints from petrology and geochemistry. Paleogeogr. Paleoclim. Paleoecol. 450, 91-110.

Gillikin, D.P., Dehairs, F., 2013. Uranium in aragonitic marine bivalve shells. Paleogeogr. Palaeoclim. Palaeoecol. 373, 60-65.

Goldberg, T., Gordon, G., Izon, G., Archer, C., Pearce, C. R., McManus, J., Anbar, A. D. and Rehkämper, M., 2013. Resolution of inter-laboratory discrepancies in Mo isotope data: an intercalibration. Journal of Analytical Atomic Spectrometry, 28(5), 724. doi: 10.1039/c3ja30375f.

Goto, K.T., Anbar, A.D., Gordon, G.W., Romaniello, S.J., Shimoda, G., Takaya, Y., Tokumaru, A., Nozaki, T., Suzuki, K., Machida, S., Hanyu, T., Usui, A., 2014. Uranium isotope systematics of ferromanganese crusts in the Pacific Ocean: Implications for the marine $^{238}U/^{235}U$ isotope system. Geochim. Cosmochim. Acta 146, 43-58.

Hammond, D.E., Cummins, K.M., McManus, J., Berelson, W.M., Smith, G., Spagnoli, F., 2004. Methods for measuring benthic nutrient flux on the California Margin: Comparing shipboard core incubations to in situ lander results. Limnol. Oceanogr. Methods 2, 149-159.

Helz, G.R., Miller, C.V., Charnock, J.M., Mosselmans, J.L.W., Pattrick, R.A.D., Gamer, C.D., Vaughan, D.J., 1996. Mechanisms of molybdenum removal from the sea and its concentration in black shales: EXAPS evidences. Geochim. Cosmochim. Acta 60, 3631-3642.

Henderson, G.M., 2002. Seawater (234U/238U) during the last 800 thousand years: Earth and Planet. Sci. Lett. 199, 97-110.

Herrmann, A. D., Kendall, B., Algeo, T. J., Gordon, G. W., Wasylenki, L. E. and Anbar, A. D., 2012. Anomalous molybdenum isotope trends in Upper Pennsylvanian euxinic facies: Significance for use of δ98Mo as a global marine redox proxy. Chemical Geology, 324-325, 87-98. doi: 10.1016/j.chemgeo.2012.05.013.

Hibbard, J.P., van Staal, C.R., Rankin, D.W., Williams, H., 2006. Lithotectonic map of the Appalachian Orogen Canada-United States of America. Geological Survey of Canada, Map 2096A, scale 1:1 500 000.

Hibbard, J.P., van Staal, C.R., Rankin, D.W., 2007. A comparative analysis of pre-Silurian crustal building blocks of the northern and the southern Appalachian orogeny. American Journal of Science.

Hua, B., Xu, H.F., Terry, J., Deng, B.L., 2006. Kinetics of uranium (VI) reduction by hydrogen sulfide in anoxic aqueous systems: Environ. Sci. Tech. 40, 4666-4671.

Jacobi, R.D., 1981. Peripheral bulge – a causal mechanism for the Lower/Middle Ordovician unfonformity along the western margin of the northern Appalachians. Earth and Planet. Sci. Lett. 56, 245-251. Doi: 10.1016/0012-821X(81)90131-X.

James, N. P., Stevens, R. K., 1986. Stratigraphy and Correlation of the Cambrian-Ordovician Cow Head Group, Western Newfoundland. Geological Survey of Canada Bulletin 366.

James, N.P., Stevens, R.K., Barnes, C.R., Knight, I., 1989. Evolution of a Lower Paleozoic continental–margin carbonate platform, northern Canadian Appalachians In: Crevello, P. D. Wilson, J. L. Sarg, J. F. Read, J. F. (eds.), Controls on Carbonate Platform and Basin Development, Society of Economic Paleontologists and Mineralogists Special Publication 44, 123–146.

Johnson, K.S., Berelson, W.M., Coale, K.H., Coley, T.L., Elrod, V.A., Fairey, W.R., Iams, H.D., Kilgore, T.E., Nowicki, J.L., 1992. Manganese flux from continental margin sediments in a transect through the oxygen minimum zone. Sci. 257, 1242-1245.

Jones, B.J., Manning, A.C., 1994. Comparison of geochemical indices used for the interpretation of paleoredox conditions in ancient mudstones. Chem. Geol. 111, 111-129.

Kelly, S.D., Newville, M.G., Cheng, L., Kemner, K.M., Sutton, S.R., Fenter, P., Sturchio, N.C., Spotl, C., 2003. Uranyl incorporation into natural calcite. Environ. Sci. Technol. 37, 1284-1287.

Kelly, S.D., Rasbury, E.T., Chattopadhyay, S., Kropf, A.J., Kemner, K.M., 2006. Evidence of a stable uranyl site in ancient organic-rich calcite. Environ. Sci. Technol. 40, 2262-2268.

Kendall, B., Reinhard, C.T., Lyons, T.W., Kaufman, A.J., Poulton, S.W., Anbar, A.D., 2010. Pervasive oxygenation along late Archaean ocean margins. Nature Geoscience 3, 647–652.

Kendall, B., Gordon, G.W., Poulton, S.W., Anbar, A.D., 2011. Molybdenum isotope constraints on the extent of late Paleoproterozoic ocean euxinia. Earth and Planet. Sci. Let. 307, 450-460.

Kendall, B., Komiya, T., Lyons, T.W., Bates, S.M., Gordon, G.W., Romaniello, S.J., Jiang, G., Creaser, R.A., Xiao, S., McFadden, K., Sawaki, Y., Tahata, M., Shu, D., Han, J., Li, Y., Chu, X., Anbar, A.D., 2015. Uranium and molybdenum isotope evidence for an episode of widespread ocean oxygenation during the late Ediacaran Period. Geochim. Cosmochim. 156, 173-193.

Kendall, B.*, Dahl, T.W.*, Anbar A.D., 2017. Good golly, why moly? The stable isotope geochemistry of molybdenum. In: Teng F.-Z.., Watkins J., Dauphas N. (Eds.), *Reviews in Mineralogy and Geochemistry: Non-traditional stable isotopes*. Mineralogical Society of America and Geochemical Society, v. 82, pp. 683-732. *These authors contributed equally.

Klinkhammer, G.P., Bender, M.L., 1980. The distrivution of manganese in the Pacific Ocean. Earth. Planet. Sci. Lett. 46, 361-384.

Klinkhammer, G.P., Palmer, M.R., 1991. Uranium in the oceans: where it goes and why. Geochim. Cosmochim. Acta 55. 1799-1806.

Knight, I., James, N.P., Lane, T.E., 1991. The Ordovician St. George Unconformity, northern Appalcachians: the relationship of plate convergence at the St. Lawrence Promontory to the Sauk/Tippecanoe sequence boundary. GSA Bulletin 103.1200-1225.

Knight, I., James, N.P., Williams, H., 1995. Cambrian-Ordovician carbonate sequence. In Chapter 3 of Geology of the Appalachian-Caledonian Orogen in Canada and Greenland. Edited by H. Williams. Geological Survey of Canada. Geology of Canada, 6, 67-87.

Knight, I., Azmy, K., Greene, M., Lavoie, D., 2007. Lithostratigraphic setting of diagenetic, isotopic, and geochemistry studies of Ibexian and Whiterockian carbonates of the St. George and Table Head groups in western Newfoundland. Current Research Newfoundland and Labrador Department of Natural Resources Geological Survey. Report 07-1. 55–84.

Knight, I., Azmy, K., Boyce, D., Lavoie, D., 2008. Tremadocian Carbonates of the Lower St. George Group, Port au Port Peninsula, Western Newfoundland: Lithostratigraphic of diagenetic Isotopic, and Geochemistry Studies. Current Research Newfoundland and Labrador Department of Natural Resources Geological Survey. Report 08-1, 1-43.

Krestou, A., Panias, D., 2004. Uranium (VI) speciation diagrams in the $UO_2^{2+}/CO_3^{2-}/H_2O$ system at 25^{O}C. Eur. J. Miner. Process. Environ. Prot. 4 (2), 113-129.

Land, L.S., 1986. Limestone diagenesis – some geochemical considerations. U.S. Geol. Surv. Bull. 1578, 129-137.

Langmuir, D., 1978. Uranium solution-mineral equilibria at low temperatures with applications to sedimentary ore deposits. Geochim. Cosmochim. Acta 42, 547-569.

Lavoie, D., Burden, E., Lebel, D., 2003. Stratigraphic framework for the Cambrian – Ordovician rift and passive- margin successions from southern Quebec to western Newfoundland: Canadian Journal of Earth Science, 40, 177–205; in Tollo, R.P., Bartholomew, M.J., Hibbard, J.P., Karabinos, P.M. (2010) From Rodinia to Pangea: The lithotectonic Record of the Appalachian Region. The Geological Society of America, Memoir 206.

Lavoie, D., Desrochers, A., Dix, G., Knight, I., Salad Hersi, O., 2012. The great American carbonate bank in eastern Canada: An overview, in K.R. Derby, R.D. Fritz, S.A. Longacre, W.A. Morgan, and C.A. Sternbach, eds., The great American carbonate bank: The Geology and economic resources of the Cambrian-Ordovician Sauk megasequence of Laurentia: AAPG Memoir 98, 499-523.

Lovley, D.R., Phillips, E.J.P., Gorby, Y.A., Landa, E.R., 1991. Microbial reduction of uranium. Nature 350, 413-416.

Lovley, D.R., Roden, E.E., Phillips, E.J.P., Woodward, J.C., 1993. Enzymatic iron and uranium reduction by sulfate-reducing bacteria: Marine Geology. 113, 41-53.

Lu X., Kendall B., Stein H.J., Li C., Hannah J.L., Gordon G.W., Ebbestad J.O.R., in press. Marine redox conditions during deposition of Late Ordovician and Early Silurian organic-rich mudrocks in the Siljan ring district, central Sweden. Chemical Geology.

Luo, W., Gu, B., 2008. Dissolution and mobilization of uranium in a reduced sediment by natural humic substancs under anaerobic conditions. Environ. Sci. Technol. 43 (1), 152-156.

McKee, B.A., DeMaster, D.J., Nittrouer, C.A., 1987. Uranium geochemistry on the Amazon shelf. Evidence for uranium release from bottom sediments. Geochim. Cosmochim. Acta 51, 2779-2786.

McManus, J., Berelson, W.M., Coale, K.H., Johnson, K.S., Kilgore, T.E., 1997. Phosphorus regeneration in continental margin sediments. Geochim. Cosmochim. 61, 2891-2907.

McManus, J., Hammond, D.E., Cummins, K., Klinkhammer, G.P., Berelson, W.M., 2003. Diagenetic Ge-Si fractionation in continental margin environments: Further evidence for a nonopal Ge sink. Geochim. Cosmochim. Acta 67, 4545-4557.

McManus, J., Berelson, W.M., Klinkhammer, G.P., Hammond, D.E., Holm, C., 2005. Authigenic uranium: relationship to oxygen penetration depth and organic carbon rain. Geochim. Cosmochim. Acta 69, 95-108.

McManus, J., Berelson, W.B., Severmann, S., Poulson, R.L., Hammond, D.E., Klinkhammer, G.P., Holm, C., 2006. Molybdenum and uranium geochemistry in continental margin sediments: paleoproxy potential. Geochim. Cosmochim. Acta 70, 4643-4662.

Morford, J.L., Emerson, S., 1999. The geochemistry of redox sensitive trace metals in sediments. Geochim. Cosmochim. Acta 63, 1735-1750.

Morford, J.L., Martin, W.R., Francois, R., Carney, C.M., 2009a. A model for uranium, rhenium, and molybdenum diagenesis in marine sediments based on results from coastal locations. Geochim. Cosmochim. Acta 73, 2938-2960.

Morford, J.L., Martin, W.R., François, R., Carney, C.M., 2009b. A model for uranium, rhenium, and molybdenum diagenesis in marine sediments based on results from coastal locations. Geochim. Cosmochim. Acta 73, 2938-2960.

Nägler, T.F., Neubert, N., Böttcher, M.E., Dellwig, O., Schnetger, B., 2011. Molybdenum isotope fractionation in pelagic euxinia: Evidence from the modern Black and Baltic Seas. Chem. Geol. 289, 1-11.

Nägler, T. F., Anbar, A. D., Archer, C., Golderg, T., Gordon, G. W., Greber, N. D., Siebert, C., Sohrin, Y. and Vance, D., 2014. Proposal for an Internatinal Molybdenum Isotope Measurement Standard and Data Representation. Geostand. Geoanal. Res. 38(2), 149-151. doi: 10.1111/j.1751-908X.2013.00275.x.

Nakagawa, Y., Takano, S., Lufti Firdaus, M., Norisuye, K., Hirata, T., Vance, D., Sohrin, Y., 2012. The molybdenum isotopic composition of the modern ocean. Geochem. Journ. 46, 131-141.

Neubert, N., Nägler, T.F., Böttcher, M.E., 2008. Sulfidity controls mylybdenum isotope fractionation into euxinic sediments: Evidence from modern Black Sea. Geol. 36, 775-778.

Nowlan, G.S., Barnes, C.R., 1987. Thermal maturation of Paleozoic strata in eastern Canada from conodont colour alteration index (CAI) data with implications for burial history, tectonic evolution, hotspot tracks and mineral and hydrocarbon potential. Geological Survey of Canada. Bulletin 369.

Partin, C.A., Bekker, A., Planavsky, N.J., Scott, C.T., Gill, B.C., Li, C., Podkovyrov, V., Maslov, A., Konhauser, K.O., Lalonde, S.V., Love, G.D., Poulton, S.W., Lyons, T.W., 2013. Large-scale fluctuations in Precambrian atmospheric and oceanic oxygen levels from the record of U in shales. 369-370, 284-293.

Piper, D.Z., Calvert, S.E., 2011. Holocene and late glacial paleoceanography and paleolimnology of the Black Sea: Changing sediment provenance and basin hydrography over the past 20, 000 years. Geochim. Cosmochim. Acta 75, 5597-5624.

Piper, D.Z., 2016. Geochemistry of the Black Sea during the last 15 kyr: A protracted evolution of its hydrography and ecology. Paleooceanogr. 31, 1117-1137.

Poulson, R.L., Siebert, C., McManus, J., Berelson, W.M., 2006. Authigenic molybdenum isotope signatures in marine sediments. Geol. 34, 617-620.

Poulson Brucker, R.L., McManus, J., Severmann, S., Berelson, W.M., 2009. Molybdenum behavior during early diagenesis: insights from Mo isotopes. Geochem. Geophys. Geosys 10 (6). Doi: 10.1029/2008GC002180.

Reeder, R.J., Nugent, M., Lamble, G.M., Tait, C.D., Morris, D.E., 2000. Uranyl incorporation into calcite and aragonite: XAFS and luminescence studies. Environ. Sci. Technol. 34, 638-644.

Reeder, R.J., Nugent, M., Tait, C.D., Morris, D.E., Heald, S.M., Beck, K.M., Hess, W.P., Lanzirotti, A., 2001. Coprecipitation of uranium (VI) with calcite: XAFS, micro-XAS, and luminescence characterization. Geochim. Cosmochim. Acta 65, 3491-3503.

Reitz, A., Willie, M., Nägler, T.F., de Lange, G.J., 2007. Atypical Mo isotope signatures in eastern Mediterranean sediments. Chem. Geol. 2245, 1-8.

Romaniello, S.J., 2012. Fractionation of $^{238}U/^{235}U$ during carbonate diagenesis: Results from the ODP leg 166 Bahamas Transect. Chapter 4 in Romaniello, S.J., Anbar, A., Hartnett, H., Hermann, A., Shock, E., Wadhwa, M., 2012. Incorporation and Preservation of Molybdenum and Uranium of Isotope Variations in Modern Marine Sediments. Thesis, Arizona State University.

Romaniello, S.J., Herrmann, A.D., Anbar, A.D., 2013. Uranium concentrations and $^{238}U/^{235}U$ isotope ratios in modern carbonates from the Bahamas: Assessing a novel paleoredox proxy. Chem. Geol. 362, 305-316.

Romaniello, S.J., Herrmann, A.D., Anbar, A.D., 2016. Syndepositional diagenetic control of molybdenum, isotope variations in carbonate sediments from the Bahamas. Chem. Geol. 438, 84-90.

Sahoo, S.K., Planavsky, N.J., Kendall, B., Wang, X., Shi, X., Scott, C., Anbar, A.D., Lyons, T.W., Jiang, G., 2012. Ocean oxygenation in the wake of the Marinoan glaciation. Nature, 489, 546-549.

Sani, R.K., Peyton, B.M., Amonette, J.E., Geesey, G.G., 2004. Reduction of uranium(VI) under sulfate-reducing conditions in the presence of Fe(III)-(hydr)oxides. Geochim. Cosmochim. Acta 68, 2639-2649.

Savrda, C.E., Bottjer, D.J., 1001. Oxygen-related biofacies in marine strata: an overview and update. In: Tyson, R.V., Pearson, T.H., (Eds.), Modern and ancient continental shelf anoxia. Geol. Sco. London Spec. Publ. 58, 201-219.

Scheiderich, K., Helz, G.R., Walker, R.J., 2010. Century-long record of Mo isotopic composition in sediments of a seasonally anoxic estuary (Chesapeake Bay). Earth Plan. Sci. Lett. 289, 189-197.

Scott, C., Lyons, T.W., 2012. Contrasting molybdenum cycling and isotopic properties in euxinic versus non-euxinic sediments and sedimentary rocks: Refining the paleoproxies. Chem. Geol. 324-325, 19-27.

Shaw, T.J., Gieskes, J.M., Jahnke, R.A., 1990. Early diagenesis in differing depositional environments: the response of transition metals in pore waters. Geochim. Cosmochim. Acta. 54, 1233-1246.

Siebert, C., Nagler, T.F., von Blanckenburg, F., and Kramers, J.D., 2003. Molybdenum isotope records as a potential new proxy for paleoceanography: Earth and Planetary Science Letters, 211, 159–171, doi: 10.1016/ 0012-821X(03)00189-4.

Siebert, C., McManus, J., Bice, A., Poulson, R., Berelson, W.M., 2006. Molybdenum isotope signatures in contental margin marine sediments. Earth Planet. Sci. Lett. 241, 723-733.

Śliwiński, M.G., Whalen, M.T., Day, J., 2010. Trace element variations in the Middle Frasnian punctata zone (late Devonian) in the western Canada sedimentary Basin–changes in oceanic bioproductivity and paleoredox spurred by a pulse of terrestrial afforestation? Geologica Belgica 4. 459–482.

Stevens, R.K., 1970. Cambro-Ordovician flysch sedimentation and tectonics in west Newfoundland and their possible bearing on a proto-Atlantic Ocean. In Flysch Sedimentology in North America. Edited by J. Lajoie. Geolog. Associ. Canada. Special Paper 7, 165-177.

Stockmal, G.S., Waldron, J.W.F., Quinlan, G.M., 1995. Flexural modeling of Paleozoic foreland basin subsidence, offshore western Newfoundland: evidence for substantial post-Taconian thrust transport. Journal of Geology 103, 653-671.

Stockmal, G.S., Slingsby, A., Waldron, J.W.F., 1998. Deformation styles at the Appalachian structural front, western Newfoundland: implications of new industry seismic reflection data: Canadian Journal of Earth Sciences 35, 1288-1306.

Sturchio, N.C., Antonio, M.R., Soderholm, L., Sutton, S.R., Brannon, J.C., 1998. Tetravalent Uranium in Calcite. Science 281, 971-973.

Taylor, S.R., McLennan, S.M., 1985. The continental crust: its composition and evolution. Blackwell, Oxford. 257-277.

Tribovillard, N., Algeo, T.J., Lyons, T., Riboulleau, A., 2006. Trace metals as paleoredox and paleoproductivity proxies: an update. Chem. Geol. 232. 12-32.

Tribovillard, N., Bout-Roumazeilles, V., Algeo, T., Lyons, T.W., Sioneau, T., Montero-Serrano, J.C., Roboulleau, A., Baudin, F., 2008a. Paleodepositional conditions in the

Orca Basin as inferred from organic matter and trace metal contents. Mar. Geol. 254, 62-72.

Tribovillard, N., Lyons, T.W., Riboulleau, A., Bout-Rounazeilles, V., 2008b. A possible capture of molybdenum during early diagenesis of dysoxic sediments. Bulletin de la Société Géologique de France. 179, 3-12.

Tribovillard, N., Algeo, T.J., Baudin, F., Riboulleau, A., 2012. Analysis of marine environmental conditions based on molybdenum-uranium covariation – Applications to Mesozoic paleoceanography. Chem. Geol. 324-325, 46-58.

Tripathy, G.R., Hannah, J.L., Stein, H.J., Yang, G., 2014. Re-Os age and depositional environment for black shales from the Cambrian-Ordovician boundary, Green Point, western Newfoundland. Geochem. Geophys. Geosys. 15 (4). 1021-1037.

Veizer, J., 1983. Chemical diagenesis of carbonates: theory and application of trace element technique. In: Arthur, M.A., Anderson, T.F., Kaplan, I.R., Veizer, J., Land, L.S. (eds.), Stable Isotopes in Sedimentary Geology. V. 10,. Society of Economic Paleontologists and Mineralogists Short Course Notes, pp. III-1-III-100.

Voegelin, A.R., Nägler, T.F., Samankassou, E., Villa, I.M., 2009. Molybdenum isotopic composition of modern and Carboniferous carbonates. Chem. Geol. 265, 488-498.

Voegelin, A.R., Nägler, T.F., Beukes, N.J., Lacassie, J.P., 2010. Molybdenum isotopes in late Archean carbonate rocks: Implications for early Earth oxygenation. Precambrian Research 182, 70-82.

Waldron, J.W.F., 1985. Structural history of continental margin sediments beneath the Bay of Islands Ophiolite, Newfoundland. Can. Journal of Earth Sci. 22, 1618-1632.

Waldron, J.W.F., Turner, D., Stevens, K.M., 1988. Stratal disruption and development of mélange, western Newfoundland: effect of high fluid pressure in an accretionary terrain during ophiolite emplacement. Journ. Struct. Geol. 10, 861-873.

Wedepohl, K.H., 1971. Environmental influences on the chemical composition of shales and clays. In: Ahrens, L.R., Press, F., Runcorn, S.K., Urey, H.C. (Eds.). Physics and Chemistry of the Earth. Pergamon. Oxford. 305-333.

Wedepohl, K.H., 1991. The composition of the upper Earth's crust and the natural cycles of selected metals. In: Merian, E. (Ed.), Metals and their Compounds in the Environment. VCH-Verlagsge-sellschaft, Weinheim. 3-17.

Wen, H., Fan, H., Zhang, Y., Cloquet, C., Carignan, J., 2015. Reconstruction of early Cambrian ocean chemistry from Mo isotopes. Geochim. Cosmochim. Acta 164, 1-16.

Wignall, P., 1994. Black Shales, 127 pp., Oxford Univ. Press, New York.

Wignall, P.B., Zonneveld, J.-P., Newton, R.J., Amor, K., Sephton, M.A., Hartley, S., 2007. The end Triassic mass extinction record of Williston Lake, British Columbia. Paleogr. Paleoclim. Paleoecol. 253, 385-406.

Williams, H., 1975. Structural succession, nomenclature and interpretation of transported rocks in western Newfoundland. Can. Journal of Earth Sci. 12, 1874-1894.

Williams, H., 1979. Appalachian Orogen in Canada. Can. Journal of Earth Sci. 16, 792–807.

Williams, H. (ed.), 1995. Geology of the Appalachian-Caledonian Orogeny in Canada and Greenland. G.S.C. Geology of Canada 6.

Williams, H., Svevens, R.K., 1974. The ancient continental margin of eastern North America. In Geology of Continental Margins. Edited by C.A. Burk and C.L. Drake. Springer Verlag, New York, pages 871-796.

Xu, L., Lehmann, B., Mao, J., Nägler, T.F., Neubert, N., Böttcher, M.E., Escher, P., 2012. Mo isotope and trace element patterns of Lower Cambrian black shales in South China: Multi-proxy constraints on the paleoenvironment. Chem. Geol. 318-319, 45-59.

Zheng, Y., Anderson, R.F., van Geen, A., Kuwabara, J., 2000. Authigenic molybdenium formation in marine sediments: a link to pore water sulfide in the Santa Barbara Basin. Geochim. Cosmochim. Acta 64, 4165-4178.

Zheng, Y., Anderson, R.F., van Geen, A., Fleischer, M.Q., 2002a. Preservation of non-lithogenic particulate uranium in marine sediments. Geochim. Cosmochim. Acta 66, 3085-3092.

Zheng, Y., Anderson, R.F., van Geen, A., Fleischer, M.Q., 2002b. Remobilization of authigenic uranium in marine sediments by bioturbation. Geochim. Cosmochim. Acta 66, 1759-1772.

Zhou, L., Wignall, P.B., Su, J., Feng, Q., Xie, S., Zhao, L., Huang, J., 2012. U/Mo ratios and $\delta^{95}/^{95}$Mo as local and global redox proxies during mass extinction events. Chem. Geol. 324–325. 99-107.

Chapter 4

Conclusions

Geochemical evidence points to the occurrence of a significant environmental change during the Cambrian–Ordovician transition within the Green Point Formation.

On the other hand, no significant diagenesis or post-depositional hydrothermal alteration and catagenesis are thought to have significantly altered the investigated shales. This is based on physical observations, organic carbon and ∑REE data. This supports the preservation of at least near-primary geochemical signatures in the investigated shales at Green Point.

The most influential control of the final organic matter concentrations was its preservation, controlled by the prevailing redox conditions, based on the close relationship with shale coloration and Mo, U concentrations, enrichments and their ratios. It is supported by the poor correlation between TOC and both detrital and bioproductivity proxies evaluated. Futhermore, the $\delta^{13}C_{org}$ values, representing phototrophic activity, indicate that sealevel may have indirectly affected redox conditions or bioproductivity.

Carbonate dilution was found to have a major and variable impact on the geochemical signatures of the shales at Green Point, especially with regards to detrital proxies. Once this effect was accounted for, detrital proxies were found to be reliable. The siliciclastic sediments are derived from the Laurentian Craton, with little to no input from the approaching Taconic Arc. Comparing carbonate content and detrital proxies indicates the shales became much more carbonate-rich up-section within the Broom Point Member, as the source platform flooded when sealevel rose and lime mudstone rhythmite deposition became much more frequent.

Paleoredox indicators suggest a relative decrease in O_2 levels during the LST systems tract from oxic-suboxic to more strongly suboxic conditions above the anomaly level in the TST sytems tract as sea level rose, with more frequent anoxic intervals. The most reliable indicators were found to be Mo and U enrichment factors and ratios. Though relative changes across the anomaly were in line with other paleoredox indicators, absolute values for several ratios, such as V/Cr, V/(V+Ni), authigenic U and Th/U are not reliable when identifying paleoredox conditions within the slope environment of the Green Point Formation. Fe_T/Al and Ce/Ce* should also be used cautiously. No correlations with other proxies or the lithologies were observed.

The study of bioproductivity proxies yielded mixed results. Phototrophic activity was the main driver of bioproductivity, based on $\delta^{13}C_{org}$ values. Overall bioproductivity was found to be low, based on Ni, Cu, P and TOC. Variations across the anomaly could not be ascertained with any certainty, however. Preservation potential, which affects TOC and P, was very inconsistent due to the short-term redox fluctuations within the pore-waters and near the seafloor.

When the observed geochemical variations were evaluated in concert with lithological changes within the shales, sealevel variations could be tracked in a predictable manner. The observed variations were correlated to the previously interpreted sea-level fluctuations, based on the carbonate isotope stratigraphy of the interbedded carbonates. Clear detrital, redox or bioproductivity proxy variations separate the systems tracts and patterns of change within each systems tract.

The relationships between the U, Mo and the U/Mo ratio paleoredox indicators provide valuable insight regarding the redox conditions and variations within marine sedimentary environments and degree of restriction within the basins.

In the Green Point shales, the correlations between U/Mo_{auth} ratios and Mo_{EF} or U_{EF} are good redox indicators in the oxic-anoxic range. The U/Mo_{auth} and Mo_{EF} ratios in particular have significant inverse correlations. This concept was then applied to other datasets representing a wide range of environments. The plots of U/Mo_{auth} vs Mo_{EF} or U_{EF} differentiated the redox the basin restriction patterns delineated in the U_{EF} vs Mo_{EF} plot of Algeo and Tribovillard (2009). Most promising, these plots can help evaluate whether significant pore-water sulfide levels developed within the suboxic range, based on relative U_{EF} and Mo_{EF} variations compared to U/Mo_{auth}. If a significant sulfidic zone did not developed (i.e. oxic-slightly suboxic), U_{EF} and U/Mo_{auth} were positively correlated. If it did (i.e. highly suboxic), then an inverse correlation is observed.

When this method was applied to the Green Point carbonates, comparing U/Mo ratios to Mo and U concentrations and enrichment factors yielded very different results. The dominant control on U concentrations observed was not redox-controlled authigenic enrichment, due to the poor relationship observed between U and U/Mo. Rather, it was the dominant carbonate species being calcite. The decrease across the anomaly level is likely due to low and decreasing TOC. This is enhanced by the presence of carbonate material, mainly low pore-water sulfide levels and suboxic conditions. This results in low authigenic enrichment. Mo concentrations on the other hand are in the range of previously evaluated carbonates deposited in conditions with low pore-water sulfides. This may indicate Mo is not strongly affected by pH or incorporation within different carbonate species, though verification would be required. Mo concentrations and enrichment factors increased across the geochemical anomaly, as in the shales. This is a good indication that pore-water sulfide levels increased above the anomaly level, and that Mo may be a good indicator of redox conditions. The U/Mo ratios in the Green Point carbonates exhibited a similar behavior to the shales, with a consistent decrease across the anomaly level. U (EF or ppm) had a low positive correlation to U/Mo ratios, indicating U is not reflective of authigenic enrichment. The U/Mo vs Mo (EF or ppm) plots had a similar trend to within the shales, and are likely reflective of redox variations. When these two plots were applied to carbonates from the Bahamas, both consistently differentiate environments with respectively low or high pore-water sulfide levels. Although more data would be necessary to verify this concept, variations in the slope of change between U/Mo_{conc} vs Mo_{ppm} or U_{ppm} may also provide a reliable proxy to differentiate potential basin restriction, as previously established for shales.

The δ^{98}Mo ratio increase was interpreted as a mixed authigenic and detrital signal. There is little indication however that post-authigenic diagenesis affected the observed values. The δ^{98}Mo signatures were thus treated minimum values. The increase suggests dissolved pore-water sulfide levels above the geochemical anomaly level in the local marine basin. This is supported by the results of multiple previous studies focusing on biostratigraphy, lithostratigraphy, shale geochemistry, and δ^{15}N and δ^{13}C trends of the Green Point section.

Appendix 2.1: Elemental, elemental ratio and isotopic geochemical data of the studied shales from the Green Point Formation in Chapter 2. Highlighted samples have low U EFs and their U contents correlate strongly with their Al counterparts. (#) refers to the relevant equation for certain ratios.

Bed	Sample #	Ca wt%	Sr ppm	Na wt%	Al wt%	K wt%	Cr ppm	Sc ppm	Th ppm	Cs ppm	V ppm	Mo ppm	U ppm
17	S112	3.27	183	0.25	3.27	2.07	33.5	4.9	4.9	1.2	75	4.3	2.4
17	S3	5.79	151	0.44	5.79	3.82	55.6	8.6	9.3	3.7	85	0.8	3.2
18	S4	5.78	114	0.40	5.78	5.11	57.7	8.6	8.7	3.8	111	7.4	6.9
18	S7	4.96	142	0.43	4.96	2.97	47.7	6.8	6.0	3.0	62	0.5	1.4
18	S8	6.70	124	0.46	6.70	4.17	68.8	9.2	6.9	4.4	88	0.8	2.4
18	S10	7.17	86	0.30	7.17	6.40	74.7	10.8	7.5	3.4	81	4.0	5.1
18	S13	5.19	136	0.36	5.19	3.93	49.9	7.9	7.5	2.9	117	13.9	6.9
18	S14	7.02	121	0.29	7.02	6.19	71.1	10.5	7.5	3.1	90	3.6	4.0
18	S16	7.14	95	0.60	7.14	4.83	72.2	9.1	5.7	4.2	88	0.4	2.4
18	S19	6.27	94	0.36	6.27	4.81	68.2	10.0	7.3	4.2	130	6.8	3.9
18	S26	7.13	73	0.23	7.13	6.82	75.8	9.8	7.4	3.6	69	2.9	4.0
20	S27	7.89	75	0.43	7.89	5.58	89.0	12.3	10.0	5.6	195	0.6	2.8
20	S30	7.23	102	0.58	7.23	4.91	66.6	11.1	8.4	4.0	77	0.3	2.3
20	S34	6.57	84	0.42	6.57	4.89	74.3	9.1	7.4	4.4	96	0.6	2.6
21	S39	5.82	124	0.35	5.82	5.29	67.2	7.6	6.9	2.8	107	0.5	2.4
21	S41	5.27	172	0.31	5.27	5.13	53.3	7.0	6.7	2.1	84	1.7	2.6
21	S44	6.84	102	0.50	6.84	4.21	65.6	10.3	7.3	4.2	77	0.6	1.6
22	S47	6.80	115	0.52	6.80	4.77	67.3	10.9	8.7	4.4	86	0.7	2.0
22	S49	5.44	114	0.41	5.44	3.76	59.5	8.0	6.4	4.5	64	1.4	1.4
22	S53	5.93	118	0.31	5.93	5.61	67.8	9.0	7.4	2.9	305	7.0	9.7
22	S57	4.36	86	0.23	4.36	2.50	51.6	5.8	5.2	2.9	58	0.4	1.0
23	S61	4.99	99	0.29	4.99	2.72	52.1	7.6	6.5	3.0	61	0.6	1.2
23	S63	5.31	86	0.33	5.31	3.15	59.6	8.0	5.5	2.9	281	1.4	2.3
23	S66	5.80	129	0.39	5.80	4.76	62.7	8.6	7.0	3.5	338	4.5	7.8
23	S68	5.11	103	0.22	5.11	5.07	59.0	7.0	4.8	2.2	57	2.4	2.7
23	S71	6.43	97	0.30	6.43	6.31	67.8	9.3	6.4	2.7	161	2.7	3.2
23	S75	3.98	134	0.30	3.98	3.32	49.2	5.1	3.6	3.1	110	1.0	1.7
24	S79	4.73	142	0.43	4.73	3.58	49.1	7.3	6.4	1.9	288	1.8	2.5
25	S82	3.22	156	0.28	3.22	1.81	33.2	5.1	3.8	1.2	43	0.6	1.8
25	S84	5.00	117	0.48	5.00	3.43	45.4	7.3	6.1	2.1	41	0.7	1.2
25	S149	5.46	75	0.31	5.46	4.63	50.8	7.5	5.1	2.1	120	1.5	2.1
25	S150	7.10	73	0.49	7.10	5.33	73.9	10.9	8.6	3.8	97	0.6	2.6
25	S151	4.37	163	0.31	4.37	4.54	50.0	5.5	4.9	1.7	78	7.3	3.3
26	S157	6.05	130	0.48	6.05	5.01	56.8	8.4	7.3	3.6	249	3.0	3.2
26	S166	5.22	131	0.39	5.22	56.7	56.7	9.1	8.7	3.9	128	24.6	13.4

Bed	Sample #	$\delta^{13}C_{org}$ ‰ VPDB	TOC % wt%	P ppm	Ni ppm	Cu ppm	Y ppm	La ppm	Ce ppm	Pr ppm	Nd ppm	Sm ppm	Eu ppm
17	S112	-29.84	0.96	434	20.0	20.3	17.10	19.15	36.01	4.30	15.87	3.04	0.75
17	S3			732	22.1	31.6	23.65	31.32	61.22	7.41	28.60	5.09	1.33
18	S4	-29.10	4.10	398	48.2	47.7	15.32	25.28	45.49	5.43	20.34	3.59	0.84
18	S7			510	18.2	28.3	17.88	24.86	48.98	5.91	22.25	3.98	0.97
18	S8	-28.46	0.25	487	27.1	30.1	14.32	20.22	37.89	4.63	17.51	3.19	0.76
18	S10	-29.02	1.80	289	42.1	36.8	9.81	17.08	27.44	3.35	13.24	2.24	0.49
18	S13			484	60.1	50.3	17.54	23.31	44.56	5.45	20.58	3.61	0.92
18	S14	-28.79	1.86	425	38.4	42.1	12.56	20.60	35.77	4.44	16.76	2.89	0.72
18	S16	-28.03	0.12	541	28.2	53.4	15.26	25.10	46.89	5.64	19.93	3.33	0.85
18	S19			500	40.5	32.2	14.21	20.14	37.27	4.55	16.84	2.94	0.77
18	S26	-29.10	1.45	259	34.5	26.0	8.16	8.11	12.95	1.66	6.39	1.15	0.36
20	S27	-28.99	0.74	576	49.0	49.1	12.80	12.73	25.48	3.24	12.89	2.49	0.65
20	S30	-27.52	0.11	632	24.7	8.5	17.76	33.21	62.62	7.63	27.87	4.80	1.11
20	S34	-28.68	0.17	455	38.0	50.7	13.08	16.74	30.14	3.72	14.12	2.50	0.63
21	S39	-29.05	0.58	657	29.6	35.3	15.27	20.15	37.97	4.74	17.20	3.06	0.81
21	S41			493	28.1	27.2	17.18	24.62	45.57	5.41	20.91	3.54	0.96
21	S44	-27.88	0.12	552	29.6	56.2	16.80	27.84	53.89	6.58	25.51	4.30	0.97
22	S47			599	27.4	22.4	18.25	30.15	55.10	6.70	25.11	4.26	1.01
22	S49	-27.52	0.11	527	32.0	41.9	20.16	28.97	54.92	6.64	25.59	4.61	1.06
22	S53	-29.86	1.79	896	39.0	45.0	19.73	25.45	51.73	6.79	26.42	4.89	1.12
22	S57	-29.13	0.24	317	27.3	30.9	8.30	10.65	20.14	2.58	9.83	1.72	0.42
23	S61	-28.82	0.20	377	24.7	32.8	10.47	13.95	25.33	3.25	12.37	2.23	0.54
23	S63	-29.71	0.58	485	31.7	45.3	11.74	13.48	25.04	3.33	12.12	2.20	0.55
23	S66			469	46.4	41.5	15.29	19.54	35.89	4.71	18.23	3.22	0.77
23	S68	-29.98	1.04	545	30.7	21.6	10.73	12.96	26.52	3.30	12.75	2.23	0.57
23	S71			420	49.5	39.2	9.99	12.32	24.52	3.08	11.96	1.96	0.51
23	S75	-29.80	0.95	271	25.1	28.5	10.32	11.90	21.98	2.60	9.94	1.84	0.47
24	S79	-29.89	1.10	633	27.9	28.2	15.05	14.22	28.31	3.54	13.79	2.62	0.68
25	S82	-29.40	0.45	377	17.9	19.2	8.31	11.29	20.51	2.47	9.47	1.79	0.41
25	S84			363	18.5	16.2	8.37	10.49	21.49	2.44	9.32	1.56	0.42
25	S149	-29.03	0.87	315	20.2	21.2	10.11	13.10	25.51	2.99	10.94	1.93	0.45
25	S150			517	48.0	105.2	15.17	34.79	78.51	7.20	25.38	4.01	0.86
25	S151	-29.02	2.37	744	32.3	34.4	19.28	21.91	45.09	4.83	18.52	3.34	0.87
26	S157	-30.1	1.24	529	36.7	29.2	14.95	16.63	32.58	4.02	15.75	2.97	0.72
26	S166	-26.01	8.81	580	30.4	45.7	17.28	19.50	39.05	4.75	18.44	3.42	0.79

Bed	Sample #	Gd ppm	Tb ppm	Dy ppm	Ho ppm	Er ppm	Tm ppm	Yb ppm	Lu ppm	∑REE ppm	Y/Ho Ratio	Ce/Ce* (1)	Ce/Ce* (2)
17	S112	2.72	0.39	2.56	0.57	1.44	0.22	1.16	0.21	105	29.9	0.91	0.96
17	S3	4.42	0.64	3.77	0.81	2.16	0.36	1.83	0.34	173	29.3	0.92	0.99
18	S4	2.82	0.41	2.34	0.52	1.45	0.23	1.20	0.20	125	29.7	0.89	0.97
18	S7	3.27	0.47	2.83	0.63	1.59	0.23	1.38	0.26	135	28.6	0.93	0.97
18	S8	2.52	0.39	2.30	0.48	1.32	0.22	1.20	0.22	107	30.1	0.90	0.96
18	S10	1.52	0.26	1.49	0.29	0.94	0.17	0.87	0.17	79	34.1	0.83	1.01
18	S13	3.20	0.45	2.76	0.60	1.53	0.23	1.33	0.22	126	29.4	0.91	0.96
18	S14	2.40	0.34	1.96	0.42	1.11	0.17	1.01	0.17	101	29.9	0.86	0.94
18	S16	2.78	0.39	2.43	0.57	1.48	0.24	1.50	0.25	127	26.6	0.91	0.91
18	S19	2.55	0.35	2.17	0.48	1.30	0.19	1.10	0.18	105	29.7	0.89	0.94
18	S26	1.04	0.16	1.13	0.25	0.75	0.11	0.75	0.13	43	32.2	0.81	0.93
20	S27	2.17	0.33	2.11	0.45	1.25	0.19	1.07	0.19	78	28.6	0.91	0.98
20	S30	3.66	0.49	2.97	0.63	1.74	0.26	1.58	0.25	167	28.2	0.90	0.93
20	S34	2.10	0.31	2.06	0.45	1.31	0.20	1.19	0.20	89	28.9	0.88	0.96
21	S39	2.74	0.36	2.24	0.50	1.25	0.18	1.13	0.18	129	30.7	0.89	0.90
21	S41	3.30	0.46	2.74	0.60	1.54	0.21	1.27	0.21	129	28.8	0.91	1.01
21	S44	3.27	0.47	2.83	0.60	1.58	0.24	1.42	0.23	147	28.1	0.92	0.99
22	S47	3.42	0.48	2.83	0.60	1.65	0.24	1.53	0.27	152	30.3	0.89	0.96
22	S49	3.54	0.52	3.21	0.67	1.79	0.28	1.57	0.25	154	30.1	0.91	0.99
22	S53	4.06	0.52	2.99	0.64	1.62	0.24	1.26	0.22	148	30.9	0.90	0.92
22	S57	1.38	0.20	1.30	0.29	0.82	0.12	0.68	0.11	59	29.0	0.88	0.93
23	S61	1.76	0.24	1.60	0.36	0.99	0.15	0.88	0.15	74	28.8	0.87	0.92
23	S63	1.90	0.28	1.72	0.38	1.02	0.17	0.94	0.15	75	30.8	0.86	0.85
23	S66	2.61	0.37	2.38	0.51	1.45	0.22	1.35	0.22	107	29.8	0.86	0.92
23	S68	1.93	0.26	1.52	0.35	0.93	0.14	0.82	0.14	75	31.0	0.93	0.97
23	S71	1.70	0.24	1.46	0.34	0.94	0.15	0.89	0.16	70	29.2	0.91	0.96
23	S75	1.55	0.23	1.49	0.34	0.94	0.14	0.78	0.15	65	30.4	0.91	1.01
24	S79	2.28	0.34	2.26	0.51	1.43	0.22	1.35	0.23	87	29.5	0.92	0.97
25	S82	1.34	0.20	1.28	0.28	0.74	0.11	0.61	0.11	59	30.2	0.89	0.99
25	S84	1.42	0.20	1.32	0.30	0.80	0.13	0.75	0.12	59	28.4	0.98	1.04
25	S149	1.64	0.24	1.43	0.35	0.95	0.15	0.92	0.15	71	29.0	0.94	0.96
25	S150	3.03	0.38	2.37	0.51	1.49	0.23	1.43	0.24	176	29.9	1.14	1.19
25	S151	3.20	0.45	2.80	0.61	1.56	0.24	1.28	0.22	124	31.5	1.01	1.12
26	S157	2.45	0.36	2.26	0.51	1.45	0.24	1.35	0.23	96	29.3	0.92	0.99
26	S166	2.92	0.40	2.56	0.55	1.41	0.25	1.31	0.22	113	31.3	0.93	0.99

Bed	Sample #	Pr/Pr* (3)	Mg/Ca Ratio	Sr/Ca Ratio	Th/Sc Ratio	K/(Fe+Mg) Ratio	Th/U Ratio	Authigenic U (4)	V/Cr Ratio	V/(V+Ni) Ratio	U/Mo_{auth} (5)	Fe_T/Al Ratio
17	S112	1.02	0.46	0.0013	1.00	0.25	2.05	0.76	2.2	0.79	0.18	0.66
17	S3	1.00	0.60	0.0036	1.08	0.74	2.88	0.13	1.5	0.79	1.25	0.45
18	S4	1.01	0.73	0.0033	1.01	0.97	1.27	3.96	1.9	0.70	0.30	0.47
18	S7	1.02	0.85	0.0022	0.88	0.35	4.22	-0.58	1.3	0.77	0.89	0.59
18	S8	1.02	1.36	0.0039	0.74	0.56	2.88	0.10	1.3	0.77	0.96	0.46
18	S10	1.00	1.41	0.0045	0.69	1.17	1.47	2.59	1.1	0.66	0.41	0.39
18	S13	1.02	0.62	0.0023	0.96	0.60	1.09	4.41	2.3	0.66	0.16	0.56
18	S14	1.03	1.13	0.0045	0.72	0.99	1.87	1.52	1.3	0.70	0.36	0.46
18	S16	1.05	3.51	0.0093	0.63	0.70	2.35	0.52	1.2	0.76	1.84	0.47
18	S19	1.03	1.21	0.0032	0.72	0.71	1.85	1.51	1.9	0.76	0.19	0.52
18	S26	1.03	1.03	0.0031	0.75	1.38	1.85	1.52	0.9	0.67	0.45	0.36
20	S27	1.01	5.35	0.0110	0.81	0.73	3.58	-0.54	2.2	0.80	1.57	0.50
20	S30	1.04	2.65	0.0080	0.76	0.78	3.62	-0.48	1.2	0.76	2.54	0.41
20	S34	1.02	1.73	0.0042	0.82	0.73	2.84	0.14	1.3	0.72	1.50	0.50
21	S39	1.05	1.00	0.0042	0.92	0.92	2.88	0.10	1.6	0.78	1.58	0.48
21	S41	0.99	0.31	0.0021	0.96	1.08	2.57	0.37	1.6	0.75	0.49	0.41
21	S44	1.01	2.07	0.0042	0.71	0.47	4.55	-0.83	1.2	0.72	0.84	0.58
22	S47	1.02	1.35	0.0041	0.80	0.68	4.37	-0.91	1.3	0.76	0.90	0.47
22	S49	1.00	1.16	0.0026	0.80	0.44	4.40	-0.68	1.1	0.67	0.34	0.63
22	S53	1.04	0.81	0.0037	0.82	1.15	0.76	7.27	4.5	0.89	0.45	0.39
22	S57	1.04	1.22	0.0022	0.89	0.30	4.98	-0.68	1.1	0.68	0.83	0.77
23	S61	1.04	1.33	0.0027	0.86	0.34	5.51	-0.99	1.2	0.71	0.63	0.60
23	S63	1.08	2.11	0.0036	0.69	0.38	2.39	0.47	4.7	0.90	0.52	0.61
23	S66	1.04	1.21	0.0046	0.81	0.78	0.90	5.46	5.4	0.88	0.56	0.47
23	S68	1.02	1.14	0.0029	0.68	0.76	1.77	1.11	1.0	0.65	0.37	0.50
23	S71	1.02	1.38	0.0034	0.69	0.93	2.02	1.03	2.4	0.76	0.38	0.45
23	S75	1.00	0.36	0.0017	0.69	0.64	2.07	0.54	2.2	0.82	0.53	0.60
24	S79	1.01	0.68	0.0020	0.88	0.51	2.54	0.39	5.9	0.91	0.46	0.43
25	S82	1.00	0.35	0.0013	0.74	0.30	2.10	0.54	1.3	0.70	1.02	0.60
25	S84	0.98	0.86	0.0019	0.84	0.44	5.13	-0.85	0.9	0.69	0.52	0.51
25	S149	1.02	1.14	0.0026	0.68	0.86	2.44	0.39	2.4	0.86	0.44	0.38
25	S150	0.91	3.64	0.0069	0.79	0.71	3.35	-0.30	1.3	0.67	1.38	0.52
25	S151	0.95	0.30	0.0022	0.89	1.01	1.47	1.68	1.6	0.71	0.15	0.52
26	S157	1.00	0.48	0.0027	0.87	1.01	2.28	0.76	4.4	0.87	0.35	0.44
26	S166	1.00	0.34	0.0030	0.95	1.34	0.65	10.51	2.3	0.81	0.18	0.41

Appendix 2.2: PAAS-normalized (6) and Average Shale-normalized (7) ratios of the studied shales from the Green Point Formation in Chapter 2. Highlighted samples have low U EFs and their U contents correlate strongly with their Al counterparts.

Bed	Sample #	Mo	U	V	Ni	Cu	Cr	P	Mo	U
		EF_{PAAS}	EF_{PAAS}	EF_{PAAS}	EF_{PAAS}	EF_{PAAS}	EF_{PAAS}	EF_{PAAS}	$EF_{Average\ Shale}$	$EF_{Average\ Shale}$
17	S112	11.02	1.99	1.38	0.85	0.70	0.86	1.60	8.97	2.17
17	S3	1.20	1.51	0.88	0.53	0.61	0.81	1.52	0.98	1.65
18	S4	10.70	3.22	1.15	1.17	0.92	0.84	0.83	8.71	3.52
18	S7	0.87	0.78	0.75	0.51	0.64	0.81	1.24	0.71	0.85
18	S8	1.01	0.97	0.79	0.57	0.50	0.86	0.87	0.82	1.06
18	S10	4.69	1.92	0.68	0.82	0.57	0.88	0.48	3.82	2.10
18	S13	22.44	3.61	1.35	1.62	1.09	0.81	1.12	18.27	3.95
18	S14	4.33	1.55	0.77	0.77	0.67	0.85	0.73	3.52	1.70
18	S16	0.50	0.92	0.74	0.55	0.84	0.85	0.91	0.41	1.01
18	S19	9.06	1.70	1.25	0.91	0.58	0.91	0.96	7.38	1.86
18	S26	3.36	1.51	0.58	0.68	0.41	0.89	0.44	2.73	1.65
20	S27	0.61	0.96	1.48	0.87	0.70	0.95	0.88	0.50	1.05
20	S30	0.34	0.87	0.64	0.48	0.13	0.77	1.05	0.28	0.96
20	S34	0.72	1.07	0.87	0.81	0.86	0.95	0.83	0.58	1.18
21	S39	0.71	1.12	1.11	0.71	0.68	0.97	1.36	0.58	1.23
21	S41	2.72	1.34	0.95	0.75	0.58	0.85	1.12	2.21	1.46
21	S44	0.76	0.64	0.67	0.61	0.92	0.81	0.97	0.62	0.70
22	S47	0.88	0.80	0.76	0.57	0.37	0.83	1.06	0.72	0.87
22	S49	2.13	0.72	0.70	0.82	0.86	0.92	1.16	1.74	0.79
22	S53	9.98	4.45	3.09	0.92	0.85	0.96	1.82	8.12	4.86
22	S57	0.78	0.64	0.79	0.88	0.79	0.99	0.88	0.63	0.70
23	S61	1.03	0.64	0.73	0.69	0.74	0.88	0.91	0.84	0.71
23	S63	2.25	1.18	3.18	0.84	0.96	0.94	1.10	1.83	1.29
23	S66	6.54	3.64	3.50	1.12	0.80	0.91	0.97	5.32	3.98
23	S68	3.90	1.43	0.67	0.84	0.47	0.97	1.28	3.18	1.57
23	S71	3.55	1.33	1.50	1.08	0.68	0.89	0.79	2.89	1.46
23	S75	2.20	1.17	1.66	0.88	0.80	1.04	0.82	1.79	1.28
24	S79	3.16	1.45	3.66	0.83	0.67	0.87	1.61	2.58	1.59
25	S82	1.49	1.52	0.79	0.78	0.67	0.87	1.41	1.21	1.66
25	S84	1.26	0.65	0.49	0.52	0.36	0.76	0.87	1.02	0.71
25	S149	2.37	1.04	1.32	0.52	0.43	0.78	0.69	1.93	1.13
25	S150	0.71	0.98	0.82	0.95	1.66	0.87	0.88	0.58	1.07
25	S151	14.07	2.05	1.07	1.03	0.88	0.96	2.05	11.46	2.24
26	S157	4.11	1.43	2.47	0.85	0.54	0.79	1.05	3.34	1.56
26	S166	34.96	6.13	1.30	0.72	0.87	0.80	1.18	28.46	6.71

Appendix 2.3: Results from the calculations using the modified method of Organo (1997), see Chapter 2. Highlighted samples have low U EFs and their U contents correlate strongly with their Al counterparts. (#) refers to the relevant equation for the ratios.

Bed	Sample #	$(\%ter)_x$ (8)	$(U_{ter})_x$ (9)	$(\%U_{ter})_x$ (10)	$(\%U_{bio\text{-}auth})_x$ (11)
17	S112	32.8	0.87	36.3	63.7
17	S3	57.4	1.53	47.5	52.5
18	S4	57.5	1.53	22.3	77.7
18	S7	45.3	1.20	84.8	15.2
18	S8	61.6	1.64	68.6	31.4
18	S10	72.2	1.92	37.7	62.3
18	S13	52.3	1.39	20.1	79.9
18	S14	69.9	1.86	46.2	53.8
18	S16	60.4	1.61	66.0	34.0
18	S19	67.0	1.78	45.3	54.7
18	S26	65.3	1.74	43.7	56.3
20	S27	82.3	2.19	78.3	21.7
20	S30	73.8	1.96	84.2	15.8
20	S34	60.5	1.61	61.7	38.3
21	S39	50.5	1.34	55.8	44.2
21	S41	46.4	1.23	47.3	52.7
21	S44	68.6	1.82	113.1	-13.1
22	S47	72.6	1.93	96.8	3.2
22	S49	53.3	1.42	97.8	2.2
22	S53	60.0	1.60	16.4	83.6
22	S57	38.8	1.03	99.7	0.3
23	S61	50.9	1.35	114.1	-14.1
23	S63	53.4	1.42	61.6	38.4
23	S66	57.2	1.52	19.5	80.5
23	S68	46.8	1.25	46.0	54.0
23	S71	62.1	1.65	52.2	47.8
23	S75	34.3	0.91	53.1	46.9
24	S79	48.8	1.30	51.1	48.9
25	S82	34.3	0.91	50.7	49.3
25	S84	49.0	1.30	109.0	-9.0
25	S149	49.7	1.32	63.3	36.7
25	S150	72.5	1.93	75.2	24.8
25	S151	36.5	0.97	29.4	70.6
26	S157	55.7	1.48	46.4	53.6
26	S166	60.6	1.61	12.0	88.0

Appendix 3.1: Elemental and elemental ratio geochemical data of the studied shales from the Green Point Formation in Chapter 3. Highlighted samples have low U EFs and their U contents correlate strongly with Al concentrations.

Bed	Sample #	**Al**	**Mo**	**U**	**U/Mo$_{conc}$**	**Mo**	**U**	**U/Mo$_{PAAS}$**
		wt%	ppm	ppm	Concentration Ratio	EF PAAS	EF PAAS	PAAS Ratio
17	S112	3.27	4.29	2.40	0.56	11.02	1.99	0.18
17	S3	5.79	0.83	3.22	3.87	1.20	1.51	1.25
18	S4	5.78	7.36	6.86	0.93	10.70	3.22	0.30
18	S7	4.96	0.51	1.42	2.76	0.87	0.78	0.89
18	S8	6.70	0.81	2.39	2.96	1.01	0.97	0.96
18	S10	7.17	4.00	5.09	1.27	4.69	1.92	0.41
18	S13	5.19	13.87	6.93	0.50	22.44	3.61	0.16
18	S14	7.02	3.62	4.03	1.11	4.33	1.55	0.36
18	S16	7.14	0.43	2.43	5.71	0.50	0.92	1.84
18	S19	6.27	6.76	3.93	0.58	9.06	1.70	0.19
18	S26	7.13	2.85	3.98	1.39	3.36	1.51	0.45
20	S27	7.89	0.58	2.79	4.85	0.61	0.96	1.57
20	S30	7.23	0.30	2.33	7.88	0.34	0.87	2.54
20	S34	6.57	0.56	2.61	4.65	0.72	1.07	1.50
21	S39	5.82	0.49	2.41	4.91	0.71	1.12	1.58
21	S41	5.27	1.71	2.60	1.53	2.72	1.34	0.49
21	S44	6.84	0.62	1.61	2.62	0.76	0.64	0.84
22	S47	6.80	0.72	2.00	2.79	0.88	0.80	0.90
22	S49	5.44	1.38	1.45	1.05	2.13	0.72	0.34
22	S53	5.93	7.05	9.74	1.38	9.98	4.45	0.45
22	S57	4.36	0.40	1.04	2.56	0.78	0.64	0.83
23	S61	4.99	0.61	1.19	1.94	1.03	0.64	0.63
23	S63	5.31	1.42	2.31	1.62	2.25	1.18	0.52
23	S66	5.80	4.51	7.79	1.73	6.54	3.64	0.56
23	S68	5.11	2.37	2.71	1.14	3.90	1.43	0.37
23	S71	6.43	2.72	3.17	1.16	3.55	1.33	0.38
23	S75	3.98	1.04	1.72	1.65	2.20	1.17	0.53
24	S79	4.73	1.78	2.54	1.42	3.16	1.45	0.46
25	S82	3.22	0.57	1.80	3.15	1.49	1.52	1.02
25	S84	5.00	0.75	1.19	1.60	1.26	0.65	0.52
25	S149	5.46	1.54	2.09	1.36	2.37	1.04	0.44
25	S150	7.10	0.60	2.56	4.28	0.71	0.98	1.38
25	S151	4.37	7.32	3.30	0.45	14.07	2.05	0.15
26	S157	6.05	2.96	3.19	1.08	4.11	1.43	0.35
26	S166	5.92	24.63	13.40	0.54	34.96	6.13	0.18

Appendix 3.2: Elemental, elemental ratio and isotopic geochemical data of the studied carbonates from the Green Point Formation.

Bed	Sample ID #	**δ98/95Mo ‰**	**±2s**	**Al**	**Sr**	**Mo**	**U**	**U/Mo$_{conc}$**	**Mo**	**U**	**U/Mo$_{PAAS}$**
		ratio		ppm	ppm	ppm	ppm	Concentration Ratio	PAAS EF	PAAS EF	PAAS Ratio
17	GP 1			1539	312	0.10	0.90	9.07	5.39	15.79	2.93
17	GP 2	0.71	0.01	372	285	0.17	1.32	7.68	38.88	96.28	2.48
18	GP 3			1043	215	0.13	0.61	4.57	10.78	15.90	1.47
18	GP 4			540	301	0.05	4.31	80.49	8.34	216.62	25.96
18	GP 5			1328	296	0.07	0.93	12.63	4.68	19.07	4.07
18	GP 6			492	260	0.09	1.48	16.83	15.06	81.72	5.43
18	GP 7	0.66	0.01	520	261	0.07	1.27	18.81	10.95	66.45	6.07
18	GP 8			1935	294	0.09	1.42	15.07	4.09	19.89	4.86
18	GP 9			568	266	0.08	0.84	10.33	12.08	40.24	3.33
18	GP 10			633	239	0.09	0.62	7.13	11.53	26.52	2.30
18	GP 11			11754	279						
18	GP 12			4902	206						
18	GP 13			302	211	0.09	0.54	5.80	25.81	48.25	1.87
20	GP 14	-0.30	0.12	878	227	0.29	2.25	7.81	27.59	69.53	2.52
20	GP 15			3162	490	0.28	0.29	1.05	7.31	2.47	0.34
21	GP 16			647	364	0.96	0.78	0.81	125.16	32.85	0.26
21	GP 17			1102	210	0.07	2.05	27.92	5.59	50.35	9.01
21	GP 18	0.94	0.03	640	297	0.09	1.85	19.95	12.21	78.55	6.44
21	GP 19			687	257	0.07	1.29	19.41	8.12	50.85	6.26
21	GP 20			483	272	0.08	0.70	9.17	13.21	39.07	2.96
21	GP 21			489	276	0.19	2.00	10.69	32.08	110.64	3.45
21	GP 22	0.82	0.04	371	250	0.10	2.68	27.91	21.75	195.87	9.00
21	GP 23			692	255	0.04	0.45	10.69	5.09	17.56	3.45
22	GP 24			614	282	0.23	1.48	6.51	31.04	65.21	2.10
22	GP 25			1083	190	0.04	0.79	22.08	2.78	19.81	7.12
22	GP 26			1558	175	0.03	0.78	23.83	1.76	13.54	7.69
22	GP 27			1785	510	0.26	3.00	11.60	12.17	45.53	3.74
23	GP 28	0.10	0.04	1104	482	0.41	1.52	3.68	31.37	37.29	1.19
23	GP 29			766	179	0.05	0.38	7.14	5.88	13.54	2.30
23	GP 30			703	246	0.03	0.16	5.04	3.76	6.12	1.63
23	GP 31			725	196	0.04	0.17	4.54	4.26	6.24	1.46
23	GP 32			686	258	0.03	0.19	6.03	3.87	7.52	1.94
23	GP 33	1.26	0.03	1571	397	1.91	1.51	0.79	102.16	26.12	0.26
23	GP 33A			1137	197	0.01	0.37	36.35	0.76	8.90	11.72
23	GP 34	0.93	0.04	920	222	0.09	0.60	6.61	8.33	17.77	2.13
23	GP 35	-0.10	0.18	1188	180	0.20	2.08	10.25	14.37	47.51	3.31
23	GP 36			910	203	0.71	0.88	1.24	65.92	26.34	0.40
23	GP 37			1142	189	0.06	1.19	18.88	4.63	28.17	6.09
23	GP 38	1.48	0.05	706	379	0.10	0.16	1.51	12.42	6.06	0.49
23	GP 39			1010	286	0.05	0.19	4.18	3.78	5.10	1.35
23	GP 40	0.55	0.02	745	215	0.02	0.24	13.71	1.95	8.62	4.42
23	GP 40 A										
25	GP 41			2010	222	0.17	0.63	3.61	7.28	8.47	1.16
25	GP 41 A			579	243	0.21	0.30	1.45	29.77	13.93	0.47
25	GP 42			496	177	0.19	0.20	1.10	31.39	11.18	0.36
25	GP 43			671	367	0.44	0.14	0.31	55.63	5.53	0.10
25	GP 44			473	342	0.34	0.36	1.07	60.32	20.83	0.35
25	GP 45			427	189	0.08	0.27	3.29	15.91	16.90	1.06
25	GP 46	2.34	0.19	286	213	0.09	0.15	1.67	26.15	14.11	0.54
25	GP 47	1.03	0.10	644	211	0.17	0.28	1.67	22.18	11.94	0.54
25	GP 48	1.24	0.07	1371	232	0.38	0.72	1.91	23.15	14.27	0.62
26	GP 49			230	398	1.28	0.78	0.61	468.49	92.21	0.20
26	GP 50			1064	262	0.74	0.69	0.94	58.34	17.61	0.30
26	GP 51			1036	272	0.52	0.36	0.69	42.36	9.36	0.22
26	GP 52			472	293	0.26	0.29	1.13	46.08	16.82	0.37
26	GP 53	1.38	0.06	406	325	0.19	0.10	0.52	39.15	6.61	0.17
26	GP 54			380	254	0.68	0.14	0.20	151.09	9.69	0.06
26	GP 55			783	309	0.33	0.60	1.83	35.30	20.79	0.59
26	GP 56			532	282	0.81	0.75	0.94	127.21	38.40	0.30
26	GP 57			677	269	0.34	0.97	2.90	41.68	38.98	0.94
26	GP 58			611	268	0.30	0.82	2.68	41.87	36.17	0.86
26	GP 59	0.89	0.04	487	295	0.62	1.06	1.70	107.57	58.99	0.55
26	GP 60			690	279	0.47	1.77	3.79	56.97	69.68	1.22